Technical Report
TR-18-03
January 2021

Evaluation of hydrogeological modelling in Task 7 of SKB Task Force GWFTS

Reduction of performance assessment uncertainty through modelling of hydraulic tests at Olkiluoto, Finland

Bill Lanyon

SVENSK KÄRNBRÄNSLEHANTERING AB

SWEDISH NUCLEAR FUEL
AND WASTE MANAGEMENT CO

Box 3091, SE-169 03 Solna
Phone +46 8 459 84 00
skb.se

SVENSK KÄRNBRÄNSLEHANTERING

ISSN 1404-0344
SKB TR-18-03
ID 1898162

January 2021

Evaluation of hydrogeological modelling in Task 7 of SKB Task Force GWFTS

Reduction of performance assessment uncertainty through modelling of hydraulic tests at Olkiluoto, Finland

Bill Lanyon
Fracture Systems Ltd

Keywords: Olkiluoto, DFN model, Groundwater flow, Solute transport, Site characterisation, Hydraulic testing, Posiva Flow Log.

Abstract

This report provides an overview and critical evaluation of the work performed by the seven modelling groups that participated in Task 7 of the SKB Task Force on Groundwater Flow and Transport of Solutes. Task 7 considered the hydraulic characterisation of the fractured bedrock at Olkiluoto in Finland. The task focused on:

- Use of the Posiva Flow Log (PFL) to characterise flow within the fracture system.
- The influence of open boreholes (required for PFL) on both the acquired data and on the site hydrogeology.
- Reduction of performance assessment uncertainty through modelling of hydraulic tests.

Use of the PFL requires long open hole intervals and the impacts of these open hole conditions are also considered.

The modelling work considered datasets from: the KR24 large scale cross-hole test (Task 7A); the KR14–18 pumping tests where both PFL and multi-packer systems tests were performed (Task 7B) and a set of PFL tests performed in low permeability rock at high drawdown during shaft sinking (Task 7C). A feature of the modelling work was the use of PFL flow data to condition and calibrate groundwater flow models of the fractured rock.

Sammanfattning

Denna rapport ger en översikt och kritisk utvärdering av det arbete som utförts av de sju modelleringsgrupperna som deltog i modelleringsuppgift 7 inom SKBs Task Force för grundvattenflöde och transport av lösta ämnen. Task 7 beaktade den hydrauliska karakteriseringen av den sprickiga berggrunden vid Olkiluoto i Finland. Uppgiften fokuserade på:

- Användning av Posiva Flow Log (PFL) för att karakterisera flödet i spricksystemet.
- Inverkan av öppna borrhål (som krävs för PFL) på både erhållna data och på platsens hydrogeologi.
- Minskad osäkerhet inom bedömningen av förvarsfunktionen genom modellering av hydrauliska tester.

Användning av PFL kräver långa intervaller med öppna borrhål och effekterna av dessa förhållanden med öppna borrhål beaktas också.

Modelleringsarbetet beaktade datamängder från: det storskaliga KR24-mellanhålstest (Task 7A); pumptester i borrhålen KR14–18 där både PFL- och multi-packersystemtest utfördes (Task 7B) samt en uppsättning PFL-tester utförda i berg med låg permeabilitet vid hög grundvattennivåsänkning under konstruktion av ett schakt (Task 7C). Ett inslag i modelleringsarbetet var användningen av PFL-flödesdata för att konditionera och kalibrera grundvattenflödesmodeller av det sprickiga berget.

Contents

1 Introduction

This report is an evaluation of Task 7 of the SKB Task Force on Groundwater Flow and Transport of Solutes. Task 7 considered the hydraulic characterisation of the fractured bedrock at Olkiluoto in Finland. The task focused on:

- Use of the Posiva Flow Log (PFL) to characterise flow within the fracture system.
- The influence of open boreholes (required for PFL) on both the acquired data and on the site hydrogeology.
- Reduction of performance assessment uncertainty through modelling of hydraulic tests.

The report aims to present both an overview and an evaluation of the work of the different modelling groups so that it represents a summary of Task 7. The detailed descriptions and interpretations from each modelling group have been separately reported by the modelling groups themselves.

1.1 Report organisation

This chapter describes how the Task Force worked during Task 7. This includes the composition of the Task Force, how the tasks were managed (task descriptions and data) and the numerical codes used. The remainder of the report is organised as follows:

- Chapter 2 provides some background information on the characterisation and interpretation of flow in fractured low-permeability rocks.
- Chapter 3 provides a short description and evaluation of Task 7A (a longer evaluation is given in Lanyon 2009).
- Chapter 4 provides a description and evaluation of Task 7B.
- Chapter 5 provides a description and evaluation of Task 7C together with additional work aimed at integrating models across different scales (Task 7ABC).
- Chapter 6 provides an overall evaluation of Task 7.
- Chapter 7 provides conclusions and recommendations.

Additional material is provided in the appendices.

1.2 The Äspö Task Force (TF GWFTS)

The Äspö Task Force on Modelling of Groundwater Flow and Transport of Solutes is a forum for the international organisations supporting the Äspö Hard Rock Laboratory to interact in the area of conceptual and numerical modelling of groundwater flow and solute transport in fractured rock. Emphasis is put on building confidence in the approaches and the methods used to model groundwater flow and solute transport in order to demonstrate their use for performance and safety assessments.

The overall objective of the Task Force is “to increase the understanding of the processes that govern retention (retention here refers to both reversible and irreversible immobilisation processes) of radionuclides transported in crystalline rock and to increase the credibility in the computer models used for groundwater flow and radionuclide transport” (Gustafson et al. 2009).

The Task Force is made up of:

- The Task Force Secretariat who manage the day-to-day operation of the Task Force.
- The delegates of the participating organisations.
- Modelling teams appointed and funded by the participating organisations.

The delegates together with the Chair, Scientific Chair and the Scientific Secretary constitute the Steering Committee of the SKB Task Force. The Steering Committee selects tasks and appoints principal investigators (PIs) and an evaluator (or reviewer) for each task. Interested scientists may participate at Task Force Meetings as observers.

The operation of the Task Force is governed by a charter approved by the participating organisations. The previous tasks performed within the Task Force are:

- Task 1 – The Large-scale Pumping and Tracer test 2 (LPT2) experiments, evaluation modelling.
- Task 2 – Äspö field tracer experiments, design modelling.
- Task 3 – The Äspö tunnel experiment, predictive/evaluation modelling.
- Task 4 – Tracer Retention and Understanding Experiments – TRUE-1, predictive modelling.
- Task 5 – Integration of hydrogeology and hydrochemistry.
- Task 6 – Performance Assessment Modelling Using Site Characterisation Data (PASC).

These tasks typically related to specific aspects of the hydrogeology of the Äspö Hard Rock Laboratory or to particular experiments at the laboratory (e.g. TRUE-1 in Task 4). Within the Task Force a significant effort has been made to integrate the understanding of groundwater flow derived from experiments at Äspö into models of radionuclide transport. This culminated in the work of Task 6 where understanding developed within the TRUE experiments was considered within the context of performance assessment (see Hodgkinson 2007).

In 2005, the Äspö Task Force initiated Task 7 which focused on the Olkiluoto site in Finland. Task 7 breaks away from previous work within the Task Force in:

- Considering a different site: Olkiluoto, the planned site for a deep high-level radioactive waste repository in Western Finland.
- Returning to surface borehole-based site characterisation issues, last considered within the Task Force in Task 1[1].

Within Task 7 the participating organisations and modelling groups were:

- CRIEPI: Central Research Institute of Electric Power Industry, Japan.
- JAEA/Golder: Japan Atomic Energy Agency in cooperation with Golder Associates Inc.
- KAERI: Korea Atomic Energy Research Institute.
- NWMO/University of Laval: Department of Geology and Geological Engineering of Laval University sponsored by the Nuclear Waste Management Organization, Canada.
- POSIVA/VTT: VTT Technical Research Centre of Finland, sponsored by Posiva Oy, Finland.
- SKB/KTH: Royal Institute of Technology (KTH), Stockholm in cooperation with SERCO, sponsored by SKB.
- SKB/CFE: Computer-aided Fluid Engineering AB, sponsored by SKB.

A group from Commissariat à l'Energie Atomique (CEA), Paris sponsored by ANDRA participated in the early parts of Task 7 (up until Task Force Meeting 23), while KAERI joined Task 7 at the end of Task 7A. During Task 7B, the team from CRIEPI withdrew from Task 7 due to the illness of a key investigator.

The PIs for Task 7 were Patrik Vidstrand and Henry Ahokas.

Following on from Task 7, work has been performed on two further tasks:

- Task 8 – Modelling of the Bentonite Rock Interaction Experiment, BRIE.
- Task 9 – Modelling REPRO, and LTDE-SD.

At the time of writing, reporting of Task 8 has been completed and Task 9 is ongoing.

[1] **Gustafson G, Ström A, 1995.** The Äspö Task Force on modelling of groundwater flow and transport of solutes. Evaluation report on Task No 1, the LPT2 large scale field experiments. SKB ICR-95-05, Svensk Kärnbränslehantering AB. (Internal report.)

1.3 The Olkiluoto site

Posiva Oy is responsible for the geological disposal of spent nuclear fuel generated in the Olkiluoto and Loviisa nuclear power plants. Posiva's reference design is based on the emplacement of canisters containing the spent nuclear fuel in vertical deposition holes (KBS-3V). The present safety case is based on the reference design. The repository is constructed on a single level with the floor of the deposition tunnels at a depth of between 400 and 450 m below the ground surface in the Olkiluoto bedrock. An underground rock characterisation facility (Onkalo URCF) has been constructed at the site. Investigations in Onkalo have been an essential support for the application of the construction license and will serve also for the operation license application of the repository. The license for the construction of a final disposal facility for spent nuclear fuel was granted in 2015 to Posiva. The operation license will be applied in a couple of years.

As given in the site description available for Task 7 (Anttila et al. 1999) the Olkiluoto site is located on an island of about 10 km^2 in the municipality of Eurajoki, in Western Finland. The investigations of geology and hydrology of the whole island began in 1987, when the preliminary site characterisation was launched. Since then more than 40 deep boreholes and a large number of shallow boreholes have been drilled. Most of the boreholes are located in the central part of the island (the Well Characterised Area, or WCA). This part of the island has been studied as the location for the deep repository. The geology of Olkiluoto is characterised by composite gneisses containing veins of tonalite and granite. The rock mass has an average fracture density of 1–3 fractures/m (Anttila et al. 1999). The bedrock is traversed by deformation zones of different magnitudes and orientation. The dominant rock types and the significant fracture zones in the area of the deep repository are presented in Figure 1-1. The planned extent of the Onkalo facility and its relationship to borehole KR24 is illustrated in Figure 1-2.

The bedrock is fractured and has several distinct hydrogeological zones, which have higher hydraulic conductivity than the surrounding sparsely-fractured rock. Of these zones, the most important were identified and have been included in the hydrogeological structural models of Olkiluoto used for this work. Within Task 7, the structural models from the Olkiluoto Bedrock Model (Vaittinen et al. 2003) and the updated hydrogeological structure model 2008 (Vaittinen et al. 2009) were used as the bases for the description of the major zones.

The fracture system within the background rock between the major zones shows a strong depth dependence with significantly more highly transmissive features in the upper 50 m of rock and a continuing reduction in the number and transmissivity of flowing features with depth. Similar patterns of depth dependence have been observed in crystalline rocks in Canada (Gascoyne et al. 1988, Raven and Gale 1986), Sweden[2] (Andersson et al. 1991, Juhlin et al. 1998), Southern Germany (Stober 1996 for gneissic rocks) and Switzerland (Thury et al. 1994). A reduction in transmissivity with depth may be explained by the combined influences of increased stresses and the absence of near-surface weathering and destressing.

A well-defined salinity profile has been developed from borehole data from Olkiluoto as shown in Figure 1-3. The water is essentially fresh until about −400 metres above sea level (m.a.s.l.) below which the salinity increases to about 70 g/l at −800 m.a.s.l. Below −800 m.a.s.l. the salinity is expected to be roughly constant. For the purposes of the current study a linear trend between 0 and −400 m.a.s.l. was assumed (Vidstrand et al. 2015) although many modelling groups assumed constant salinity within the models of the region of interest.

The Olkiluoto site description has been updated in 2011 for the construction license application (Posiva 2012) around the end of Task 7 activities

[2] Also in **Gale J E, Macleod R, Welhan J A, Cole C, Vail L, 1987.** Hydrogeological characterisation of the Stripa site. SKB Stripa Project Technical Report 87-15, Svensk Kärnbränslehantering AB. (Internal report.)

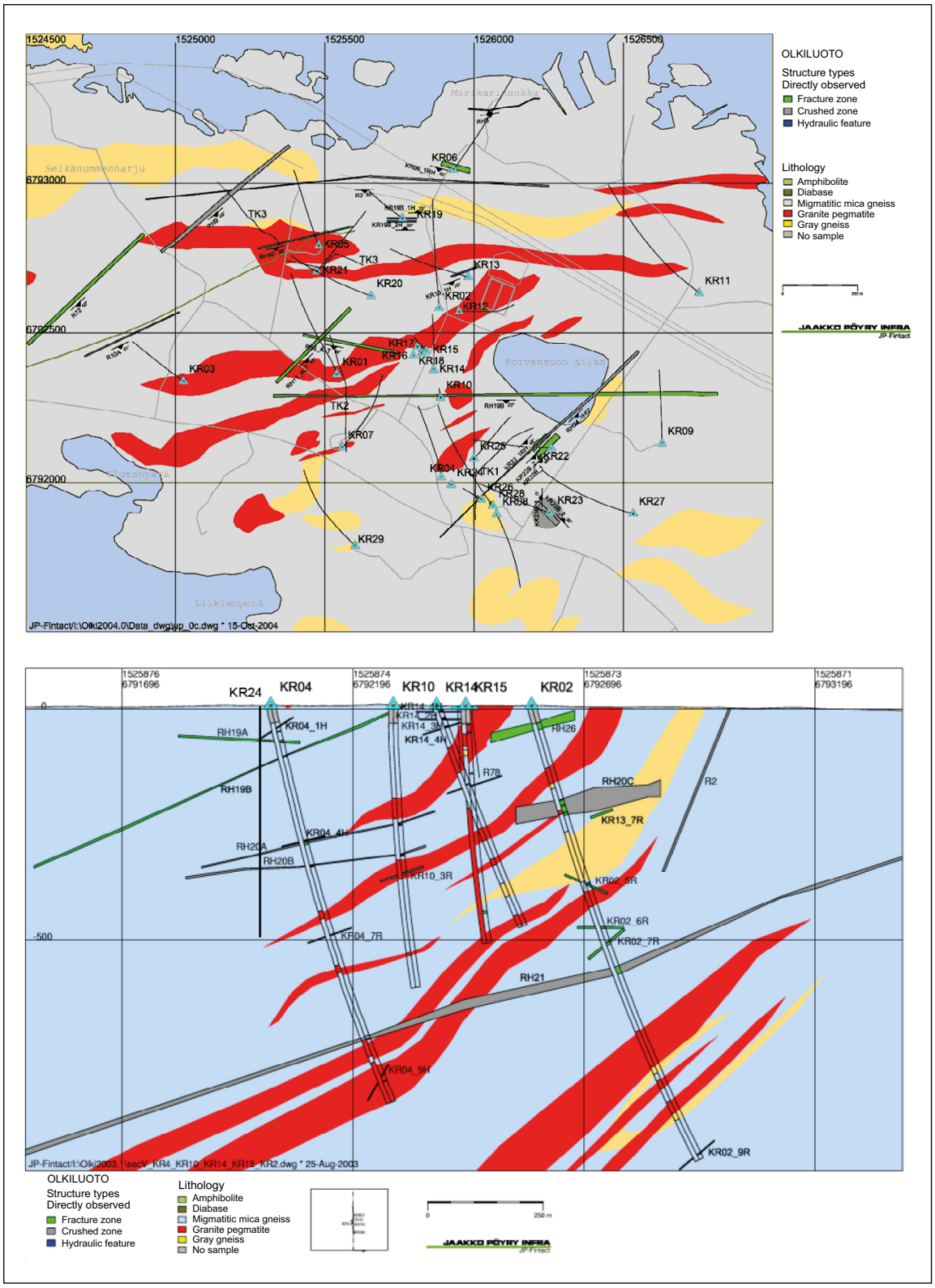

Figure 1-1. *Rock types and fractured zones within the main interest area for the deep repository at Olkiluoto according to the Olkiluoto bedrock model 2003/1 (Vaittinen et al. 2003).*

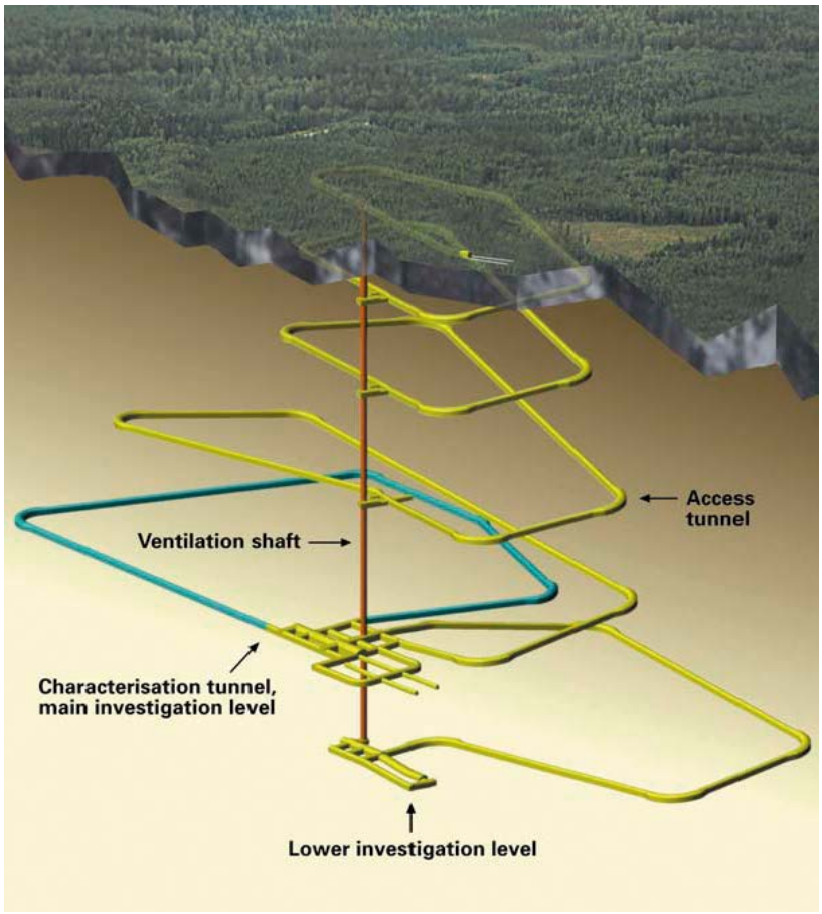

Figure 1-2. *The planned Onkalo rock characterisation facility. The construction of Onkalo started in July 2004 and is expected to take about six years. Borehole KR24 was located along the centre line of the ventilation shaft (from Vidstrand et al. 2015).*

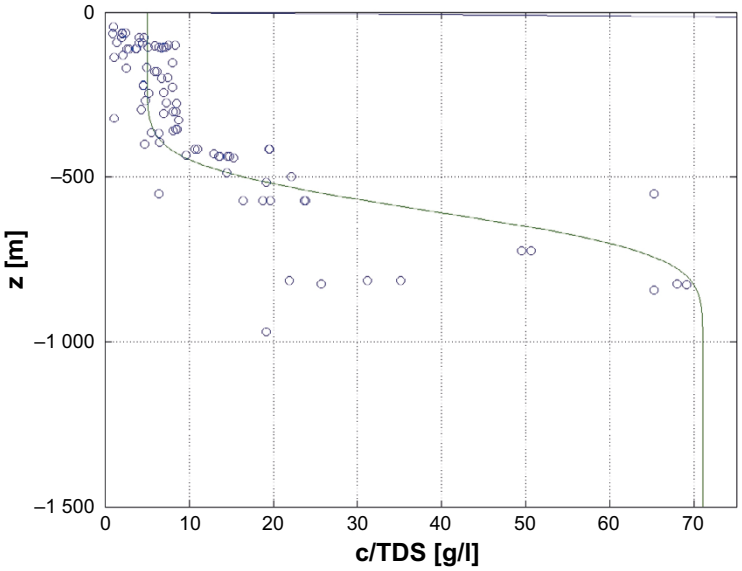

Figure 1-3. *Salinity profile for Olkiluoto island taken from Vidstrand et al. (2015). A linear trend between 0 and 6 g/litre between 0 and −400 m.a.s.l. was specified for use within Task 7.*

1.4 Task Management

The progress of each task is guided by the Task Force Secretariat using task definitions and structured data deliveries. The task definitions and datasets were developed by the Task 7 PIs and presented and discussed with the modelling groups at Task Force Meetings and Task Force Workshops.

During the course of Task 7 a series of Task Force Meetings and workshops were held (Table 1-1). Task Force Meetings considered the current tasks and included representatives of the modelling groups, delegates of the participating organisations and the Task Force Secretariat, whilst workshops typically focused on detailed modelling issues associated with the task. There was initially some overlap with Task 6 and towards the end of Task 7, with Task 8.

Decisions concerning the progress of the Task were taken during executive sessions at the TF Meetings. More routine management of the task included monthly Task Force planning telephone meetings of the Task Force Secretariat.

Table 1-1. Task Force Meetings and Workshops during Task 7.

Meeting	Location	Date
TF meeting #20	Äspö HRL, Sweden	May 17–19, 2005
TF Workshop – Task 7	Stockholm, Sweden	September 5–6, 2005
TF meeting #21	Montparnasse, Paris, France	March 6–9, 2006
TF Workshop – Task 7	Rauma, Finland	September 12–13, 2006
TF meeting #22	Långholmen, Stockholm, Sweden	January 16–18, 2007
TF Workshop – Task 7	Gothenburg, Sweden	June 11–12, 2007
TF meeting #23	Toronto, Canada	October 29–31, 2007
TF Workshop – Task 7	Oxford, UK	May 13–14, 2008
TF meeting #24	Äspö HRL, Sweden	September 9–11, 2008
TF Workshop -Task 7	Lund, Sweden	January 28–29, 2009
TF meeting #25	Mizunami, Japan	October 14–16, 2009
TF Workshop – Task 7/8	Vuojoki, Finland	January 12–14, 2010
TF Meeting #26	Barcelona, Spain	May 3–5, 2010
TF Workshop – Task 7/8	Lund, Sweden	December 1–2, 2010
TF Meeting #27	Äspö HRL, Sweden	March 15–17, 2011
TF Workshop – Task 7/8	Gothenburg, Sweden	October 25–26, 2011
TF Meeting #28	Berlin, Germany	January 17–19, 2012
TF Workshop – Task 8	Äspö, Sweden	April 24–25, 2012
TF Meeting #29	Lund, Sweden	November 27–29, 2012
TF Meeting #30	Helsinki, Finland	June 3–5, 2013

1.5 Tasks, subtasks, and task descriptions

Task 7 was organised as a series of subtasks considering fracture flow and use of the Posiva Flow Log (PFL) at decreasing spatial scales:

- Task 7 pre-studies: Test cases for September 2005.
- Task 7A: Reduction of performance assessment uncertainty through site-scale modelling of long-term pumping in KR24 at Olkiluoto, Finland.
- Task 7B: Reduction of performance assessment uncertainty through block scale modelling of interference tests in KR14–18 at Olkiluoto, Finland.
- Task 7C: Posiva Flow Logging characterisation and analysis of low permeable fractures and assessment of flow distribution pattern at shaft wall section at Onkalo, Olkiluoto, Finland.

The structure of the subtasks was set out in individual task description documents that are included in Vidstrand et al. (2015). There was an overall task description for Task 7 and detailed individual task descriptions for each of the subtasks. The evolution of the task descriptions is described in Vidstrand et al. (2015) and briefly summarised here.

The original task description was developed in April 2005 and focused on issues concerning open boreholes, their influence on site characterisation and how to model such features in a groundwater system perturbed by a long-term pumping test. The Task was initiated with a generic set of modelling exercises ("Test cases for September 2005") designed to test the ability of the modelling teams and their numerical codes to simulate flow into, out of and along boreholes.

Following the completion of these exercises and the development of a first definition of Task 7A (modelling of the KR24 long-term pump test) a revised task definition was developed. The revised description states that: "Task 7 aims at providing a bridge between the site characterisation (SC) and performance assessment (PA) approaches to pumping tests and measurement from borehole flow logging. Open boreholes are, during certain periods of the investigations, a feature at many sites and Task 7 aims to develop an understanding of the effects of open boreholes on the groundwater system and the use of data from such boreholes in site characterisation and performance assessment." The inclusion of i) the link to PA, ii) the focus on reduction of uncertainty and iii) the consideration of multiple scales resulted in a significant increase in the scope of the task.

The strategy of the revised Task 7 was to proceed from the largest scale (site-scale with focus on fracture zones) to smaller scales (rock block). Task 7 finished with measurements at the scale of the engineered barrier in a low permeability rock block. In addition, some work was done to integrate models across the spatial scales (see Chapter 5).

A more detailed discussion of the individual task descriptions is included in the relevant chapters.

1.5.1 Data

Data was provided to the modelling groups in a set of data deliveries. These were made available on the Task Force web pages on the SKB website. A list of the deliveries is given in Table 1-2. The main data are also presented within the individual Task Descriptions (see Vidstrand et al. 2015).

In Task 7B2 and 7C3 data was held back for comparison to allow modellers to make "blind-predictions". These were "Class B" (Lambe 1973) predictions, in that the data had already been acquired and was in some cases available in reports prior to the modellers' presentation of their predictions.

The datasets for each subtask are discussed later in the context of each subtask; however, each Task's dataset contained large amounts of data in multiple formats reflecting the extent of the Olkiluoto site characterisation dataset. In all, over 70 different items were delivered to the modellers, contained within 37 distributions. Henry Ahokas (one of the Task 7 PIs) worked extensively within the Olkiluoto programme and was an invaluable guide to the data.

Table 1-2. Data deliveries for Task 7.

#	Content
1	Definition of Task 7 – Modelling the KR24 long-term pumping test at Olkiluoto
2	Presentation files from TF#20
3	Installation files for viewers needed for some files in Data Delivery 2
4	General data a) Borehole information b) Bedrock model
5	Flow responses of pumping tests
6	Pressure responses of pumping tests
7	Test cases for Task 7 Workshop, September 5–6, 2005
8	Task 7A a) Task Description for Task 7A, part I – Specifications for Task 7A1 and Task 7A2 b) Data package for Task 7A c) Geometry of the zones d) Replies concerning some questions e) Task Description for Task 7A
9	Updated topography data for Task 7
10	a) Information on Data Delivery 10, December 5, 2006 b) Corrected groundwater table c) Grid format for the topography information
11	Questionnaire and Performance Measures Task 7A.
12	Updated groundwater table file to cover a larger domain
13	a) Memo from the Technical Session at TF#22 b) Spreadsheet on fresh water head values in some of the boreholes at the site
14	Task 7 Overall document
15	Questions and answers on Casing data.
16	Task Description Task 7A3–5
17	CAD file representing Olkiluoto
18	a) Measured values of drawdown and zone information b) Updated Task 7A3–5 Description c) Updated Task 7 Overall Document
19	Task 7B Related Information a) Report including flow responses: Rouhiainen and Pöllänen (2003) b) Report including pressure responses: Klockars et al. (2006). c) Summary made by Lasse Koskinen and Pekka Rouhiainen concerning interference tests made in boreholes KR14–18 d) Presentation concerning the interference tests in KR14–18
20	Task 7A Related Information Draft Memo – Preliminary analysis on the effect of natural trend of groundwater-table on head below the packer during long-term pumping test in KR24 in 2004.
21	Task 7A1 and A2 Reporting a) Task 7 Report Outline b) General SKB report template c) User's Guide for the template d) Example of an International Technical Document e) General SKB report template as dot file
22	Task Description of Task 7B

#	Content
23	Task Description and Background reports for Task 7B a) Task Description Task 7B b) Hydraulic crosshole interference test at the Olkiluoto site in Eurajoki, boreholes KR14–KR18 and KR15B–KR18B, WR 2003-30 c) Hydraulic Crosshole Interference Tests at Olkiluoto, Eurajoki in 2004, Boreholes KR14–KR18 and KR15B–KR18B, WR 2006-01 d) Appendices 43–45 for WR 2003-30 Additional background reports on single-hole measurements, April 2008. Basis for some single-hole data: e) Difference flow and electric conductivity measurements at the Olkiluoto site in Eurajoki, boreholes KR13 and KR14, Pöllänen and Rouhiainen (2002a) (Work2001-42.pdf) f) Difference flow and electric conductivity measurements at the Olkiluoto site in Eurajoki, boreholes KR15–KR18 and KR15B – KR18B, Pöllänen and Rouhiainen (2002b) (Work2002-29KR15- KR18B.pdf)
24	Updated Task Description and Data for Task 7B a) Overview of Data Delivery 24 b) Data package
25	Task 7B a) Task 7B Data including updated Task Description (Task7_DataDelivery25.zip) b) Surface fracture data (Task7_DataDelivery25b.zip) c) Fracture trace data (TK10_TK11.dxf.zip)
26	Task 7A and 7B a) Draft reports on Task 7A1–3 from MG b) Draft Task 7A Evaluation report c) Spreadsheet template for Task 7B results
27	Review Form, templates
28	Task 7B Description and Performance measures Updated Task Description Task 7B and Performance measures. Corrected Calibration data spreadsheet (October 28, 2008)
29	Fractures in boreholes surrounding KR14–18. Geological fracture information in boreholes KR01–13 and 19–40
30	Task 7B Plots of calibration data.
31	Task 7B Questionnaire and updated spreadsheet for model calibration
32	Task Description for Task 7C
33	Updated Task Description for Task 7C – Specifications for Task 7C
34	Revised Task Description for Task 7C – Specifications for Task 7C Fracture and PFL data for Task 7C
35	Task 7B – Updated questionnaire for Task 7B
36	Task 7C – Description of the cross-flow/interference test sequence using boreholes PP125, 127 and 129.
37	Task 7A-C report template

1.6 Numerical codes

The different groups used a range of numerical tools to build and populate numerical meshes and solve for groundwater flow and transport. Table 1-3 lists the main numerical codes used by each group in Task 7.

Table 1-3. Numerical codes used in Task (see glossary for abbreviations).

Group	Numerical tools	Task 7A	Task 7B	Task 7C
		KR24 pump test	**KR14–18 crosshole tests**	**PFL characterisation of low permeable fractures**
		Deterministic model of major zones	**Block containing deterministic zones and "background rock"**	**Block of background rock containing low permeability fractures**
CRIEPI	FEGM Kawanishi et al. (1994)	DFN with EPM surface layer.	DFN with EPM surface layer (not reported).	Did not participate.
JAEA/Golder	Fracman (Dershowitz et al. 2007)	DFN with EPM surface layer.	DFN with deterministic zones (from cross-hole test interpretation) and stochastic background rock fracture network.	Deterministic fracture plane with heterogeneous transmissivity and background stochastic fracture network.
KAERI	FEFLOW (Diersch 2005a,b)	CPM model conditioned on major zones and low permeability background rock.	CPM model conditioned on major zones with stochastic background rock fracture network.	Kriged heterogeneous transmissivity fracture plane.
NWMO/Laval	HydroGeosphere (Graf and Therrien 2007).	Continuum model containing embedded fracture elements in low permeability background rock.	Continuum fractured rock facies model with embedded discrete fractures.	Deterministic fracture plane with heterogeneous transmissivity and uniform permeability background rock.
Posiva/VTT	FEFTRA (Löfman and Mészáros 2013)	Continuum model containing embedded fracture elements in low permeability background rock. EnkF inverse modelling approach.	EPM and DFN models with deterministic zones and background rock fracture network.	Deterministic fracture plane with heterogeneous transmissivity and background stochastic fracture network.
SKB/KTH	CONNECTFLOW (Hartley and Holton 2008) Fup model (Gotovac 2009a,b)	DFN zone model and surface layer.	DFN based on fracture growth model.	Adaptive "multi-resolution fup model of heterogeneous transmissivity fracture plane.
SKB/CFE	DarcyTools (Svensson et al. 2010, Svensson 2010)	Smeared fracture zone model and continuum surface layer.	Smeared fracture zone model and continuum surface layer.	Smeared fracture model of deterministic single fractures and stochastic background fracture network.

1.6.1 Representation of the fracture system

In general, the models contained elements representing:

- Deterministic features (fractures or fracture zones, often based on geometries provided within the task descriptions and data deliveries).
- Stochastic fractures generated from probability distributions describing the fracture geometric, hydraulic and transport properties.

The hydraulic properties of the deterministic features were either specified in the task description or estimated by the modellers (calibration). The transmissivity of deterministic features was not always uniform (see for example the method of conditioning "patches" implemented in Task 7A, the segmentation of features by VTT in Task 7A, or spatially varying transmissivity models in Task 7C).

Stochastic fractures typically had power-law or log-normal length-scale distributions and log-normal transmissivity distributions. Transmissivity was often statistically correlated with fracture length scale such that the longest features were likely to be of highest transmissivity. Transmissivity was uniform across stochastic fractures. Almost all models assumed a homogeneous Poisson process for the stochastic fracture centres within the rock. The only exception is the fracture-growth model used by SKB/KTH in Task 7B which is discussed later. The homogeneous Poisson process represents a "purely random" process where fracture centre positions are statistically independent of one another (i.e., it is assumed that there are no interactions between fracture locations)[3].

The only model that was not based on the generation of a geometric fracture network was the fractured rock facies approach of NWMO/Laval in Task 7B. In this approach a "Transition Probability" method (T-PROGS, Carle 1999) was used to generate spatial distributions of different fractured rock facies: (unfractured, slightly fractured, moderately fractured and highly fractured). The different facies were associated with different hydraulic properties (permeability).

In addition to the fracture system, models included representations of the boreholes (often as 1D elements) and continuum representations of the near surface rock.

1.6.2 Numerical methods for solving flow and transport in the fracture network

Many of the numerical codes represent the fracture system geometry as an assemblage of 2D planar elements (triangles, rectangles, polygons or circles) embedded in a 3D model volume. The 2D planar elements represent fractures or parts of fractures with the assumption that the thickness of the fracture is of minor significance for the geometry. The numerical codes implement three ways of using this geometric model of the fracture network as the basis for solving flow and transport in the fracture system:

- Direct representation of the geometric model as 2D elements in an impermeable medium (discontinuum).
- Embedding (and possible adjustment) of the 2D elements within a 3D continuum.
- Calculation of equivalent continuum element properties based on the geometric fracture model.

A short summary of the approaches is given in Table 1-4.

[3] Or that such interactions have no significant impact on the model outputs.

Table 1-4. Treatment of geometric model of fracture network within the numerical tools.

Treatment	Codes	Comment
2D elements in impermeable medium	FRACMAN	Fracture intersections are discretised and mesh-making tools used to ensure high resolution grids around “pathological” intersection geometries.
	CONNECTFLOW	Regular gridding of fracture elements with response functions calculated for stepwise linear pressure variations along fracture intersection (adjusted to lie on grid nodes) followed by global flow solution using calculated response functions (static condensation). Options to control refinement (number of nodes) on each fracture plane and along intersections.
	FEFTRA/VINTAGE	Discretisation of fracture geometry as 2D finite elements in 3D space using integer arithmetic.
Volumetric element with equivalent properties (e.g. permeability and porosity) to the fracture network within the element	FEFLOW	Geometric estimate of tensor (Oda’s method).
	DarcyTools	Adaptive gridding to represent flow in fractures greater than a specified minimum size. Below this size fractures are treated as sub-grid porosity.
	CONNECTFLOW	Options to fit a permeability tensor to flow across the element volume from fluxes at the element surface or within element, under multiple gradients.
2D element embedded in 3D porous medium	HydroGeosphere	Feature geometry was adjusted to map to nodes within the model mesh (Graf and Therrien 2007).

1.6.3 Feature connectivity

Hydraulic connections between fractures in most of the models are based on purely geometric considerations. In models that solve for flow on the DFN (FRACMAN, CONNECTFLOW, FEFTRA/VINTAGE) the geometric intersection of the 2D planar elements are calculated and an assumption of hydraulic head continuity is made. This assumption is justified if:

- There are no special hydraulic properties of the fracture intersection different from the fracture plane.
- Flow is uniform across the fracture plane.

Where geometric DFNs are upscaled using approximate methods, fractures within an upscaling cell are assumed to be connected and the flow conductance within the equivalent cell is the (tensor) sum of those of the individual fractures.

Both of these assumptions potentially result in “over-connection” where for example:

- fractures whose internal heterogeneity do not connect well are assumed within the model to be in perfect connectivity,
- fracture intersections are the locus for fracture fill or gouge resulting in reduced connection between fractures,
- otherwise disconnected (or poorly connected) small fractures within a cell may contribute to the estimated cell permeability.

The JAEA/Golder model in Task 7B randomly reduced connectivity in the stochastic fracture network to address this issue.

Some previous studies have postulated enhanced permeability along fracture planes or even situations where flow is dominated by the network of fracture intersections (e.g. Abelin et al. 1987, Nordqvist et al. 1992).

Under-connectedness in the models may occur where the unfractured rock is of sufficient permeability (due to the matrix or fractures not included in the DFN) that flow can occur in thin “bridges” of rock between features in the DFN (see Matthäi and Belayneh 2004). High hydraulic gradients may occur within such bridges if the fracture network itself is poorly connected.

1.6.4 Other tools

The different models were used in combination with either general purpose (e.g. Microsoft Excel) or purpose-built pre- and post-processing software for model-building, visualisation and presentation of results. Two inverse modelling codes were used in conjunction with the groundwater flow codes: NWMO/Laval used PEST (Doherty 2004) and POSIVA/VTT used EnKF (Evensen 1994).

JAEA were the only group to use a detailed well-test analysis model as part of their workflow. This was used in Task 7B in an interpretation phase prior to model development.

A range of numerical tools were used to generate 2D random transmissivity fields in Task 7C e.g. HYDROGEN (Robin et al. 1993).

1.7 Task 7 timeline

An approximate timeline for Task 7 is shown in Figure 1-4. Starts and ends of tasks have been chosen to roughly coincide with Task Force meetings. The long period of Task 7 reporting reflects the period from the delivery of the first draft modelling report to the receipt of the last final draft and does not include time spent in the final SKB publication process.

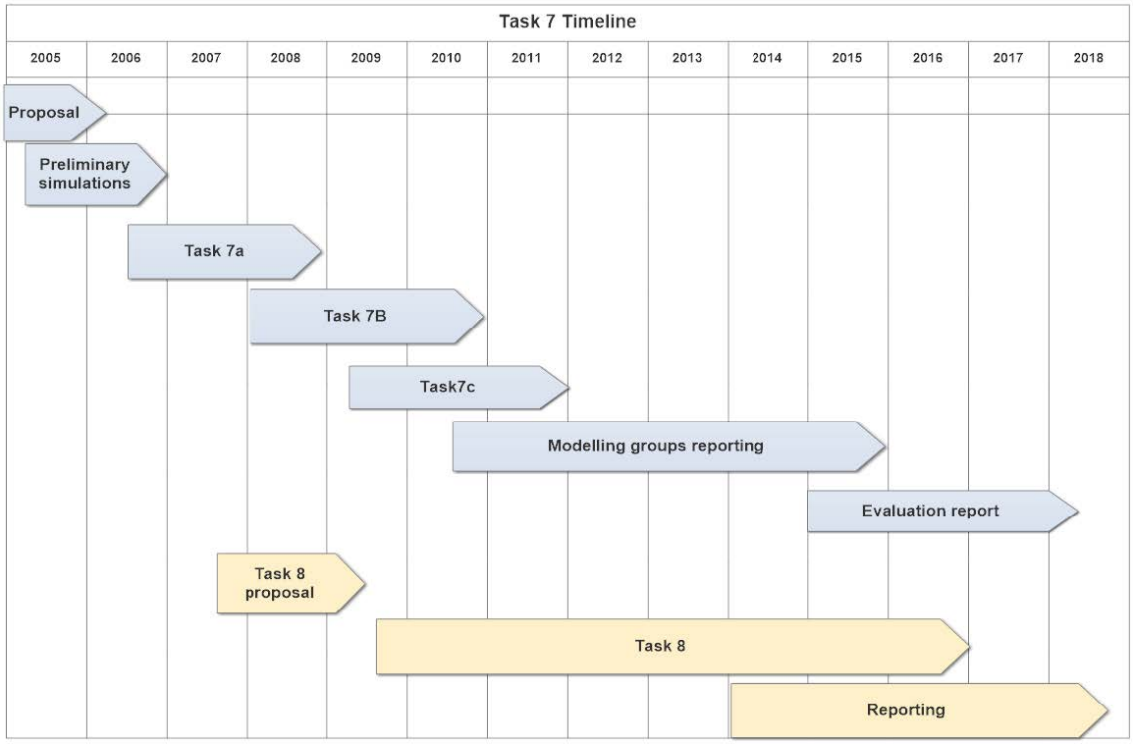

Figure 1-4. *Task 7 timeline.*

2 Characterising flow in fractured rock

The characterisation of flow and transport in fractured rock poses particular difficulties due to the heterogeneity of fracture properties and the extreme contrast between the rock matrix and fractures. The main hydrogeological characterisation methods (see Andersson et al. 1993, National Research Council 1996, Gustafson 2012) discussed in the next sections of this chapter are:

- Hydraulic head measurements.
- Pump tests.
- Flowmeter tests.
- Tracer tests.
- Groundwater sampling.

The different methods are combined within a site characterisation programme to acquire the key hydrogeological system properties:

- Spatial distribution of water conducting features (WCF e.g. channels, fractures or fracture zones depending on the nature of the flow system and scale of investigation).
- Geometric and geological properties of the WCF.
- Distribution of WCF transmissivity (or equivalent flow properties).
- Hydraulic head magnitudes and gradients.
- Spatial distribution of water chemistry (within both the advective and diffusive pore water systems).

Paillet (2004) suggests that successful characterisation of fractured rock aquifers requires integration of three basic tools:

1. Surface geophysics providing non-destructive imaging of the volume, but which is typically ambiguous and unable to identify individual fracture conduits.
2. Borehole geophysics providing detailed characterisation of fractures but only in the immediate vicinity of the borehole.
3. Hydraulic measurements in boreholes to generate direct relationships between geophysical and hydraulic properties adjacent to the boreholes.

Posiva's approach to the characterisation of the Olkiluoto site (including large volumes of low conductivity rock) utilises these three tools, as is demonstrated by the dataset provided within Task 7.

Berkowitz (2002) reviews characterisation of flow and transport in fractured rock and emphasises issues associated with measurement scale. In particular, he poses three questions to be considered prior to developing a conceptual picture, selecting a modelling approach and/or embarking on a data acquisition or field monitoring program:

- What is the scale of the problem of interest?
- What are the data to be used for?
- What is the required level of detail?

Berkowitz (2002) goes on to conclude that recurring research issues include those of scale (of process, problem and measurements) and non-uniqueness (e.g., interpretation of fluid and tracer tests; quantitative models). He sees progress coming from two technical developments: (1) improved characterisation of geometrical and hydraulic properties, based largely on improved geophysical measurement techniques, and (2) improvements in computing power and computational techniques, allowing consideration of flow and transport in large scale, 3D fracture systems. Task 7 in its focus on the Posiva Flowmeter Log (PFL- see Section 2.5) methodology and large-scale simulations contributes to both areas.

2.1 Hydraulic head measurements

Hydraulic heads in a borehole or borehole interval (isolated by temporary packer strings or permanent multi-packer systems) can be measured either from water level (e.g. in a piezometer) or as a gauge pressure. The conversion of gauge pressures to hydraulic heads requires knowledge of the gauge elevation relative to the head datum and the fluid density between the measurement interval and the gauge.

Two types of head measurement are typically used: (equivalent) fresh water head and environmental head. Where water density varies strongly with depth through an aquifer, it is not appropriate to use fresh water heads to estimate the vertical hydraulic gradient and the "environmental head" should be used. This issue was addressed by Lusczynski (1961) who defined "environmental head" as illustrated in Figure 2-1.

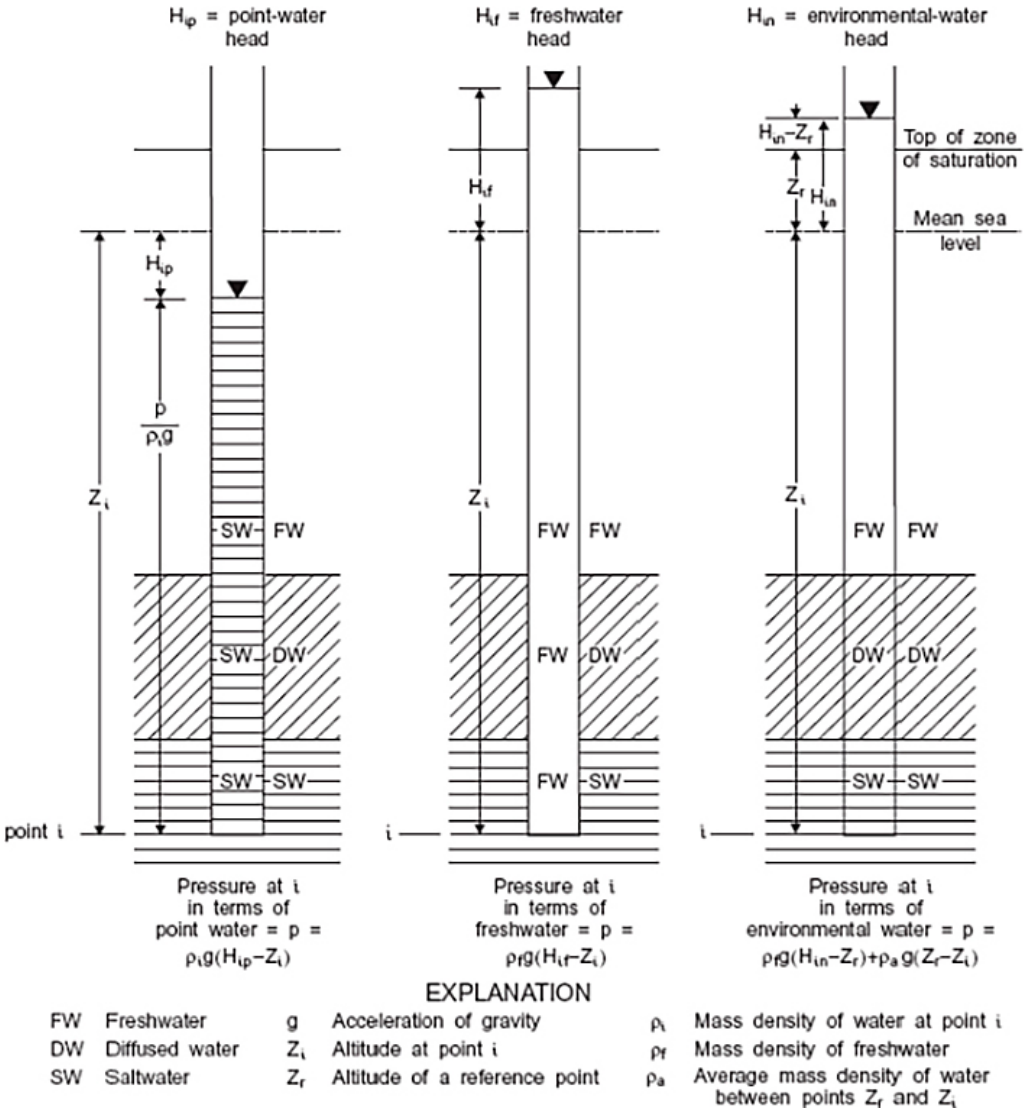

Figure 2-1. *Definitions of point-water, fresh water and environmental heads in groundwater with variable density (from Lusczynski 1961).*

At Olkiluoto heads have been measured since 1990 (Ahokas et al. 2008) using permanent piezometers, multi-packer systems, double packer tests and from analysis of flow logging (see later). Three types of hydraulic head have been defined:

- **Measured head** = the elevation of water level (m.a.s.l.) in a measuring hose conducted from a packed-off section onto the ground surface.
- **Fresh water head** = the calculated elevation of water level (m.a.s.l.) in a measuring hose assuming constant density (e.g. ρ_w = 1 000 kg/m^3) for water in the measuring hose.
- **In situ fresh water head** = the elevation of water level (m.a.s.l.) in a measuring hose filled with fresh water (the density of the water in the line depends largely on the temperature and salinity of the water).

The most commonly used head measurement method has been from multi-packer systems either manually using a contact meter or by means of pressure transducers linked to data acquisition systems. Regular measurements (one per week for manual measurements or at 1–6 hour intervals for automatic systems) reveal the influence of barometric responses, seasonal fluctuations and site activities (e.g. sampling, pumping or the influence of excavation). The main errors associated with such head measurements relate to either leakages in the measuring hoses or assumptions of the density of water in the measuring hose.

2.2 Single hole pump tests

Single hole pump tests can be applied in boreholes or packed-off borehole intervals. The main forms of test are:

- PI/PW: Pulse injection or pulse withdrawal.
- RI/RW: Rate controlled injection or withdrawal (e.g. constant rate test).
- HI/HW: Head controlled injection or withdrawal (e.g. constant head test).

In each test method the response to the imposed conditions (e.g. in RI tests the pressure change for the imposed flow-rate, see Figure 2-2) is monitored and interpreted in the light of one or more (usually simple) conceptual models. One special case of rate control uses sinusoidal flow rates (see for example Rasmussen et al. 2003).

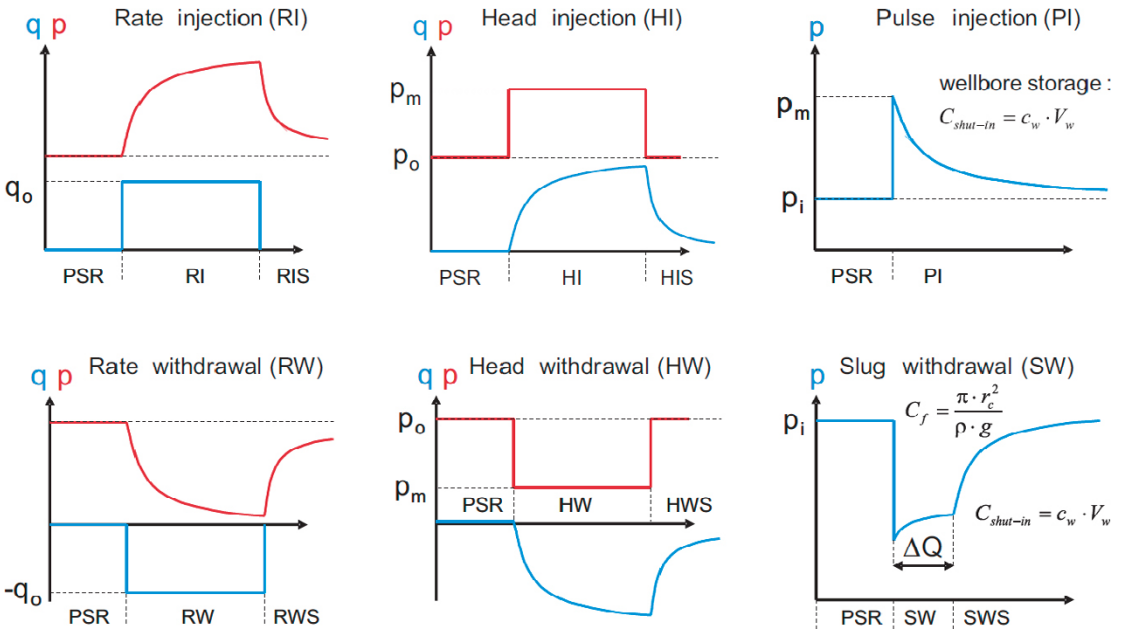

Figure 2-2. *Typical packer test procedures applied for hydraulic characterisation of rock formations (from Marschall and Lunati 2006). PSR = static pressure recovery period.*

The testing objectives together with practicalities of testing such as:

- Knowledge of the likely flow-rates.
- Ability to accurately measure flow.
- Expected test duration.
- Limits on injected or produced water volumes.

dictate the choice of pumping test. Well-test responses typically show an unsteady or transient flow period (influence of well-bore storage and WCF properties) followed by a late-time steady-state or quasi-steady state period. The duration of the test determines the distance over which the hydraulic properties are "averaged". In a homogeneous medium the radius of action (or investigation) can be estimated as $2.25\sqrt{Tt/S}$ where T/S is the hydraulic diffusivity (m^2/s) and t the test duration (s).

2.2.1 Analysis

Analysis of late-time data often assumes the existence of steady state conditions and either radial flow to the borehole (Thiem equation) or a simplified 2/3D flow model (e.g. Moye's equation assuming cylindrical flow to a radius of half the interval length). These models provide a description of the productivity or injectivity of the interval (flow-rate normalised by pressure change). The assumption of steady state means that this can be treated as a formation parameter and is representative of long-term flow (i.e. would be appropriate for any sufficiently long testing period).

Traditional analysis methods of the unsteady flow period match the observed response to testing to analytical (or semi-analytical) solutions assuming homogeneous WCF properties such as the Theis solution (Theis 1935) or the Cooper-Jacob approximation (Cooper and Jacob 1946). Diagnostic analysis for constant rate (or head) tests can be used to: identify flow dimension (Barker 1988) and estimate WCF parameters. More recent work has aimed to relate the transient response to lateral variation in hydraulic properties (Butler and Liu 1993, Oliver 1993, Enachescu et al. 2004, Copty et al. 2011).

Flow dimension analyses (see Barker 1988, Walker and Roberts 2003, Walker et al. 2006) provide a useful tool for considering deviations from radial flow e.g. flow within a linear channel or pipe-like fracture system (1D) or at the other extreme where flow spreads spherically (3D) or in a fractal flow system (Acuna and Yortsos 1995). Note however that the property controlling flow dimension is the rate of change of flow-area × permeability (or equivalently length × transmissivity) so that flow dimension is influenced by both changes in hydraulic properties and geometry of the flow conduits (this can result in flow dimensions less than 1 or greater than 3).

2.2.2 Assumptions and biases

The most important assumption regarding well-test analysis usually relates to the assumed geometry of the flow conduit, although other assumptions regarding the flow processes may result in significant bias, particularly in low permeability systems.

At high fluid velocities (Elsworth and Doe 1986) it is possible that fracture flow may become turbulent in the near-borehole region resulting in non-linear flow behaviour. Experimental work within fractures suggests significant Non-Darcy effects at Reynolds Numbers ~10 (Zimmerman et al. 2004).

Coupled mechanical effects may also be important as most analytic approaches assume that the rock is undeformed by the testing procedure. This assumption is reasonable where pressure drawdown or build-up is small compared to the minimum in situ stress and the critical pressure for shearing. Fransson et al. (2010) present data from hydraulic testing and grouting in tunnels at Nygård and the Äspö HRL, both in Sweden, to identify grout-induced fracture opening, to estimate fracture stiffness of such fractures, and to evaluate its impact on the grout performance. Further discussion of these and other coupled effects can be found in Rutqvist (2016).

For a discussion of other effects (e.g. thermally induced pressure, borehole pressure history and equipment compliance) which may become important when testing low permeability intervals see Pickens et al. (1987).

2.3 Cross-hole pump tests

Cross-hole pumping tests involve the monitoring of responses to pumping in multiple observation boreholes or borehole intervals. The objectives of such tests are:

- Estimation of large-scale or effective hydraulic properties (or more generally scaling behaviour).
- Identification of connectivity (e.g. of fracture zones).
- Confidence-building in site-descriptive models.

The design of cross-hole tests concerns the form and duration of the pumping signal and the layout of monitoring intervals (often multi-packer systems). Large-scale cross-hole tests have been a feature of major site-investigations (often prior to shaft-sinking) and the LPT-2 test at Äspö was the subject of Task 1 of the Task Force.

2.3.1 Analysis

Cross-hole pump test responses can be analysed in similar ways to single-hole tests:

- Assumed steady-state: maps of drawdown/build up pressures (sometimes normalised to source).
- Transient responses: Cooper-Jacob or type-curve/diagnostic analysis.

Black and Kipp (1977) showed that significant lags may occur in observation interval response due to the storage associated with the observation interval in unconfined conditions. The same effect can also be significant in very low permeability intervals.

Several authors have considered the observation response to constant rate testing in a heterogeneous 2D aquifer (or WCF) using the Cooper-Jacob method to derive observation zone transmissivity T_{obs} (m^2/s) and storativity S_{obs} (-). Meier et al. (1998) and Wu et al. (2005) show that:

- The derived transmissivity T_{obs} is an effective property of the feature[4],
- The derived storativity S_{obs} is an indicator of the connectivity between the source and the observation interval. Small values of storage indicate good connectivity while large values indicate poor connectivity.

Best estimate properties of the aquifer are given by:

- T_{WCF}: The geometric mean of the derived transmissivity.
- S_{WCF}: The arithmetic mean of the derived storativities.

Enachescu et al. (2004) and Copty et al. (2011) consider analysis approaches based on time-dependent estimates of transmissivity and storage for 2D heterogeneous aquifers and relate these to the spatial variability of the aquifer. The use of the derived diffusivity T_{obs}/S_{obs} as an indicator of connectivity is discussed in Knudby and Carrera (2006) and Trinchero et al. (2008).

2.4 Flowmeter tests

Flowmeter logging has been commonly used to identify permeable features within boreholes (Molz et al. 1989) although use of spinner (or impeller) flowmeters limited the application to relatively high flows (~100 l/min). Subsequent development of higher resolution tools including heat-pulse and electromagnetic flowmeters allowed application to lower flow-rates and lower permeability environments. Typical outputs are borehole flow profiles (for some minimum resolution) and correlations with geological structures. Paillet (1995) describes the use of flowmeter data to optimise subsequent packer testing. Paillet (1998, 2000) sets out a method to derive a steady-state flow model of transmissivity and head from multiple flow logs under different pumping conditions. Measurements of flow transients have also been used by Paillet (1998) at the Mirror Lake site in New Hampshire.

[4] Related results for anisotropic formations were derived by Streltsova (1987).

2.4.1 Cross-hole flowmeter testing

Williams and Paillet (2002) present results from cross-hole flowmeter pulse tests at the Watervliet, New York site to identify inter-borehole connections. Le Borgne et al. (2006) present data from flowmeter testing in six boreholes at the Plœmeur site in crystalline bedrock in Brittany using a method outlined by Paillet (1998):

- Measuring along-borehole flow at selected depths between inflow/outflow zones in each observation borehole, and at an additional point above all inflow points.
- At each depth measurements are repeated for:
  - Short period to establish a baseline ambient flow.
  - Period (10–20 minutes) with a given production well turned off.
  - Equal period of measurement after the production well is brought back on line.

Le Borgne et al. (2006) comment that the approach is an "efficient method to image the geometry of preferential permeable flow paths in heterogeneous aquifers where packer testing is not possible. On the Plœmeur site, it was possible to characterise inter-borehole connectivity with borehole separation distances ranging from 7 to 150 m." In a comparison of alternative characterisation methods Le Borgne et al. (2007) comment that "flowmeter tests are used to characterise which of the fracture zone in the observation well is connected to the pumping well, whereas single packer tests allow determining which of the fracture zone in the pumping well is connected to observation wells."

2.5 The Posiva Flowmeter Log (PFL)

The PFL is a development of previous flowmeter logging methods suited to the particular conditions of fractured crystalline rock that has been extensively used in the Posiva and SKB site investigation programmes. Unlike traditional borehole flowmeters, rather than measuring the total cumulative flow-rate along the borehole, the PFL DIFF tool measures the flow-rate in/out of short intervals providing significantly improved detection limits for incremental flow along the borehole (Rouhiainen 2001).

The PFL DIFF tool measures the local in/outflow from a short interval of borehole isolated by the two sets of rubber flow guides (Figure 2-3). The interval length between the guides can be altered. The PFL measurements include:

- Flow-rate by the thermal pulse method.
- Flow-rate by the thermal dilution method.
- Temperature of borehole water.
- Electric conductivity of borehole- and fracture-specific water.
- Single point resistance (SPR) of the borehole wall.
- Depth of the probe based on the cable counter.

Commonly used interval lengths include 0.5 and 2 m. Logging speed with the 0.5 m interval and 0.1 m depth steps is about 10 m/hour. The PFL DIFF tool can measure the in/outflow to the section in the range 6–300 000 ml/hr ($\sim 2 \times 10^{-9}$ to 8×10^{-5} m^3/s) using either the thermal pulse or thermal dilution method. The lowest flow-rate (6 ml/h) can only be measured using the thermal pulse method and only then when conditions are favourable. Measurement properties are summarised in Table 2-1.

There are two main PFL logging methods:

- Normal (or sequential) mode, in which both the thermal pulse and thermal dilution flow measurement techniques are used resulting in a wide flow measurement range.
- Detailed (or overlapping) mode, in which only the thermal dilution method is used and depth increments between measurements are usually small resulting in a more detailed flow characterisation along the hole (Ludvigson et al. 2002).

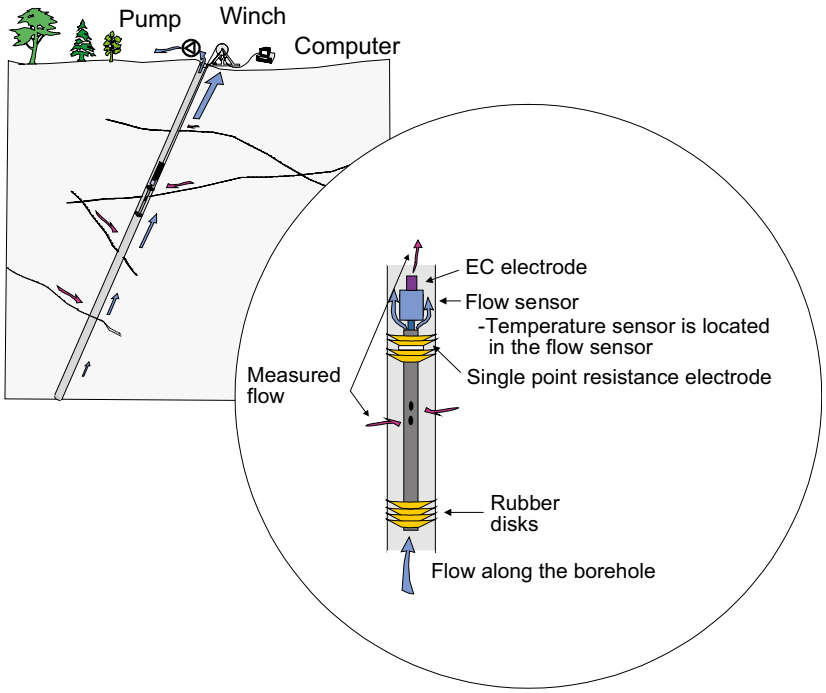

Figure 2-3. *Schematic of single-hole PFL setup and detail of PFL DIFF tool.*

Table 2-1. PFL DIFF measurement range and accuracy.

Measurement	Location	Range	Accuracy
Thermal dilution		2–5 000 ml/min	
Thermal pulse		0.1–10 ml/min	
Temperature	Central thermistor	0–50 °C	±0.01 °C
Temperature difference	Between outer thermistors	−2–+2 °C	0.0001 °C
Water level in borehole		0–0.1 MPa	±1 % fullscale
Absolute pressure		0–20 MPa	±0.01 % fullscale
Air pressure		800–1 060 hPa	±5 hPa
Electrical conductivity (EC)	Above flow sensor	0.02–11 S/m	±5 %
Singlepoint resistance	between upper rubber disks	5–500 000 Ω	

2.5.1 Analysis

The main output from the PFL log is the estimated in/outflow from each depth interval for the given flow conditions determined by borehole pumping conditions. This can be converted into estimates of feature transmissivity and undisturbed head when measurements are made at least in two different conditions. The normal method assumes that flow is steady and radial and can be described by the Thiem equation:

$$Q = \frac{2\pi T \Delta h}{\ln\left(r_{bc} / r_0\right)}$$

where Q is the volumetric flow, T is the fracture transmissivity, r_0 is the borehole radius, Δh is the head drop between the borehole and a fixed head boundary condition at distance r_{bc}. For PFL analyses r_{bc} is commonly assumed to be 500 r_0 (Pekkanen and Pöllänen 2008). For a 76 mm diameter borehole this is equivalent to a distance to the constant head boundary of 19 m. Note that over half of the total drawdown is estimated to occur within the first metre. The equation can be solved for multiple flow conditions (different borehole drawdowns) to estimate both transmissivity and undisturbed head.

2.5.2 Assumptions and biases

The major assumptions relate to the estimation of transmissivity from the measured flow. The assumption of radial steady flow in a homogeneous feature with constant head at known distance (500 r_0) may clearly not be appropriate in fractured rock. However, it represents the simplest case and can be taken as an indicative reference situation. The effect of near-wellbore heterogeneity (skin) is considered in Appendix C.

Follin et al. (2014), when developing site -descriptive models for Forsmark and Laxemar chose to match the flow/drawdown statistics rather than the derived transmissivity. By doing this they were able to address the influence of the fracture network geometry on the flow in/out of the borehole assuming geometric descriptions of the flowing fractures (uniform transmissive rectangles or circles with length and orientation following probability distributions fitted to the fraction of flowing fractures and the orientations of these fractures).

A potential uncertainty relates to flow past the rubber discs in very fractured or rough borehole intervals. This may cause the recorded flow to be significantly underestimated or missed completely. Another potential uncertainty may arise from changing salinity and density conditions along the hole during pumping. This may cause changes in the hydraulic head conditions with time, which will affect determinations of transmissivity and undisturbed head.

Muddy water and gas bubbles may also increase the noise in the measurements and consequently increase the detection limit. Measures to minimise these problems include post-drilling clean up of the borehole and the avoidance of high drawdowns that might cause degassing.

2.6 Flow localisation

The aim of flow localisation is to identify the water conducting features in the borehole with high spatial resolution for the purposes of:

- Correlation with geological (core) and geophysical data (e.g. borehole camera, televiewer, resistivity imager).
- Optimisation of future hydraulic testing.
- Identifying suitable groundwater monitoring sampling locations.
- Supporting and adding information to conventional double packer hydraulic measurements with longer intervals.

Potential methods are:

- High resolution flowmeter, e.g. PFL as used at Olkiluoto.
- Electrical conductivity and temperature “flow logging” (Tsang et al. 1990, Doughty et al. 2004).
- ”Telescopic[5]” packer testing.

Additional data can be acquired from high resolution mud logging (Dyke et al. 1995) which can identify the most significant in/outflows (depending on the drilling conditions i.e. over or underbalanced). The sensitivity is, however, much less than that of other measurement methods.

The choice of localisation method is dependent on a wide range of different conditions, in particular:

- Availability of drilling rig and equipment.
- Available budget and time.
- Nature of the water conducting features.
- Downhole conditions (state of the borehole wall, borehole deviation, temperature and pore fluid).

[5] An efficient method of packer testing that can deliver moderately high spatial resolution. The “Telescopic” approach is discussed by Follin et al. (2007) where the choice of interval location of short interval tests is based on the results from longer interval tests.

2.7 Summary

Task 7 largely focuses on modelling using data derived from PFL campaigns, both single-hole and cross-hole. PFL tools, operating methods, interpretation and modelling approaches have been specifically developed to address the challenges of site characterisation for repositories in fractured crystalline rock. These developments have largely occurred within Posiva and SKB's site characterisation and performance assessment studies (Follin et al. 2014) and so Task 7 provides an opportunity to test out alternative approaches to utilising PFL data.

- Subtask 7A considers the KR24 large-scale pump test utilising a large number of monitoring boreholes. Many of the monitoring boreholes were open and used for PFL logging of the cross-hole flow response.
- In Subtask 7B, the modelling groups were able to compare cross-hole PFL and pressure monitoring data in terms of their ability to constrain aspects of the flowing fracture system.
- In Subtask 7C the extension of the PFL tool and methodology to lower transmissivity features is examined using data from boreholes around the Olkiluoto shafts with significantly higher drawdowns than were used in the borehole-based site investigations.

3 Task 7A Reduction of performance assessment uncertainty through site-scale modelling of long-term pumping in KR24

The modelling work performed in Task 7A is documented in a series of SKB reports:

- CRIEPI: Tanaka and Hasegawa[6].
- JAEA: Sawada et al. (2015).
- NWMO/Laval: Therrien and Blessent (2017).
- Posiva/VTT: Keto and Koskinen (2009).
- SKB/CFE: Svensson (2015).
- SKB/KTH: Frampton et al. (2015).

A short summary of the modelling work by KAERI is included as an appendix in a report written by Lanyon[7] which provides an evaluation of Task 7A. This chapter is a shortened version of that report and is included here so that a picture of the whole of Task 7 is given in this report.

3.1 Task 7A Objectives

Initially Task 7 had been planned to consider only the KR24 pump test and the aims of Task 7A were to:

- Determine proper means of incorporating open boreholes in the hydrogeologic models and estimate their significance to the observed and calculated response fields.
- Implement the calculation of results corresponding to flow logging measurements in numerical models.
- Condition the models with borehole-specific data.
- Implement the pumping in the numerical models with suitably determined boundary conditions.
- Assess the need for free surface/unsaturated flow modelling.

Successful completion of an initial series of test cases demonstrated that the facilities needed for simulation of the pump test were already available in most of the codes, so the scope of Task 7A was extended. Although the test cases were useful in building confidence in the capabilities of the numerical codes, problems arose with comparison of the results due to the modelling groups' use of different distant boundary conditions in their simulations.

[6] **Tanaka Y, Hasegawa T, 2009.** Äspö Hard Rock Laboratory. Äspö Task Force on modelling of groundwater flow and transport solutes – Task 7A. Application of FEGM-B to Task 7A: Reduction of performance assessment uncertainty through site scale modelling of long-term pumping in KR24 at Olkiluoto, Finland. SKB ITD-09-03, Svensk Kärnbränslehantering AB. (Internal report.)

[7] **Lanyon G W, 2009.** Äspö Hard Rock Laboratory. Äspö Task Force on modelling of groundwater flow and transport of solutes – Task 7A: Evaluation report on Task 7A reduction of performance assessment uncertainty through site scale modelling of long-term pumping in KR 24 at Olkiluoto, Finland. SKB ITD-09-10, Svensk Kärnbränslehantering AB. (Internal report.)

3.2 Task 7A definition and structure

The Task 7A definition is included in Vidstrand et al. (2015). The scope of Task 7A was extended to include the following subtasks:

- 7A1: Hydrostructural model implementation.
- 7A2: Pathway simulation within fracture zones.
- 7A3: Ideas for calculation of PA-relevant parameters from open borehole information.
- 7A4: Quantification of compartmentalisation from open borehole information.
- 7A5: Quantification of transport resistance (Hodgkinson 2007) distributions along pathways.

Subtasks 7A1, A2 were to be reported jointly and 7A3-A5 separately.

The goals of Task 7A were also revised and became

1. to understand the major features of the groundwater system,
2. to understand the consequences of the tests and measurement systems used, e.g. the open boreholes,
3. to understand how to model open boreholes within site characterisation studies and for the provision of parameters for PA,
4. to understand how PFL measurements could reduce uncertainty in models as compared to models calibrated with only head measurements,
5. to increase understanding of compartmentalisation and connectivity at the Olkiluoto site and more generally in fractured crystalline rock,
6. to evaluate how uncertainty in PA can be reduced based on the analysis of the Olkiluoto dataset.

These extended goals placed much more emphasis on a) understanding of the groundwater flow system and the influence of open boreholes, and b) integration with performance assessment. The interest in compartmentalisation arose partly from examination of the KR24 drawdown data which shows a strong late-time linear trend, together with similar observations of flow at other sites in crystalline rock.

The Task Description set out a structured series of simulations to be performed by the modelling groups. The simulation list (Table 3-1) was focused on allowing a series of comparisons to be made to identify

1. the influence of the open boreholes on the measured hydraulic heads and flows,
2. the influence of the open monitoring boreholes on the KR24 pump test,
3. the impact of model calibration (forward/inverse simulations),
4. the impact of steady-state versus transient simulation.

Most modelling groups followed the simulation structure but it required a relatively large number of results to be presented and collated and some groups performed only a subset of the simulations.

Table 3-1. Task 7A simulation list from Vidstrand et al. (2015).

Name	Task	Description	Forward/Inverse	Boreholes
SS01	7A1	Steady state flow conditions without pumping	Forward	No boreholes
SS02a	7A1	Steady state flow conditions with open boreholes	Forward	Boreholes are open and free to cross-flow.
SS02b	7A1	Steady state flow conditions with open boreholes	Calibrated/Inverse	Boreholes are open and free to cross-flow.
SS02c	7A1	Steady state flow conditions without pumping	Based on SS02b final set-up	No boreholes
SS03	7A1	Steady states flow with extraction from KR24	Forward	KR24 only
SS04a	7A1	Steady states flow with extraction from KR24	Forward	KR24 + monitoring boreholes
SS04b	7A1	Steady states flow with extraction from KR24	Calibrated/ Inverse	KR24 + monitoring boreholes
TR01	7A1	Transient simulation of KR24 test	Forward	KR24 only
TR02a	7A1	Transient simulation of KR24 test	Forward	KR24 + monitoring boreholes
TR02b	7A1	Transient simulation of KR24 test	Calibrated/Inverse	KR24 + monitoring boreholes
PA01	7A2	Transport pathway simulation from KR24 to discharge under PA-relevant boundary conditions[8].		No boreholes (particles start from a position along KR24 trajectory)

3.3 Task 7A dataset

The dataset provided to the modellers for Task 7A, although only a small part of the total dataset for the Olkiluoto site, was extensive and required significant effort to implement from the modellers. In all there were some 19 data deliveries including task definitions and clarifications. The major elements of the dataset were:

- Geometry of the major deterministic structures.
- Topography and surface water table.
- Borehole locations and trajectories.
- PFL data in “undisturbed” conditions (measured flows, interpreted transmissivity based on radial flow assumption and head).
- Short interval single hole pump test data.
- Description of the pump test and measured responses (flow and head/ drawdowns).

3.3.1 Task 7A common hydro-structural model

The very large amount of site characterisation data available from Olkiluoto meant that it was not possible for each modelling group to analyse the data and develop their own site-scale hydro-structural model and so the Task Force provided the hydro-structural model as described within the Task Description (Vidstrand et al. 2015) and supporting documents. The hydro-structural model adopted within the task specification was a highly simplified version of the then current version of the Olkiluoto Bedrock Model (Vaittinen et al. 2003). The model assumed:

- Deterministic major fracture zones.
- Homogeneous hydraulic properties of the zones using the geometric mean transmissivity.
- A very simple representation of the near-surface flow system 0–80 mbgl.
- No significant effect of the background rock between the deterministic fracture zones.

The modelling groups had the option to vary/test these simplifications but in general the work needed for the simulations and data analysis meant that most modellers used the structural model as specified.

[8] I.e. after borehole sealing without any significant influence of the boreholes.

3.4 Modelling approaches

3.4.1 CRIEPI

CRIEPI's objectives in Task 7 were:

- To demonstrate the usefulness of CRIEPI's numerical code FEGM-B to simulate site-scale groundwater flow in crystalline rock.
- To understand the usefulness of a large-scale pumping test to build and calibrate a site-scale geohydrological model.
- To understand the influence of major fracture zones on site-scale groundwater flow in crystalline rock.
- To understand the influence of open monitoring boreholes on groundwater flow.
- To investigate the usefulness of Posiva Flow Log to validate geohydrological models.
- To investigate the relation between travel time of groundwater to discharge area and depth of release point.

Model structure

The modelling group from CRIEPI developed a custom-built mesh made from triangular and tetrahedral elements representing the fracture zones and 80 m-thick surface layer (Figure 3-1). Boreholes were represented by 1D elements. The mesh was highly refined around the borehole intersections (especially KR24).

The boundary conditions for the island surface were set as specified head (for SS01 and SS02a) or as an infiltration boundary (for all other simulations) based on recharge of 5 or 80 mm/yr. The seabed and the sides of the model were treated as constant hydrostatic head boundaries, while the base of the model was treated as a no-flow (impermeable) boundary. No account was taken of the salinity variation at the site within the model although the salinity information was used to correct the measured head data (under natural conditions) and the calculated heads were compared with the corrected measured head data.

Model conditioning and calibration

CRIEPI chose to condition, rather than calibrate the fracture zone transmissivity using a "patch model" where, while the main part of each zone was assigned the geometric mean transmissivity as specified in the common structural model, the region around each borehole intersection used the measured local transmissivity from the PFL measurement for the borehole. The approach is illustrated in Figure 3-2. A patch radius of 100 m was used within the models; the basis for the selection of this radius was not documented.

In addition to the fracture zone conditioning described above, the recharge was increased from 5 mm/yr to 80 mm/yr as part of the model calibration.

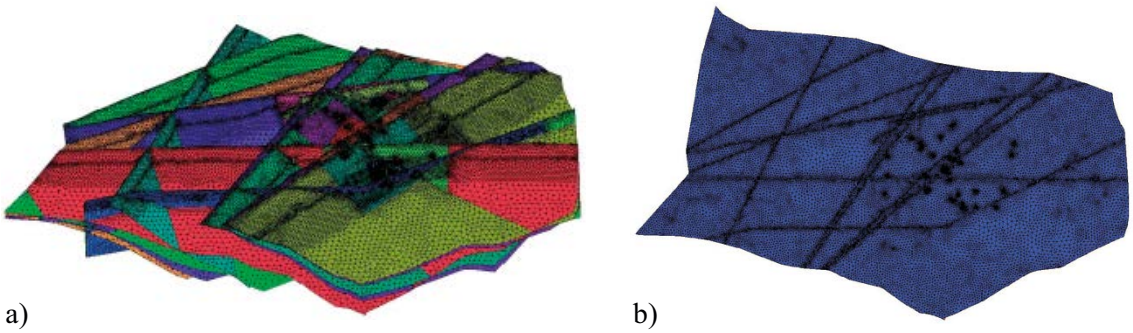

a) b)

Figure 3-1. *CRIEPI Task 7A model geometry: (a) The network of major zones and (b) the surface layer.*

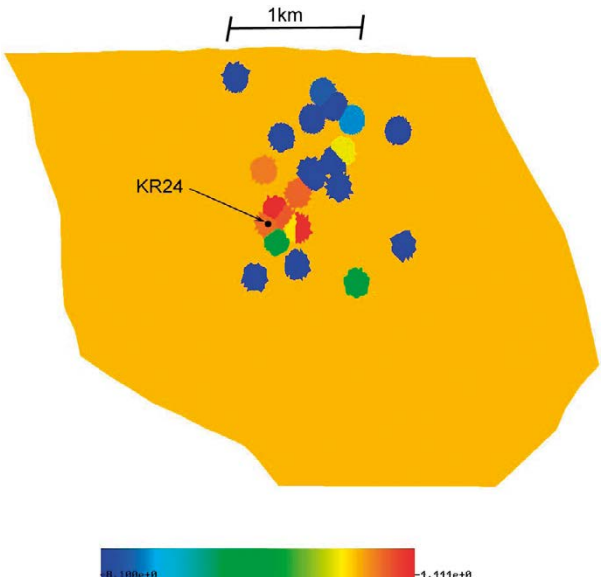

Figure 3-2. *Conditioned model of zone HZ20a showing the borehole intersection "patches" where the measured local transmissivity has been assigned (from Tanaka and Hasegawa[1]).*

3.4.2 JAEA

Model structure

JAEA also used the "large" deterministic fracture zone meshes together with an equivalent porous medium representation of the near-surface layer as the basis for their model (Figure 3-3). The model used a tetrahedral mesh with 20 m × 20 m × ~20 m cells to represent the surface layer. The zone transmissivity was given by the geometric mean transmissivity defined in the common structural model and the hydraulic conductivity of the near-surface layer was taken to be isotropic with a uniform value of 2×10^{-7} m/s (as given in Vidstrand et al. 2015). The transport apertures of zones were as specified in the Task Definition using Doe's Law (Dershowitz et al. 2003).

The boundary conditions for the island were specified head (for SS01, SS02a) or an infiltration boundary (for all other simulations) with a recharge of ~5 mm/yr. The seabed was treated as a constant hydrostatic head boundary while the sides and base of the model were treated as no-flow (impermeable) boundaries (Figure 3-3). No account was taken of salinity variation at the site within the model.

Model conditioning and calibration

JAEA calibrated their model to the measured "undisturbed heads" by implementing an infiltration boundary (phreatic surface) and adjusting the recharge to the island to approximately 5 mm/yr. The transmissivity of selected fracture zones (HZ19A, HZ19C, HZ20A, HZ20B_ALT, HZ21, HZ21B) was adjusted using a set of 6 sensitivity cases. The sensitivity cases were based on increasing or decreasing the transmissivity of key fracture zones by approximately 1 standard deviation ($\log_{10}$ transmissivity) of the transmissivity measurements in each zone.

[1] **Tanaka Y, Hasegawa T, 2009.** Äspö Hard Rock Laboratory. Äspö Task Force on modelling of groundwater flow and transport solutes – Task 7A. Application of FEGM-B to Task 7A: Reduction of performance assessment uncertainty through site scale modelling of long-term pumping in KR24 at Olkiluoto, Finland. SKB ITD-09-03, Svensk Kärnbränslehantering AB. (Internal report.)

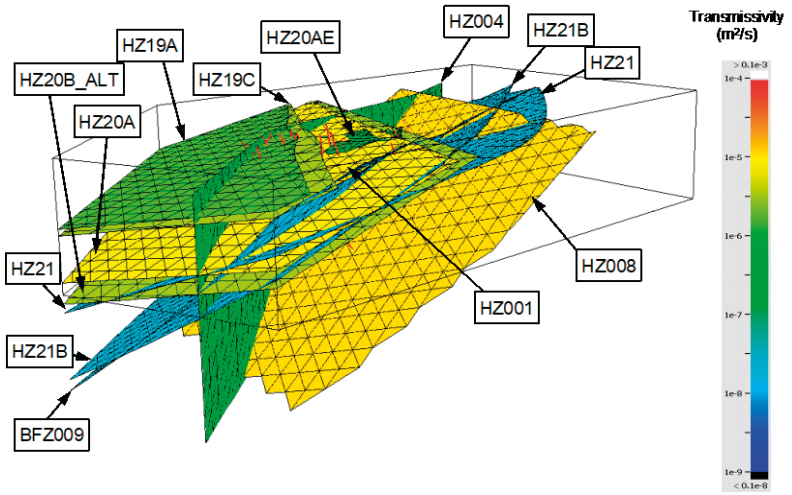

a)

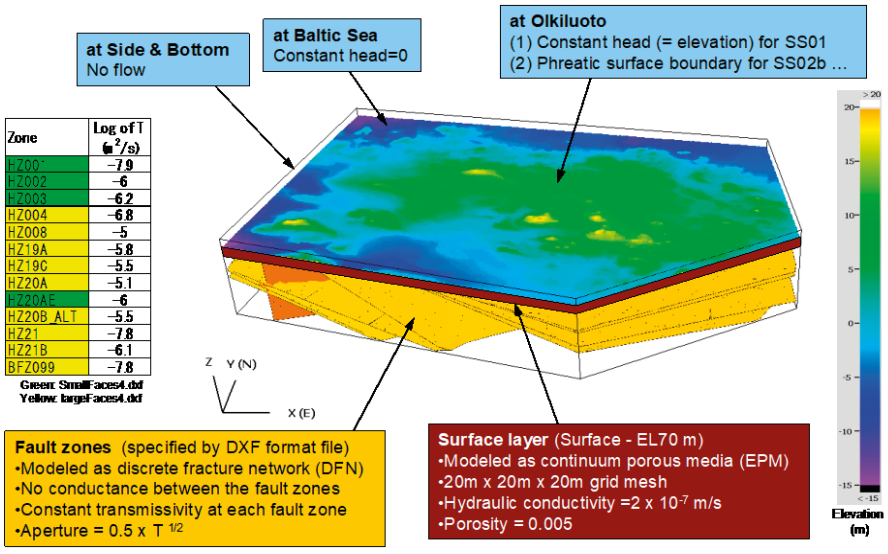

b)

Figure 3-3. *JAEA model showing a) zones b) surface layer and boundary conditions.*

3.4.3 KAERI

The modelling group from KAERI joined the Task Force near the end of Task 7A when other modelling groups had for the most part already completed the modelling simulations. KAERI chose to perform simulations from Task 7A as a preparatory step for participating fully within Task 7B. KAERI's modelling aims were to

- conceptualize the groundwater flow system of the Olkiluoto site,
- understand the effects of variables used for calibration on PA condition simulation,
- understand the influences of open boreholes on the flow system.

Model structure

KAERI modelled the site as a 3D continuum model representing the deterministic fracture zones using Oda's method (Oda 1985) to convert feature transmissivity to element hydraulic conductivity. For each cell, the flow under uniform gradient due to the individual structures that cross the cell is computed and summed to derive an anisotropic conductivity tensor due to the structures, which is then added to the hydraulic conductivity of the rock matrix (treated as an isotropic hydraulic conductivity of 10^{-11} m/s). The rock in the top 30 m (near-surface layer) was modelled with a uniform calibrated hydraulic conductivity of 7×10^{-7} m/s. The deeper background rock was modelled with a lower hydraulic conductivity of 10^{-11} m/s. The specified fracture zones and model hydraulic conductivity distribution are shown in Figure 3-4.

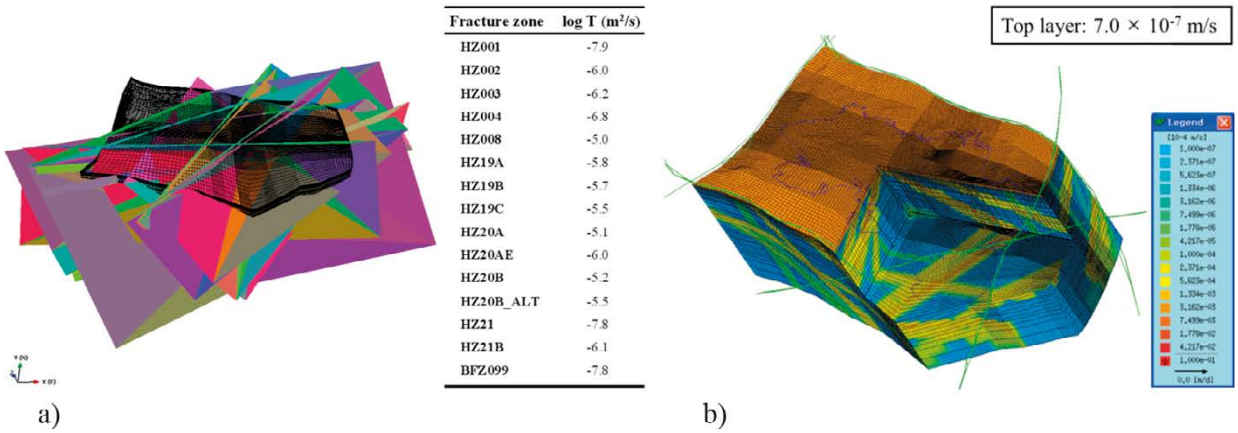

Figure 3-4. *KAERI Task 7A model geometry: (a) The network of major zones and (b) the hydraulic conductivity distribution of the groundwater flow model.*

The upper model surface was controlled by the topography of the island. The lateral boundaries of the model domain were set by the large-scale lineaments surrounding the Olkiluoto island. The recharge was specified on the island creating the initial water table within the near-surface layer. The upper model surface corresponding to the sea and the lateral boundaries were set to a constant 0 m.a.s.l.

Model conditioning and calibration

The model was calibrated to the observed hydraulic heads during undisturbed and pumped conditions.

3.4.4 NWMO/Laval

Model structure

The NWMO/Laval model was based on a 3D mesh with embedded lower dimension elements (fracture zones and boreholes). The fracture zones were represented by two-dimensional rectangular or triangular elements and one-dimensional elements were used to represent boreholes. A total of 9 open boreholes and 9 packed-off intervals were represented in the model with 1D line elements. The mesh was refined around the location of KR24. The background rock throughout the model domain was discretised with 3D hexahedral elements. The upper section of the rock mass, above an elevation of −70 m.a.s.l. was assigned a hydraulic conductivity of 10^{-7} m/s and below −70 m.a.s.l. the rock was assumed to have a very low hydraulic conductivity of 10^{-12} m/s. The mesh and fracture zone representations are shown in Figure 3-5a,b.

The boundary conditions were constant heads for the nodes located at the top of the mesh and on the lateral boundaries. The imposed heads at the top of the mesh were interpolated from the ground water table elevation, and the heads on the lateral boundaries were set to sea level (0 m.a.s.l.). The base of the model was treated as a no-flow boundary.

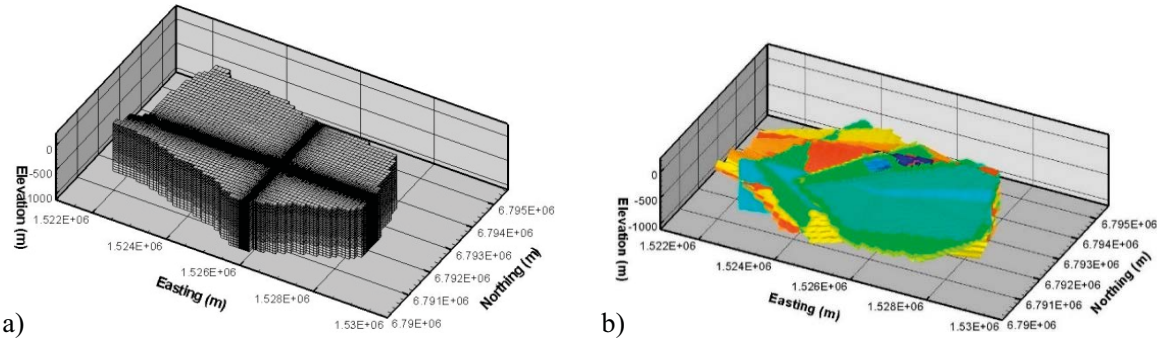

Figure 3-5. *NWMO/Laval Task 7A model geometry: (a) complete mesh and (b) the representation of the 13 fracture zones (from Therrien and Blessent 2017).*

Model conditioning and calibration

Both manual and automatic inverse modelling was attempted. During the manual inverse modelling, the transmissivities of entire zones were adjusted. Transmissivity values for each zone were taken in the interval between the mean transmissivity ± one standard deviation of the PFL transmissivity from different boreholes for that zone. No attempt was made to locally modify the zone transmissivity.

NWMO/Laval also used an automated approach to model calibration using PEST (Doherty 2004). The calibration parameters were the logs of the hydraulic apertures (equivalent to transmissivity) for each fracture zone. The parameter ranges were taken from the log mean transmissivity plus or minus two standard deviations ($\log_{10} T$). Neither manual calibration nor automatic calibration was successful. The automatic calibration typically failed, indicating lack of sensitivity of the objective function (heads/drawdowns) to the inverse model parameters (zone transmissivity). This failure may, at least in part, have been due to a lack of experience with the large number of different PEST control parameters (Therrien and Blessent 2017).

3.4.5 Posiva/VTT

Model structure

Initially VTT used both the "large" and "small" fracture zone representations as two model variants (see Figure 3-6). The VTT models were meshed using a tetrahedral mesh for background rock with a 2D triangular mesh based on the surfaces of the 3D elements for the zones using the OCTREE code. Boreholes were modelled as 1D elements.

Fracture zone transmissivities were initially set to the geometric mean value but were adjusted during calibration. The background rock above −70 m.a.s.l. was assigned a hydraulic conductivity of 2×10^{-7} m/s while below this the hydraulic conductivity was set to 10^{-11} m/s.

The upper model surface boundary conditions were based on the topography and set to the long-term average of the water table. All other model surfaces were treated as no-flow boundaries.

Model conditioning and calibration

VTT performed a manual calibration/conditioning of the "small zone" model variant guided by an interpretation of the results of the KR24 pump test. The calibration involved significant changes to the structural model including:

- Addition of an extra highly transmissive local fracture zone.
- Modification of zone transmissivity and connectivity to the surface boundary.
- Removal of parts of some zones.
- Inclusion of borehole "skins".

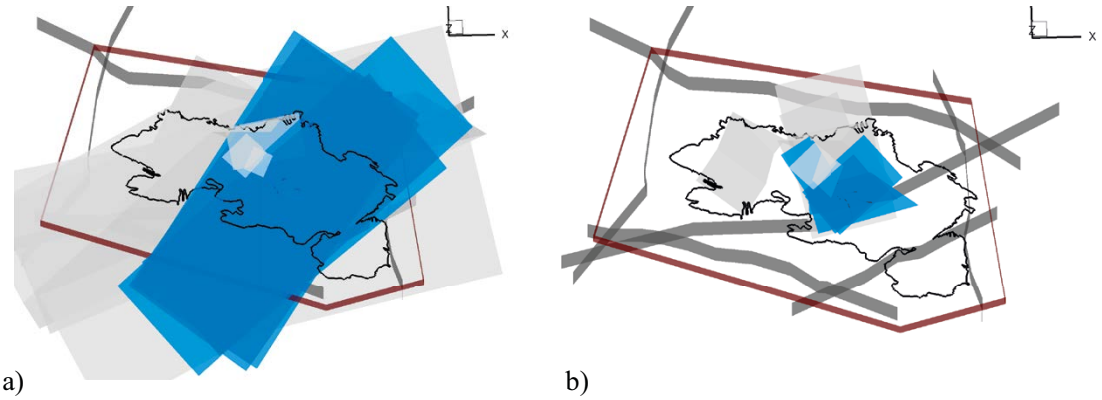

a) b)

Figure 3-6. *VTT model: a) large zone representation, b) small zone representation (from Keto and Koskinen 2009).*

In the latter part of Task 7A, VTT implemented an Ensemble Kalman Filtering approach (Evensen 1994) to the analysis of the KR24 pump test. The model parameters are the major zone transmissivities and the transmissivity of the upper part of the zones connecting to the surface. The parameters considered were the log transmissivity of zones HZ004, HZ19A, HZ19C, HZ20A, HZ20AE, HZ20B_ALT and their surface connections. The calibration data were 17 drawdown measurements and 16 PFL measurements (change in flow due to pumping).

3.4.6 SKB/CFE

Model structure

CFE implemented the structural model using the large zone representations. The background rock was included within the upper 80 m of the model while below this, only elements including fractures zones or around the boreholes were present in the model (see Figure 3-7). The model was highly refined around the boreholes. The model was implemented with the DarcyTools (Svensson 2010) numerical code for simulation of flow and transport in porous and/or fractured media. Fractured media can be treated via a "Smeared fracture" approach where the grid cell hydraulic properties are calculated from an underlying stochastic Discrete Fracture Network.

CFE introduced a high permeability near-surface layer, the permeability of which declined exponentially with depth to allow simulation of runoff, and they applied an upper boundary condition equivalent to the estimated potential recharge (100–150 mm/yr, Vidstrand et al. 2015). The boundary conditions applied were net recharge of 100 mm/yr, constant head on the model sides and seabed and no flow on the model base.

Model conditioning and calibration

The parameters of the near-surface exponential decay of hydraulic conductivity and the average recharge were adjusted to match the observed heads in undisturbed conditions (SS02b). In addition the effective conductivity of the local DFN in the top 80 m was adjusted and local fracture networks were added around borehole intersections, which in effect provided a "skin-term" that could also be adjusted to better match observation. The three different calibration terms act almost "independently" in that:

- Hydraulic conductivity of the very near-surface layer matches infiltration and undisturbed heads.
- Near-surface DFN matches the KR24 upper zone head/flow during pumping.
- Local "skin" around KR24 aims to match the lower zone drawdown.

Only the heads and/or drawdowns were used in the calibration process. PFL data were subsequently compared with the model results.

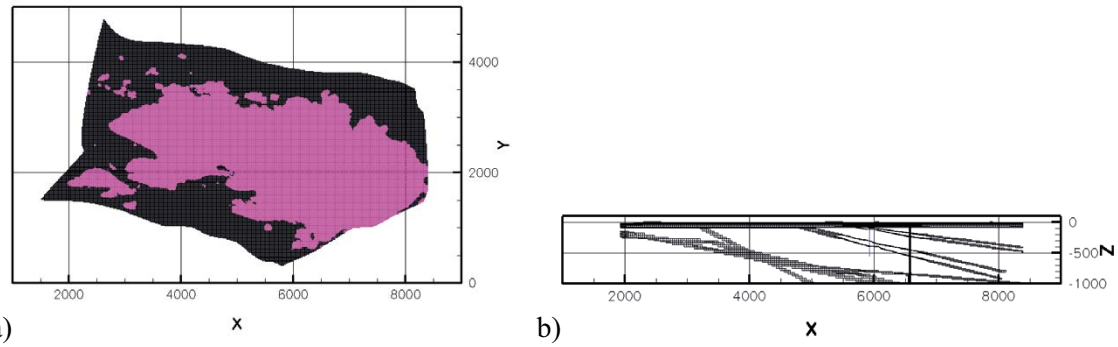

Figure 3-7. *CFE model mesh: a) top surface, b) side view showing surface layer and zones (from Svensson 2015).*

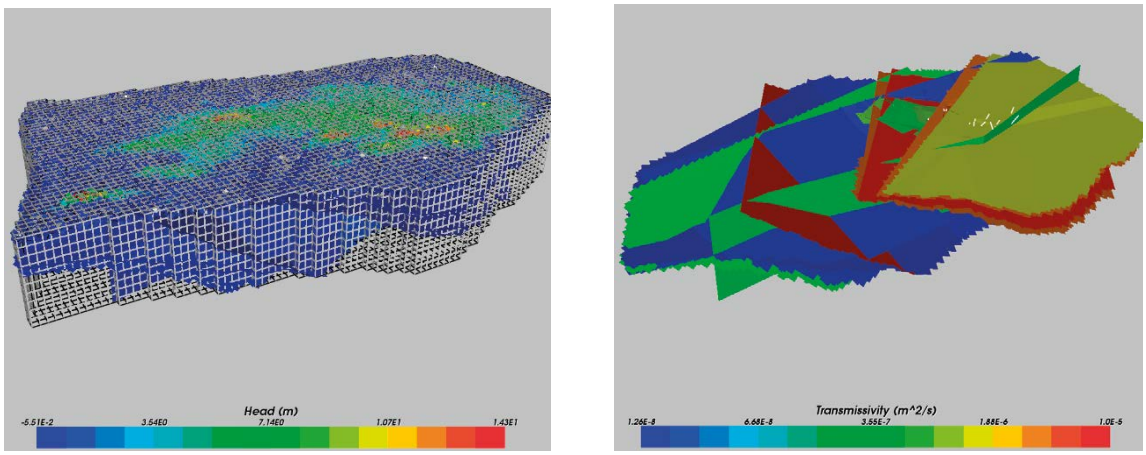

a) b)

Figure 3-8. *KTH fracture network model: a) model region and surface DFN and zones coloured by undisturbed head, b) fracture zone coloured by transmissivity (from Frampton et al. 2015).*

3.4.7 SKB/KTH

Model structure

KTH implemented the large zone representation and used the geometric mean transmissivity for each zone. The top 80 m of the model included a DFN with uniform size and orientations and constant transmissivity of $10^{-5.9}$ m^2/s such that the effective hydraulic conductivity was 10^{-7} m/s. The model (coloured by undisturbed hydraulic head) is shown in Figure 3-8.

The boundary condition of the upper surface was based on the elevation (or sea level as shown in Figure 3-8a), and constant head (= 0 m.a.s.l.) was assumed on the model sides. The elevation values were interpolated onto the 78 m × 78 m grid used to define the model volume. The model base was assumed to act as a no-flow boundary.

Model conditioning and calibration

A trial and error calibration approach was used (an "adjoint method" inverse approach was being developed within CONNECTFLOW during the task – Cliffe et al. 2011). The calibration aim was not to perform a robust calibration procedure, but rather to identify the valid parameter range for transmissivity (specified as hydraulic aperture), assuming homogenous fracture zones. The first calibration simulations considered varying only the transmissivity of HZ19C which was felt to be the dominant feature controlling pump test response. Subsequently the transmissivities of all zones were changed by a constant factor of 1/1 000, 1/8, 8 or 1 000 (corresponding to factors of 2 and 10 in hydraulic aperture).

3.5 Modelling results

The Task Description set out a series of simulations to be performed (Table 3-1). The details of all the simulations performed can be found in the modelling group reports and an evaluation of the complete set of simulations can be found in Lanyon (2009). This section concentrates on the simulations related to the KR24 pump test and the influence of the different calibration or conditioning methods. The motivation to concentrate on this subset of the simulations is that the KR24 pump test simulations show the strongest influence of the modelling choices made by the groups and relate to the overall theme of DFN calibration and conditioning covered by this report. The simulations regarding the influence of open boreholes on the groundwater flow system and site characterisation are discussed more fully in Lanyon (2009) and Ko et al. (2012).

3.5.1 CRIEPI

Task 7A1, 7A2

CRIEPI used the heterogeneous "patch" model for simulation SS04b and did not make any further model modifications to match the pump test data. The improvement in the match to drawdown and change in flow from SS04a to SS04b is clearly shown in Figure 3-9 and Figure 3-10. The general shape of the distance-drawdown curve appears to be well-captured by the heterogeneous patch SS04b model; also the direction of flow change and magnitudes are better matched by the model. The improvements probably derive from the increased transmissivity zone local to KR24 (see Figure 3-2) resulting in an overall reduction in drawdown and in changes in inflow from the zones to the boreholes (and hence change in flow along the boreholes).

Transient simulations of the KR24 pumping test were also performed for cases with and without monitoring boreholes. The fracture zone and surface layer diffusivity were both set to 0.5 m^2/s. The effect of the presence of monitoring boreholes is illustrated in Figure 3-11. For the case with monitoring boreholes, the drawdowns at the end of simulation period (1 708.8 hrs) were similar to those for the steady state simulations for all boreholes apart from KR14.

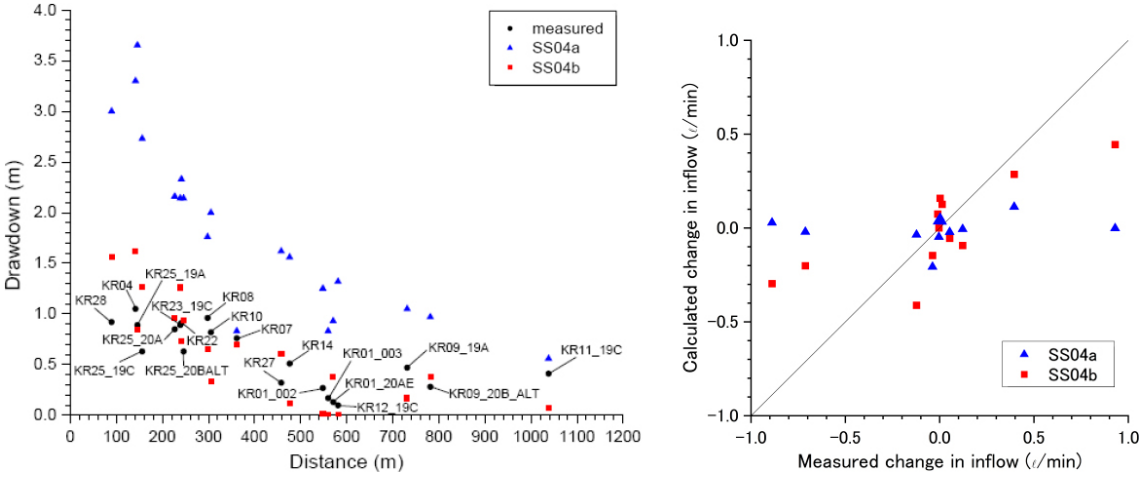

Figure 3-9. *Simulated and measured a) drawdowns and b) borehole inflow for homogeneous transmissivity and patch model.*

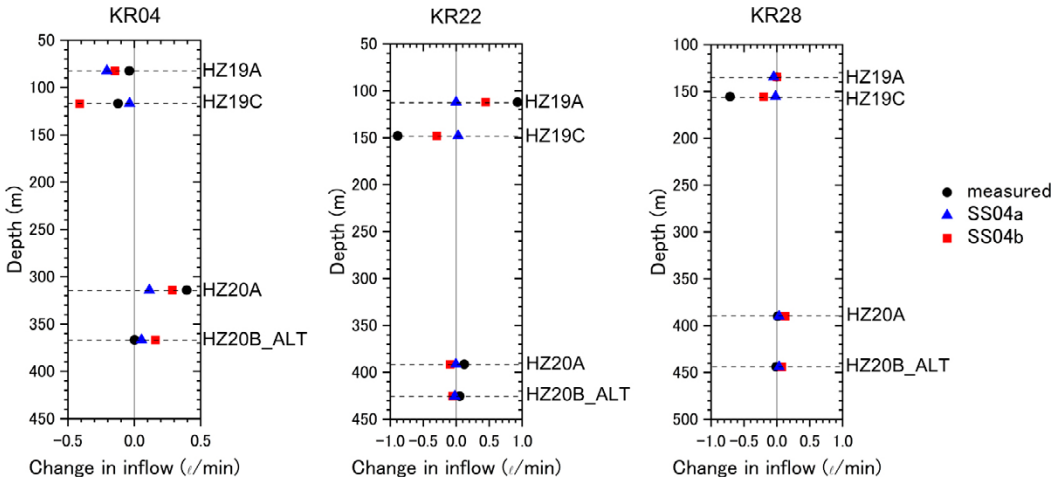

Figure 3-10. *Simulated and measured borehole inflows for selected boreholes.*

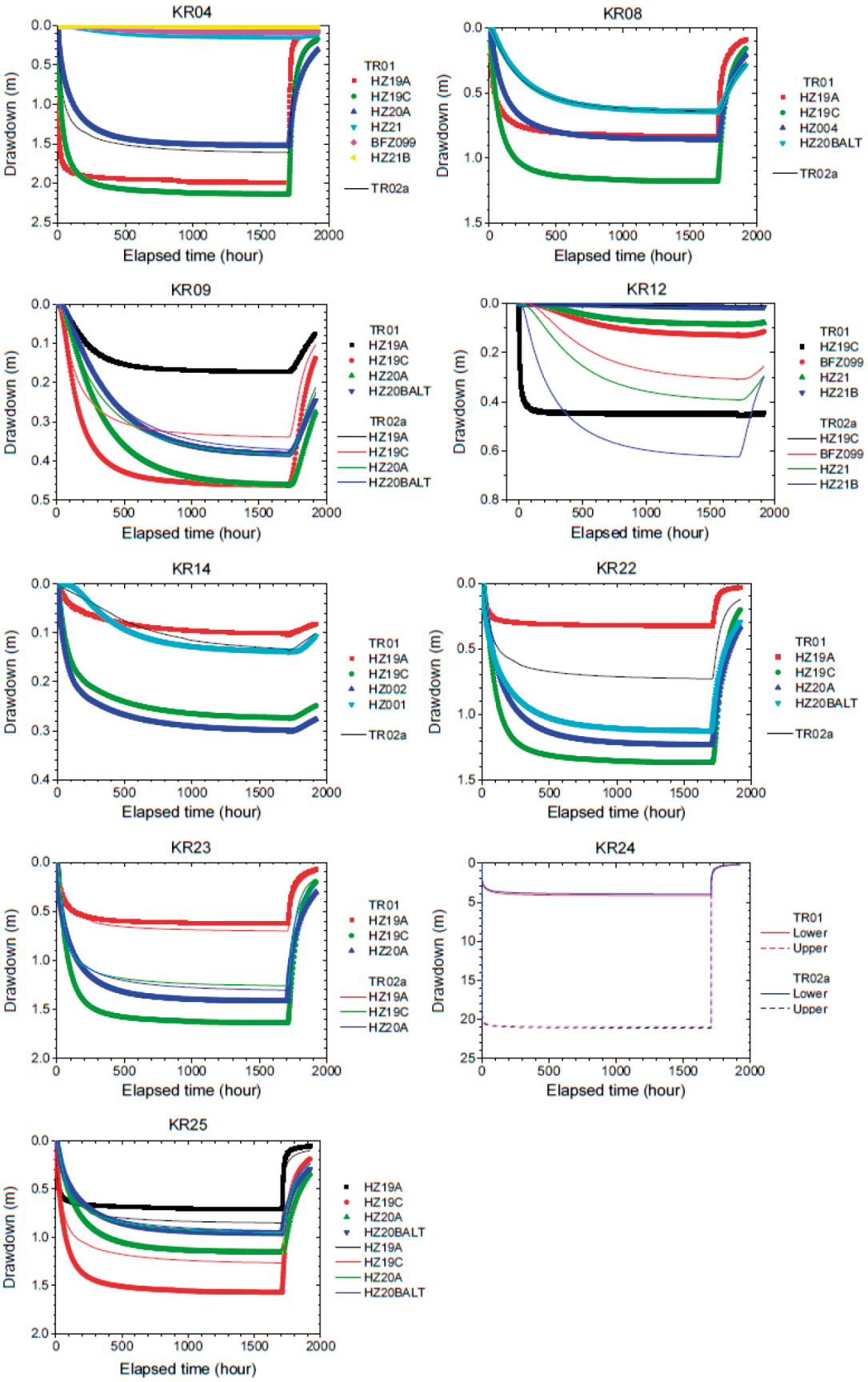

Figure 3-11. *Simulated drawdowns for selected boreholes for case without monitoring boreholes (TR01) and with monitoring boreholes (TR02a).*

Task 7A2, 5: Transport simulations

CRIEPI performed particle tracking simulations using 1 000 particles from each release point (RP1-3) in the "patch" model used within SS02c. The release points were specified in the task description and used by all modelling groups were located along KR24 at:

- RP1: intersection with HZ19B/C at 115.5 mah.
- RP2: intersection with HZ20A at 304.3 mah.
- RP3: intersection with HZ20B at 331.6 mah.

Particle tracking considered only advective transport through the zones and near surface layer. The tracks are shown in Figure 3-12. Travel times increased with depth and and mean travel times from RP3 were a factor 24 greater than those from RP1. CRIEPI split the tracks from each release point into different routes.

- RP1: mean particle travel time 6.5years, 90 % of particles travelled via the HZ19C zone.
- RP2: mean particle travel time 19.6 years, all particles travelled via HZ20A→HZ004→HZ20B ALT.
- RP3: mean particle travel time 156.5 years, 99 % of particles travelled via HZ20B ALT→HZ004→HZ20B ALT.

Overall the trajectories show only very limited dispersion. CRIEPI did not split out the time in the fracture zones from that spent in the near-surface layer.

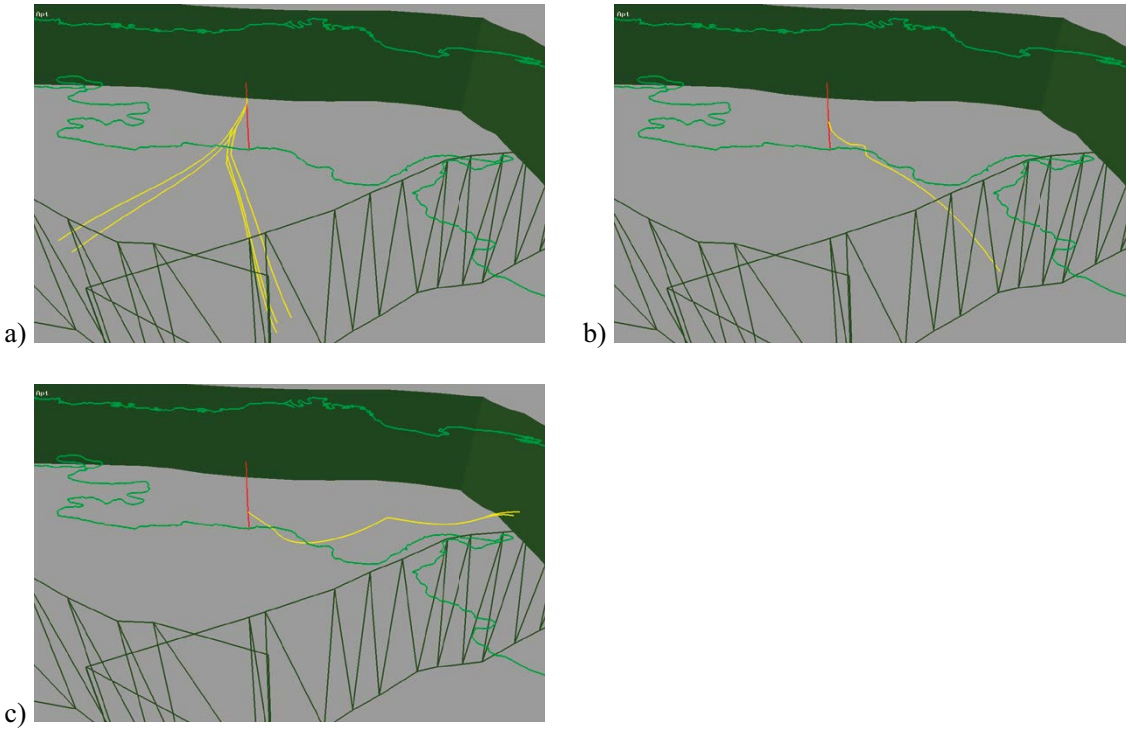

Figure 3-12. Simulated particle trajectories from the different release points a) RP1, b) RP2, c) RP3.

3.5.2 JAEA

Task 7A1, 7A2

JAEA followed the series of simulations specified within the Task Description using the properties defined in Vidstrand et al. (2015) for the reference case. After calibrating the model boundary conditions (recharge) they examined the impact of 6 sensitivity cases based on increasing or decreasing the transmissivity of key fracture zones. The average infiltration was reduced from 19.8 to 5 mm/year resulting in very limited discharge areas (Figure 3-13) and a reduction in the simulated head provided a better match to measurements.

Comparison of measured and simulated steady state borehole heads indicated that the T4 case (lower transmissivity for zones HZ20A and HZ20B_ALT) provided an improved match to the measured data. None of the cases captured the increase in head with depth in KR01, 09 and 12 probably indicating a limitation in the conceptual model (e.g. omission of salinity gradient). While the magnitude of PFL inflows was consistent with observations, it was difficult to judge between the different sensitivity cases based on the simulated inflows although Case T4 appeared to be a slightly better match to the average magnitude and pattern of PFL flow.

JAEA noted that locally high PFL flow rates were measured which did not appear in the simulations (for example, at a depth of 100–150 m in KR22), and that there were high simulated PFL flows rates that did not appear in the in situ measurements (for example, at a depth of 440–460 m in KR27). They concluded that this was due to the simplification in the structural model (only major fracture zones), and that this resulted in an overall increase from 5 significant inflows in the measurements to 7 inflows in the model boreholes. A comparison of the calibrated T4 model variant with/without boreholes showed that the presence of the open boreholes resulted in increased head at depth and a more uniform head field.

For the KR24 pump test simulations, the same set of variants were used and labelled SS04b-T1-6. An additional variant T0 was added which used the model parameters implemented prior to SS02b. The measured and simulated drawdowns and flows are shown in Figure 3-14 and Figure 3-15. In general, the SS04a case matched the measurements better than any of the calibration variants.

JAEA noted that the relatively high simulated drawdowns were probably due to a mismatch in the model representation of the near surface rather than the fracture zones. Further, mismatches in the spatial distribution of PFL inflow were probably due to limitations in the structural model.

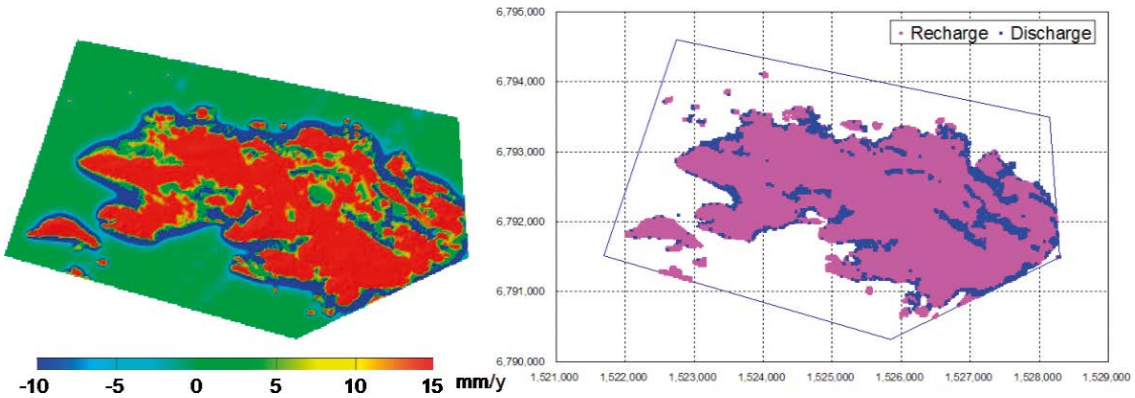

Figure 3-13. *Calculated discharge and recharge distribution at Olkiluoto site; results of calibration of infiltration rate of first calibration step in SS02b case.*

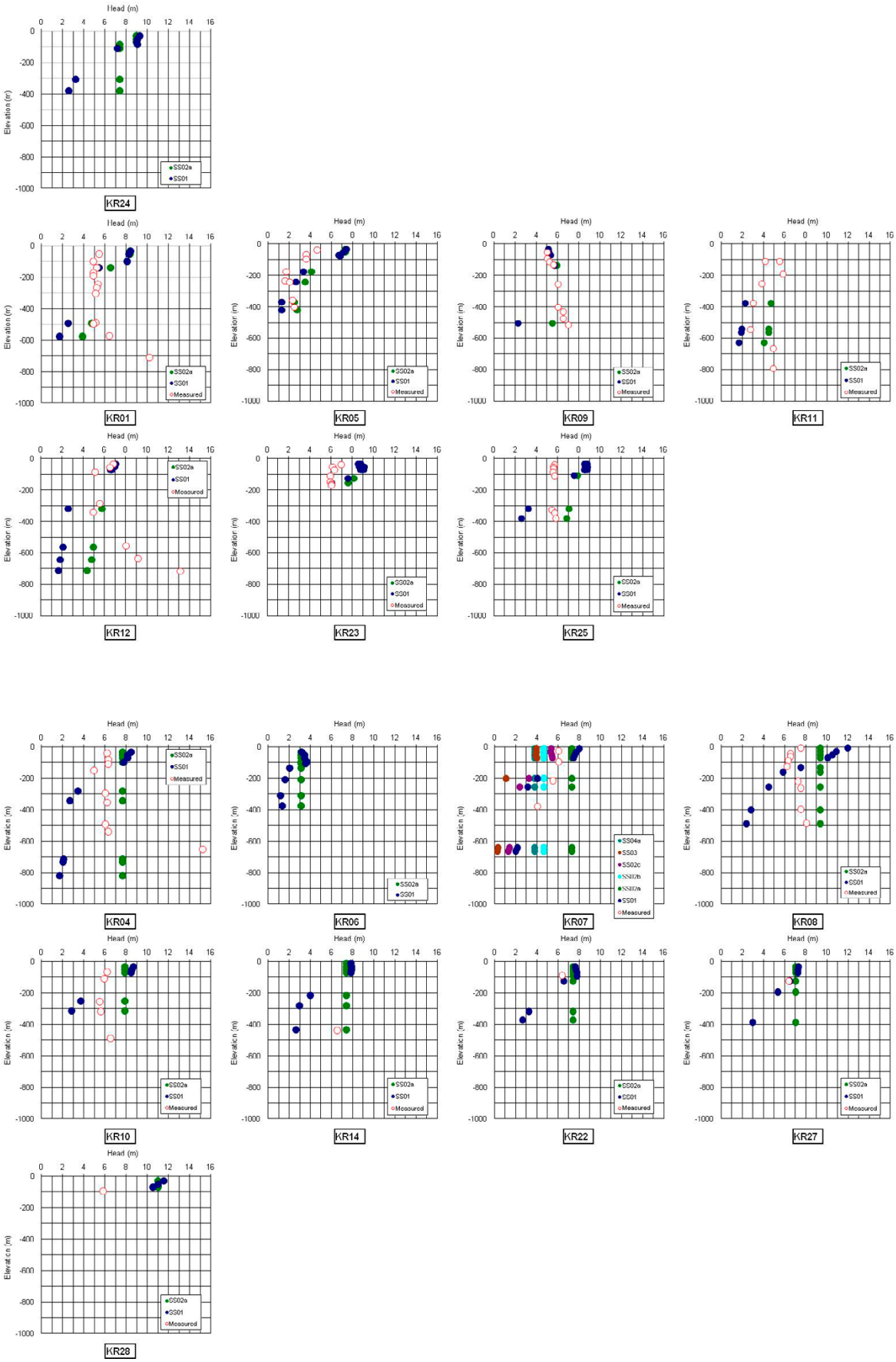

Figure 3-14. *Simulated drawdowns for the forward (SS04a dark green) and the different conditioned models (SS04b T0-T6) together with the measured drawdown (hollow red symbols).*

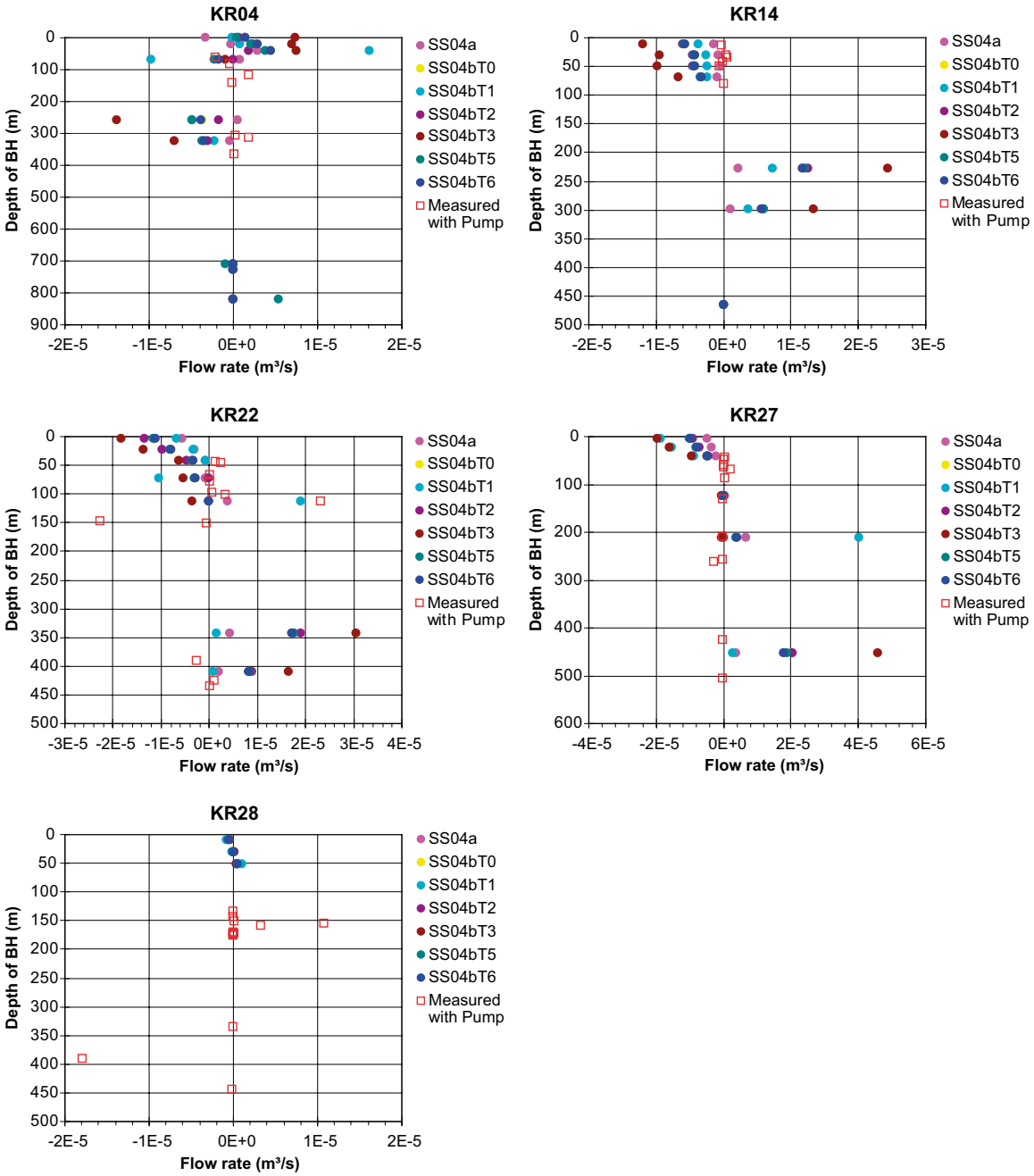

Figure 3-15. *Simulated and measured borehole inflows for the forward (SS04a) and conditioned models (SS04b cases T0-T6).*

Task 7A2, 5: Transport simulations

JAEA simulated particle trajectories for the head fields corresponding to each of the seven cases without pumping or open boreholes. 100 trajectories were calculated for each release point and case. A longitudinal dispersion of 1 m and transverse dispersion of 0.1 m were used to generate a range of advective paths. Simulated trajectories are shown in Figure 3-16.

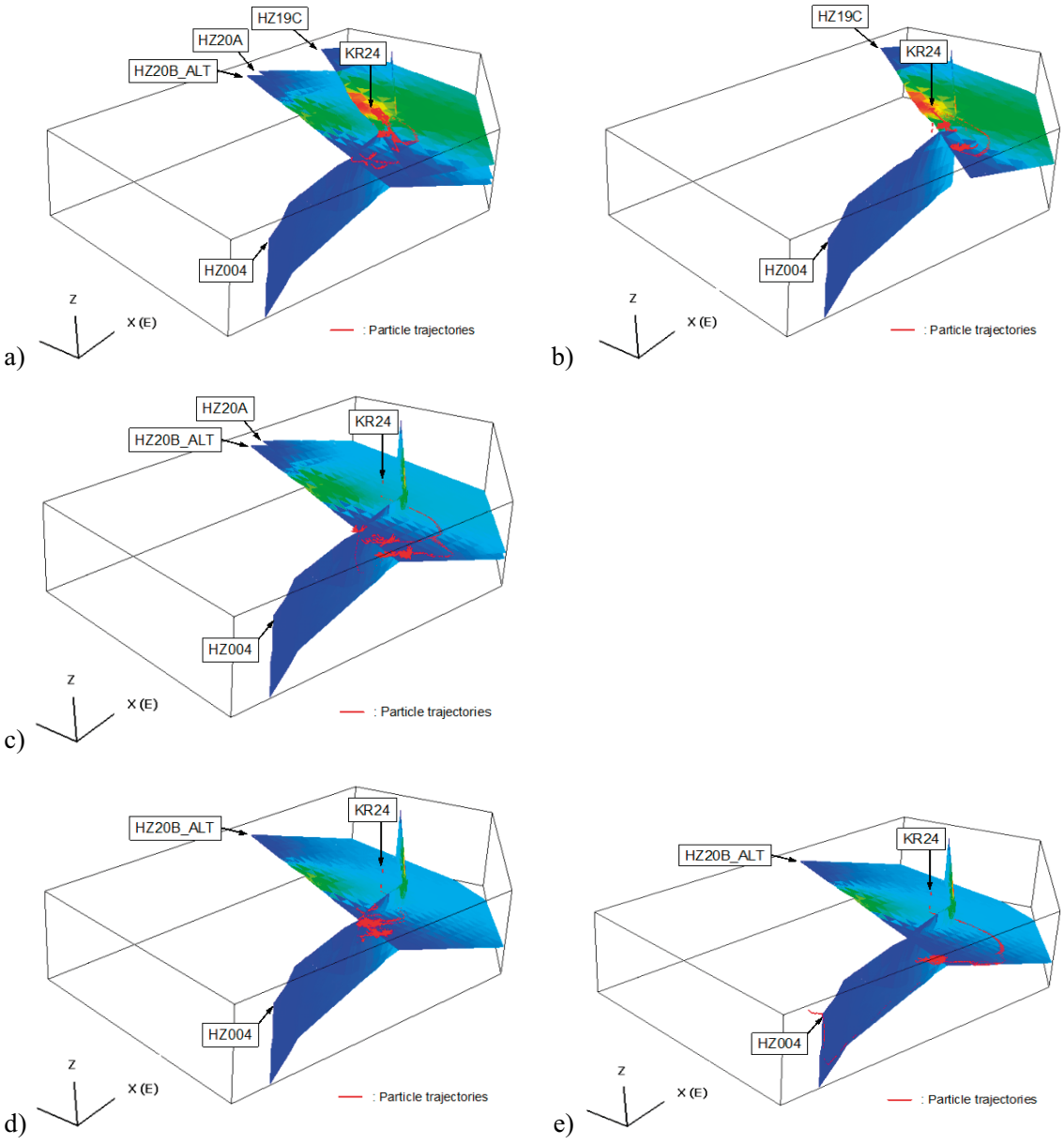

Figure 3-16. *Particle trajectories for selected release points and model cases: a) RP1 case T4, b) RP1 case T1, c) RP2 case T4, d) RP3 case T4, e) RP3 case T6.*

The travel time and distance probability distributions were calculated for each release point and case and the T4 distributions are shown in Figure 3-17. Comparison of the distributions and trajectories led JAEA to conclude that:

- Particle travel times were dominated by the time in the surface layer and hence it is necessary to separate the travel time in the fracture zone network from that spent in the continuum surface layer.
- Particle trajectories from RP1 were sensitive to the transmissivity of HZ19. For high transmissivity case T1 all trajectories stayed within the zone, while in other cases paths traversed multiple zones. Modelling had shown that pumping and PFL tests were insufficient to distinguish between such cases.
- Particle trajectories from RP2 were largely insensitive to zone transmissivity and the main variability related to travel in the surface layer.
- Particle trajectories from RP3 were generally similar to the results for RP2, indicating that within a certain range, uncertainty in fault zone transmissivity caused only a small uncertainty in the travel distance. However, cases T4 and T5 had significantly different travel distances from the other cases.

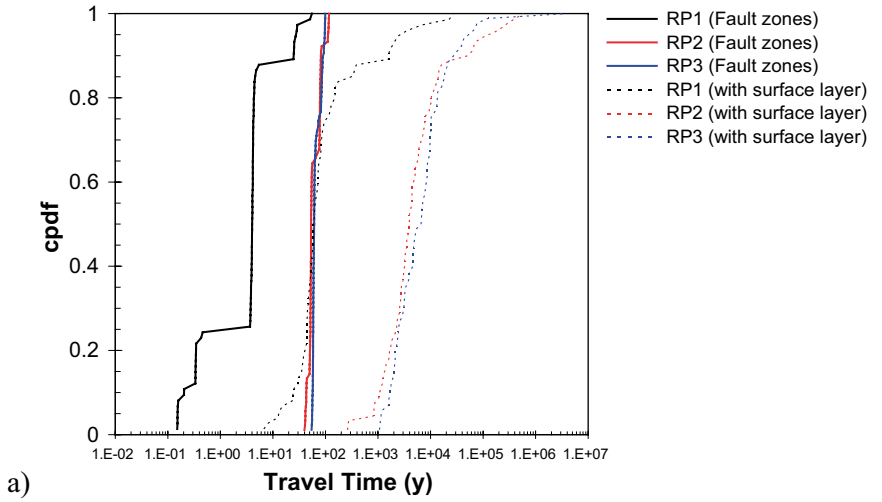

a)

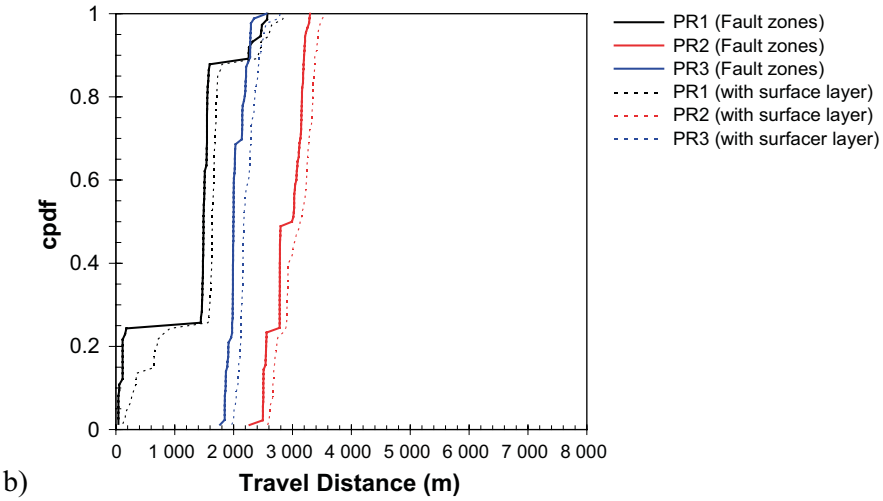

b)

Figure 3-17. *Cumulative probability density functions for travel time and distance for case T4. Solid line shows travel time within fracture zones and dotted line shows travel time to the boundary including surface layer.*

3.5.3 KAERI

Task 7A1, 7A2

Figure 3-18 shows the measured and predicted heads from simulations SS02b (with boreholes) and SS02c (without boreholes). The SS02b simulated heads show good agreement with the measured heads with the exception of the deeper parts of KR09 and KR12. The model assumed a constant fluid density of 1 000 kg/m^3 and so did not reproduce the high heads at depths below −500 m.a.s.l. that are due to the observed salinity profile.

The effect of the boreholes can be clearly seen by comparing the two simulations. In the simulation without boreholes, heads are increased in the upper part of the models while heads decrease significantly in the lower part. This may be partially a result of the assumed lateral constant head boundaries, although it also reflects the ability of the boreholes to disturb the natural head field due to their high vertical permeability, suggesting that the Discrete Fracture Element (DFE) method can successfully describe the open borehole effects.

Figure 3-19 shows the measured and predicted drawdowns and flows from SS04a and SS04b. Drawdowns are typically slightly lower in the calibrated model (SS04b) with higher recharge. The difference between the measured and simulated drawdowns is relatively large even with the increased recharge and adjustments to the structural model such as inclusion of zone heterogeneity would be required to achieve a better match.

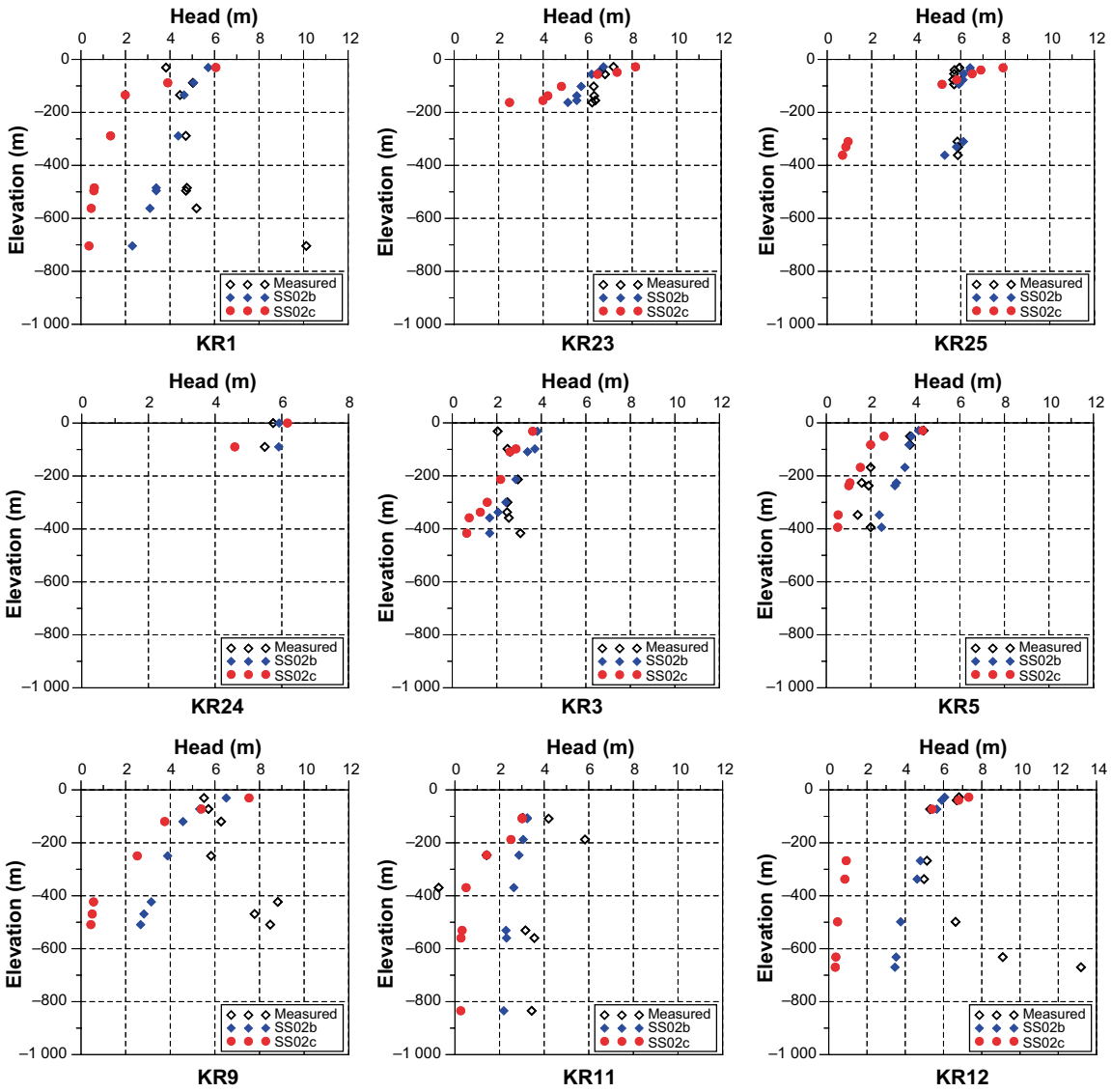

Figure 3-18. *Measured and predicted heads for selected boreholes.*

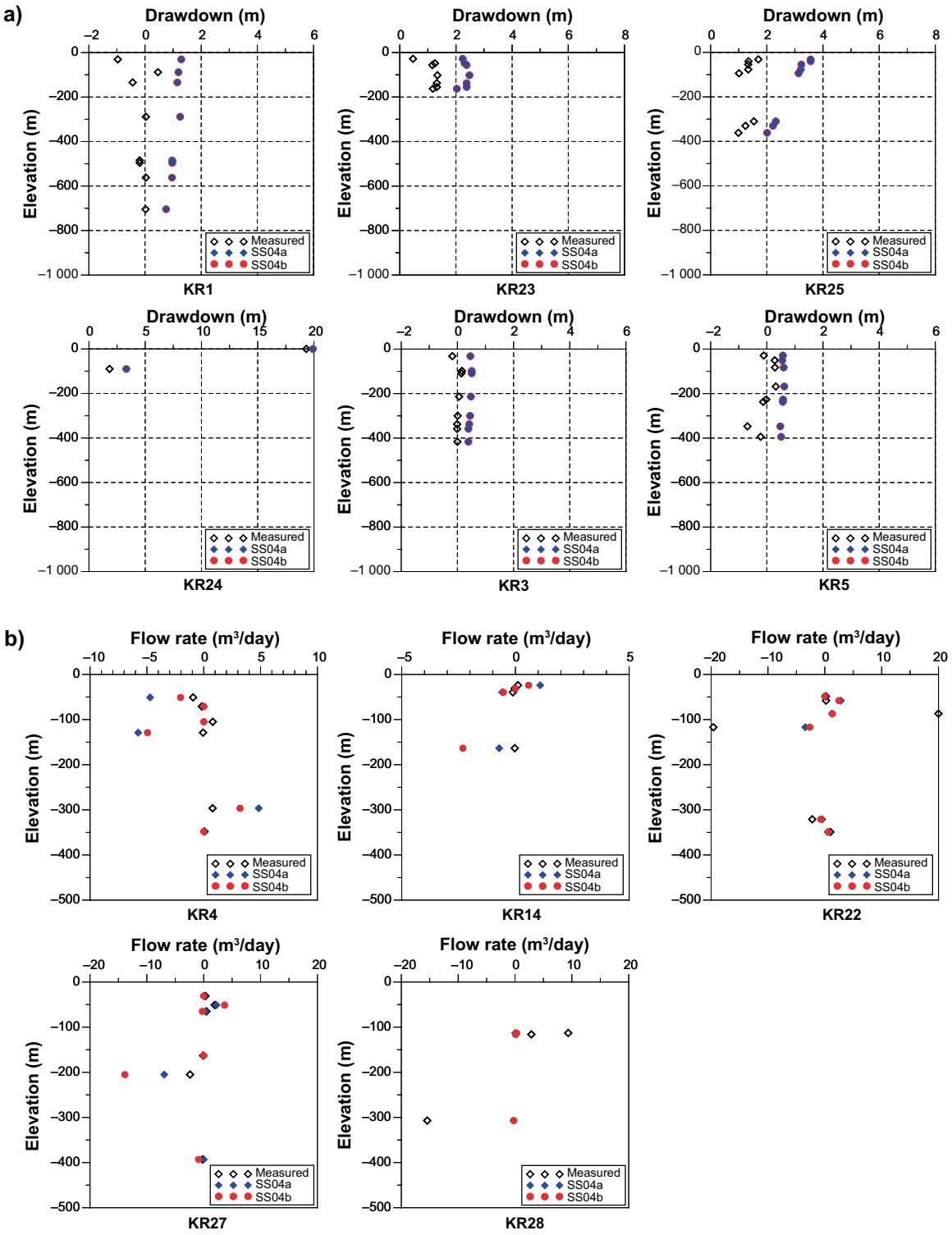

Figure 3-19. *Measured and predicted (SS04a and SS04b) drawdowns and flows for pumping in KR24/ a) drawdowns, b) flows.*

In general the match to flow magnitude and direction is reasonable, although some major flow features in KR28 are not predicted by the simulations.

Transient simulations were performed using the SS04b calibration assuming a calibrated storage coefficient of 10^{-7} m^{-1}. Reasonable matches were achieved to the source interval in KR24 and monitoring zones as shown in Figure 3-20. The difference between steady state drawdowns and those calculated at the end of pumping in the transient models were small due to the small storage coefficient and consequent high diffusivity of the zones within the simulation.

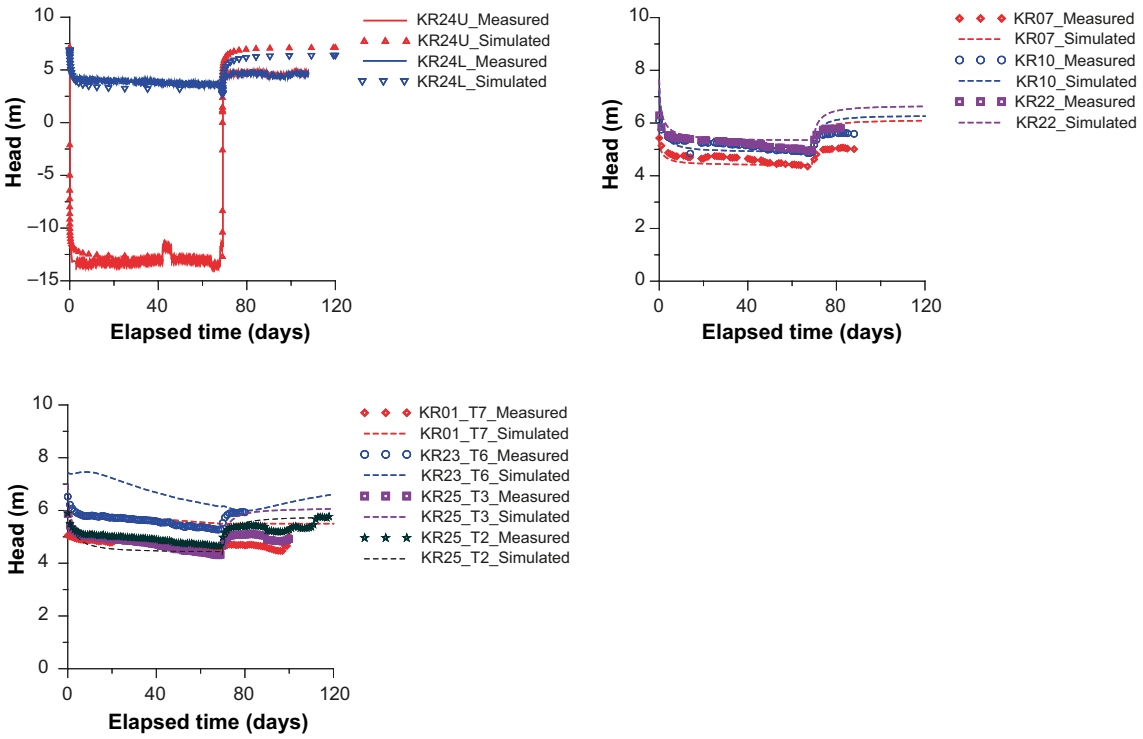

Figure 3-20. *Measured and predicted transient heads for TR02a simulation with pumping in KR24.*

Task 7A4

Simulations SS11 and SS13 used the results of the calibrated models to consider the differences due to the presence of the boreholes. They clearly show a strong effect of the boreholes on the observed head field (Figure 3-21). KAERI conclude that the effect of open boreholes should be considered in any calibration of groundwater flow models of fractured rock aquifers with low permeable matrix.

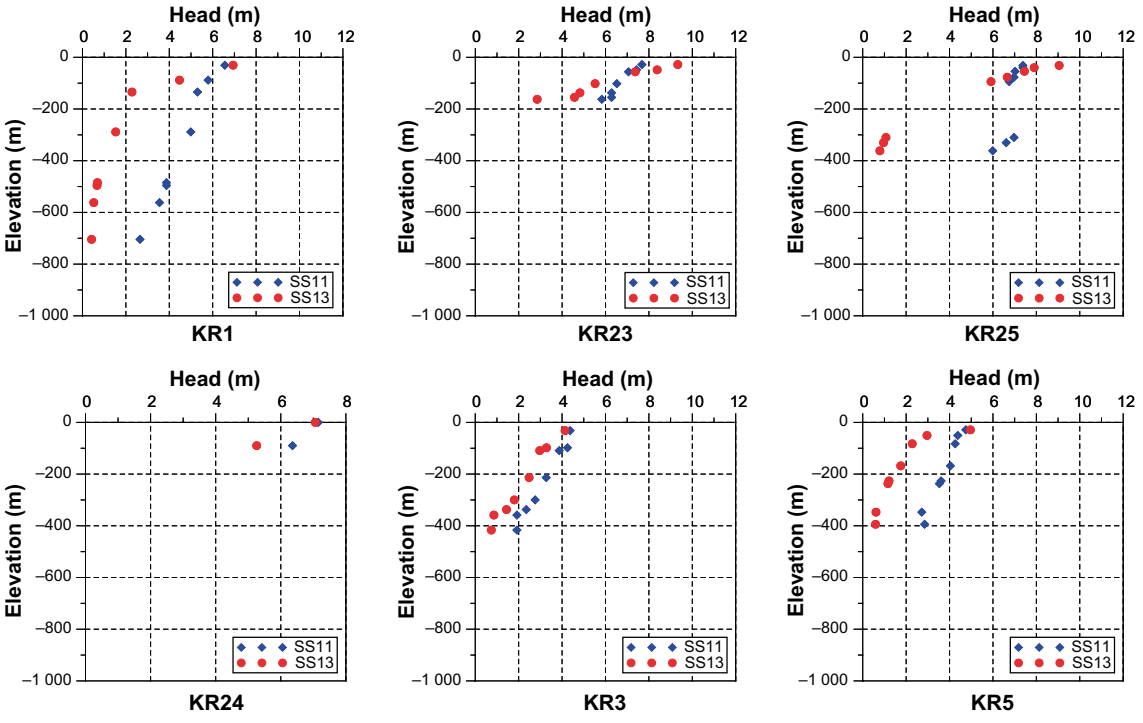

Figure 3-21. *Heads from SS11 (open boreholes) and SS13 (no boreholes) simulations showing the difference between calibrated models due to the presence of open boreholes.*

Task 7A2, 5: Transport simulations

Particle transport calculations were performed using the SS02b and SS13 flow fields assuming a uniform subsurface porosity of 5 %. Statistics for the advective travel time for the transport paths from the three release points are shown in Table 3-2. The transport paths appear to be identical in the two simulations. Only median advective travel times were reported and these were typically much higher than those reported by other modelling groups due to the assumed uniform high porosity (other modelling groups used a porosity based on zone transmissivity from either Doe's Law or the cubic law). Travel time is approximately 10 % lower when using the SS13 flow model (presumably due to higher specified recharge).

Table 3-2. KAERI Particle tracking advective travel time (s) from SS02b and SS13 flow fields.

Flow simulation	Release Point 1			Release Point 2			Release Point 3		
	Mean	Median	95 %	Mean	Median	95 %	Mean	Median	95 %
SS02b		4.5E12			2.1E13			1.4E14	
SS13		3.9E12			1.8E13			1.3E14	

3.5.4 NWMO/Laval

NWMO/Laval performed all the forward simulations within the Task but could not complete the inverse models because of problems using PEST[9]. Figure 3-23 shows the simulated hydraulic heads on the model surfaces and fracture zones. The effect of the island topography is clearly seen. Inclusion of open boreholes (SS02a) produce higher simulated hydraulic heads at greater depths (elevation <−300 m) and typically decreased hydraulic gradients. In the uncalibrated models the simulated heads showed greater variability than the measured heads probably due to the upper boundary conditions used.

Forward steady-state simulations of the KR24 pump test were performed with (SS04a) and without (SS03) monitoring boreholes. The simulated drawdowns are shown in Figure 3-24. The effect of the monitoring boreholes is clearly seen in the plot versus horizontal distance where much greater variability is seen without the monitoring boreholes.

Transient models of the pump test were also performed for cases with and without monitoring boreholes. The case with monitoring boreholes (TR02a) provided a reasonable match to the "detrended" drawdowns (Figure 3-25). Matches to head were less good due to inconsistencies in the imposed initial conditions. The observed roughly linear head trend of 1 cm/day was thought to relate to annual changes in recharge rather than the pump test.

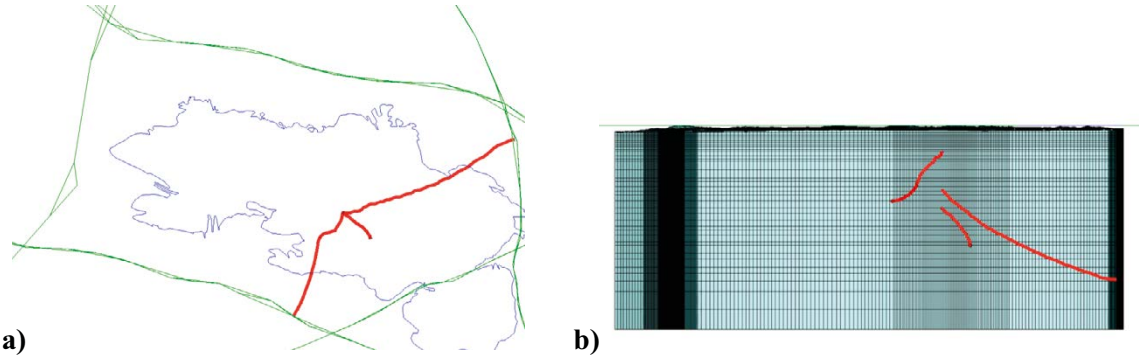

Figure 3-22. *Plan view and section view of transport paths for SS02b and SS13 flow models.*

[9] At least partly due to inexperience during Task 7A– see later applications in Task 7B.

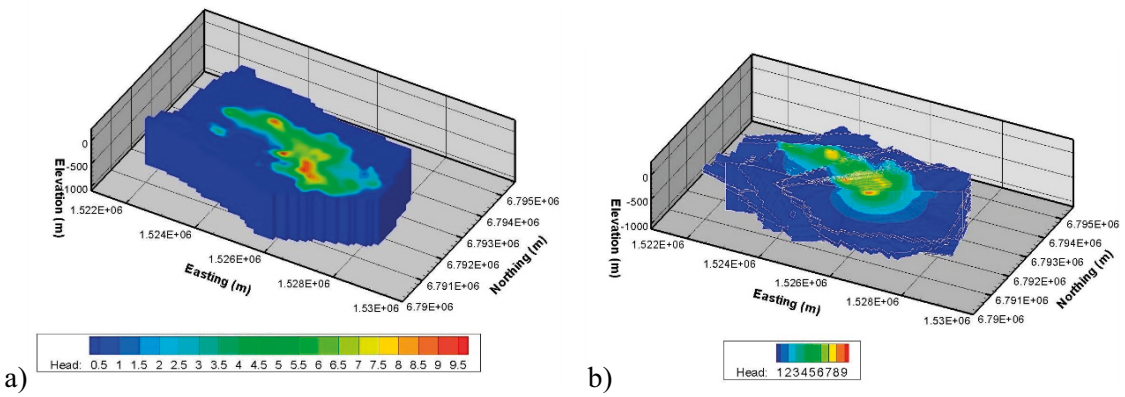

Figure 3-23. Hydraulic heads for natural conditions (SS01) without open boreholes contoured on a) model surfaces and b) fracture zones.

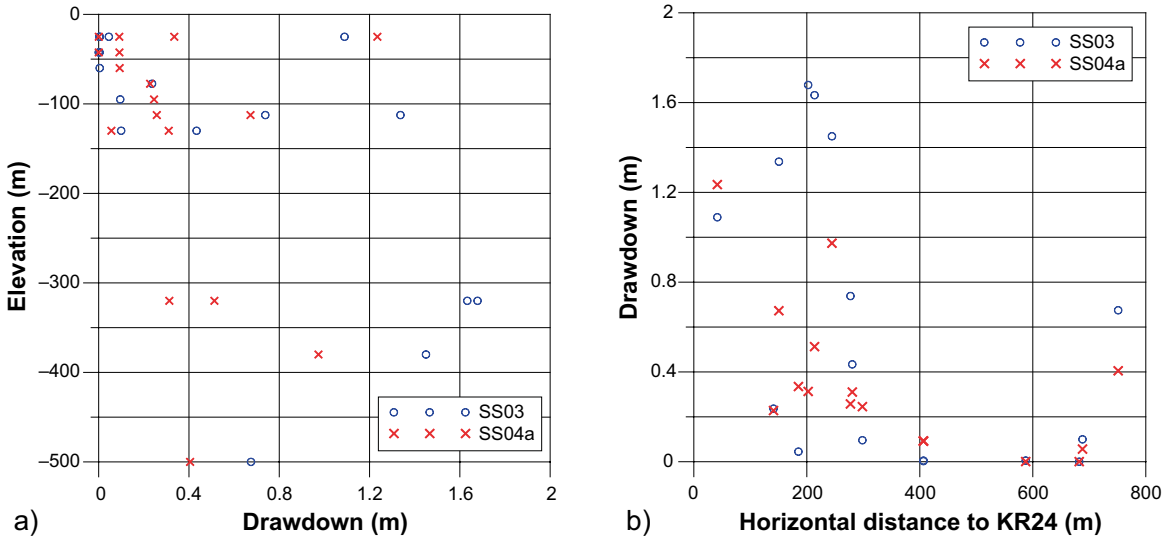

Figure 3-24. *Drawdown for KR24 pump test with (SS04a) and without (SS03) monitoring boreholes: a) drawdown versus elevation, b) drawdown versus horizontal distance from KR24.*

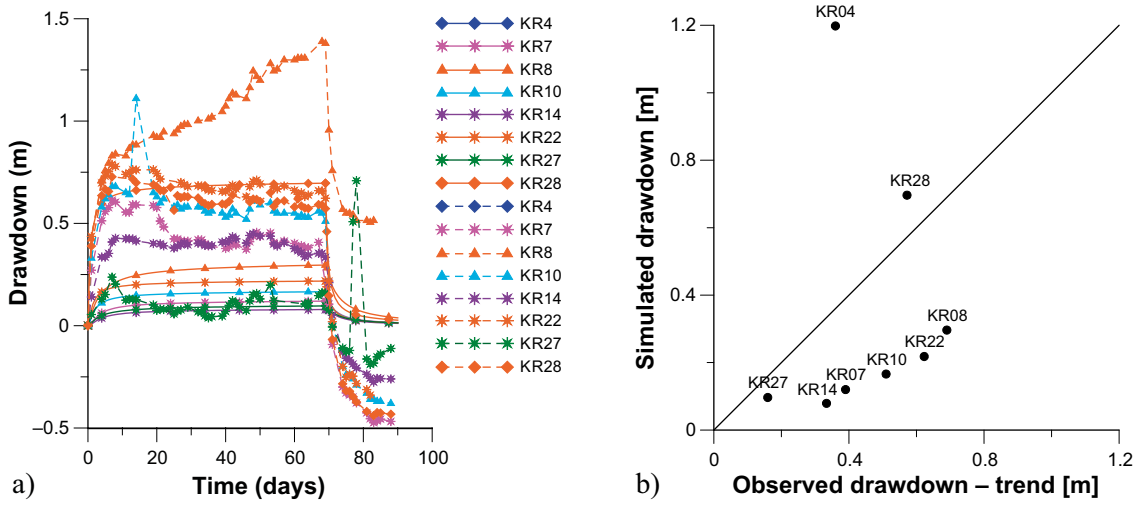

Figure 3-25. *a) Simulated transient drawdowns (solid lines) from TR02a with measured drawdowns after trend removal (dashed line) for KR24 pump test. A 1 cm/day trend has been subtracted from the observed drawdowns; b) crossplot of simulated and observed (detrended) drawdowns.*

NWMO/Laval performed transport calculations using three methods:

1. Particle tracking using the facilities within the TECPLOT visualisation package.
2. Advective-dispersive transport simulation within Hydrogeosphere.
3. A “life expectancy” simulation.

The TECPLOT calculations were performed as a check on the advective-dispersive transport simulation.

Both particle tracking and the advective-dispersive transport simulation showed that the transport paths from the release point went to the South (Figure 3-26) with preferential transport along HZ19C and HZ20A and more limited transport along HZ20B_ALT.

The life-expectancy simulations are run in a backward-in-time mode – reversing the flow field. The groundwater life expectancy at a point is the time of travel from the location to an exit boundary (Therrien et al. 2009). A life expectancy of zero is assigned at the outflow boundaries and a backward-in-time simulation is then run to compute the mean life expectancy for every node in the domain. In addition to the mean life expectancy, the model also computes the probability density function and the cumulative density function of life expectancy at every node. Figure 3-27 shows the computed probability distributions for the 3 release points. The transport times increase with depth. The longer travel times and low probability at 55 000 days for RP3 reflects the low hydraulic conductivity of the rock around this release point.

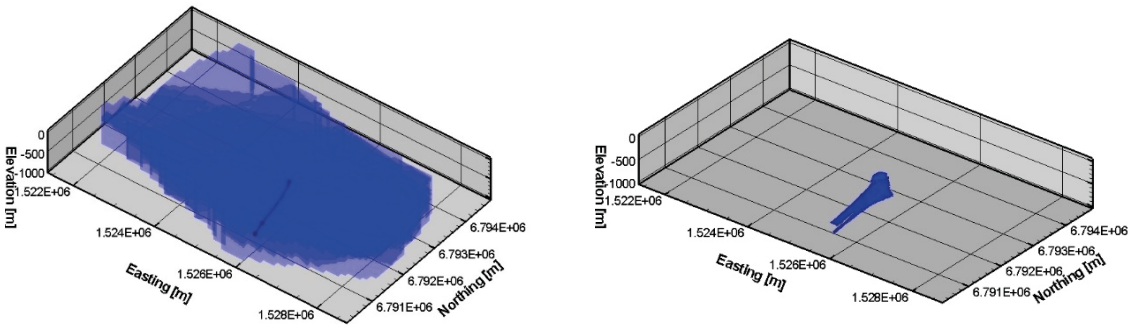

a) b)

Figure 3-26. *NWMO/Laval transport simulations a) trajectories of particles as computed by TECPLOT and b) contour of relative concentration = 0.001 at 30 years, for a solute source located at KR24.*

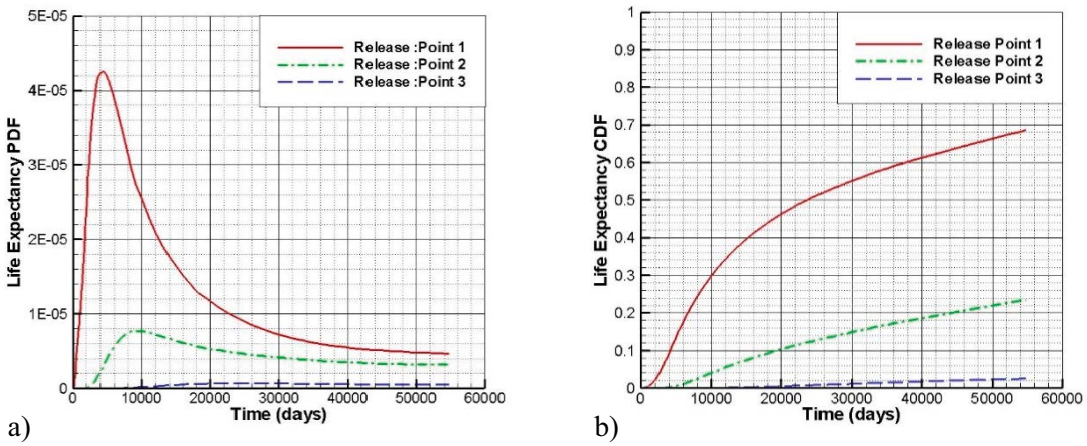

a) b)

Figure 3-27. *Distribution of particle life-expectancy for release points RP1, RP2 and RP3 a) probability density function and b) Cumulative density function.*

3.5.5 Posiva/VTT

Posiva/VTT used both the small and large representations of the fracture zones. The model variant using the small zones is significantly less well connected. The hydraulic heads for undisturbed conditions with (SS02a) and without monitoring boreholes (SS01) show the influence of both the reduced connectivity (model variant S) and the open boreholes in Figure 3-28.

The effect of the monitoring boreholes is also clearly seen in Figure 3-29. The monitoring boreholes spread the response to pumping to greater depth. Without the monitoring boreholes, the drawdown is focused in a sub-horizontal layer related to the major zones intersected by the lower borehole section. The inclusion of the boreholes results in drawdowns reducing more quickly with radial distance but extending in the vertical direction as flow is diverted from fracture zones into KR24.

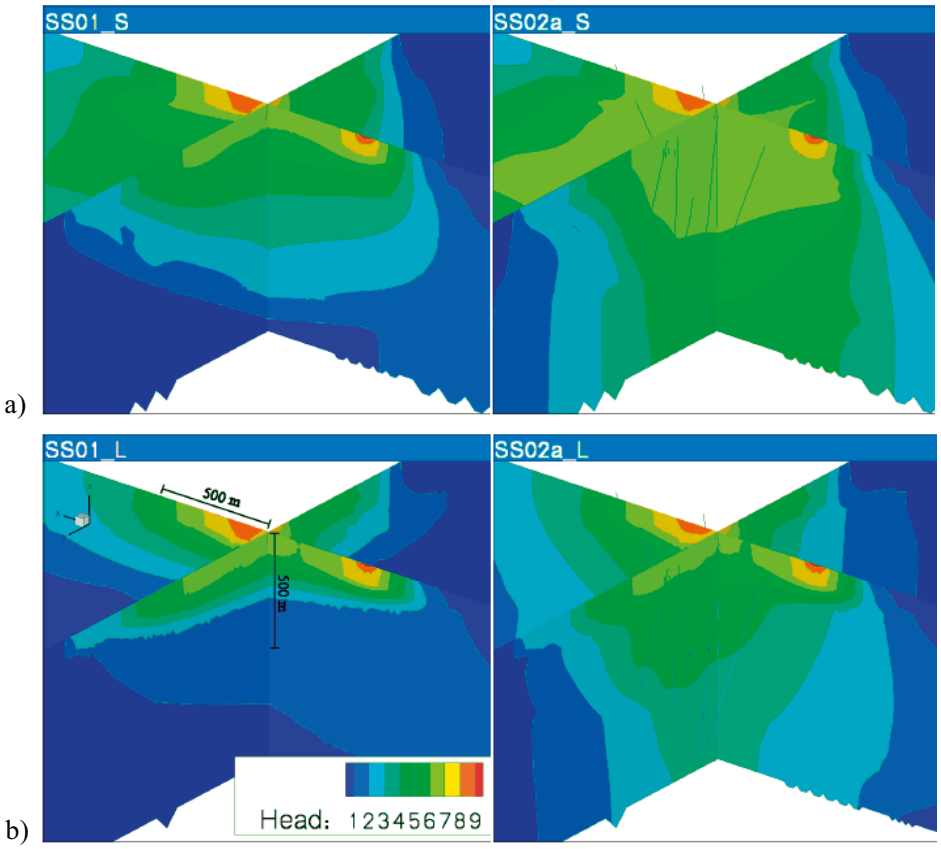

Figure 3-28. *Contoured head for the Posiva/VTT models for SS01 and SS02a: a) small zone models; b) large zone models (from Keto and Koskinen 2009).*

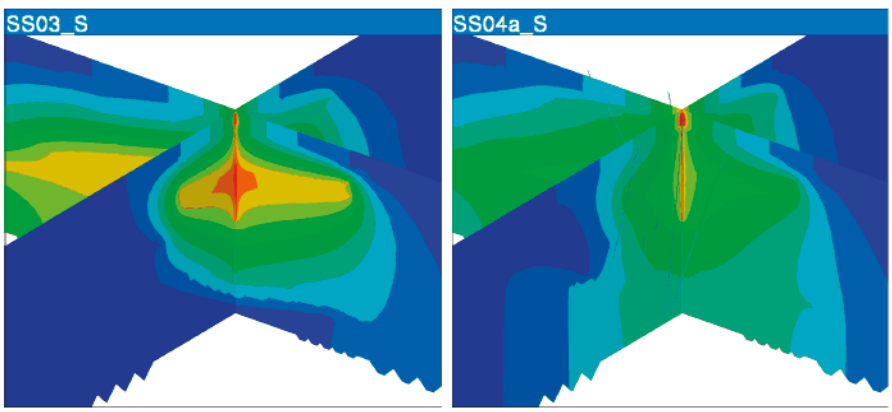

Figure 3-29. *Contoured "normalised" drawdown for the Posiva/VTT small zone models for SS03 (no monitoring boreholes) and SS04a (including monitoring boreholes) uncalibrated models (from Keto ad Koskinen 2009).*

The distance drawdown curve for Posiva/VTT's calibrated model of the KR24 pumping test is shown in Figure 3-30. At greater distance the model over-estimates the drawdowns (KR12, KR27 and KR09) because these boreholes are not connected to KR24 by the zones but high drawdowns are simulated because of the assumed steady state. A comparison of the initial and calibrated model PFL responses is shown in Figure 3-31.

Posiva/VTT did not perform transport simulations within Task 7A.

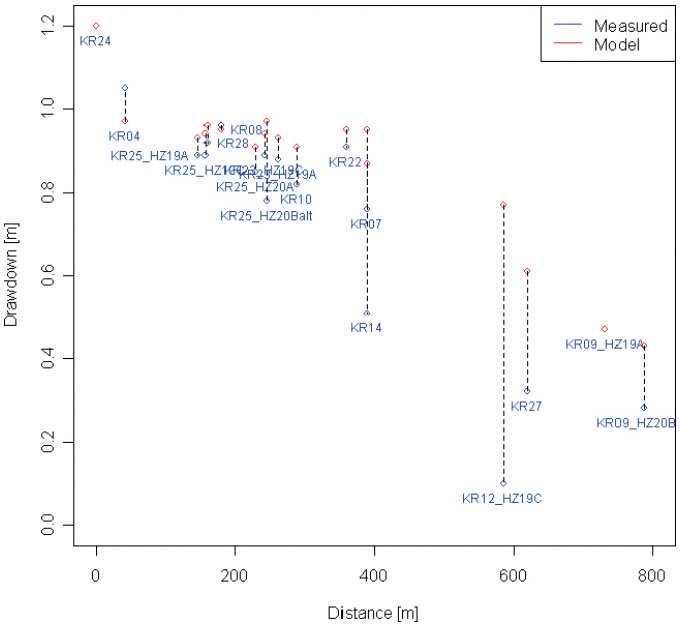

Figure 3-30. *Comparison of drawdown normalized drawdown versus distance from VTT calibrated model (from Keto and Koskinen 2009).*

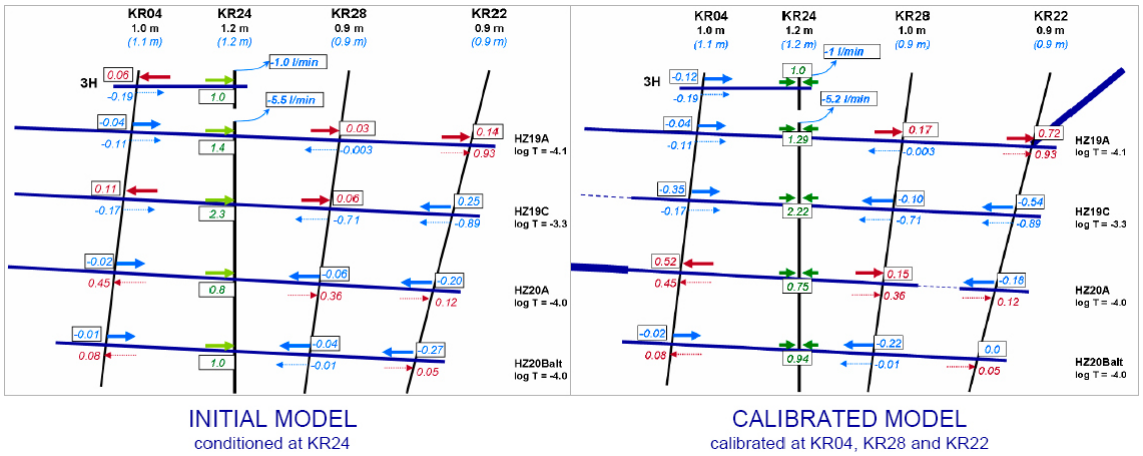

Figure 3-31. *Comparison of simulated PFL responses and data from SS04a and SS04b from VTT. Model flows shown in boxes (from Keto and Koskinen 2009).*

Task 7A4: Calibration for possible compartmentalisation or natural trends from open borehole information

POSIVA/VTT applied an Ensemble Kalman Filtering approach (Evensen 1994) to the analysis of the pump test (Keto and Koskinen 2009). Ensemble Kalman filtering is a tool for statistical calibration using the Kalman filter with a sampled covariance matrix that provides a sequentially improved estimate of model state (parameters) in the form of a collection of normally distributed random variables.

The KR24 pump test model is shown in Figure 3-32. The model parameters are the major zone transmissivities and the transmissivity of the part of the zones that connects to the surface. The parameters considered were the log transmissivity of zones HZ004, HZ19A, HZ19C, HZ20A, HZ20AE, HZ20B_ALT and their surface connections. The calibration data were 17 drawdown measurements and 16 PFL measurements (the change in flow due to pumping). The specified prior distributions of zone and surface connection transmissivities together with posterior distributions for a) fits to drawdown only and b) fits to drawdown and change in PFL flow are shown in Figure 3-33.

Comparison of the posterior distributions for calibration to drawdowns only and both drawdowns and PFL data shows that the uncertainty is considerably lower when including the PFL data. This may in part be due to the increase in number of observations but it would appear that the PFL data is providing a stronger constraint on the model parameters than the drawdowns.

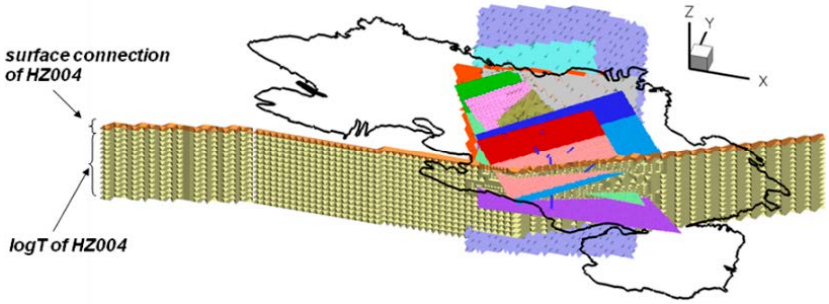

Figure 3-32. *Fracture zone model showing different zones and surface connections from VTT Ensemble Kalman Filtering model.*

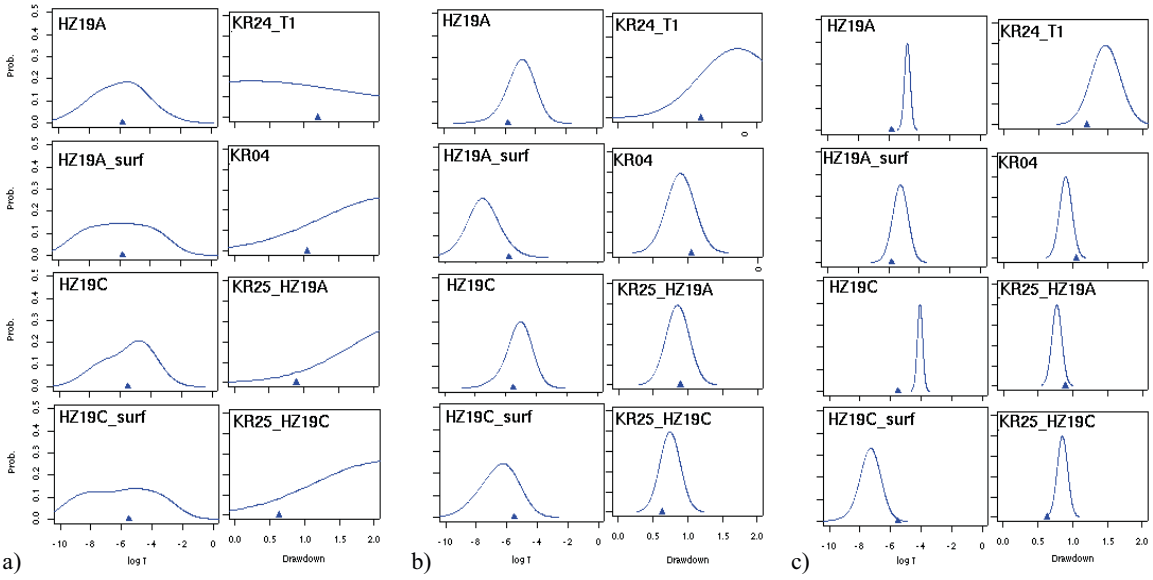

Figure 3-33. *Fracture zone parameters a) prior distribution, b) posterior distribution calibration to head data only, c) posterior distribution calibration to head and PFL data.*

3.5.6 SKB/CFE

Task 7A1, 2

SKB/CFE included a high hydraulic conductivity near-surface layer with a negative exponential depth trend and adjusted the average recharge to match heads in undisturbed conditions. The resulting groundwater table and "wet" areas are shown in Figure 3-34.

SKB/CFE presented only the results from a calibrated model (SS04b) and did not make a forward simulation (SS04a). The calibration was to head/drawdown only and flow measurements were then compared with the results from the calibrated models. The calibration involved the adjustment of the background hydraulic conductivity of the layer down to 80 m to match the drawdown in the upper section of the borehole and adjustment of the local fracture networks around fracture zone intersections in the deep section. This allowed a good match to be achieved between the measured and simulated inflows (see Figure 3-35).

The simulated inflows show greater uniformity in the upper 80 m where the background rock is represented by a layer of uniform hydraulic conductivity than in the deeper part where only the fracture zones are modelled.

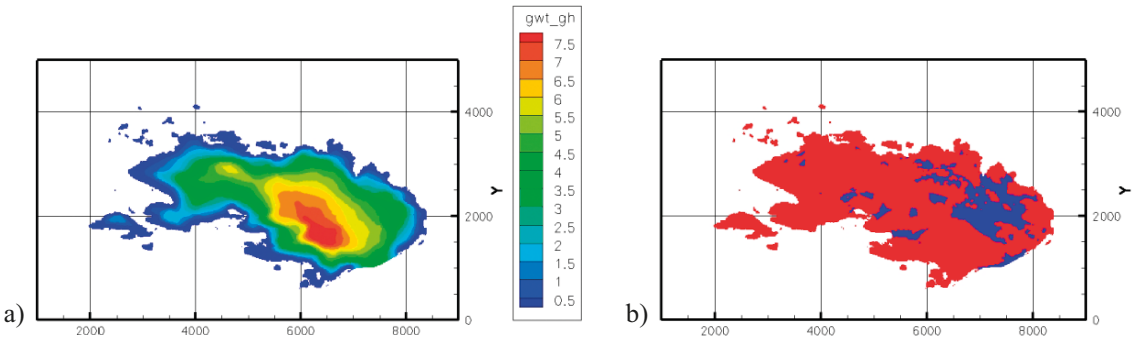

Figure 3-34. *Simulated a) groundwater table and b) wet areas (blue) from SKB/CFE calibrated model.*

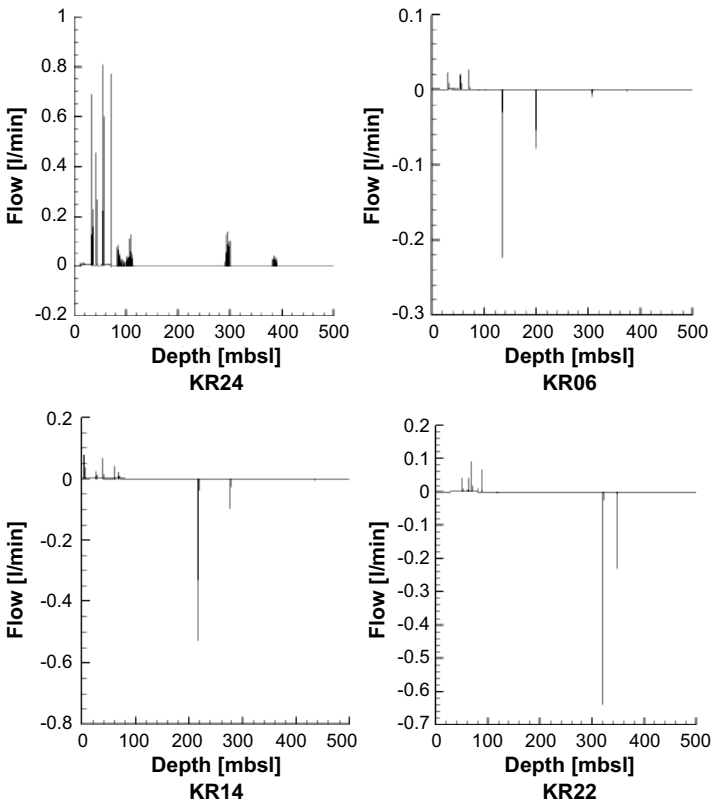

Figure 3-35. *Simulated borehole inflows for the SKB/CFE calibrated model.*

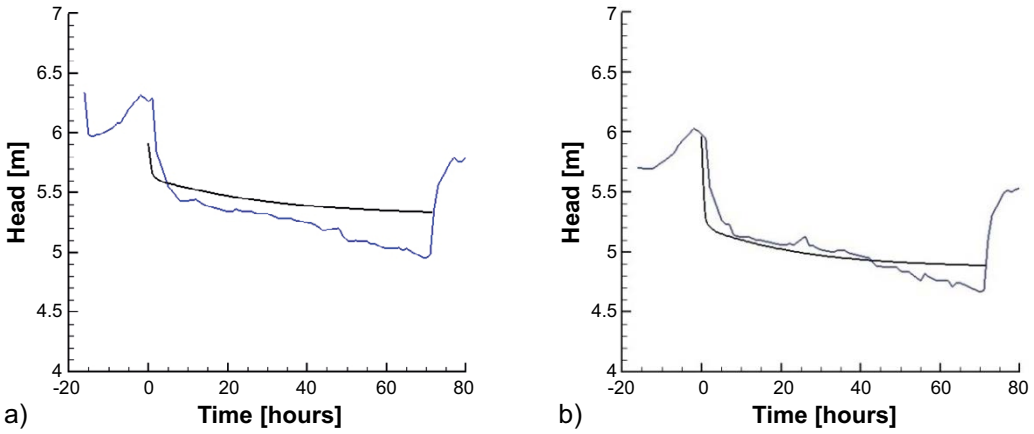

Figure 3-36. *Simulated (black) and measured (dark blue) transient heads in a) KR22 and b) KR28.*

Transient simulations

SKB/CFE performed a transient simulation using the calibrated model and assuming a specific storage of $S_s = 10^{-6}$ m^{-1} for cells within the model. Heads at the end of the transient simulation were close to those from the steady state simulation. The simulated and measured heads in KR22 and KR28 are shown in Figure 3-36. A reasonable match to observation was achieved.

Task 7A2, 5: Transport simulations

SKB/CFE performed a particle tracking simulation for the calibrated model and the simulated tracks are shown in Figure 3-37.

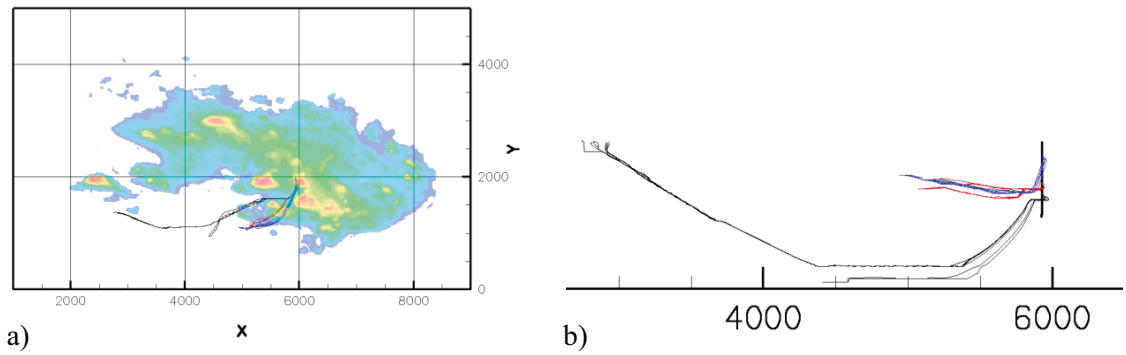

Figure 3-37. *SKB/CFE plan and vertical section (XZ) of particles tracks from the three release points (RP1-RP3).*

Task 7A3 Ideas for calculation of PA-relevant parameters from open borehole information

SKB/CFE was the only group to report on 7A3. The report (Svensson 2015) draws on recent studies (RETROCK 2005, Black et al. 2007) that argue for highly channelled flow systems within crystalline rock and presents work from two related modelling studies: one concerning modelling of the inflow distribution to repository tunnels (see Figure 3-38) and a second concerning detailed simulations of flow in a single fracture and the surrounding matrix.

The repository models illustrate the potential for description of the flow distribution around deposition holes and its dependence on the "channelling model". A second block scale model (from Task 6C) shows how the inclusion of transmissivity variability within 2D fractures increases flow heterogeneity.

The report also presents a detailed scale model (1 m scale with resolution down to ~0.03 mm) coupling flow in a fracture using the Navier-Stokes equations and flow in the matrix using a linear resistance term. The matrix itself is assumed to contain permeable microfractures. Results from both 2D (cross-section through matrix and fracture) and 3D models are presented. The models demonstrate the potential for coupling of flow and transport between the two porosity systems. The models are computationally intense due to the fine spatial discretisation used.

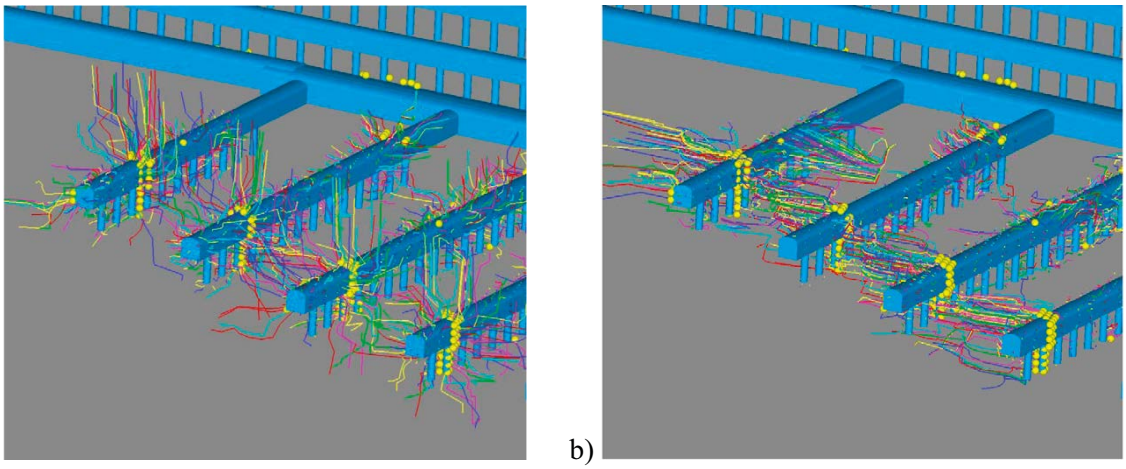

Figure 3-38. *Backtracking of particles for a) open repository and b) after backfilling of the repository. Integration time is one hour for the open repository (a) and 100 days for undisturbed conditions (b) (from Svensson 2015).*

3.5.7 SKB/KTH

Task 7A1, 7A2

For the simulations without open boreholes, SKB/KTH included the boreholes but with a low borehole permeability of 10^{-15} m^2. This had the advantage that borehole-fracture zone intersections were well defined and pressures and flows could be easily compared with simulations with open boreholes[10]. Figure 3-39 shows the measured and simulated heads for the case a) without and b) with open boreholes (SS01); both simulations show significantly greater variability than the measurements.

SKB/KTH made six variant calculations where the transmissivity of selected fracture zones was altered by factors of 8 or 1 000 (hydraulic aperture variation by factor 2 or 10). The model variants were compared in terms of their match to the measured flows at 40 fracture zone intersections under open borehole conditions without pumping (SS02b). The variants showed limited improvement over the base case (SS02a shown in Figure 3-39c) although for variant-5 the mean and sample variance of the flow values was closer to that measured (Figure 3-39d) and hence it was felt that this variant produced a better model description than the base case, at least in a statistical sense.

[10] In fact SKB/KTH performed a sensitivity study using a range of internal borehole permeabilities and found that for a borehole permeability of 10^{-5} m^2 the results were equivalent to simulations with open boreholes where the resistance to flow along the borehole is given by the Hagen-Poiseuille equation.

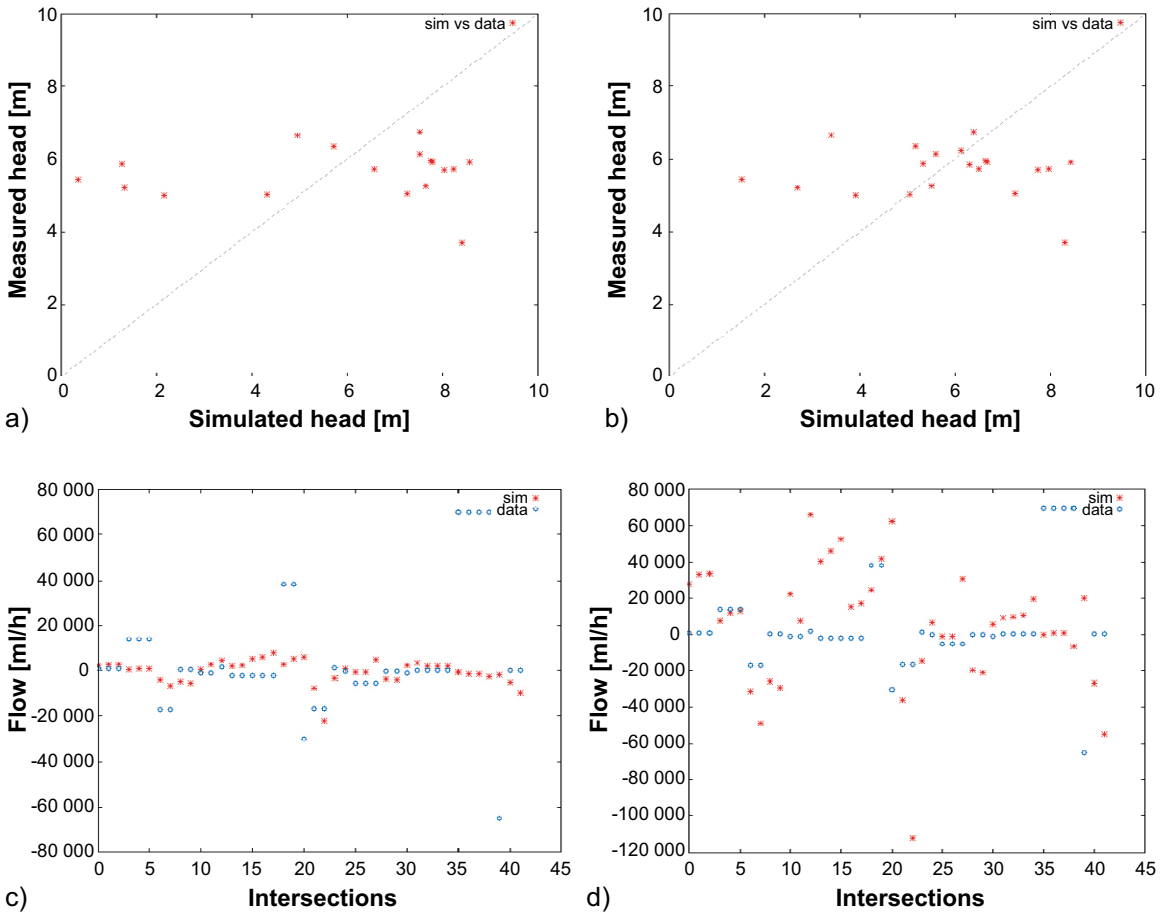

Figure 3-39. *Simulated and measured heads and flows a) simulated heads without open boreholes (SS01) versus measured (y-axis), b) simulated heads versus measured with open boreholes (SS02a), c) simulated (red) and measured (blue) flows at identified intersections for forward model (SS02a), d) flows at identified intersections for model variation SS04b-5.*

Simulations of the KR24 pumping test were performed for the base case only but considered two different methods of implementing the KR24 pumping boundary condition

1) as three linked borehole sections and

2) as two (upper and lower) independent borehole sections.

The second method was felt to provide a better match to observations (Figure 3-40).

Transient simulations

SKB/KTH performed a transient simulation for the KR24 pumping test (TR02a). The storativity S in m/m for the fracture zones was chosen such that the diffusivity $T/S = 0.5$ m^2/s, where T is fracture transmissivity in m^2/s. This value of diffusivity for all fracture zones results in relatively fast pressure equilibration. Figure 3-41 shows the head evolution for selected boreholes and in/outflow evolution for KR22. It is notable that while pressure transients typically last 100–200 hours in some boreholes (e.g. KR22) the induced flow transient extends over the first ~300–400 hours.

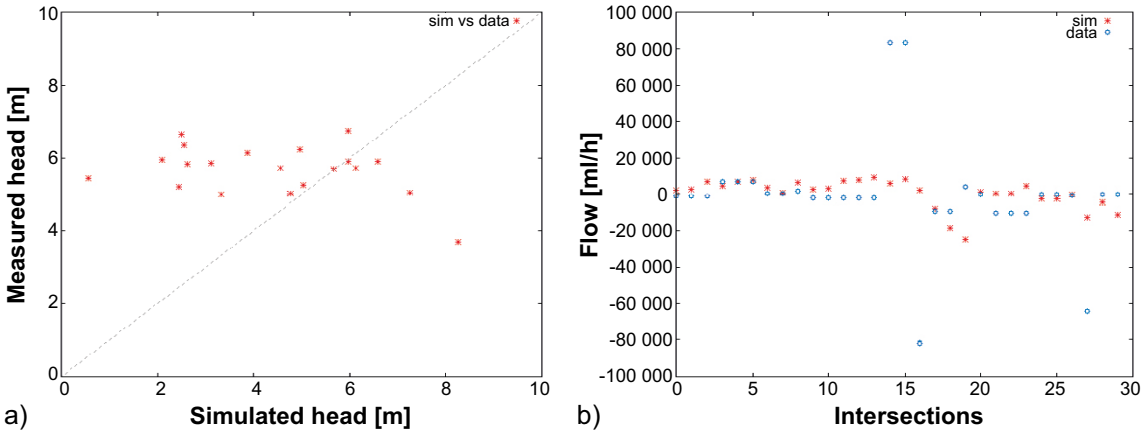

Figure 3-40. *Simulated and measured heads and flows for KR24 pumping test(SS04a) a) model heads for versus measured (y-axis); b) flows at identified intersections.*

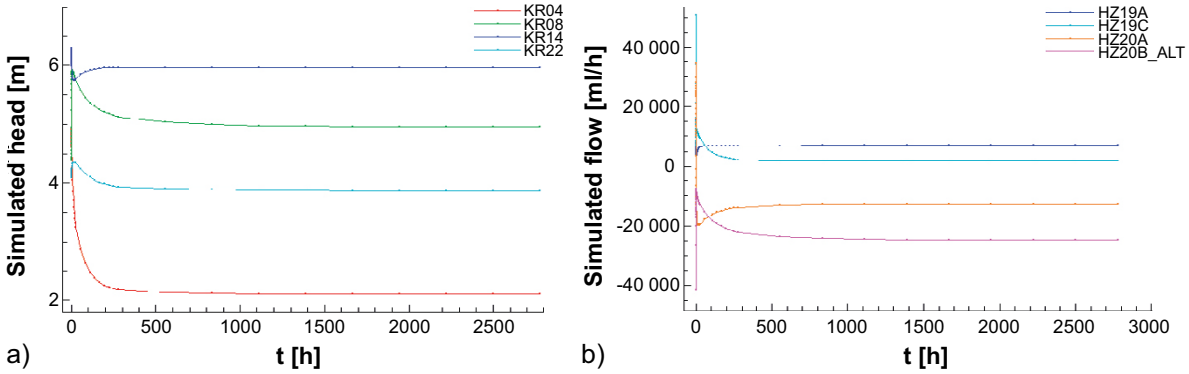

Figure 3-41. *TR02a results: a) simulated heads, b) simulated flows in KR22.*

Task 7A2, 5: Transport simulations

SKB/KTH performed particle tracking calculations (PA01) based on the undisturbed conditions without boreholes (SS01). 1 000 particles were started at each release point. The path lines are shown in Figure 3-42. The path lines show similar trends but vary by release point:

- Release Point 1: most particles traverse through fracture zones HZ19C and HZ20A. Travel times were typically shortest for RP1.
- Release Point 2: most particles traverse through fracture zones HZ19C and HZ20A. A high percentage of the particles released at RP2 became ‘stuck’ and other particles travelled down KR24 (when represented as a low permeability feature k = 10^{-15} m^2) and into HZ20B_ALT. In another simulation where boreholes were completely removed practically no trajectories were obtained from particles injected at RP 2.
- Release Point 3: most particles traverse through fracture zones HZ20A and HZ20B_ALT. Travel times were typically longest for RP3.

For all particle trajectories regardless of release point, fracture zone HZ004 acted as a vertical conductor between zones HZ19C, HZ20A, and HZ20B_ALT, and these latter zones acted as major transport pathways to the model boundaries, i.e. the fracture zones in direct contact with the Baltic Sea. This is most clearly seen in the “side-view” plots in Figure 3-42 where the tracks follow the major zones to the model boundaries.

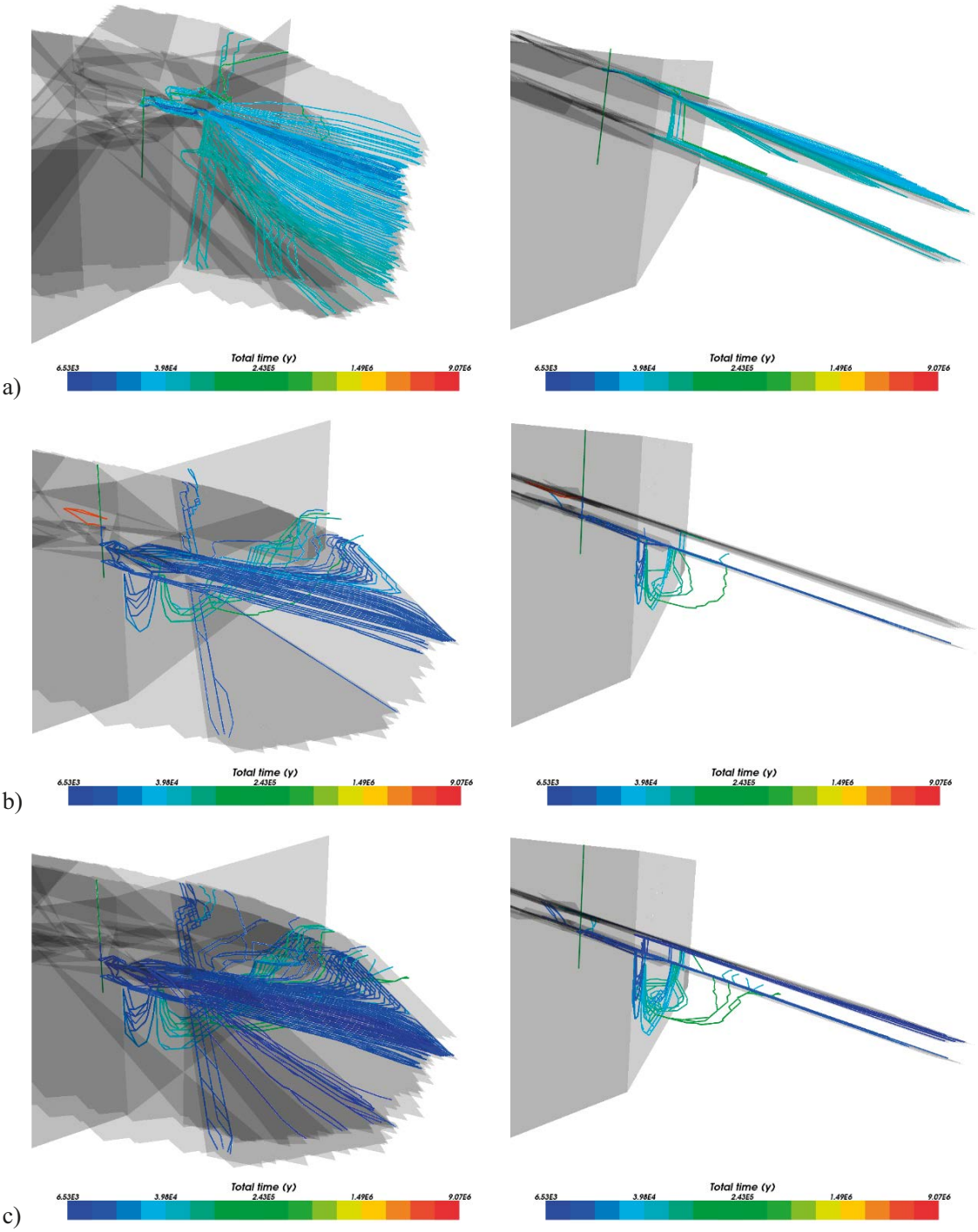

Figure 3-42. *PA01 particle tracks aerial (left) and side view (right): a) Release Point 1, b) Release Point 2, c) Release Point 3.*

Task 7A3 Ideas for calculation of PA-relevant parameters from open borehole information

KTH presented an approach to the use of PFL data at the 23rd Task Force Meeting in Toronto. The approach has not been documented within the Task 7 reporting but related ideas are discussed in Frampton and Cvetkovic (2007). The KTH proposal relates to the hypothesis that:

- PFL measurements may correspond to an approximation of the Eulerian distribution of sub-fracture flow velocities.
- Lagrangian distributions may be approximated by mapping of the PFL measurements.

The methodology is illustrated in Figure 3-43 and is similar to that set out in Frampton and Cvetkovic (2007) whereby Eulerian distributions of travel time created from simulations are mapped and upscaled to Lagrangian distributions suitable for large scale safety assessment. At the Toronto meeting it was suggested that PFL measurements might be used as an approximation of the Eulerian distribution of sub-fracture flow velocities.

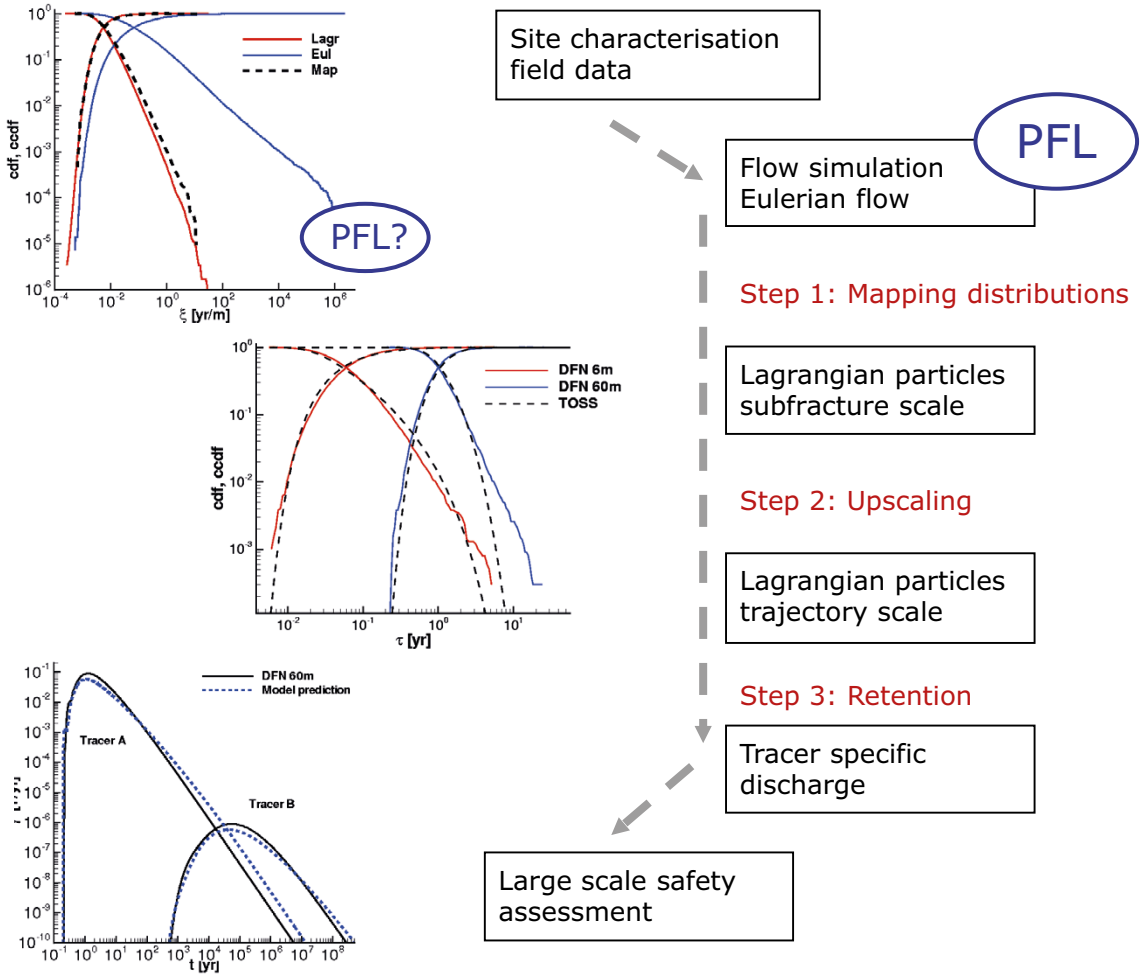

Figure 3-43. *Outline methodology for prediction of transport based on mapping of Eulerian distribution (PFL) to Lagrangian distribution and subsequent upscaling.*

3.6 Model comparison

The modellers' individual evaluations of modelling group results can be found in their own Task 7a reports and within questionnaires (summarised in Lanyon 2009). A short evaluation of different aspects of Task 7A (e.g. the 7A3 work documented in Svensson 2015) is also given in the relevant sections of Lanyon (2009). Here the emphasis is placed on inter-comparison between the groups and extracting common themes.

3.6.1 Task 7A1: steady state flow in undisturbed conditions (SS01, SS02)

For the models without boreholes (SS01) the forward models show relatively high heads near the surface with heads reducing with depth (Figure 3-44a). Heads are highest at depth for the JAEA/Golder and Posiva/VTT-SZ (Small Zone) models, which assume lateral no-flow boundaries. The Posiva/VTT-SZ model is considerably less well-connected than the other models which use the large zone representation (including Posiva/VTT-LZ).

Given that the modelling groups implemented the same structural model (with the exception of the Posiva/VTT-SZ models), differences between the models arise from differences in the boundary conditions and minor differences in the treatment of the near-surface layer. Some differences may also arise from the numerics of the different codes and meshes. The choice of the upper boundary condition drives the near-surface heads on the island and the connectivity to the flow boundaries controls how head dissipates. The highest heads are in the JAEA forward model which assumed an upper boundary where hydraulic head was equal to elevation and the lateral boundaries were no-flow.

The effect of the boreholes on hydraulic heads can be seen in Figure 3-44a,b, and Figure 3-45 but is most clearly shown in the Posiva/VTT and NWMO/Laval models where the inclusion of the low permeability background rock facilitates contouring of heads as shown in Figure 3-46. The boreholes take high heads from the island topography deep into the bedrock, significantly changing the pattern of hydraulic head. The extent of this phenomenon is probably exaggerated within the models because:

- The absence of smaller fracture zones and the low hydraulic conductivity of the background rock within the models enhances downward flow along the boreholes as these provide almost the only significant transmissive vertical features within the models.
- Steady state simulations ignore the time taken for such head disturbances to propagate through the rock (which may be significant for large blocks of low diffusivity rock).

It should also be noted that these models are not calibrated to the site data.

The discussion has focused on the groundwater head, but the PFL data provides insights into the flows associated with the boreholes. The data from deep boreholes show strong flows from zones below the casings down to zones in the deeper bedrock. For example in KR28, the PFL data shows flow of about 1 l/min from HZ19C at about −150 m.a.s.l. down the borehole to HZ20A at about −400 m.a.s.l. Unfortunately the modellers interpreted the Task Definition as only requiring them to report flows in the two KR24 sections for SS02a and SS02b and only JAEA provided any distribution of flow within these sections.

While the models clearly show the difference in head caused by the boreholes it is not clear to what extent this resulted in changes to the pattern of groundwater flow within the models. This is largely due to the very limited reporting of flow values either in boreholes or in the rock within these simulations[11].

[11] CFE also calculated the vertical flux across a 1 200 m × 1 200 m horizontal plane centred on KR24.

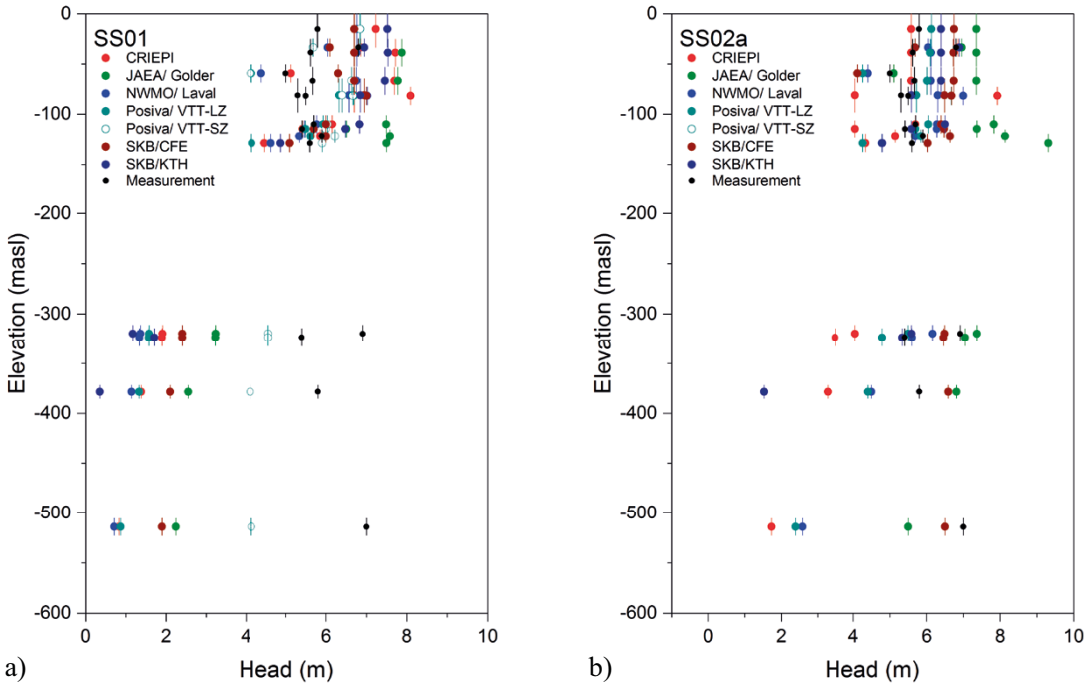

Figure 3-44. *Simulated heads a) base case without boreholes (SS01) and b) with boreholes (SS02a).*

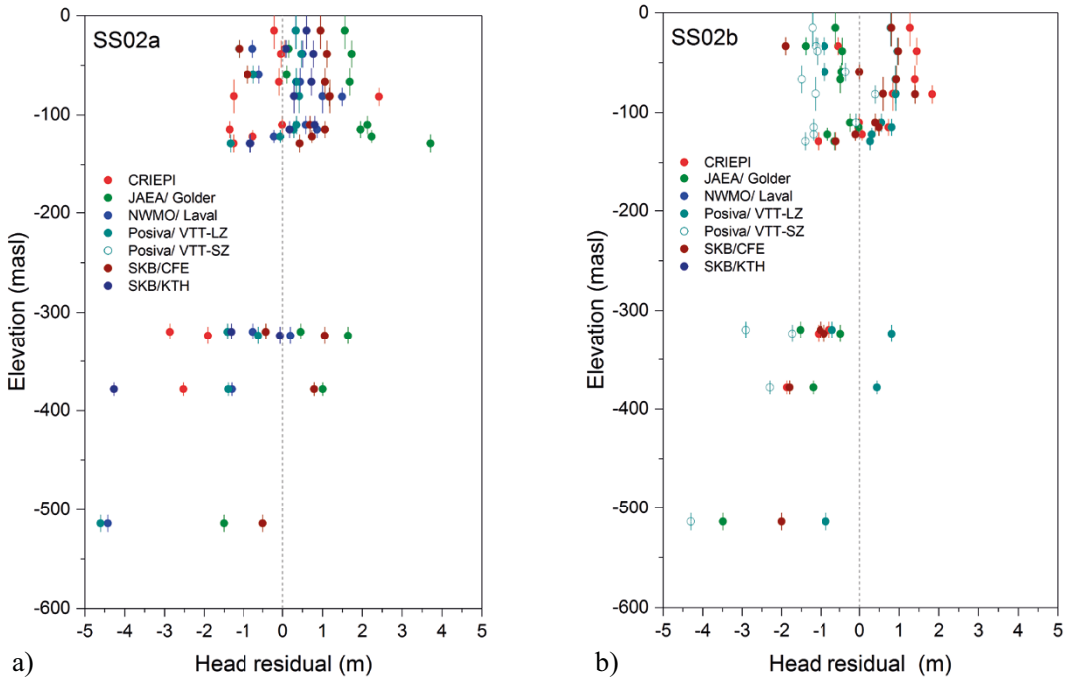

Figure 3-45. *Head residuals (simulated-measured) for a) base case with open boreholes (SS02a) and b) calibrated model (SS02b).*

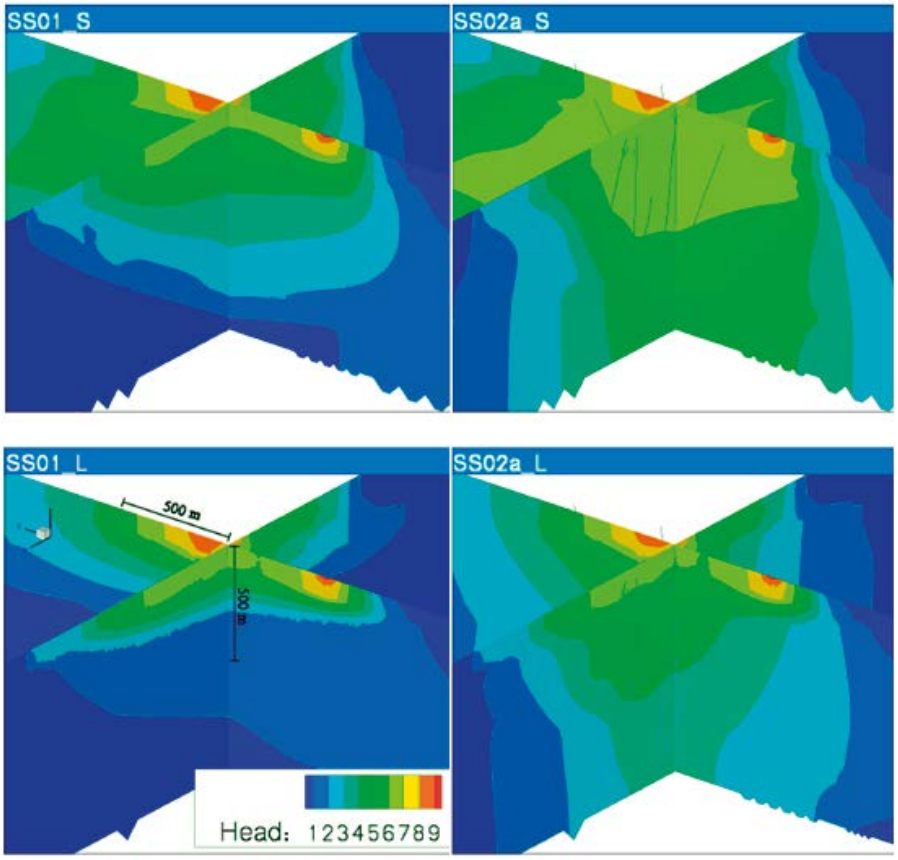

Figure 3-46. *Contoured head for the Posiva/VTT models for SS01 and SS02a: a) small zone models; b) large zone models (from Keto and Koskinen 2009).*

3.6.2 Task 7A1: steady state flow in pumped conditions (SS03, SS04)

Effect of monitoring holes

The effect of the monitoring boreholes is seen most clearly in models containing an explicit representation of the background rock (Posiva/VTT and NWMO/Laval) making it simple to contour the drawdown as shown in Figure 3-47. The monitoring boreholes clearly spread the response to pumping to greater depth. Without the monitoring boreholes, the drawdown is focused in a sub-horizontal layer related to the major zones intersected by the lower borehole section. The inclusion of the boreholes results in drawdowns reducing more quickly with radial distance but extending in the vertical direction as flow is diverted from different zones into KR24.

A comparison of the calculated drawdowns from the pumping boreholes for SS04a and SS03 (JAEA and NWMO/Laval provided calculated head rather than drawdown) is given in Table 3-3. Drawdowns are typically larger in the SS03 simulations although only very slightly so in the CRIEPI simulations. The reason for the spread in drawdown in the lower part of KR24 reported by SKB/CFE is because they calculate drawdown from the undisturbed heads (SS01).

Table 3-3. Drawdowns (m) in the upper and lower sections of pumping borehole KR24 from SS03 and SS04a.

		CRIEPI	Posiva/VTT-LZ	Posiva/VTT-SZ	SKB/CFE	Measured
SS03	Upper	29.9	21.4	23.6	19.2	n/a
	Lower	12.1	21.4	16.93	3.1–7.7	n/a
SS04a	Upper	29.9	10	23.2	18	18
	Lower	12.1	20	12.2	5.4	1.2

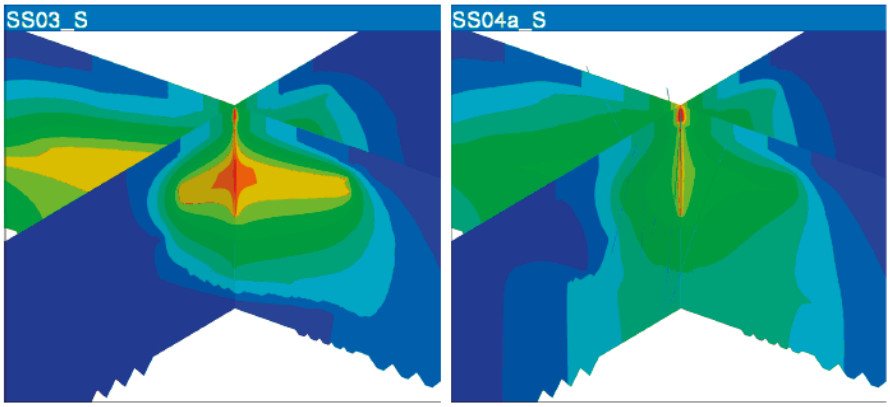

Figure 3-47. *Contoured "normalised" drawdown for the Posiva/VTT small zone models for SS03 (no monitoring boreholes) and SS04a (including monitoring boreholes) uncalibrated models (from Keto and Koskinen 2009).*

Forward and calibrated models

Figure 3-48 shows distance drawdown plots from the performance measures provided by the different modelling groups for the forward and calibrated/conditioned simulations of the KR24 pump test. The best matches to overall shape are from SKB/CFE, CRIEPI and Posiva/VTT-SZ simulations. Drawdown in the JAEA models is typically too high as are the drawdowns from SKB/KTH. Distant drawdowns from Posiva/VTT and JAEA are also high but this may relate to the steady state assumption as suggested by Posiva/VTT. Only Posiva/VTT achieve a drawdown in the lower section close to that measured but this was with a significantly reduced flow from the upper section. Otherwise the simulations from CRIEPI and SKB/CFE are the closest to the measured values.

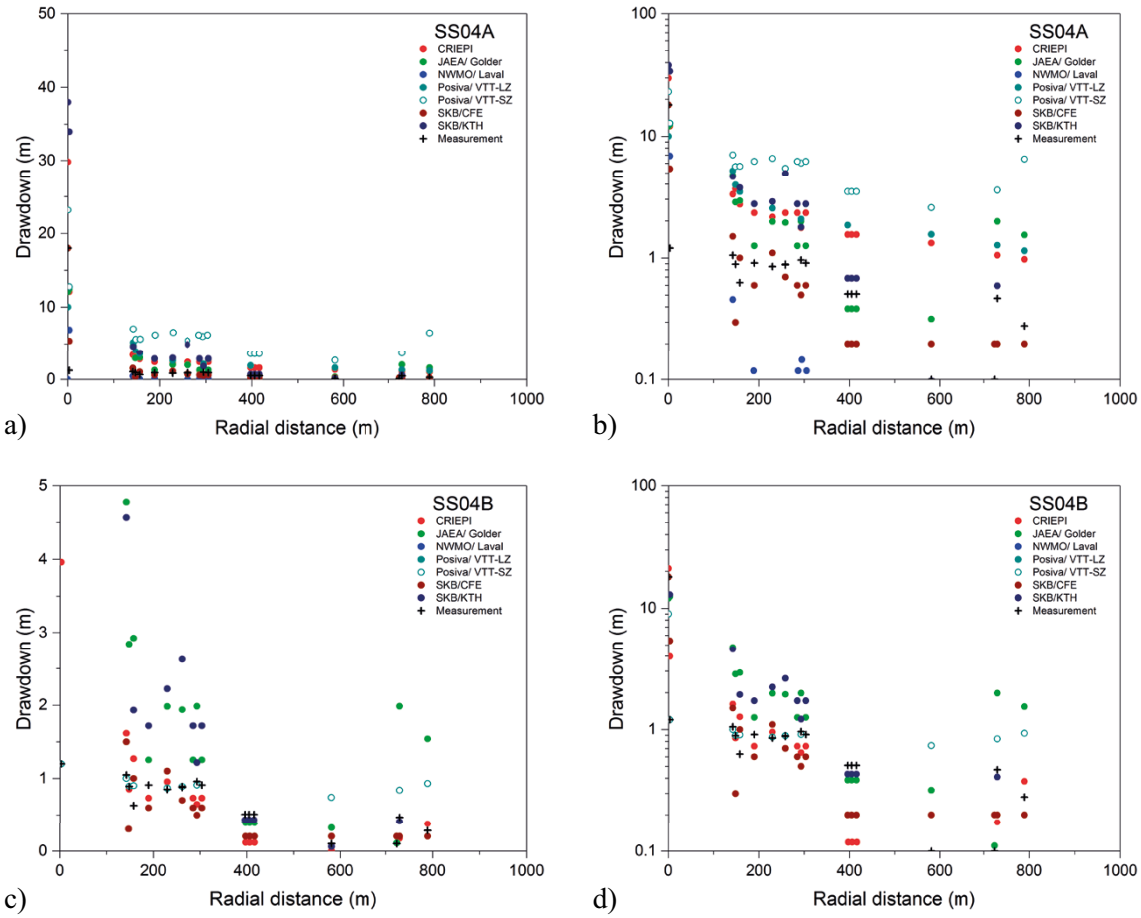

Figure 3-48. *Simulated and measured drawdowns for SS04a and SS04b for linear and logarithmic y axes.*

Although none of the models achieved both a good match to the KR24 drawdown and the overall shape of the distance drawdown curve, the models of CRIEPI, SKB/CFE and Posiva/VTT provided the best match, with the caveat that Posiva/VTT changed the flow-rate from the upper section of KR24 (arguing that much of the flow came from the overburden). All these models applied "skin terms" or assumed in some way heterogeneous fracture zones.

The JAEA, SKB/KTH and NWMO/Laval modellers all had problems in calibrating their models when assuming uniformly transmissive zones. A comparison of the different modelling group approaches to calibration to the pump test is given in Table 3-4 and an evaluation of the general approaches is given in Table 3-5.

Table 3-4. Summary evaluation of the different modelling groups' approaches to calibration of the pump test.

Modelling Group	Method	Evaluation
CRIEPI	Patch model	Inclusion of local transmissivities from PFL measurements improves match to drawdown and flow.
SKB/CFE	Local DFN (skin), near-surface layer model	Local skin and surface layer models improve fit.
JAEA	Sensitivity study based on Zone *T*	No improvement from conditioning on pump test, probably due to constraints of the conceptual model (e.g. assumption of uniform zone transmissivity).
NWMO/Laval	PEST	Fails due to lack of sensitivity when treating zones with uniform transmissivity.
Posiva/VTT	Addition of zone, modification of zone T, geometry + local skins	Most extensive model revision and change to KR24 upper section boundary conditions that significantly improves reproduction of KR24 responses. Local refinement produces "KR24 pump test model".

Table 3-5. Evaluation of different general approaches to calibration of the pump test.

Method	Evaluation
Inclusion of PFL data	Harder to match but better confidence in models than match to head data alone.
Inclusion of local transmissivity variation/skin	In general, resulted in improved model fits but fitting method added many additional largely independent parameters.
Modification of Zone T	On its own not enough to give significant improvement in model fits.
Inclusion of extra data/ knowledge (changing the CM)	VTT site knowledge and CRIEPI use of local transmissivity, helped in the development of better models.
Automated methods	Additional work in model setup and "learning curve". Clear advantage in terms of sensitivity/uncertainty information but it was not possible to apply these within Task7A1.

3.6.3 Task 7A1: Transient flow in pumped conditions (TR01,TR02)

Only results from forward transient models were presented by modelling groups as listed in Table 3-6. Several different assumptions were made concerning the storage associated with fractures and background rock. The simulated drawdowns in all the models approached approximate steady state conditions by the end of the pump test and typically did not show the late-time linear trend observed in the raw data. They were a better match to the detrended data as shown in the simulations performed by NWMO/Laval. The use of the detrended data is recommended in Vidstrand et al. (2015) who argue that the linear decline of approximately 1 cm/day is probably caused by variation in recharge at the site.

Table 3-6. Transient simulations performed by modelling groups.

Group	Transient Simulations	*T-S* relationship	Relationship to steady state
CRIEPI	TR01,TR02a	$S = 2T^{12}$ (+variant)	Approximate steady state by shut-in
SKB/KTH	TR02a	S = 2T	Approximate steady state < 300 hrs (longer for flow than head)
SKB/CFE	TR02a	$S_s = 10^{-6}$ m^{-1}	Approximate steady state by shut-in
NWMO/Laval	TR01,TR02a	$S_s = 3.5 \times 10^{-6}$ m^{-1}	Approximate steady state < 500 hrs

3.6.4 Task 7A2: Transport simulations

All groups apart from Posiva/VTT performed transport simulations. The transport simulations typically used "particle tracking" approaches although NWMO/Laval also used a "life expectancy" approach (see Therrien et al. 2005, Cornaton et al. 2008). Typical particle tracks from the different models are shown in Figure 3-49.

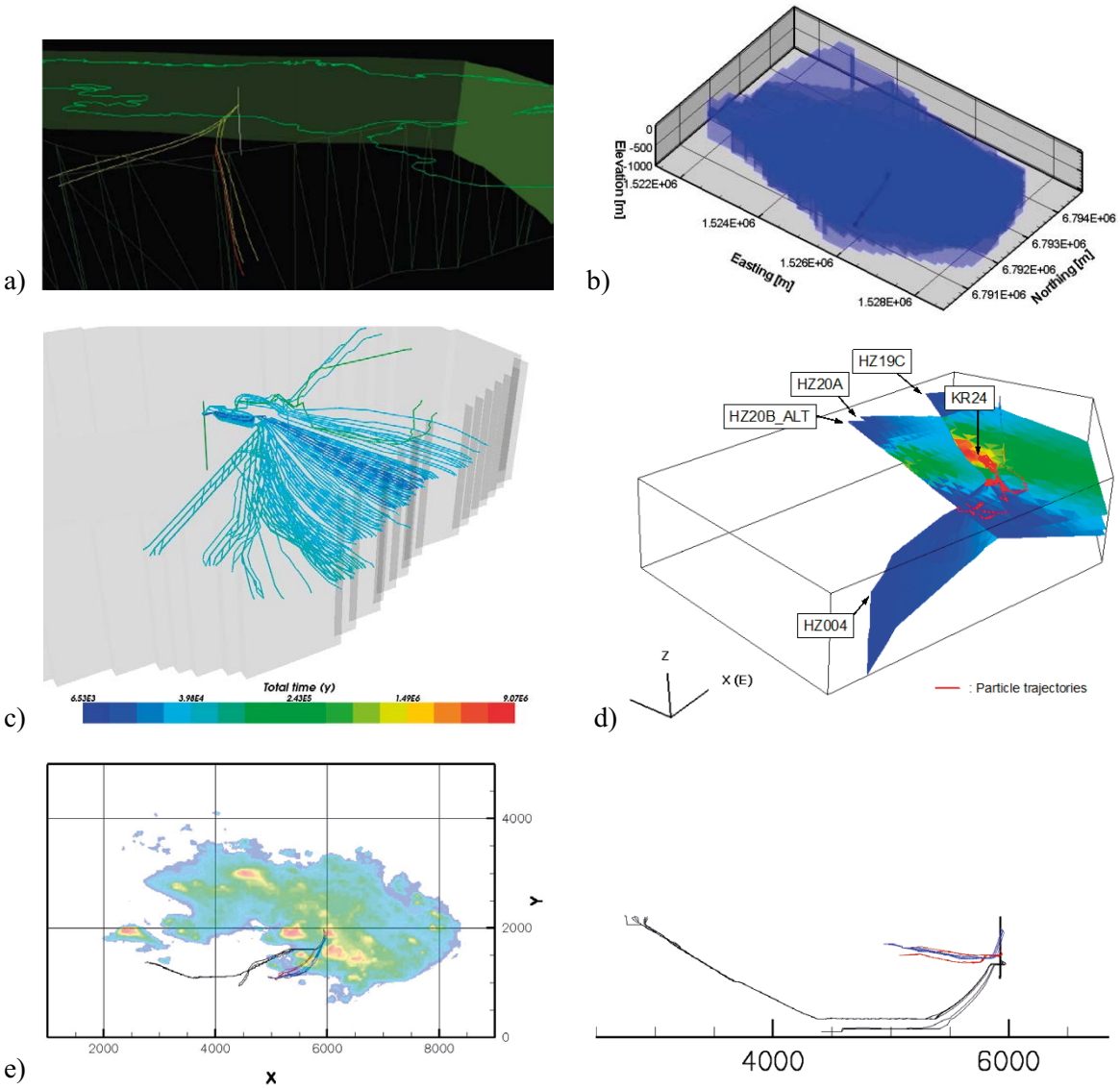

Figure 3-49. *Particle tracks from the different models. a) CRIEPI view from south, b) Laval University tracks can be seen as narrow dark shaded line from KR24, c) KTH, d) JAEA and e) CFE plan and section showing particle tracks.*

[12] This equation relates the transmissivity T (m^2/s) of a feature to its storativity (m/m). Essentially it sets the diffusivity of all features to 2 m^2/s.

The boreholes had no hydraulic effect in these simulations[13]. The end points were to be the model boundaries. In general the tracks from the three starting points along KR24 initially move south through the zones but are then influenced by the different model boundary conditions. Where the lateral boundaries are specified as constant head, particles may travel to either the model lateral boundaries or the surface through the network of deterministic zones. However in the models where the sides are treated as no-flow boundaries (JAEA), particles must migrate into the near-surface layer and discharge on the upper model surface (the seabed). Within the SKB/CFE simulations the particle tracking algorithm was stopped after simulation times of 100 years due to the very slow velocities calculated in the surface layer. Table 3-7 presents the advective travel time statistics.

Table 3-7. Advective travel times in seconds reported by modelling groups for release at 3 points along KR24 trajectory.

Group	Release Point 1			Release Point 2			Release Point 3		
	Mean	Median	95 %	Mean	Median	95 %	Mean	Median	95 % s
CRIEPI	2.0E+08	2.0E+08	3.0E+08	6.2E+08	6.2E+08	6.2E+08	3.4E+09	3.2E+09	4.9E+09
JAEA (total)	3.2E+10	1.9E+09	8.6E+10	8.5E+11	1.2E+11	4.2E+12	1.8E+12	2.1E+11	1.7E+12
JAEA (zones)	2.1E+08	1.3E+08	8.7E+08	2.0E+09	1.7E+09	3.5E+09	2.1E+09	1.9E+09	3.1E+09
KTH[14]	1.5E+10	1.2E+10	2.4E+10	5.4E+11	4.3E+11	1.4E+12	4.4E+11	3.4E+11	7.4E+11
University Laval[15]		2.1E+9			>4.8E+9			>4.8E+9	
CFE	Particles stopped at 100 years (3.16E+9 seconds)								

NWMO/Laval used a life-expectancy approach (Therrien et al. 2005, Cornaton et al. 2008) to develop the probability density functions for solute travel time. The simulations were performed for a maximum of 55 000 days and as a result only the median time for RP1 can be estimated (see Table 3-7). The approach required an advective-dispersive transport model and so is not strictly comparable with purely advective treatments.

There are differences in the numbers of particles tracked and in particle tracking assumptions between the different simulations. However the overall direction of particles appears to be similar (although the CONNECTFLOW simulation from KTH shows a much greater spread of possible paths[16]).

The JAEA results were provided as both the total travel time and the travel time spent within the major zones. The total travel time was dominated by time spent within the 80 m-thick surface layer. As the model boundaries were impermeable, particle paths were forced into the relatively high porosity surface layer where gradients were low. As a result only about 1 % of the travel time was spent in the zones. In contrast the CRIEPI model allowed flow to the lateral boundaries and so the particle paths did not enter the surface layer. The SKB/KTH travel times, although again likely to be largely through the major zones are typically an order of magnitude greater than the CRIEPI times, despite assuming lower transport apertures. This is possibly caused by the mixing assumed at fracture intersections.

[13] Some models included “low permeability” representations of the boreholes for numerical convenience e.g. to create a well-defined intersection point within the model.

[14] Many of the particles injected at the second release point became stuck.

[15] Transport simulations stopped after 55 000 days (4.8E9 seconds).

[16] CONNECTFLOW assumes “perfect mixing” at points along feature intersections within its particle tracking algorithm. In a low hydraulic conductivity network of open fractures, diffusion across the fracture intersections should result in perfect mixing of any solutes entering the intersection at the low flow velocities expected after repository closure.

The general direction of flow is similar and the “discharge” points where paths leave the models are relatively consistent (depending on the choice of lateral boundary conditions) between the different simulations (both calibrated and uncalibrated) which suggest that these features are a consequence of the specified hydrostructural model. Factors controlling the total travel time seem largely to relate to the regional boundary conditions and the treatment of the surface layer. It is unlikely that uncertainties in the treatment of these features would be reduced by analysis of the KR24 pumping test.

3.7 Evaluation

This section is taken directly from the discussion and conclusions section of Lanyon (2009).

3.7.1 PFL data analysis

Undisturbed conditions

The power of the PFL data and the possibility to reduce uncertainty are illustrated in Posiva/VTT’s EnKF models. In particular the sensitivity of the models to connections between zones and more importantly to the overburden (or near-surface water bodies) is likely to provide valuable information for site characterisation.

The PFL data sensitivity to near-surface connections and local borehole properties compared to head measurements does, however, make it more difficult to match within regional scale models. The “short-circuiting” of flow along open boreholes further complicates modelling and requires the inclusion of local properties around the borehole intersections to correctly model flow directions in the boreholes. Thus the base-case hydrostructural model presented in the Task Definition was probably not consistent with the calibration to the PFL data, which may explain the problems encountered by JAEA and KTH when calibrating to this data without using borehole skins.

Pumping tests

The methods for PFL analysis of pumping test data described by Posiva/VTT and illustrated in Figure 3-50 provide a practical framework for such studies. The calibrated model developed by Posiva/VTT illustrates how such results can then be implemented within numerical models. The emphasis on change in flow-rate as the calibration target rather than the measured flow-rate itself has clear advantages. CRIEPI also used change in flow in their evaluation of the models, while JAEA and SKB/KTH were less successful using the measured flow-rates.

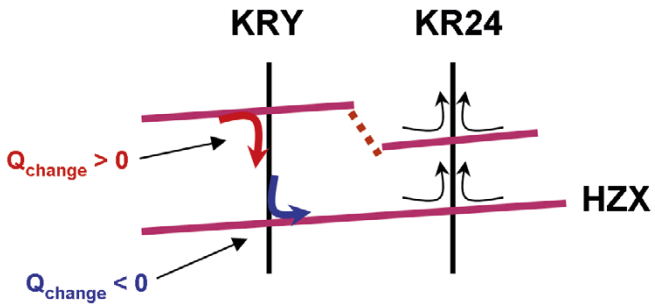

$Q_{change} < 0$	Flow from HZX to KRY decreases when pumping at KR24	There is a good connection from point KRY_HZX to KR24
$Q_{change} > 0$	Flow from HZX to KRY increases when pumping at KR24	There is a more conductive route from KRY_HZX to KR24 than through HZX

Figure 3-50. *Guidelines to interpret the observed changes in PFL measurements.*

It is clear that the PFL data is strongly affected by the local properties of the fracture zones and this requires either:

- inclusion of zone heterogeneity (e.g. heterogeneous model of CRIEPI), or
- the acceptance of "non-physical" (in Posiva/VTT's terms) changes to large scale properties and the development of models tuned to only the KR24 test (see comments by Keto and Koskinen 2009).

Conclusions

It would appear that it was more difficult to match flow data (PFL under undisturbed conditions) or induced changes in flow (PFL under pumped conditions) than to match heads and drawdowns. This is almost certainly due to the dependence of flow response in/out of the borehole on local fracture properties at the borehole and more generally on a strong dependence on "connectivity" for the induced flows along the boreholes.

Measurements of head and drawdown are typically much less sensitive[17] to local properties than measurements of flow or transport (see for example Butler 1991, Oliver 1993, Meier et al. 1998) and the effective feature transmissivity can usually estimated by the use of transient analysis (Meier et al. op cit, show this for Cooper-Jacob analyses of flow in heterogeneous 2D features, see also Walker et al. 2006) or from the geometric mean transmissivity from small-scale tests.

In their evaluation of Task 1 Gustafson and Ström (1995) comment that "The pressure field is rather insensitive to the underlying conceptual model, whereas the transport outputs like breakthrough curves are more sensitive". It appears that the PFL flow data is more like transport data than head data and hence may be helpful in developing a much stronger understanding of the flow distribution in the rock than can be achieved by head measurements alone. However the use of PFL flow data is complicated by the sensitivity to near-borehole properties and the requirement to model flow within the boreholes themselves.

3.7.2 Modelling of boreholes for site characterisation

All the modelling groups have developed site-scale models of Olkiluoto based on the hydrostructural model provided by the Task Force. The numerical codes have successfully simulated flow to/from and within the boreholes in steady state and transient modes to address the question of the effect of boreholes at the site and to simulate results from PFL logging. The ability of the numerical codes to do this was an issue at the start of the Task and it is clear that all the modelling groups possessed the facilities and experience to adequately consider such issues.

All the groups developed improved methods for handling the head and flow data from boreholes within the task, but several groups developed new facilities within the numerical codes to better address these issues:

- SKB/CFE: Borehole implementation for open, packed off and pumped conditions: development, testing.
- NWMO/Laval: More flexible treatment of fracture intersection geometry.
- Posiva/VTT: PFL result calculation within FEFTRA using FEM solution.

The codes used by CRIEPI, SKB/KTH and JAEA already included facilities for handling borehole data at the start of the task.

[17] Local low transmissivity may however result in a significant "lag" in monitoring borehole responses (see Black and Kipp 1977).

3.7.3 Effect of open boreholes

The effect of open boreholes on the groundwater flow system under natural and pumped conditions has been considered. The models suggest that the head field is significantly altered by the open boreholes and that, at least, locally flow paths are significantly changed. In addition the boreholes may induce longer term transients by mixing waters from the surface with deeper waters.

It would also appear that the boreholes play a significant role in groundwater flow during pumping where water may "short-circuit" along the boreholes to connect to the most transmissive paths into the pumping borehole. Analyses of such large-scale pump tests that do not include the effect of the open boreholes are likely to overestimate the connectivity and effective hydraulic properties of the rock mass.

While the simplified hydrostructural model with its emphasis on a small number of mostly sub-horizontal fracture zones and absence of any "background rock" is likely to exaggerate the significance of the boreholes as conduits for vertical flow, the relatively good performance of some of the calibrated models and (more significantly) the PFL measurements from the site suggest that the boreholes play a significant part in the deep groundwater flow system at the site.

3.7.4 Modelling approaches

The modelling approaches used were largely dictated by the Task Definition and the common hydrostructural model. In essence all the models were based on a single simplified structural model and the only differences were due to the different implementations within the codes (e.g. CPM vs DFN) or differences in model boundary conditions. A very limited consideration of model variants using both the "Large" and "Small" representations of the deterministic fracture zones was undertaken by VTT.

Different approaches were, however, taken with regard to the inverse modelling including:

- Trial and error calibration of zone transmissivity (KTH and VTT).
- Limited grid search on zone transmissivity (JAEA).
- Automated parameter optimisation (Laval University using PEST).
- Use of local transmissivity data to condition zone transmissivity (CRIEPI).
- Use of Ensemble Kalman Filter (VTT).
- Use of additional site knowledge (VTT).

3.7.5 Reduction in uncertainty in PA properties

With regard to transport and reduction of uncertainty in performance assessment from calibration of the models to the KR24 pump test, there has been less success. This has been due to:

- Limitations in the data quality: form of the pump test and uncertain influence of natural trends in groundwater level.
- Limitations in the ability of a single pump test to constrain large scale flow paths (e.g. influence of near-surface layers and lateral boundaries on flow paths).
- Difficulty in performing inverse modelling on either highly simplified site models or models with potentially large numbers of degrees of freedom.

Conditioning of the models by CRIEPI and manual adjustment by Posiva/VTT and SKB/CFE certainly improved the matches to observation (particularly heads) but it is hard to argue for uniqueness or for any constraint on the possible transport behaviour other than the need to include local transmissivity heterogeneity within the zones to match observed heads and flows.

The suggestions made in the studies presented for Subtasks 7A3,4 show promise in developing tools for assessing the reduction in uncertainty, modelling the pattern of post-closure flow and use of PFL data; however they need further development and demonstration.

3.7.6 Summary

A summary of Task 7A against its goals as defined in the Task Definition is given in Table 3-8.

Table 3-8. Overall evaluation of Task 7A.

Goal	Evaluation
To understand the major features of groundwater system	Achieved within the limitations of the imposed conceptual model.
Understand the consequences of the tests/ measurement systems	Achieved in general, but specifics of PFL responses are complex.
Understand how to model open boreholes within site characterisation studies	Achieved (improved methods implemented in some codes).
Understand how to model open boreholes for provision of parameters for PA	This remains a challenge for Task 7B, where it may be more appropriate given the focus on the background rock.
Understand how PFL measurements could reduce uncertainty	Better understanding but needs quantitative methods (such as Ensemble Kalman Filter)
Increase understanding of compartmentalisation and connectivity	Limited by the form of the KR24 pump test and data quality (influence of natural trends).
Evaluate how uncertainty in PA can be reduced	Not enough work on transport or range of models to demonstrate reduction in PA uncertainty. The transport properties considered in the Task were largely controlled by the model boundary conditions and the simplified regional hydrostructural model.
Introduction to Olkiluoto site	Achieved

4 Task 7B Reduction of performance assessment uncertainty through block scale modelling of interference tests in KR14–18 at Olkiluoto, Finland

Task 7B considers a smaller rock volume based on a 500 m × 500 m region surrounding the KR14–KR18A group of boreholes at the Olkiluoto site in Finland. This represents a sub-volume of the region considered within Task 7A. Task 7B is documented within the series of SKB P series reports covering Task 7:

- KAERI: Ko and Ji (2017).
- JAEA: Sawada et al. (2015).
- NWMO/Laval: Therrien and Blessent (2017).
- Posiva/VTT: Krumenacker et al. (2017).
- SKB/CFE: Svensson (2015).
- SKB/KTH: Frampton et al. (2015).

CRIEPI initially participated in Task 7B but withdrew due to the illness of a key investigator and did not submit a report on their work.

4.1 Task 7B Objectives

The aim and scope of Task 7B was to simulate the performance of the groundwater system and its response to different cross-hole pumping tests in the presence of open and sealed-off boreholes, by building and testing the sensitivity of numerical groundwater flow models of the KR14–18 region of the Olkiluoto site. An important aspect of the data from the site is the use of the Posiva Flow Log to measure flow into/out of the boreholes during "undisturbed" and pumped conditions and the possibility to compare this "flow response" data to "pressure response" data from packer tests performed in the same boreholes. The complete Task 7B Task Description is included within Vidstrand et al. (2015).

4.1.1 Task Objective

The main objectives of Task 7B were

- to assess the Posiva Flow-logging (PFL) data when analysing the rock (rock mass),
- to quantify the reduction of uncertainty in the properties of the fracture network.

A further set of goals was specified to evaluate how uncertainty in PA can be reduced based on the analysis of the Olkiluoto dataset

1. to understand how major features could be used as boundary conditions,
2. to understand the minor features of the groundwater system, (background rock),
3. to understand the consequences of the tests and measurement systems used, e.g. the open boreholes,
4. to understand how to model open boreholes within site characterisation studies and for the provision of parameters for PA,
5. to understand how PFL measurements could reduce uncertainty in models as compared to models calibrated with only head measurements,
6. to increase understanding of compartmentalisation and connectivity at the block scale.

4.2 Task Definition and Structure

The task was organised as three subtasks:

- Task 7B1 focused on documenting the modelling groups' conceptual models and planned methodology.
- Task 7B2 focused on the numerical modelling of the hydraulic tests (PFL and "classical" pump tests). The modelling included forward modelling, model calibration and "blind" prediction phases.
- Task 7B3 focused on a "Bayesian" update based on lessons learned (during 7B1,2) and collaboration within the Task Force.

4.3 Task 7B dataset

The Task 7B dataset documented a series of hydraulic tests performed in 5 deep boreholes within the 500 m × 500 m block. The tests included both PFL logging (in open boreholes) and packer tests with multiple monitoring intervals. The tests are known as the "KR14-KR18 tests". The boreholes and nearby major fractures zones are shown in Figure 4-1 and listed in Table 4-1. B-series boreholes (e.g. KR15B[18]) are drilled close to the equivalent deep borehole and completed to provide monitoring of the near-surface flow system.

Prior to packer testing, PFL logging was performed to identify the most transmissive features in each of the boreholes (Pöllänen and Rouhiainen 2002a, b). In a first phase of pump testing (between January 2000 and March 2002) each of the five deep borehole open-hole sections was pumped for about 10 days followed by a recovery period of a few days prior to pumping the next borehole (Rouhiainen and Pöllänen 2003). The drawdowns ranged from 6–11 m and the aim was to achieve steady flow conditions during the pumping.

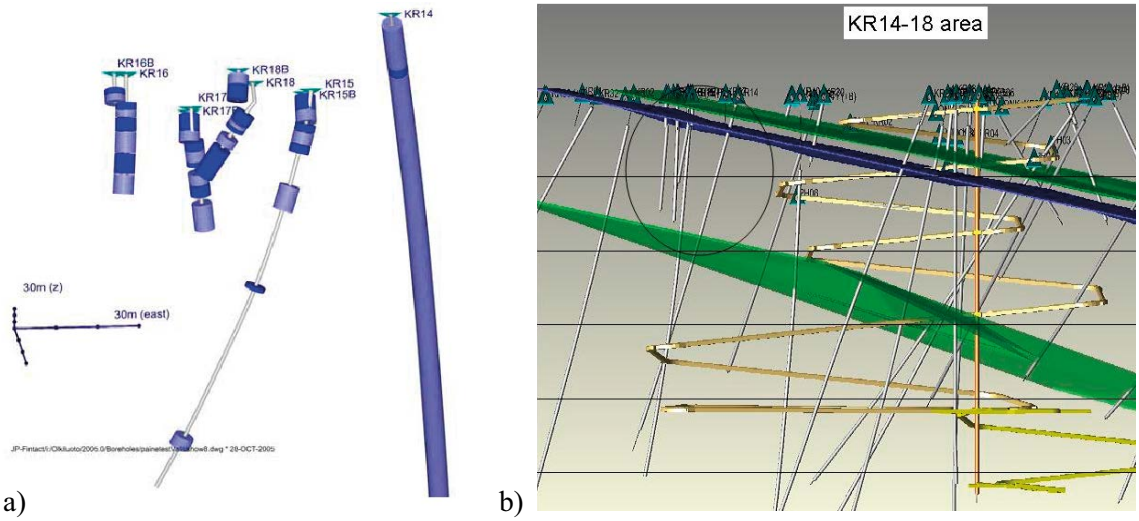

a) b)

Figure 4-1. *KR14-KR18 boreholes: a) monitored sections and b) the three major fracture zones of significance for the model domain. Structure HZ19A located at top (Site Model 2006).*

[18] Where two boreholes were drilled at the same location, the main deep borehole is given a postscript A (e.g. KR18A) and the shallow borehole B (e.g. KR1*B). In this report where no poscript is given (e.g. KR18) the references is to the deep borehole.

Subsequent to the open-hole pumping tests, packer systems were installed in the boreholes and a series of hydraulic tests were performed in the boreholes between September and November 2004:

- Phase 1: Pumping of open hole section of KR14 (outflow 25 l/min).
- Phase 2: Pumping of open hole section of KR17A (outflow 5–7 l/min).
- Phase 3: HTU Injection tests in 3 intervals of KR18A.
- Phase 4: HTU Injection tests in 4 intervals of KR18A.

Table 4-1 Boreholes and monitoring completions (see Figure 4-1a) KR14-KR18 tests.

Borehole	Casing depth (m)	Total depth (m)	Completion during KR14-KR18 tests
KR14	9.52	514.1 (70° inclination)	3 intervals L1, L2, L3
KR15A	39.98	518.8	6 intervals L1-L6
KR15B	4.48	45	2 intervals L1, L2
KR16A	40.23	170.2	6 intervals L1-L6
KR16B	4.48	45	3 intervals L1, L2, L3
KR17A	39.93	157.13	6 intervals L1-L6
KR17B	4.1	45	2 intervals L1, L2
KR18A	39.81	125.49	4 intervals L1-L4
KR18B	6.51	45	2 intervals L1, L2

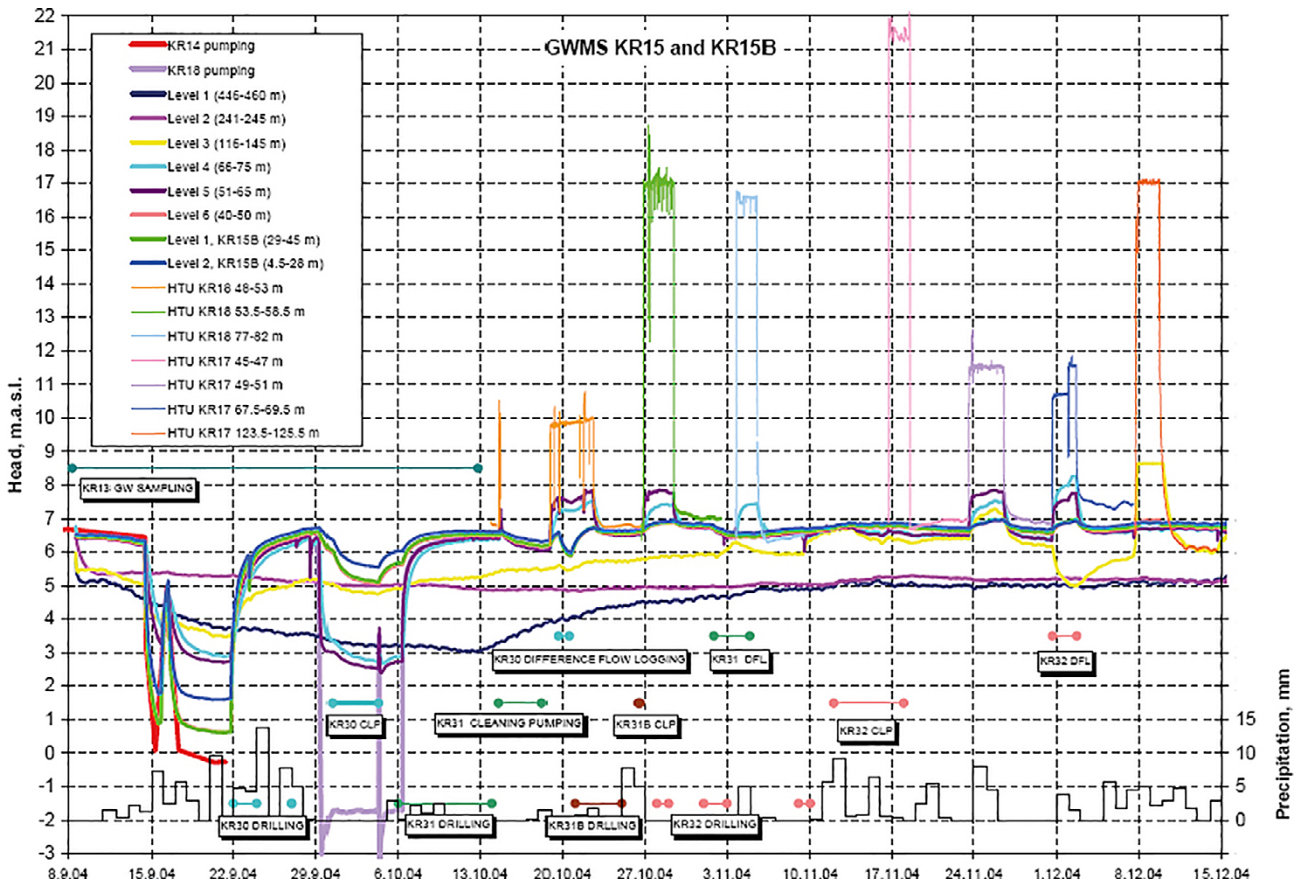

Figure 4-2. *Illustration of results of the KR14–18 pressure interference tests (September-December 2004).*

The modellers were provided with the following data:

- Borehole geometry and schedule of packer system locations.
- Single-hole PFL logging results as
  - transmissive features correlated to oriented features in core, and
  - transmissive features that could not be correlated to core.
- PFL data and measured water level responses from open hole testing phase (2001–2002).
- PFL data and measured head response from pressure interference testing phases 1–2.
- Flow and head data from pressure interference testing phases 3–4.
- Geometry of the major fracture zones (HZ-model 2008).
- Ground surface topography and water table plus digital model of wetlands estimated recharge.

4.3.1 Simulations

A list of simulations was specified in the Task Description covering:

- Undisturbed conditions with open and packed-off boreholes.
- PA-relevant conditions without boreholes.
- Pumped conditions with monitoring boreholes either open or packed-off.

The test configurations considered in the simulations are listed in Table 4-2. Both steady state and transient simulations were specified. A simulation sequence was suggested with the goal of improving "global" model performance rather than adjusting models locally for each test configuration. At each calibration stage a forward model was performed (e.g. SS23a) prior to the calibrated model (e.g. SS23b). The "predictive" simulation of the KR15A extraction was intended to provide a test of the proposed simulation scheme. The response data to pumping in KR15A was withheld from the modellers although it was potentially available via published reports.

Table 4-2 Testing configurations specified for simulations in Task 7B.

Pumping	#	Monitoring status	Simulation type	
KR14	SS23a&b	Boreholes are open and free to cross-flow	Steady state	a:forward b:calibration
	SS24a&b	Boreholes are packed-off		
KR18A	SS25a&b	Boreholes are open and free to cross-flow	Steady state	a:forward b:calibration
	SS26a&b	Boreholes are packed-off		
KR15A	TS27	Boreholes are open and free to cross-flow	Transient	Forward
KR14	TS28	Boreholes are open and free to cross-flow[19]	Transient	Forward

The head and drawdown data provided for model calibration are shown in Figure 4-3. The relatively small variation in heads in the undisturbed state is clearly seen even where packers systems were in place (SS22). The influence of the open hole conditions during testing can be seen by comparing the head responses for pumping in KR14 (SS23a&b, SS24a&b) and pumping in KR18 (SS25a&b, SS26a&b).

The PFL flow data for undisturbed and single-hole pumping are shown in Figure 4-4, while the flow data from the cross-hole pumping in KR14 (SS23a&b) and KR18A (SS25a&b) are shown in Figure 4-5. The richness of the flow data in comparison to the head/drawdown data can be seen in the increased spatial resolution and greater dynamic range of data together with flow direction.

[19] With the exception of one isolated flowing structure in a monitoring borehole.

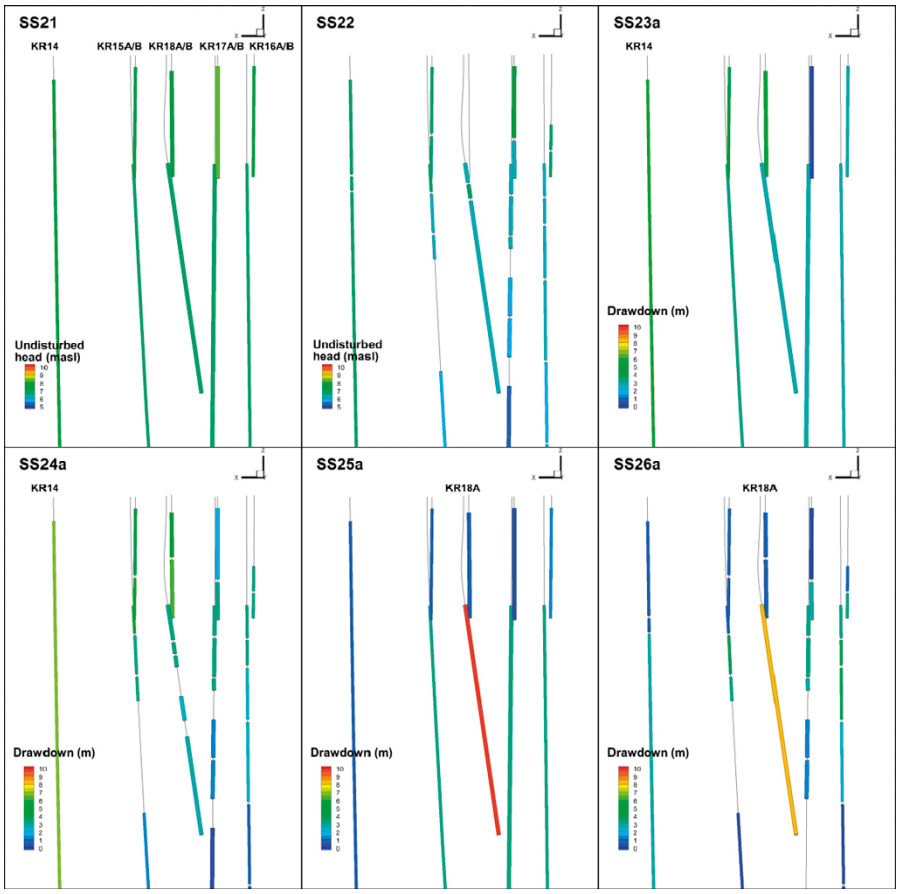

Figure 4-3. *Head and drawdown data provided to modellers for use in calibration steps for the different simulations.*

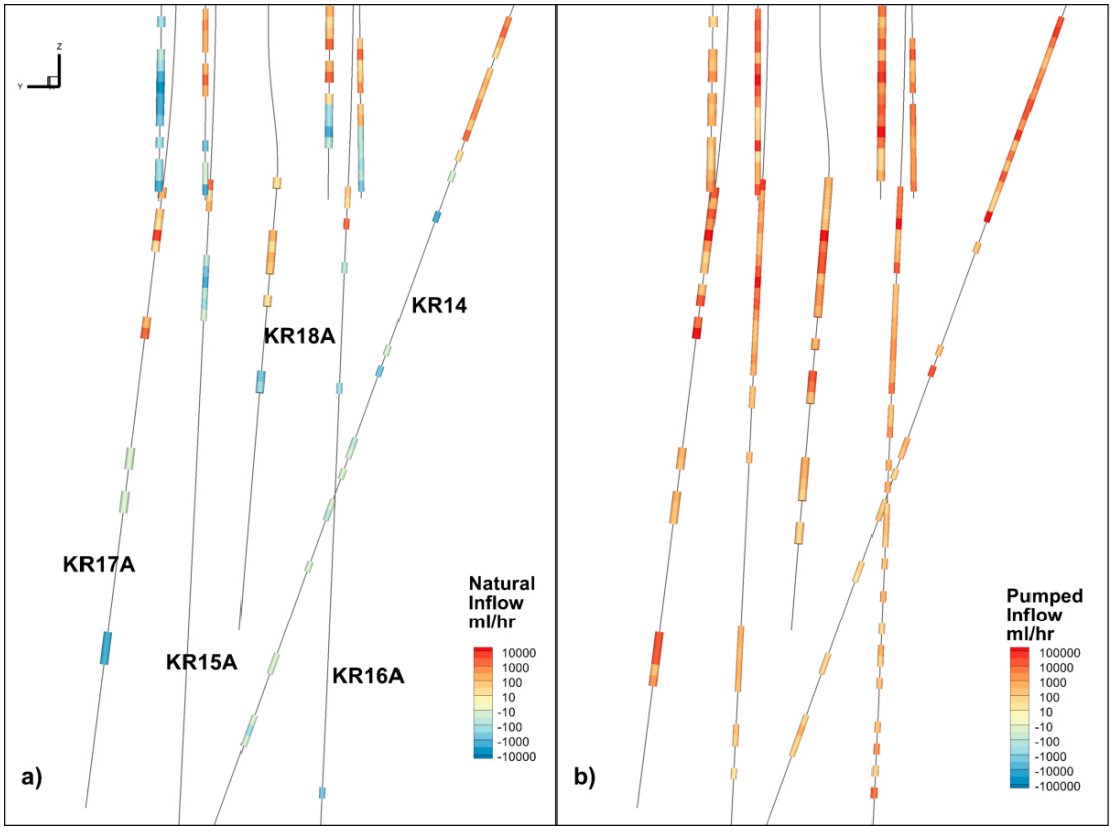

Figure 4-4. *Flow data used for calibration a) undisturbed/no pumping, b) single-hole pumping.*

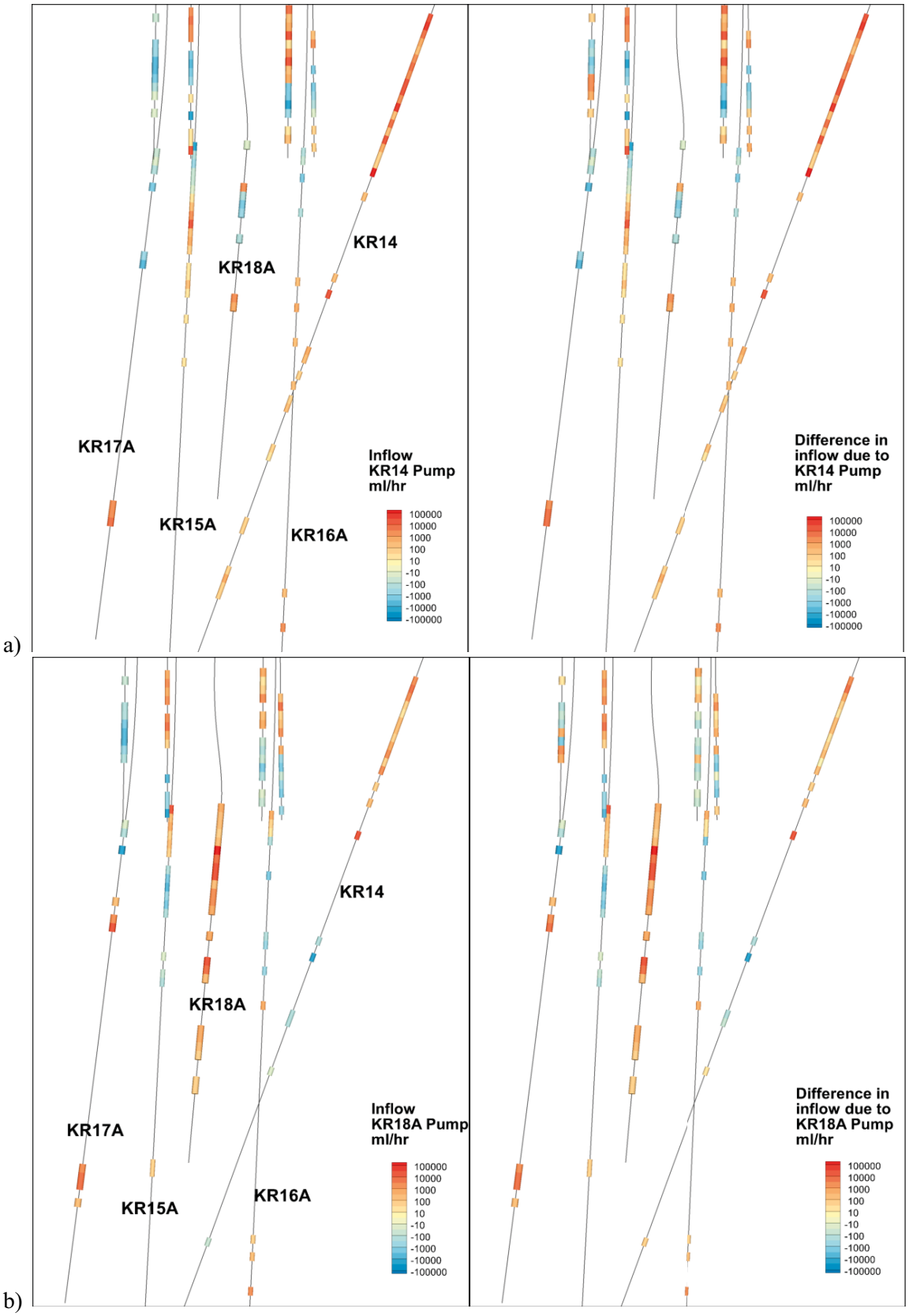

Figure 4-5. *Flow data used for calibration: a) SS23a&b pumping in KR14, b) SS25a&b pumping in KR18A.*

4.4 Modelling approaches

The numerical codes and associated tools used by each modelling group are listed in Table 1-3. For the most part the modelling groups used the same numerical codes in each subtask.

4.4.1 JAEA

JAEA's Task 7B model was constructed by combining deterministic representations of large-scale structures (fixed geometry and calibrated hydraulic properties) with a stochastic DFN representation of the background rock. The workflow for deriving the properties of the deterministic features was:

1. Pressure derivative plots were used to develop a "mapping" of transmissivity versus time and radial distance, and to identify the nature of fracture connectivity in terms of flow dimension.
2. Three alternative models for the deterministic fault zones were constructed based on the 2006 (as used in Task 7a) and 2008 hydro-structural models. The three models were compared for their consistency with the pressure transient model derived in step 1.
3. The relative plausibility of the three models was estimated from a comparison of measured and simulated flow and head. The resulting model was able to reproduce the major pressure and flow responses.

The workflow for the derivation of the background fracture DFN properties was:

1. Fracture orientations were analysed to define sets and preferred orientations from flowing features identified in the PFL dataset within the model region.
2. Fracture transmissivity distribution was derived directly from the PFL transmissivity.
3. Fracture size distributions were estimated from a correlation to transmissivity.
4. The spatial pattern of background fractures was also analysed by comparing fracture intersections with features identified by PFL.

In a later model update, the background fracture model was calibrated.

Conceptualization of deterministic fault zone model

Pressure derivative plots of the response to injection were used to identify intervals with similar late-time behaviour and associate hypothetical connections to the injection interval for three different tests in KR18A and KR17A. The models were then compared with the 2006 hydro-structural model (used in Task 7A) and the 2008 hydro-structural model as shown in Figure 4-6a,b. Neither model fully matched the concept derived from the analyses and a third model called "Modified 2008" including the HZ0002 feature from the 2006 model was defined (see Table 4-3). The three different structural models were then used to simulate the pumping tests in order to evaluate "model plausibility".

Table 4-3. Comparison of pressure transient concept and JAEA hydro-structural models.

Model	Comment	Evaluation
2006	HZ19C and HZ002 are not sufficiently connected to reproduce the flow seen between these features in boreholes KR16A, 17A and 18A.	Need to include a WCF between HZ19C and HZ002.
2008	HZ19C seems to represent the larger conductive feature estimated from the derivative plot analysis. HZ002 not present in this model version.	A structure similar to HZ002 needs to be considered to provide the observed connectivity at a depth of 70–80 metres.
Modified 2008	Fault zone HZ002 added to the 2008 model.	

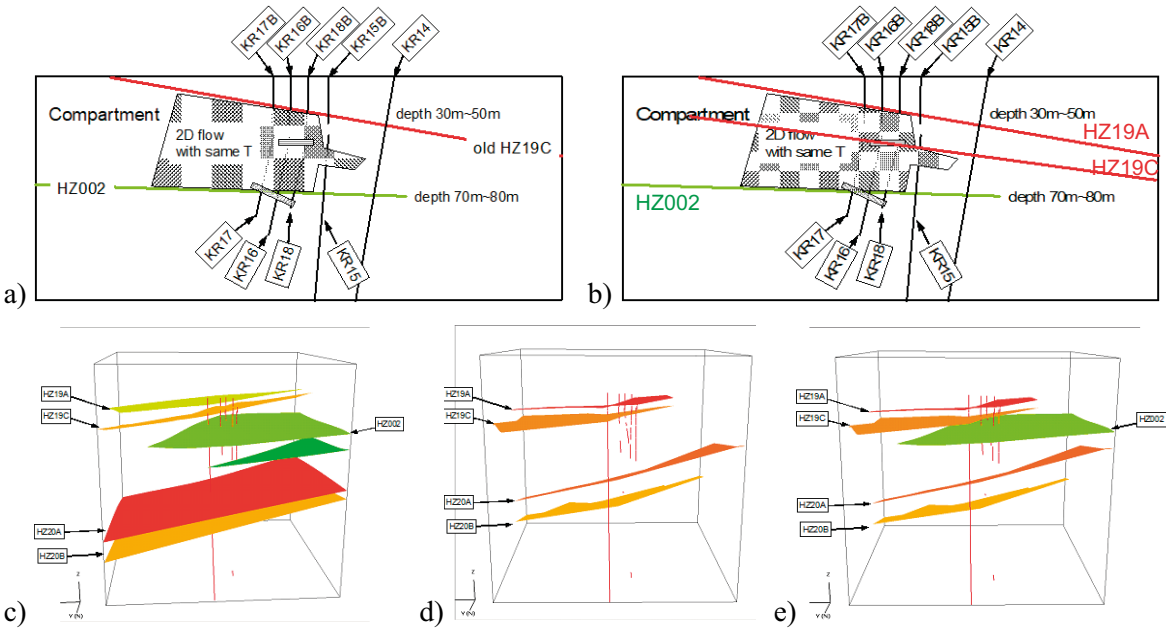

Figure 4-6. *Comparison of JAEA hydro-structural models and pressure transient conceptualisation: a) 2006 model and b) 2008 model together with 3D views of the models implemented c) 2006 model; d) 2008 model; e) modified 2008 model.*

Figure 4-6c,d,e show the 3 models. The transmissivity of each fault zone was set to the geometric mean of the measured values for that zone (taken from Vidstrand et al. 2015). Figure 4-7 shows the simulated pressure responses to pumping in KR14 and KR18A. The boundary conditions used in the simulations were:

- Upper surface: constant head = elevation, with no surface layer.
- Sides: constant head equal to average of top elevation each side.
- Base: no flow.
- Borehole: imposed flow or pressure to reproduce the test intervals and conditions.

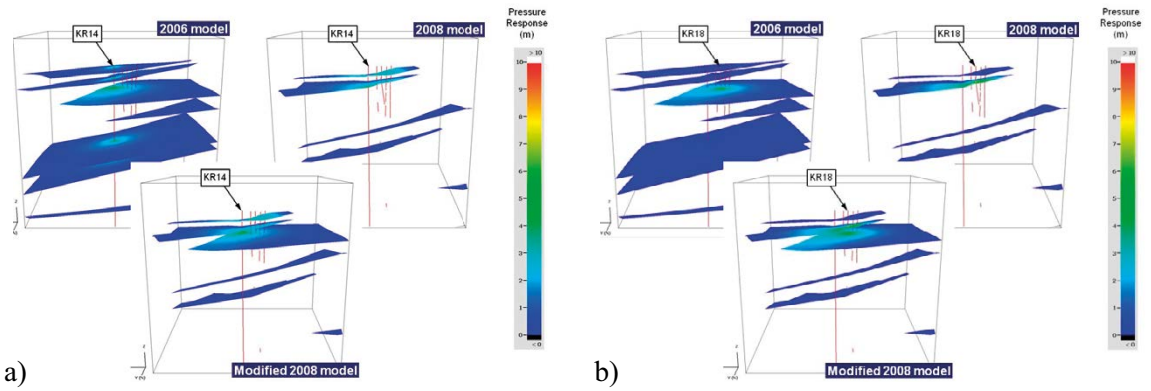

Figure 4-7. *Simulated pressure responses to pumping for the three different models: a) Phase 1 pumping in KR14; b) Phase 2 pumping in KR18A.*

The models were then evaluated based on the mean residual sum of squares (RSS) calculated over the intervals where a response could be simulated. The 2008 model provided the lowest mean RSS but the Modified 2008 model results in more simulated responses (57) than either the 2006 model (27) or the 2008 model (29). Arguably therefore, the Modified 2008 model provided the better match as the RSS was only slightly greater than that for the 2008 model.

The JAEA study also considered the uncertainty related to alternative stochastic realisations of the background fracture population in the region above fault zone HZ20A. Fracture orientation and transmissivity were taken from the integrated PFL data while fracture length was based on an empirical correlation from Task 6C (Dershowitz et al. 2003). The background fracture DFN parameters are listed in Table 4-4.

The modelling region was a 500 m cube centred on borehole KR15A shown in Figure 4-8 and the boundary conditions were the same as those used for the model plausibility simulations.

Table 4-4. Summary of background fracture network parameterisation.

Entity	Parameter	Value	Remarks
Fracture intensity	P_{32} Wang (2005)	0.3 m^2/m^3	Assumes Fisher distribution
	Intensity, P_{10}	0.23 m^{-1}	Calculated from water conducting fractures, identified by PFL
	Wang conversion factor	1.3	
Orientation	Orientation (pole, Fisher distribution) trend, plunge	229, 78	Fisher Kolmogorov-Smirnov (K-S) goodness of fit = 74 %
	Fisher *k*	4.7	
Transmissivity *T*	Lognormal mean and standard deviation	−8, 0.8 (log_{10})	
Size *L*	Mean, standard deviation of lognormal distribution	31 m, 67 m	L is correlated to transmissivity T (Dershowitz et al. 2003)

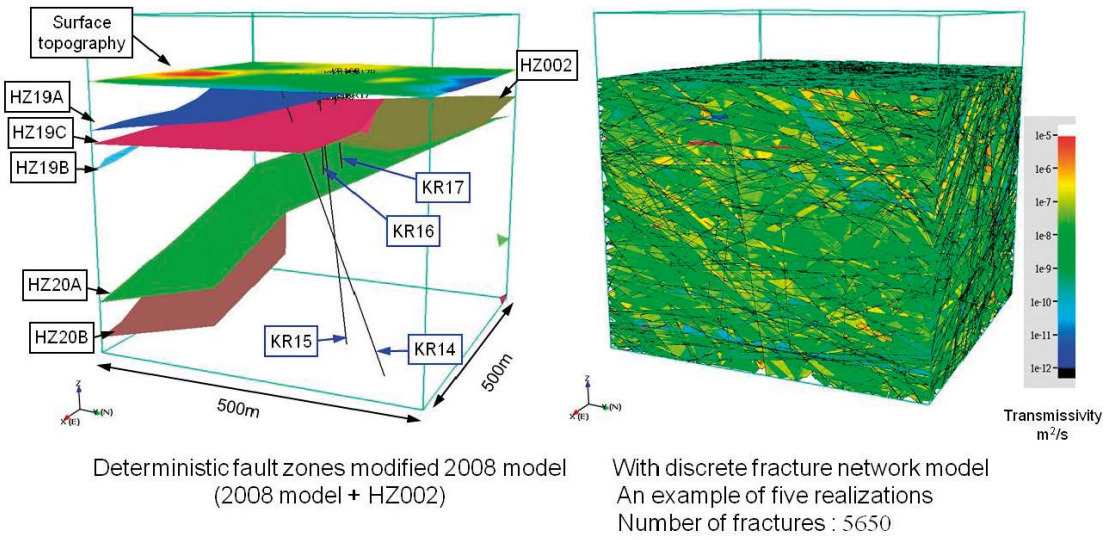

Figure 4-8. *The Modified 2008 deterministic fault zones model, and an example background fracture network model generated in the modelling region (500 m cube).*

Model Calibration

As part of an update to the model JAEA calibrated the background DFN focusing on the simulated flow and drawdown distributions rather than the absolute value of measured heads. The background DFN model was modified by

1. removing background fractures below HZ20A to avoid hydraulic connectivity from KR14 and KR15A at the deeper zone,
2. increasing fracture transmissivity above HZ002 by a factor of 5 introducing a depth dependency of transmissivity,
3. varying the fracture network connectivity by assuming no hydraulic connection at randomly selected fracture intersections between background fractures and fault zones. The probability of lack of connection varied from 0 % to 50 % for five stochastic realisations.

A further calibration step involved disconnecting KR14 from HZ002 and HZ19C to be consistent with the pressure transient analysis.

4.4.2 KAERI

KAERI's objective for modelling in Task 7B was to understand the block scale groundwater flow system in regard to flow and head responses.

Model structure

KAERI adopted a similar modelling approach to that used in Task 7A, building a 3D continuum model representing the deterministic fracture zones using Oda's method (Oda 1985) to convert structure transmissivity to element hydraulic conductivity. "Background" fractures were analysed to develop a stochastic DFN model (Ji et al. 2010) and converted to element hydraulic conductivity, again using Oda's method. The complete model hydraulic conductivity distribution is shown in Figure 4-9. There is a clear contrast between the upper part of the bedrock, the major HZ structures and the deeper background rock. The boreholes were treated as discrete elements. Groundwater flow was solved using the FEFLOW code (Diersch 2005a, b).

Model conditioning and calibration

The effective surface recharge was adjusted to match measured heads under six different pumping conditions: open and packed-off boreholes each under three pumping conditions (no pumping and pumping in KR14 and KR18A). The total Sum of Squared Errors (SSE) was then minimised relative to the recharge.

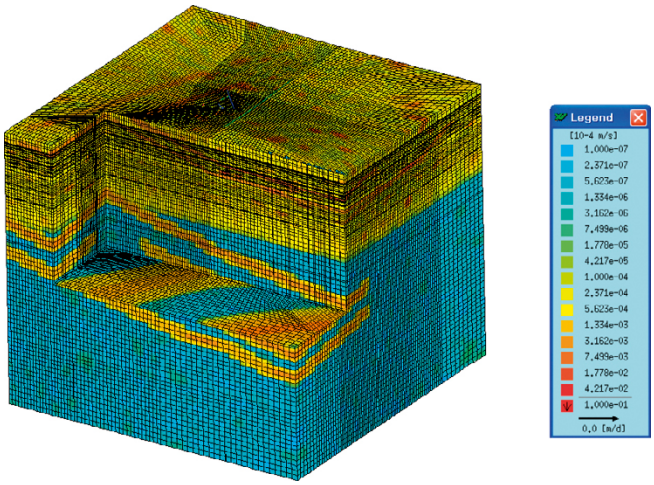

Figure 4-9. *Hydraulic conductivity distribution of the KAERI Task 7B groundwater flow model.*

4.4.3 NWMO/Laval

NWMO/Laval's objectives were to use inverse modelling of the different hydrotests to provide calibrated models and parameter estimates, and therefore reduce uncertainty in the properties of the fracture network. To do this they used a "hydrofacies" approach based on the Transition PRObability GeoStatistical (T-PROGS) model (Carle 1996) with the flow modelling performed in Hydrogeosphere (Therrien et al. 2009) coupled with PEST (Doherty 2004). Their emphasis was on the background rock and so the major zones were ignored although deterministic "sheet joints" were included in some simulations.

Model structure

The fractured rock in NWMO/Laval's Task 7B models was represented using a transition probability and Markov chain geostatistical approach based on the definition of fractured rock facies. The approach had previously been used by Park et al. (2004) in the simulation of tracer tests performed in the Moderately Fractured Rock experiment at the AECL Underground Research Laboratory in Pinnawa, Manitoba. Analysis of PFL data identified a relationship between hydraulic conductivity and fracture density based on a 5 m averaging window as shown in Figure 4-10[20]. Hydraulic conductivity was defined as the sum of PFL transmissivity divided by window length.

An initial model using 4 facies (UFB, SFB, MFB, HFB) was developed as described in Table 4-5 below. The UFB is defined as the background facies and its volume fraction is calculated automatically based on the estimated fractions of the other facies. The geometric properties used in the models are the volume fraction and transition probability matrix. The observations and fitted models for the vertical and horizontal directions are shown in Figure 4-11.

The embedded transition probability is the probability that a given facies is located above or next to a second facies. The fitted transition probability matrix is shown in Table 4-6. The model indicated that for the UFB there is a probability of 39 % that SFB occurs above it, 35 % that MFB occurs above and 26 % that HFB occurs as shown in Table 4-6. Initial estimates of the facies' hydraulic conductivity were based on the mean PFL transmissivity for each facies (Figure 4-10). The hydraulic conductivities for the different facies were then used as the targets for the optimisation performed with PEST.

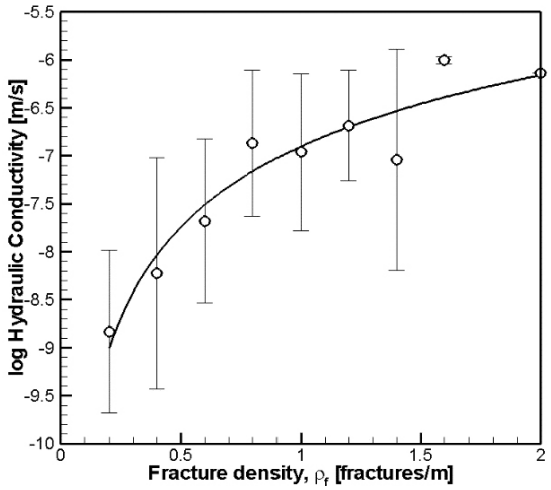

Figure 4-10. *Distribution of hydraulic conductivity versus fracture density* r_f *based on PFL data.*

[20] The relationships may derive from the higher fracture density and transmissivity observed at shallow depth and not directly from an association of transmissivity with local fracture density – see subsequent discussion in model evaluation.

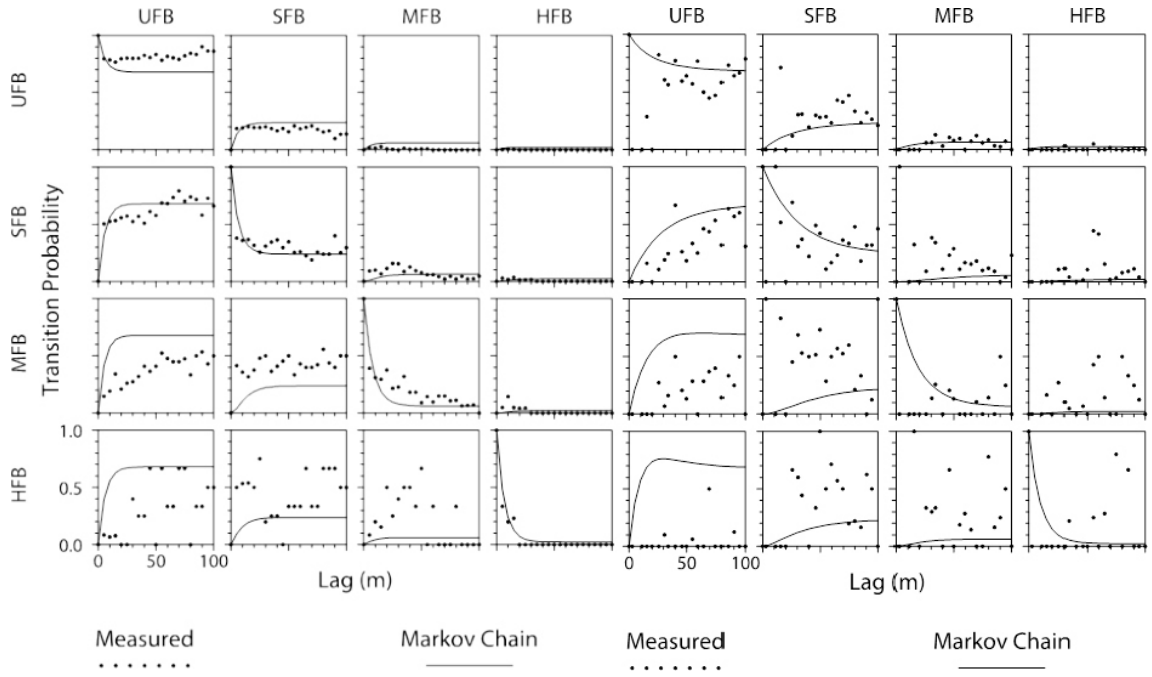

Figure 4-11. *Observed transition probabilities and initial fitted Markov chain model for vertical (left) and horizontal (right) directions for the 4 facies UFB, SFB, MFB and HFB.*

Table 4-5. Initial rock facies categories, density range and geometric properties.

Rock facies category		Fracture density range	Volume fraction (%)	Observed mean length (m)	
				Vertical	Horizontal
Unfractured Bedrock	UFB	$0 < \rho_f < 0.5$	67.93	28.5	60.6
Sparsely Fractured Bedrock	SFB	$0 < \rho_f < 0.5$	23.75	8.2	40
Moderately Fractured Bedrock	MFB	$0.5 < \rho f < 1.0$	6.10	7.8	20
Highly fractured bedrock	HFB	$\rho_f > 1.0$	2.22	6.8	10

Table 4-6. Fitted transition probability matrix (initial model).

Facies 1	Facies 2			
	UFB	SFB	MFB	HFB
UFB		39 %	35 %	26 %
SFB	99 %		1 %	1 %
MFB	96 %	2 %		2 %
HFB	91 %	5 %	4 %	

Alternative facies models were used within the simulations replacing MFB with Sparsely to Moderately Fractured Bedrock (SMFB) and Moderately to Highly Fractured Bedrock (MHFB). Figure 4-12 shows realisations of the four hydro-structural models that were tested by NWMO/Laval:

- Model-1: Base case using 4 facies (SFB, SMFB, MHFB and HFB).
- Model-2: 4 facies model with alternative spatial distribution (different random seed).
- Model-3: 4 facies plus discrete features.
- Model-4: 5 facies model (UFB, SFB, SMFB, MHFB, HFB).

The deterministic features shown in Figure 4-12c are listed in Table 4-7. These features were included in Model-3 only. HZ19A and HZ19C were not explicitly represented in the models (due to the focus on background rock) and it was assumed that the zones could be represented by the high conductivity facies (HFB). This also motivated the treatment of the upper model boundary as a flat top with heads interpolated from the water table elevation.

Table 4-7. Deterministic features used by NWMO/Laval (Klockars et al. 2006).

Name	Location	Transmissivity (m^2/s)
KR14_4H	KR14 50 mah	Forward modelling and initial value in inverse models 9×10^{-5}
Plane_1/HZ19C	KR15A 60 mah	

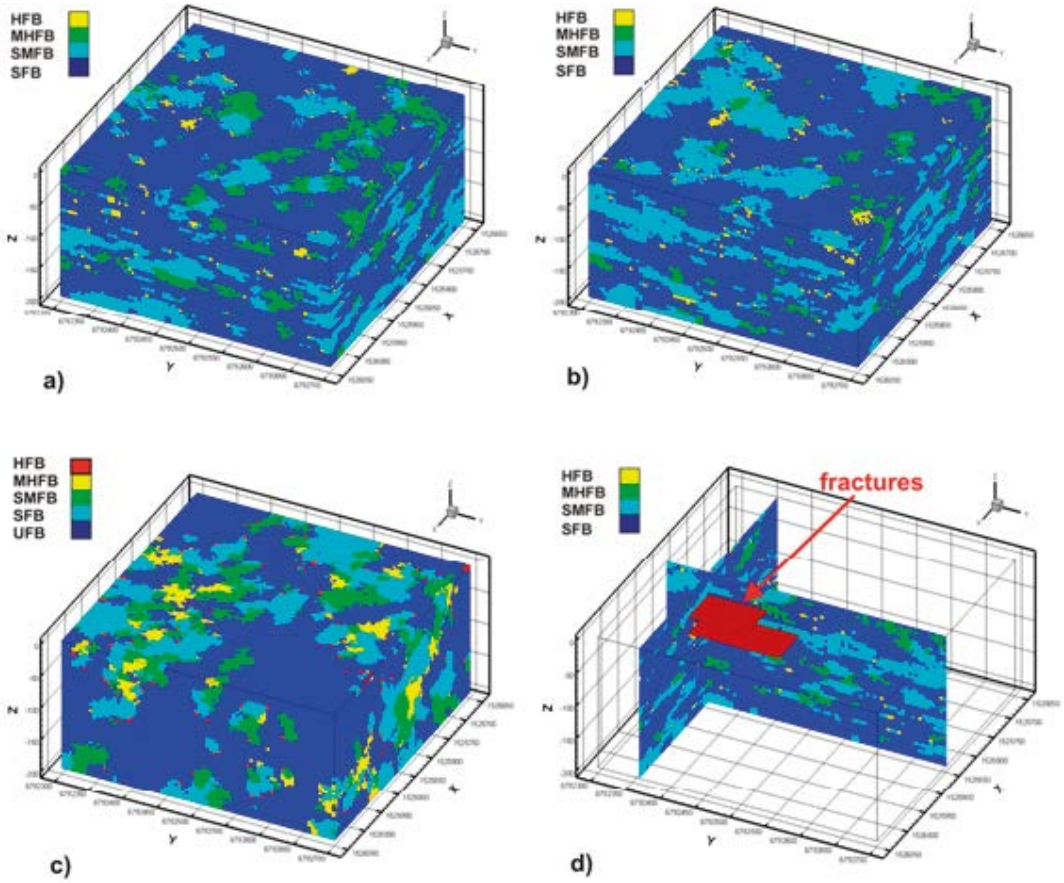

Figure 4-12. *The different hydro-structural models tested by NWMO/Laval: a) Model-1 4 facies, base case b) Model-2 4 facies, alternative spatial distribution c) Model-4 5 facies and d) Model-3 4 facies + two deterministic discrete fractures.*

4.4.4 Posiva/VTT

Posiva/VTT's interest in Task 7B related largely to the development of a new modelling tool for creating stochastic DFNs (the VINTAGE module of FEFTRA) and the quantitative assessment of the derived DFNs.

Model structure

The model volume was initially based on a 500 m × 500 m × 500 m cube centred on the KR14-KR18 boreholes. However, this was later refined to include only the space bounded by the HZ19A and HZ20A deterministic fracture zones within the cube, since the effect of these large water conducting zones proved sufficiently dominant that background fracturing above HZ19A and below HZ20A could be ignored. The transmissivity of the zones was interpolated from the borehole measurements using Ordinary Kriging (Figure 4-13a).

The major HZ Structures were based upon the 2008 hydro-structural model of those zones intersecting the volume. Two smaller sheet joints were included on the basis of observed head data. The existence of these structures cannot actually be excluded given the available fracture data. The features were called UPPER and LOWER and located at z = −20 and −50 m respectively.

Stochastic fractures were characterised as a single set of circular disks with radius defined by a truncated power-law length distribution parameterised by a minimum length r_{min} and exponent b where:

$$P(R > r) \propto \left({}^{r}/_{r_{min}}\right)^{-b}$$

The fractures followed a Fisher orientation distribution and log-normal transmissivity distribution. Terzaghi-corrected P10 intensities were used as the P32 fracture intensities.

Posiva/VTT performed a sensitivity study on the stochastic fracture network varying the degree of correlation between transmissivity and length (SL parameter). 10–20 realisations were generated for each sensitivity case. For a realisation with correlated transmissivity T and fracture radius r, where y = F1(r) is the cumulative probability distribution function for radius, the transmissivity was then calculated as T = F2−1(y'+N(0,SLi)), where N(μ,σ) is a normally distributed random variable with μ mean and σ standard deviation (see Figure 4-14).

Prior to the implementation of the DFN approach, scoping calculations were performed with an Equivalent Porous Medium (EPM) model. The purpose of this was twofold: first, to assess and understand the basic properties of the flow on the block-scale and second, to provide reasonable boundary conditions for the smaller DFN model. The EPM model was built upon the structural model of 2008 (Vaittinen et al. 2009). The rock matrix extended from z = 0 m down to 1 500 m in depth and was partitioned into horizontal layers of increasing thickness with depth to model the depth-dependent hydraulic conductivity.

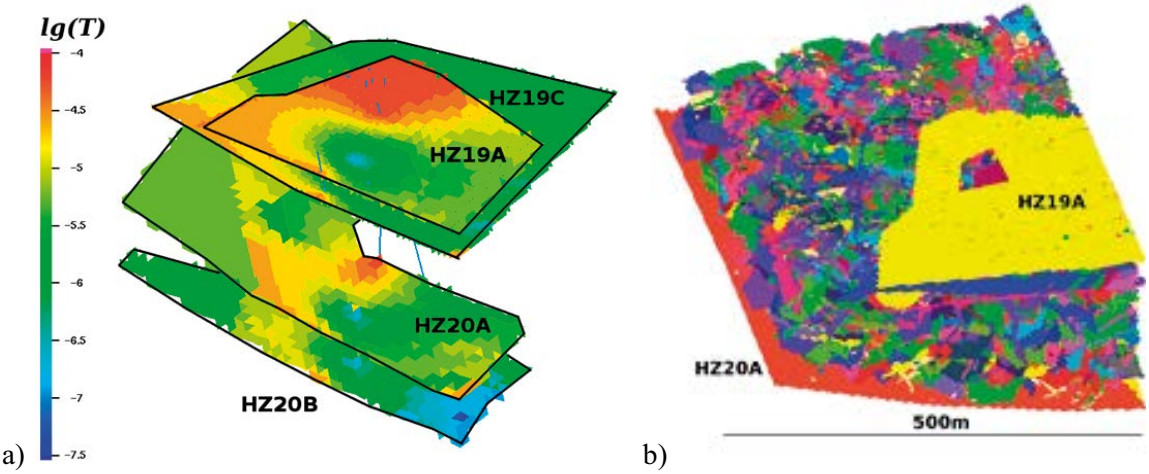

Figure 4-13. *Posiva/VTT model a) zones within the model showing the interpolated transmissivity field and b) example realisation of the stochastic fracture network.*

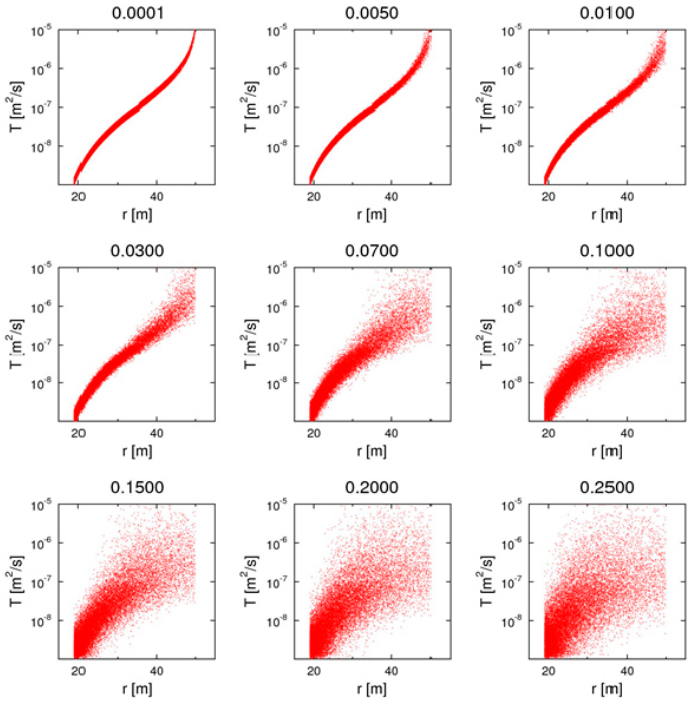

Figure 4-14. *Cross-plots of transmissivity and fracture size (radius) for varying S_L. Low S_L values represent strong correlation, high S_L values represent weak correlation. In the example shown the log-normal transmissivity distribution was truncated to $-9.0 \leq lg(T) \leq -5.0$ and the power-law size distribution was truncated to $19.0\ m \leq r \leq 50.0\ m$.*

Model Calibration

For the case of pumping in KR14 with boreholes open and free to flow, an extensive search was made using 130 cases each with 10 realisations (i.e. a total of 1 300 model realisations). The fracture parameters considered are listed in Table 4-8. The calibration was based on an *ad hoc* scoring system using simulated flows and heads. The scores were derived from

- Kolmogorov-Smirnov (K-S) statistics (distance and relevance) for the simulated and measured distribution of flow magnitudes,
- root mean square deviation (RMSD) of observed and calculated heads in the open boreholes,
- variability of the flow.

The transmissivities of the sheet joints were estimated in a further set of test cases using the EnKF method used in Task 7A as discussed in the previous chapter.

Table 4-8. Parameter variations used in Posiva/VTT models in Task 7B.

Property	Type	Description
Orientation	Fixed	Mean trend 192°, Mean plunge 79°, Dispersion Fisher κ: 3.1
Intensity	Fixed	P_{32} = 0.41 m^2/m^3, Terzaghi-corrected P_{10}. Mean intensity of different boreholes weighted by the used borehole section
Transmissivity	Calibrated	$-7 \le \lg T_{max}, 0 \le \sigma(T) \le 1.8$ Truncated log-normal $\sigma(T)$, $\mu(T)$ $Tmax_{min}$
	Fixed	$\mu(\lg T) = -8.3$ $\log_{10}$ mean transmissivity[21]
	Calibrated	$0.0001 \le S_L \le 0.2500$ Connection between size and transmissivity
Size distribution	Calibrated	50 m $\le r_{max}$ Truncated power-law upper limit
	Fixed	r_{min}, b Minimum fracture size and power law exponent
Sheet joints	Calibrated	Present only in a subset of cases. T was not calibrated; only the presence/absence of the features.

Table 4-9. Summary table of Posiva/VTT model configuration in Task 7B.

Structure/ Feature	Deterministic zones	Background rock
Description	Site-scale major fracture zones included in the block-scale model wo/re-interpretation	EPM model: rock matrix between major structures DFN models: stochastic small scale fractures modelled as circular disks of variable orientation and size
Location and spatial distribution	As specified in Posiva bedrock model 2008	EPM model: volume enclosing the deterministic zones. DFN model: between HZ19A and HZ20A. Distributions defining geometry: Spatial: uniform random (Baecher) Orientation: Fisher Size: power-law
Hydraulic properties (T or K) and storage	EPM model: geometric mean T from observations of zones. $S_S = 10^{-6}$ m^{-1} obtained experimentally. DFN model: interpolated T-field from observations.	Uniform within the fracture. Fracture transmissivities are truncated log-normal $\mu(T) = -8.3$, $\sigma(T) = 1.2$ $\lg(T_{min}) = -9$, $\lg(T_{max}) = -5$ connected to their size, strength of connection (S_L) varied.
Heterogeneity/microstructure	Interpolation w/ Ordinary Kriging	None
Aperture/porosity	0.001 m	0.001 m
Orientation	As specified in Posiva bedrock model 2008	Trend: 192 Pole: 79 Fisher κ: 3.1
Length scale	As specified in Posiva bedrock model 2008	Truncated power-law distribution $P(X>x) = (x/x_{min})^{-b}$ xm_{min} = 19 m b = 2.5 xm_{max} = 50 m
Likely numerical representation	Finite element mesh of linear triangular elements	Finite element mesh of linear triangular elements
Significant uncertainties in description	None	Single set of fractures may be a crude approximation
Prior probability distributions for key parameters	N/A	Orientation: Fisher Size: power-law T: log-normal (see parameter values above)
Approach to choice of model volume and setting model boundary conditions	500 m × 500 m × 500 m block centred on KR15A. Side boundaries constant head or upper boundary over HZ19A from larger EPM model (for which the groundwater table was applied on its top surface).	
Treatment of boreholes and features intersecting boreholes (e.g. conditioning)	EPM models: Mesh refinement around the boreholes, the Kriged T-field was conditioned on the transmissivities at the boreholes. DFN models: No refinement around the boreholes, no conditioning of realisations on borehole data.	

[21] Posiva/VTT sometimes use Brigg's logarithm lg notation equivalent to log and $\log_{10}$.

4.4.5 SKB/CFE

Model structure

SKB/CFE again used an adaptive gridding structure to represent the fracture network and boreholes as shown in Figure 4-15. A grid size of 16 m was used to represent the upper surface topography, with successive reduction in grid-size down to 0.0625 m for the boreholes. The upper 80 m of rock are included while below this only the cells containing fracture zones or "background" rock fractures are included. The upper model boundary was assigned a constant pressure where the surface was below sea level while above sea level a free groundwater table was simulated with net recharge of 100 mm/year. Hydrostatic boundary conditions are applied to the model sides and a no-flow condition to the model base.

The updated 2008 structural model superseded the 2006 structural model specified in Task 7A (see Vidstrand et al. 2015). The main change impacting Task 7B simulations is that boreholes KR14 and KR15A do not intersect any zones at depth in the 2008 model. In the SKB/CFE models the updated 2008 structural model was implemented by eliminating these deep intersections.

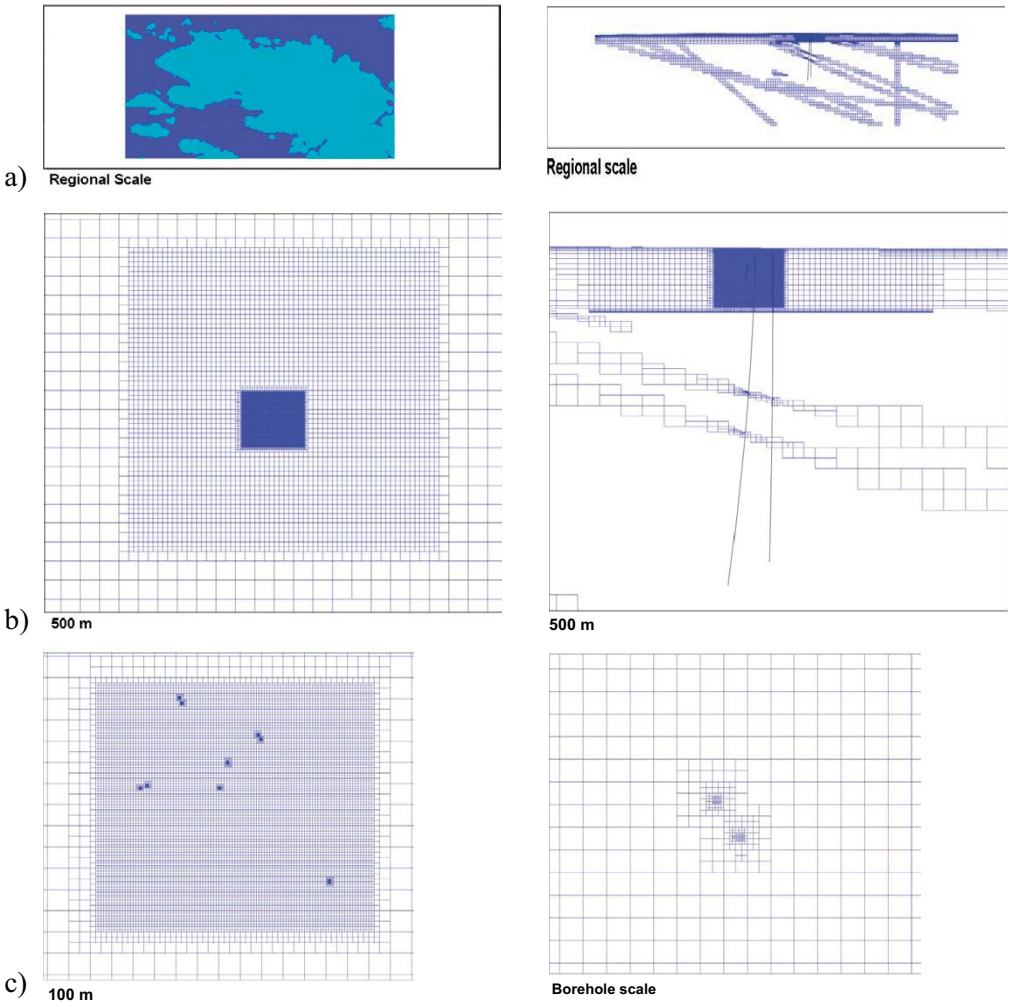

Figure 4-15. *SKB/CFE model grid at a) regional scale, b) 500 m scale and c) 100 m and "borehole" scales.*

Model Calibration

SKB/CFE's calibration strategy was based on the following guidelines:

- The calibration carried out in Task 7A was kept with respect to large scale features (lakes, wetlands, etc).
- The interference test with open boreholes was used for a calibration of the local site.
- The pump tests with packed-off boreholes were simulated in a forward manner i.e. without calibration). This was felt to be logical as the rock volume investigated is the same as that for the open borehole tests (KR14–KR18A).

The main effort was therefore put into the modelling of the tests with open boreholes. SKB/CFE noted that:

- Pumping 25 l/min in KR14 causes the same drawdown as pumping 5–7 l/min in the A-holes (KR15A-KR18A).
- Pumping in A-holes causes a uniform drawdown in A-holes, but a smaller drawdown in B-holes (KR15B-KR18B) and KR14.
- The effect of pumping in A-holes is the same, irrespective of which hole is pumped.
- The observed response in KR17B is generally small.

The introduction of two horizontal sheet joints could qualitatively explain the observed drawdowns. SKB/CFE argued that such features had been identified at the Forsmark site and that similar sub-horizontal structures might exist at Olkiluoto. The upper joint needed to be of high transmissivity to explain the limited drawdown when extracting from KR14. SKB/CFE therefore introduced two high transmissivity features (sheet joints):

- A rectangular feature at −50 m.a.s.l.
- A triangular feature (not intersecting KR17B) at −20 m.a.s.l.

SKB/CFE did not use the model calibration strategy suggested in the Task Description but instead looked for methods to simultaneously satisfy the following conditions: a local groundwater table at 6–7 m and the correct frequency of High Permeability Features (HPFs), while using the interference test data to fit the transmissivity of the sheet joints. The surface hydrology model used in Task 7A was found to provide a reasonable water table and "standard values" for DFN properties provided the right frequency of HPFs.

For the sheet joints:

- KR14 pump test was used to derive a transmissivity of 2.2×10^{-4} m^2/s for the upper sheet joint.
- The tests in KR15A and KR18A were used to derive a transmissivity of 10^{-5} m^2/s for the lower feature.

The results from the no-pumping conditions were relatively insensitive to DFN realisation but a realisation was selected (#3) as the basis for the reported results.

4.4.6 SKB/KTH

Model structure

SKB/KTH included only the "hydraulically active fractures" within their model for Task 7B. This included flowing features identified from the PFL logs and, in some model variants, fracture zones based on the definitions used in Task 7A.

SKB/KTH developed a novel "fracture-growth" DFN generation scheme to represent the flowing fractures. A model fracture is centred at each of the PFL flowing features and then extended until it intersects with a fracture connected to a neighbouring borehole (see Figure 4-16). The fracture orientation and transmissivity were taken directly from the integrated PFL analysis. This scheme "automatically" honours the position, orientation and local transmissivity at each borehole. The connectivity of the fracture network is controlled by the volume partitions and no account is taken of features not intersecting the boreholes.

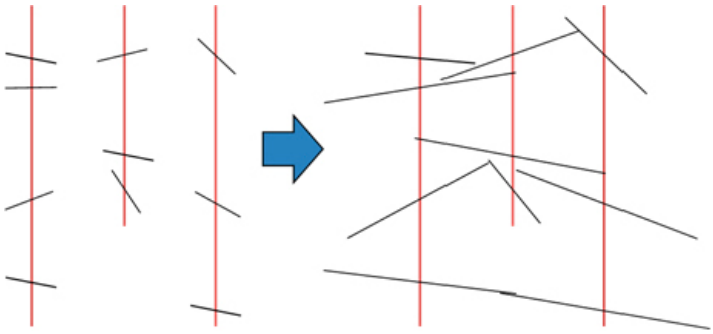

Figure 4-16. *Illustration of SKB/KTH conceptual approach. PFL flowing fractures are allowed to 'grow' from out from the borehole until they intersect neighbouring fractures.*

The fracture network was generated within a computational domain of 300 m × 300 m × 500 m centred around KR17A and KR18A (Figure 4-17). The generation scheme partitioned the volume according to the nearest borehole (excluding B-boreholes) as shown in Figure 4-17 by defining slightly overlapping cuboid regions around each of the five boreholes. Connectivity of the flowing fracture network was ensured by adjusting the size of each compartment.

The boundary conditions applied to the model volume were:

- Top surface: Head due to elevation or no-flow (according to model variant Table 4-10).
- Lateral surfaces: constant zero head boundary.
- Bottom surface: no-flow boundary.
- Pumping is simulated by using the field measured drawdown during pumping.

Model Calibration and conditioning

Model calibration was performed by defining a reference case "Configuration A", then performing a series of trial and error test cases T1–T4 and finally developing an improved model "Configuration B" based on the results of the trial and error cases. The different variants and the resulting impact on the match to observed flows are given in Table 4-10.

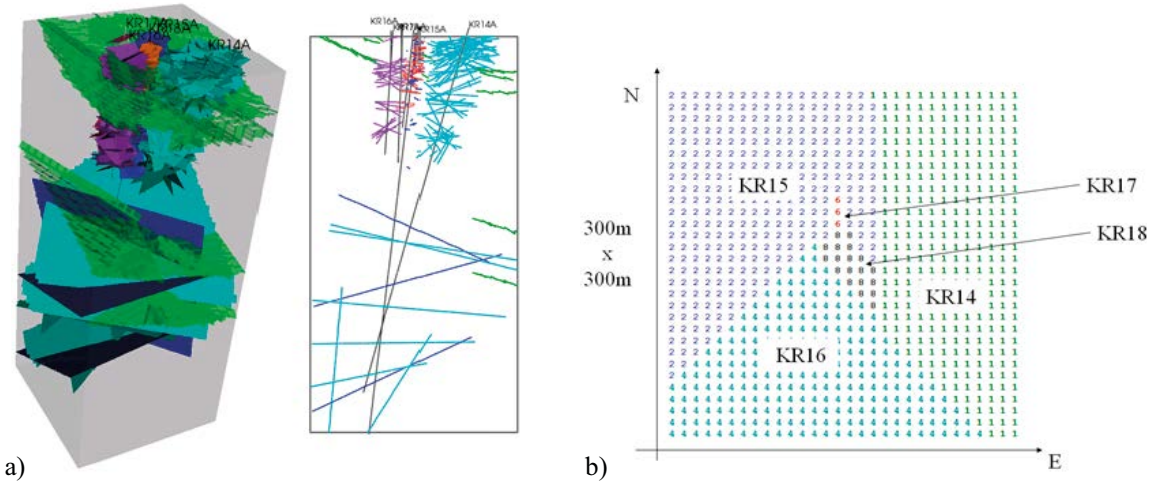

Figure 4-17. *SKB/KTH model volume and partitioning: a) 3D and vertical section view of zones and flowing fractures; b) Partitioning scheme identifying region of influence due to each borehole.*

Table 4-10. Model variants used by SKB/KTH in Task 7B.

Variant	Model features and modifications	Comparison
Configuration A	Flowing features from PFL. Hydraulic zones from Task 7A large-scale model. Top boundary condition head proportional to surface elevation, and the lateral sides head set to zero.	
Test case T1	Hydraulic zones are removed and replaced by fractures extending throughout their respective partitions, such that they extend to the model domain boundaries.	Reduction in the flow rates of pumping boreholes to below measured values and reduction in measured flows in observation boreholes. Flow magnitudes showed a better match but match to directions not improved.
Test case T2	Random removal of a defined fraction of fracture surface area (based on fracture tessellation).	Aim was to reduce DFN connectivity. For different percentages of the fracture surface area: 90 % negligible difference 75 % somewhat “underconnected” 50 % DFN is unconnected.
Test case T3	Top surface boundary condition is changed to a no-flow boundary.	Forced flow to come from lateral boundaries.
Test case T4	Horizontal near-surface, high-conductivity zone introduced by increasing fracture transmissivity by a factor 10 between −10 and −20 m.	Flow magnitudes improved in the pumping boreholes, but observation directions and magnitudes are generally not improved.
Configuration B	No hydraulic zones. Fracture transmissivity is increased by factor 10 close to the boreholes to represent possible skin effects. The top surface of the model domain is assigned a no-flow boundary.	

4.5 Modelling results

4.5.1 JAEA

Pumped conditions

JAEA focused on the examination of the flow connectivity between the boreholes by comparing pressure response (drawdown) and flow response, rather than comparing the hydraulic head using measured data which would be largely dependent on the choice of boundary conditions. Initially JAEA performed steady state simulations of the pump tests for the 5 background DFN realisations using both specified flow and specified drawdown conditions. The simulated drawdowns were typically higher than those measured for the specified flow boundary condition (Figure 4-18a), and a better match was initially achieved with constant drawdowns. The specified drawdown simulation did not honour the measured flowrates but was interpreted as indicating that reduced connections between the boreholes might be a calibration target.

The simulated flow distributions for the forward model simulations (Figure 4-19a) reproduce the major flow responses, although the match is better without the background fracture network which resulted in over-estimates of the hydraulic responses.

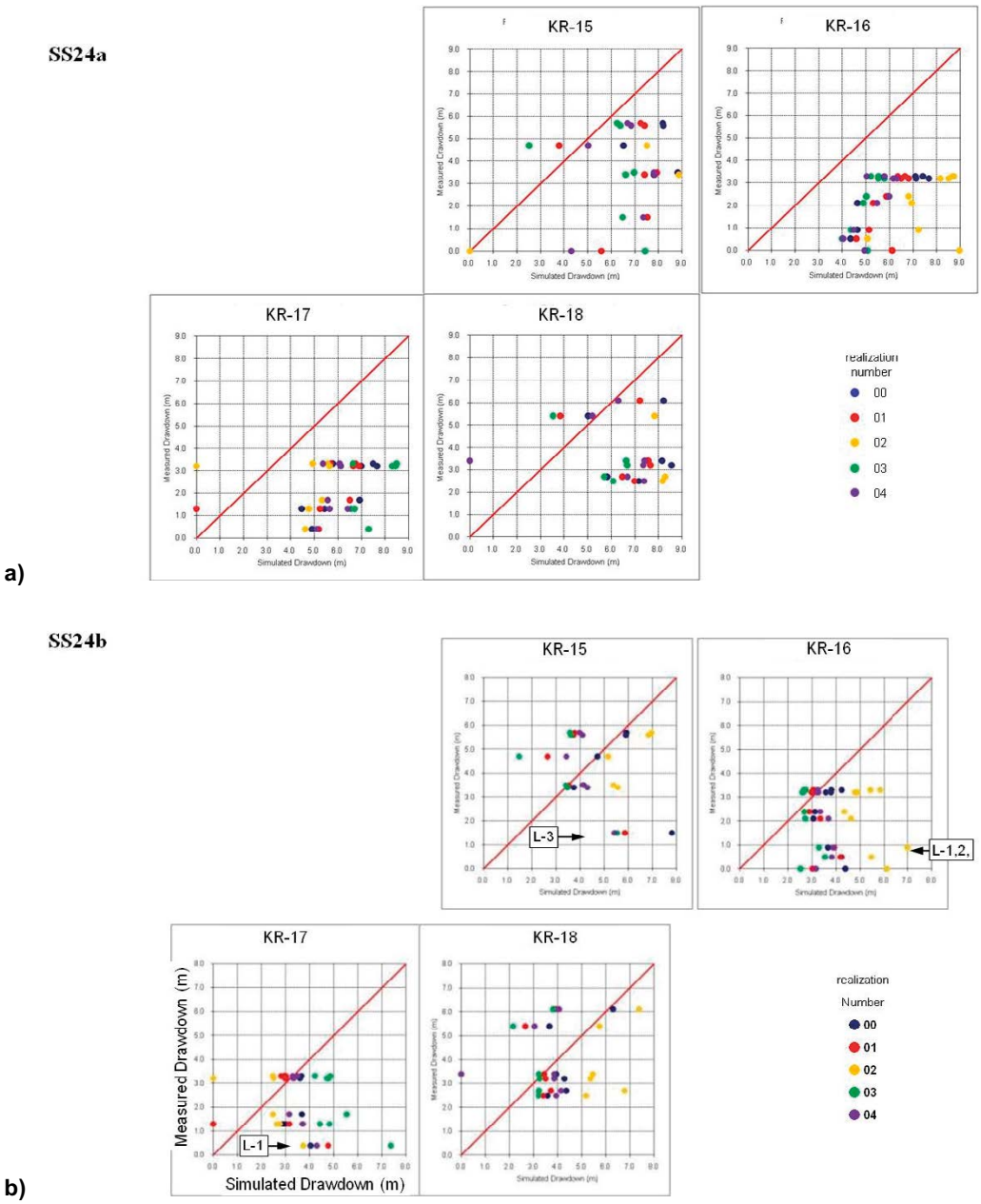

Figure 4-18. *JAEA comparison of measured and simulated drawdowns for a) forward and b) calibrated models of pumping assuming constant rate flow in KR14 (SS24a and SS24b).*

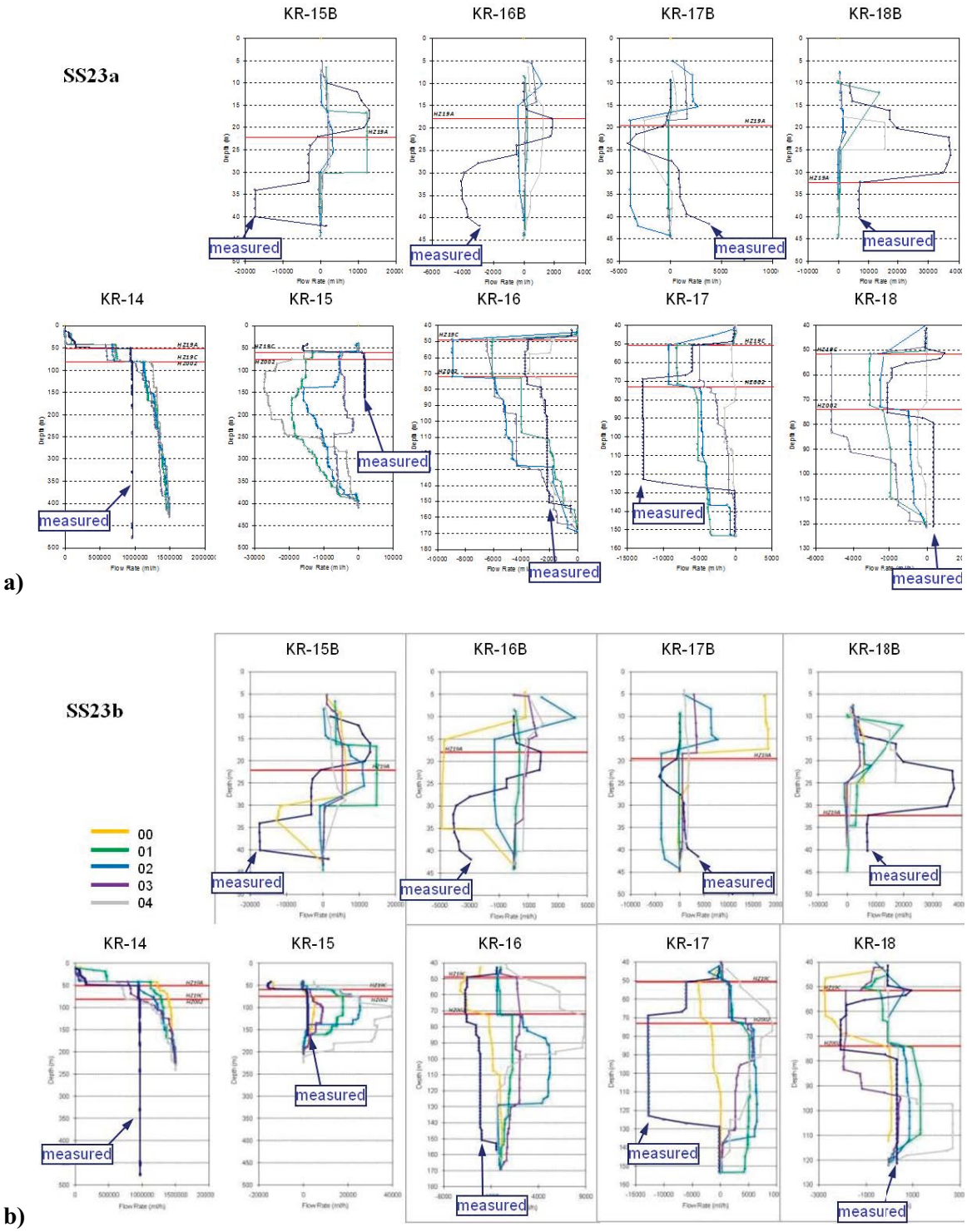

Figure 4-19. *JAEA comparison of measured and simulated flow distributions for a) forward and b) calibrated models of pumping assuming constant rate flow in KR14 (SS24a and SS24b).*

After updating the model (see Section 4.4.1) the drawdowns from the calibrated models show a better mean match (reduced drawdown) both at the pumping interval and in the monitoring intervals. The flow responses also show some improvement over the forward model. JAEA calculated a "model plausibility" value based on the pressure responses and on flow responses. The improvement due to model calibration is clearly seen (although realisation 2 results in significantly higher drawdowns than measured). The calculated plausibility value based on flow data also improved.

Transport simulations (particle tracking)

Particle tracking simulations were performed to calculate F-factors (flow dependent transport resistance, Hodgkinson 2007). Distributions were based on ~100 particles from each of the nine starting locations around KR-14. The F-factor calculated from the calibrated model is slightly decreased (particularly for release points 4 and 5) which may in part be due to the transmissivity in the region above z = −90 m.

Particle tracks were calculated for two model cases PA20C and PA29C both without boreholes. PA20C was performed using model parameters prior to calibration to the KR14–18 pump tests, while PA29 used the calibrated models. The aim was to identify the change due to model calibration to the pump test data.

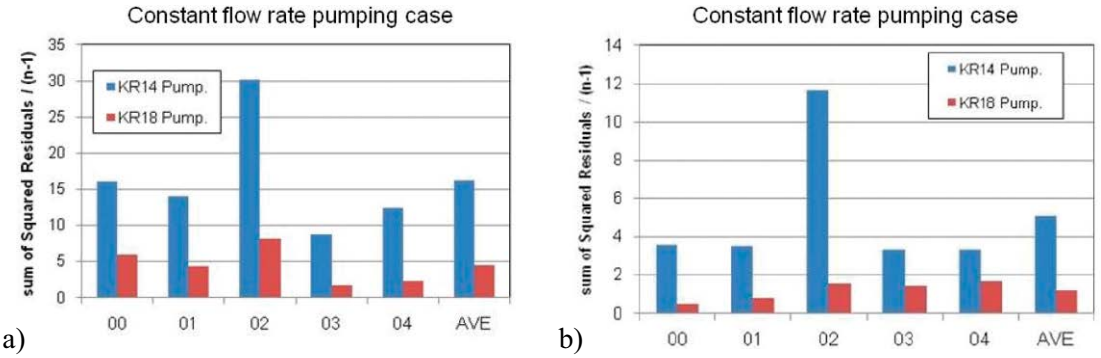

Figure 4-20. *JAEA model plausibility based on pressure responses for the 5 background fracture realisations for a) forward models and b) calibrated models.*

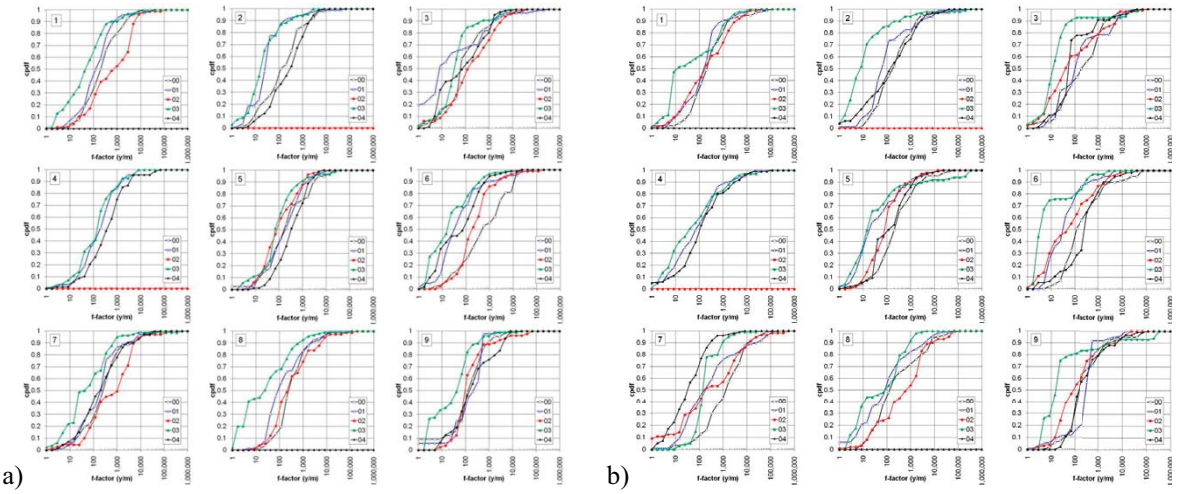

Figure 4-21. *Calculated F-factor distributions for the JAEA a) uncalibrated (PA20C) and b) calibrated (PA29) models.*

4.5.2 KAERI

Undisturbed conditions

Figure 4-22 shows the simulated heads for undisturbed conditions. Recharge rates were calibrated for the open and packed-off conditions (Table 4-11). The higher recharge rate for the open hole condition resulted in very similar simulated heads at the boreholes due to their high transmissivity significantly underestimating the observed head variation.

The simulated flow magnitudes (Figure 4-23) are in reasonable agreement with the measured values although the flow directions (+ve in, -ve out of the borehole) are not always in agreement with those measured.

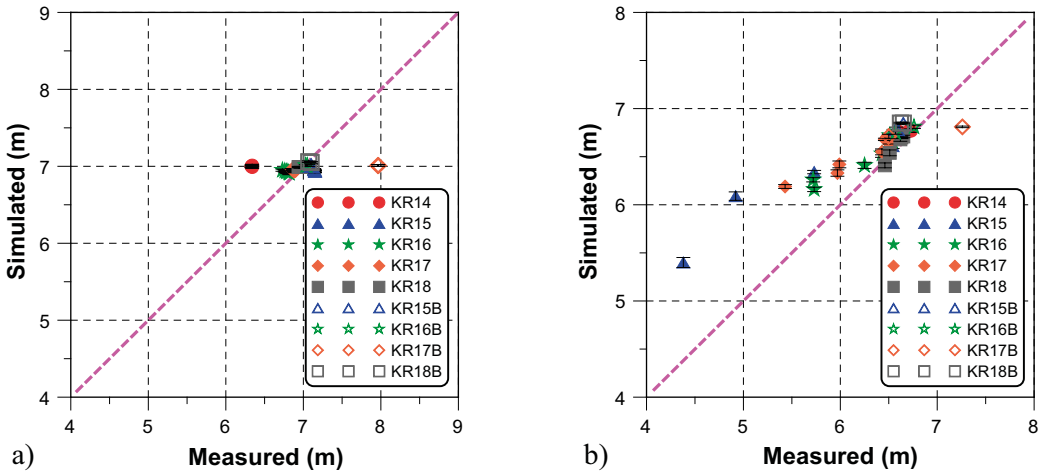

Figure 4-22. *Cross-plot of simulated and measured heads for undisturbed conditions a) open boreholes; b) packed-off boreholes.*

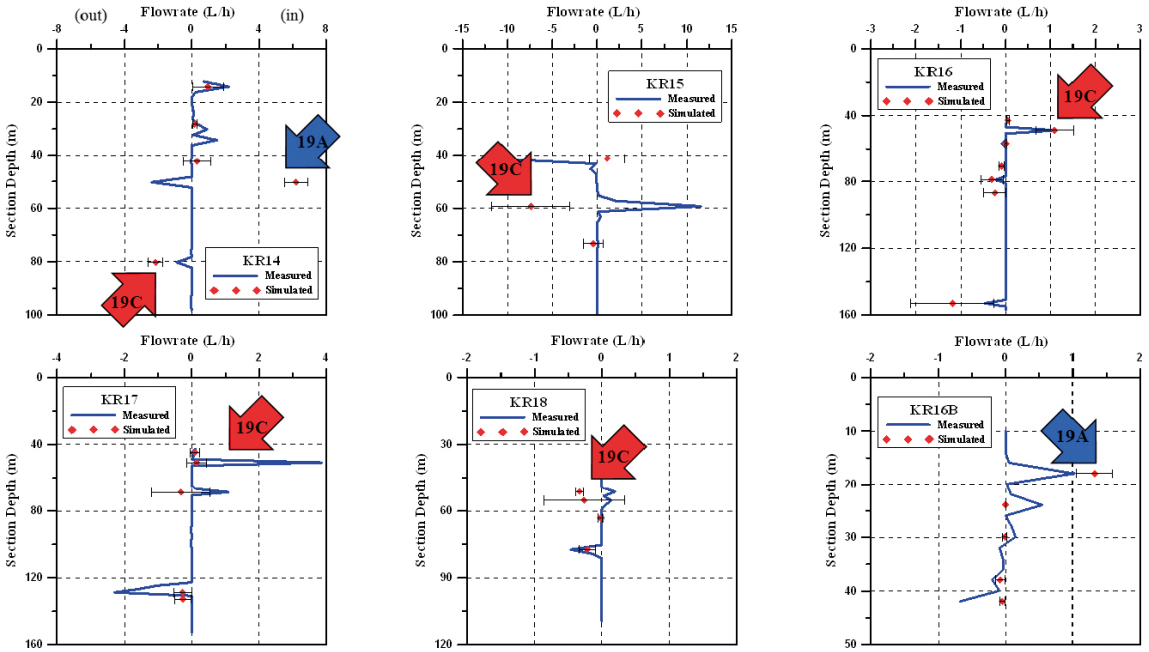

Figure 4-23. *Simulated and measured borehole flows (PFL) for undisturbed conditions.*

Pumped conditions

Recharge rates were recalibrated for the two pumping conditions (KR14 and KR18A) as given in Table 4-11. The fitted recharge rates are slightly lower for the packed-off borehole state which may reflect annual variations in head. Figure 4-24 and Figure 4-25 show the drawdowns and flow measurements for the models calibrated to the KR14 pumping condition. The results from the simulations are based on 30 realisations of the stochastic background fracture network. The drawdowns are typically better matched for the open hole state (although there are fewer measurements) and show smaller overall variability than observed in the packed-off state. A reasonable match to the observed flows is achieved although for some features the flow direction is not captured by the models.

Figure 4-26 and Figure 4-27 show the drawdowns and flow measurements for the models calibrated to the KR18A pumping condition. Again the results are based on 30 realisations of the stochastic background fracture network. The drawdowns are better matched for the open hole state (fewer measurements) and show smaller overall variability than observed in the packed-off state. Again a reasonable match to the observed flows is achieved.

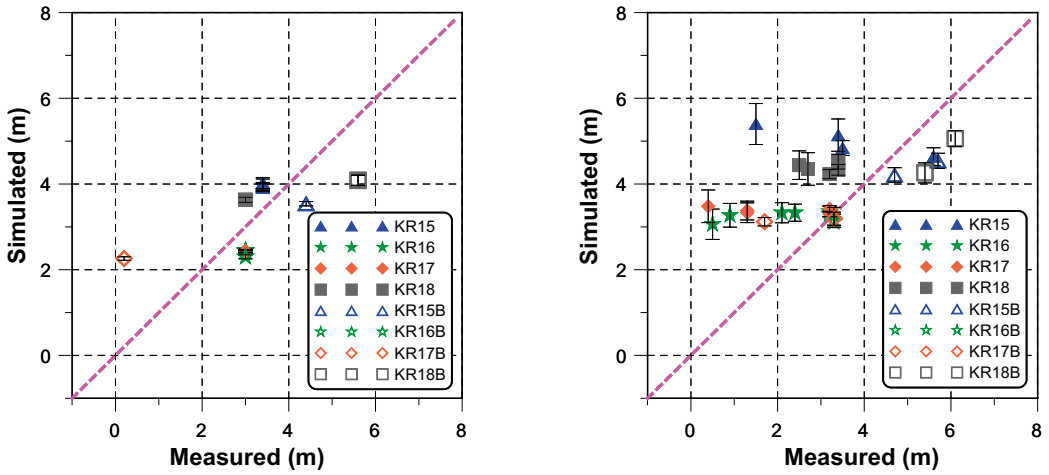

Figure 4-24. *Simulated and measured drawdowns for pumping in KR14 (SS23b, SS24b) in open and packed-off conditions.*

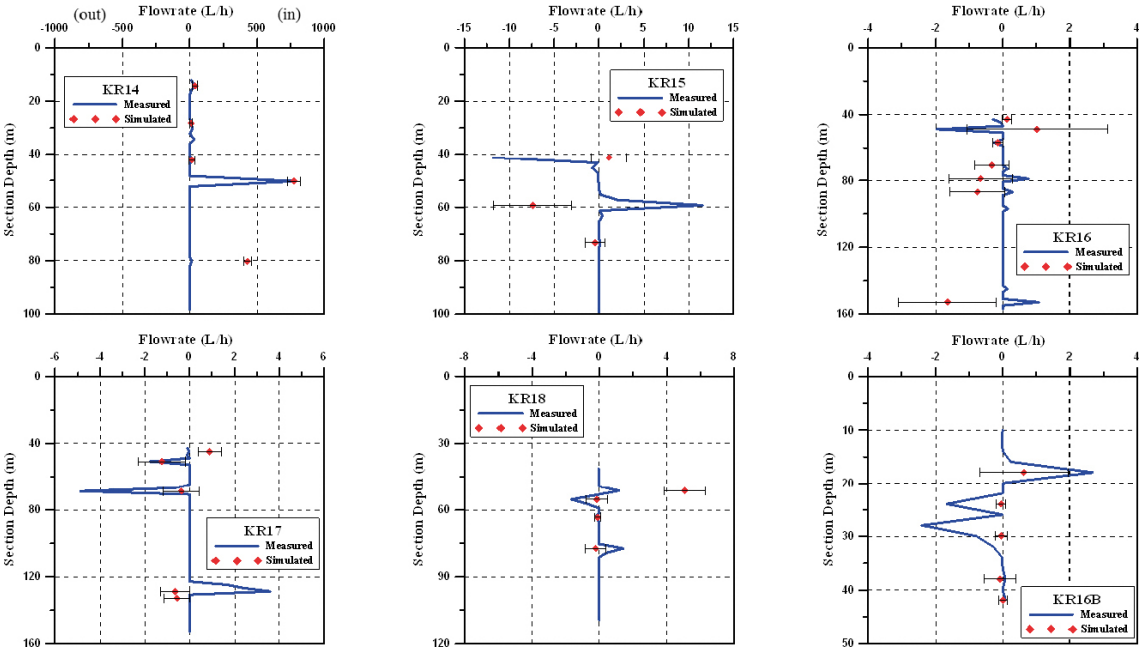

Figure 4-25. *Simulated and measured borehole inflows (PFL) for pumping in KR14 (SS23b).*

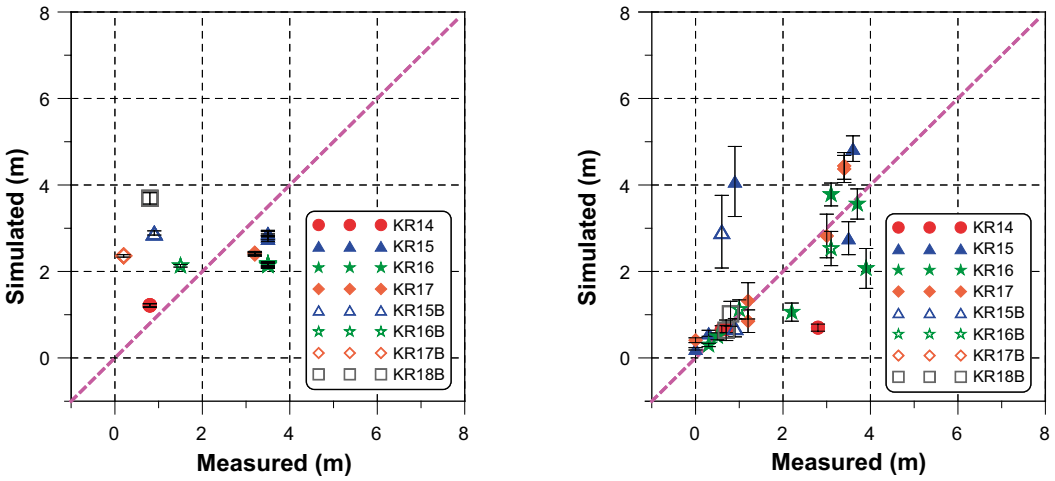

Figure 4-26. *Simulated and measured drawdowns for pumping in KR18A in open (left) and packed-off (right) conditions.*

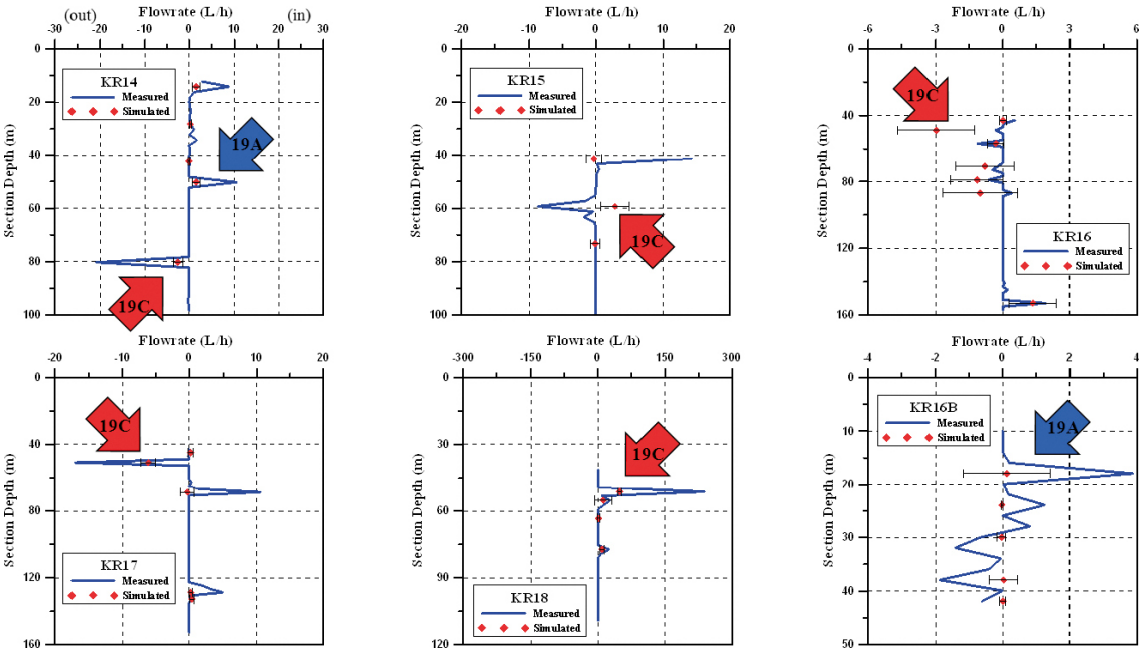

Figure 4-27. *Simulated and measured borehole inflows (PFL) for pumping in KR18A*

Table 4-11. Calibrated recharge rates for the different pumping conditions and borehole states. Uncertainty given as one standard deviation.

Pumping conditions	Calibrated recharge (mm/yr)	
	Open	Packed-off
Natural conditions	6.6±0.5	0.4±0.1
Pumping KR14	56.2±1.6	32.7±2.9
Pumping KR18A	18.6±0.8	15.7±1.6
All conditions and borehole states (used in particle tracking)	22.05±	

Transport simulations (particle tracking)

Particle tracks were simulated for pre- and post-calibration models using “no borehole” conditions. The results are very similar as would be expected since the difference is solely in the applied recharge. The tracks for the two cases are shown in Figure 4-28 and travel times in Table 4-12.

Table 4-12. Particle travel time and distance summaries for pre/post hydraulic test calibration simulations.

Release Point	Pre-calibration PA20c Travel time (× 10^3 year)	Travel distance (m)	Post-calibration PA29 Travel time (× 10^3 year)	Travel distance (m)
1	10.8±2.2	214± 3	8.3±2.0	209± 2
2	12.1±2.9	220±5	9.0±2.0	209±13
3	21.1±5.1	234±9	17.9±5.8	233±12
4	16.7±2.5	271±4	13.5±4.0	244±62
5	25.4±8.1	281± 39	16.9±4.0	267± 6
6	17.7±2.5	234± 5	15.0±2.8	236± 7
7	47.2±13.4	356±14	52.6±19.9	331±23
8	25.0±2.4	284± 7	27.3±5.3	278± 9
9	19.5±4.5	230± 7	15.0±4.6	224± 7

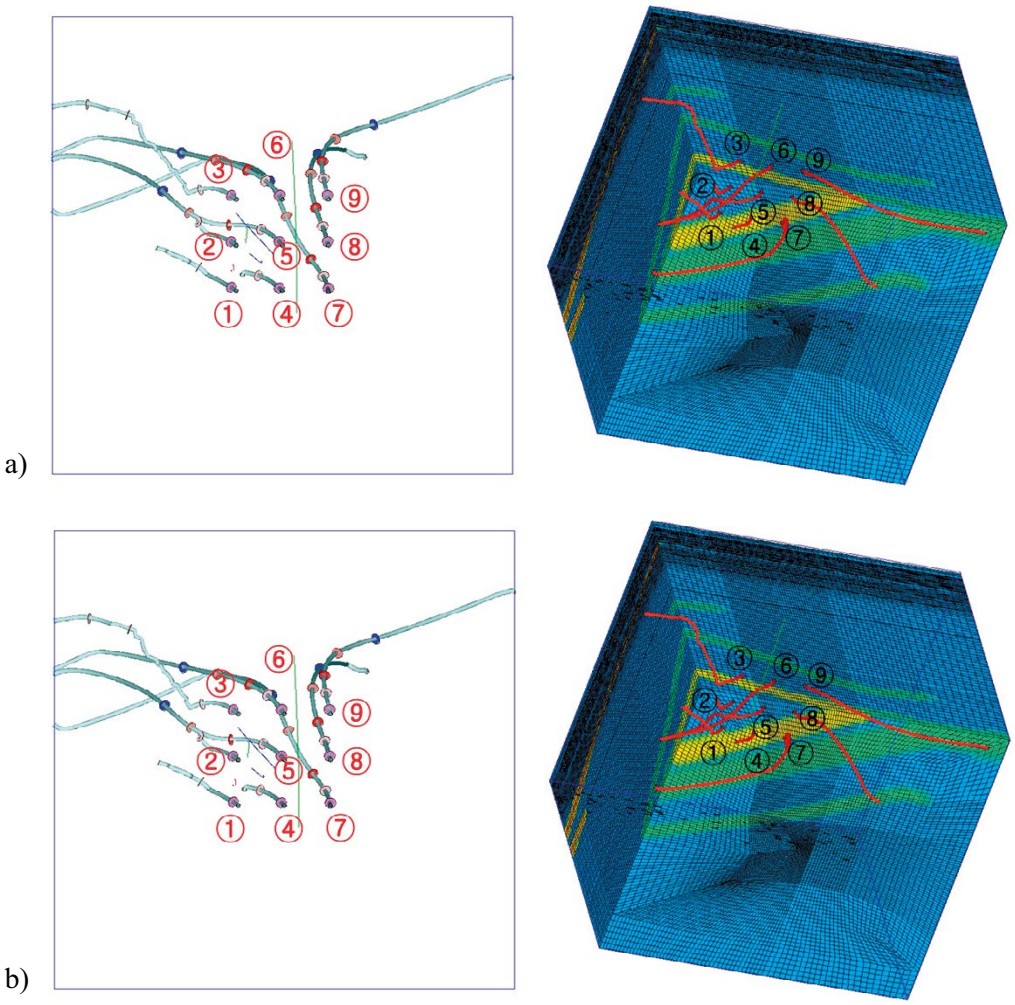

Figure 4-28. *Particle tracking paths from a) PA20c and b) PA29.*

4.5.3 NWMO/Laval

The results presented here and in Therrien and Blessent (2017) focus on model calibration, in part because the forward simulations were used as either initial conditions, or initial estimates for calibration. During the first phase of calibration only heads were used in the inverse modelling, and it was only in the latter part that the inverse modelling included flow observations as targets for calibration as developments of the HydroGeoSphere-PEST interface were required to incorporate flow observations. NWMO/Laval used four different hydro-structural models (see Figure 4-12):

- Model-1: Base case using 4 facies (SFB, SMFB, MHFB and HFB).
- Model-2: 4 facies model with alternative spatial distribution (different random seed).
- Model-3: 4 facies plus discrete features.
- Model 4: 5 facies model (UFB, SFB, SMFB, MHFB, HFB).

The structural models were all based on fractured rock facies defined by fracture density

- UFB: Unfractured Bedrock.
- SFB: Slightly Fractured Bedrock.
- SMFB: Sparsely to Moderately Fractured Bedrock.
- MHFB: Moderately Highly Fractured Bedrock.
- HFB: Highly Fractured Bedrock.

Undisturbed conditions

Figure 4-29 shows the simulated head fields without (SS20) and with open boreholes (SS21). The effect of the open borehole KR14 can be clearly seen in one vertical section. Drawdowns for pumping simulations with open boreholes were based on the simulated heads shown in Figure 4-29b. The situation for packed-off boreholes was considered in case SS22. Comparison with the measured undisturbed heads indicated that the models did not capture the low hydraulic head observed in some of the intervals.

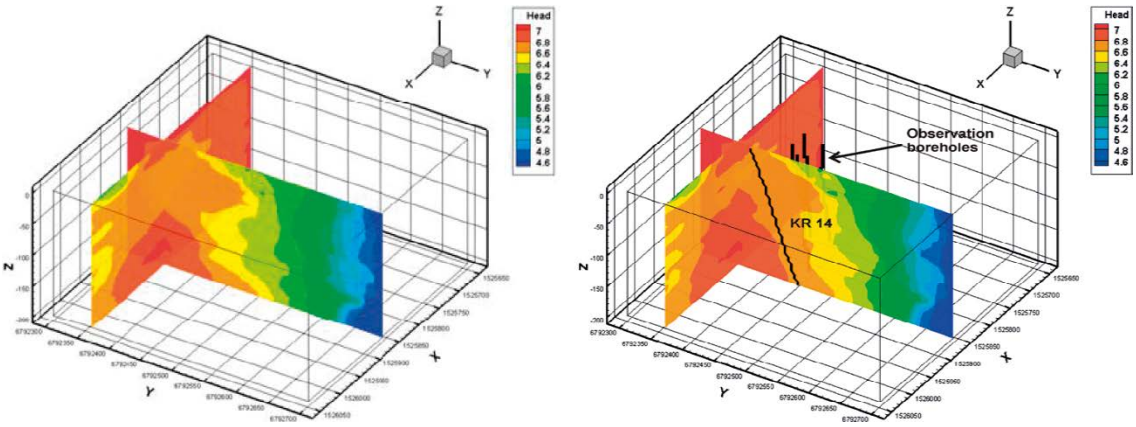

Figure 4-29. *NWMO/Laval simulated hydraulic head a) SS20 undisturbed conditions without boreholes; b) SS21 with boreholes but no pumping.*

Pumped conditions

NWMO/Laval's main goal was to perform inverse modelling to provide calibrated models and parameter estimates. Forward simulations were largely used to derive initial conditions and initial parameter estimates for the inverse simulations. A range of different approaches was used within the inverse simulations to investigate the overall match to observation via different choices of objective function:

- Using only head/drawdown data.
- Using both head/drawdown and flow data.
- Inclusion of 'Prior Information" (PI) fixing the ratios between the hydraulic conductivity of the different facies.
- Modification of the applied pumping flow rate. For pumping in KR18A with open holes (SS25) higher extraction flowrates (7 and 20 l/min) than recorded (5.3 l/min) were used in some simulations.

For pumped conditions, model comparisons focused on drawdowns rather than heads and baseline heads were calculated from the undisturbed cases (Figure 4-29). Calibrated models of open hole pumping in KR14 (SS23) with Model-1 (base case 4 facies) showed a poor fit with typically too high a drawdown at the pumping borehole and too small a drawdown in the observation holes. A better match was obtained with Model-3 (4 facies plus the two deterministic features suggested by the interpretation of Klockars et al. 2006).

Initial attempts to calibrate to the drawdown data resulted in very large uncertainties on the facies' hydraulic conductivity and so a priori information in terms of the ratio of hydraulic conductivities between the different facies was specified (KHFB=2 KMFFB=8 KSMFB). In a second phase of inverse modelling, PFL flows from the observation boreholes were included in the calibration objective function. Two cases were considered: one using all the observation boreholes (i.e. including the B holes) and the second using just the A boreholes. Flows (in ml/min) were given a relative weighting of 0.1, compared to 1 for heads (in m) to compensate for the typically higher numerical value of measured flow. Although the total flow from KR14 was specified as 25 l/min, the measured flow distribution in the pumped borehole was not included in the calibration as it resulted in too high a residual. Figure 4-30 shows a comparison of the confidence intervals for the calibrations with and without flow data. Table 4-13 gives the correlation coefficient, objective function and parameter correlations for the four different calibration targets. Inclusion of the flow data significantly reduces the parameter correlations and calculated uncertainties. This is consistent with the observation that extreme values of parameter correlation coefficients often occur when using only hydraulic heads (Hill 2000).

Table 4-13 gives the estimated hydraulic conductivity and objective functions for the various simulations. Overall the facies' hydraulic conductivities show limited variability (~factor 4) between all the simulations of the different pump tests:

- SMFB (Sparse to Moderately Fractured Bedrock): $2.2-8.8\times10^{-7}$ m/s.
- MHFB (Moderately to Highly Fractured Bedrock): $1.1-4.4\times10^{-6}$ m/s.
- HFB (Highly Fractured Bedrock): $0.5-1.8\times10^{-5}$ m/s.

This variability is only slightly greater than that for the different SS25b simulations. The hydraulic conductivity estimates for open-hole pumping (Figure 4-30a,b) and packer testing (Figure 4-30c,d) in KR14 are very similar. In general the simulations for pumping in KR14 (Figure 4-30a,b) reproduce the observations better than those simulating pumping in KR18A (Figure 4-30e,f).

Simulations were performed for pumping in KR18A with both open hole (SS25) and packed-off boreholes (SS26). In both cases NWMO/Laval found it difficult to reproduce the observed behaviour and for the open-hole pumping in KR18A, the flow-rate was increased from the measured 5.3 l/min to 7 l/min[22] in an attempt to match the observations. Despite this, the simulated drawdowns were less than 8 m compared to the measured drawdown of ~10 m. The flow-rate for pumping with packed-off boreholes was given as 5–7 l/min but drawdown was found to be best fitted with a flow-rate of 7 l/min.

[22] The case of an even higher flow-rate of 20 l/min was also considered.

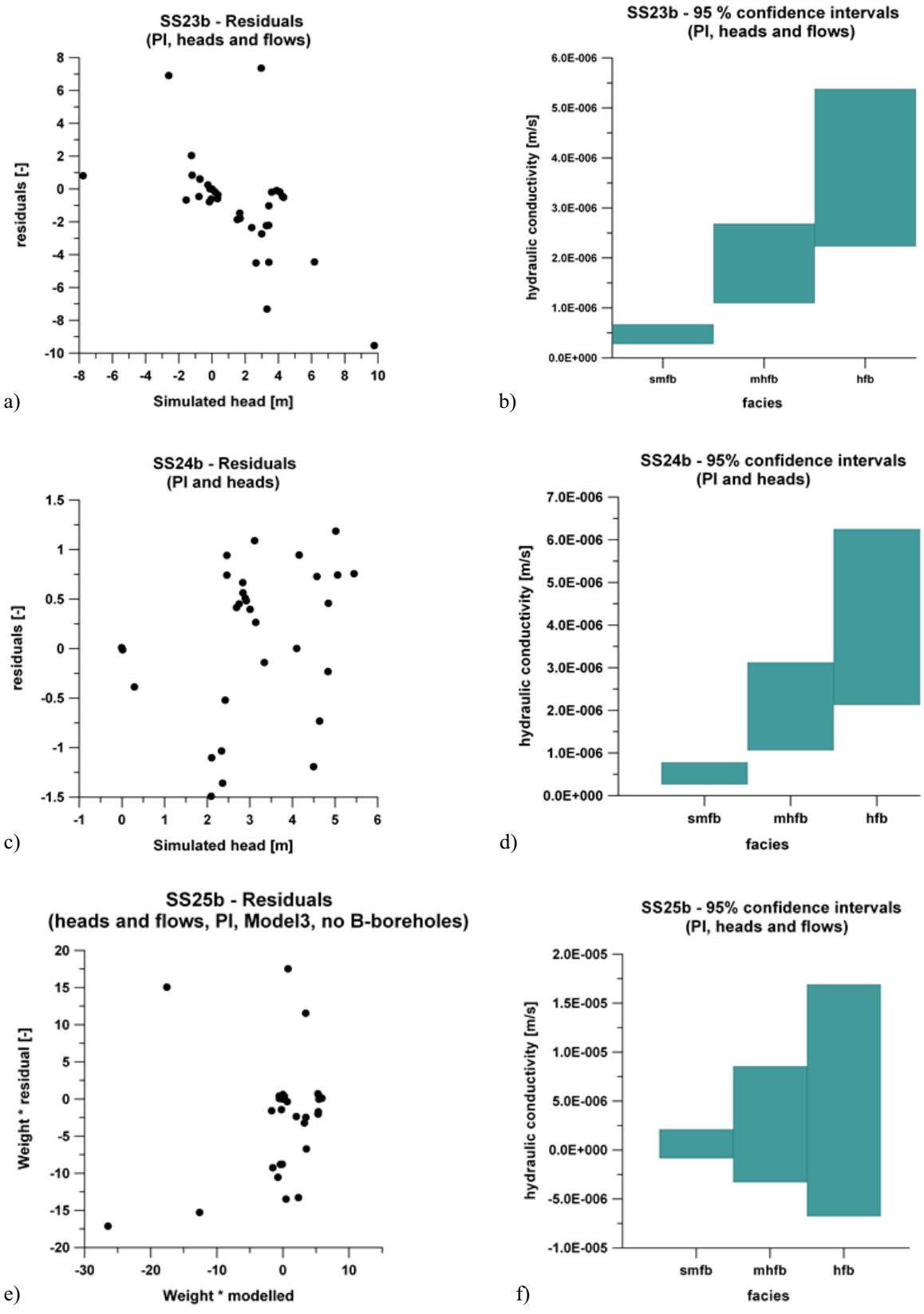

Figure 4-30. *NWMO/Laval residuals and 95 % confidence intervals for: a, b) open-hole pumping in KR14 (SS23b); c, d) packer testing in KR14 (SS24b) and e, f) open-hole pumping in KR18A (SS25b). All simulations use prior information (PI) specifying ratio of facies' hydraulic conductivity.*

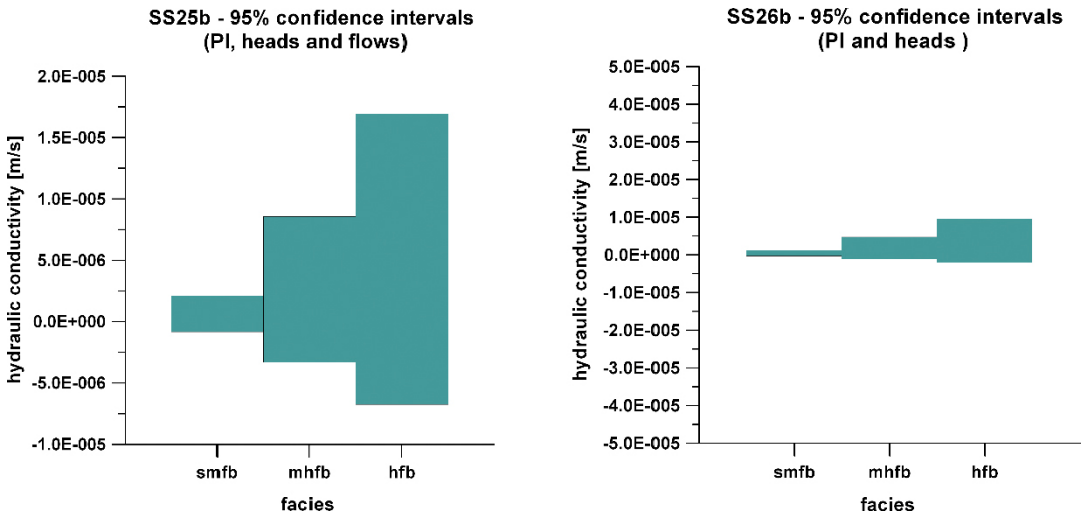

Figure 4-31. *Confidence intervals on facies' hydraulic conductivity for KR18A pumping (SS25b) a) calibration to heads and flows with prior information for open hole conditions, and b) heads and prior information for packed-off conditions.*

Parameter sensitivities for the two horizontal deterministic features were also found to be different between the simulations for KR14 and KR18A, with low sensitivity for feature hydraulic aperture (equivalent to transmissivity) in the KR18A simulations.

Better matches to the pumping in KR18A were achieved by increasing the flow-rate, which indicated that the rock was less conductive around KR18A and models with a low-conductivity around KR18A showed an improved match with the appropriate flow rate.

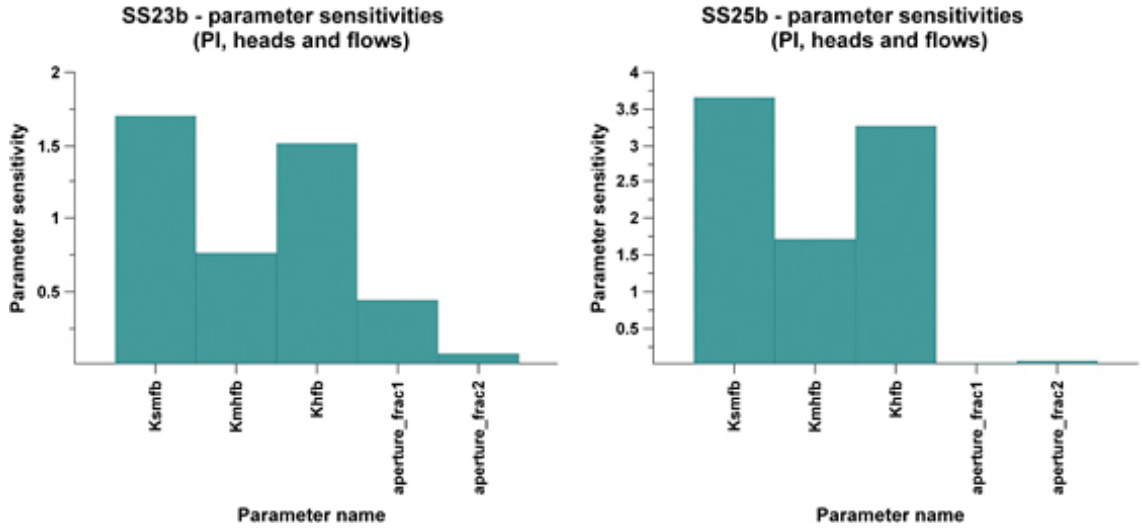

Figure 4-32. *NWMO/Laval parameter sensitivities for pumping in KR14 and KR18A.*

Table 4-13. Estimated facies' hydraulic conductivity and objective function (ϕ) value.

Pumping	Simulation	PI[1]	PFL[2]	Q[3]	SMFB [m/s]	MHFB [m/s]	HFB [m/s]	ϕ
None	SS21				2.2E−7	4.4E−6	5.3E−6	0.07
	SS22				8.8E−7	3.4E−6	1.5E−5	6.4
KR14	SS23b_PI	Y			7.5E−7	2.9E−6	5.9E−6	1.9
	SS23b_PI_flow_A	Y	Y		8.8E−7	3.5E−6	7.0E−6	381
	SS23b_PI_flow_AB	Y	Y		6.6E−7	2.8E−6	5.3E−6	897
	SS24b				8.8E−7	1.1E−6	1.8E−5	15.7
	SS24b_PI	Y			7.0E−7	2.9E−6	5.8E−6	17.5
KR18A	SS25b_Q5.3			Y	2.2E−7	1.1E−6	5.3E−6	20.9
	SS25b_Q7			Y	2.2E−7	1.1E−6	5.5E−6	12.4
	SS25b_Q7_PI_flow	Y	Y	Y	8.8E−7	3.6E−6	7.0E−6	2 119
	SS25b_Q20_PI_flow	Y	Y	Y	8.8E−7	3.5E−6	7.0E−6	1 245
	SS25b_Q5.3_5zones[4]	Y		Y	2.2E−7	1.1E−6	1.1E−5	5
	SS25b_Q5.3_5zones_PI_flow	Y	Y	Y	7.0E−7	2.8E−6	5.5E−6	2 326
	SS26b				3.5E−7	1.1E−6	5.3E−6	36.8
	SS26b_PI		Y		6.6E−7	2.6E−6	5.3E−6	52.4

[1] PI: prior information (relationship between facies' hydraulic conductivity) included in inverse process.
[2] PFL: Flow measurements used as targets for calibration.
[3] Q: withdrawal from borehole KR18A (7 and 20 l/min, respectively).
[4] Zones: additional low conductivity zone around KR18A.

Transient simulations

Transient flow simulations were performed for the case of pumping in KR15A with open boreholes (TS27) and pumping in KR14 with open boreholes except for a packed-off interval in KR15A that was used for a transverse flow measurement (see discussion of TS28). Pumping was simulated by applying a drawdown boundary condition to the pumping borehole (not a withdrawal rate) for the period of the test. Drawdowns and changes in flow from the un-pumped conditions were calculated for the monitoring boreholes. TS28 focused on measurements of the transverse flow in KR15A which are summarised in Table 4-14.

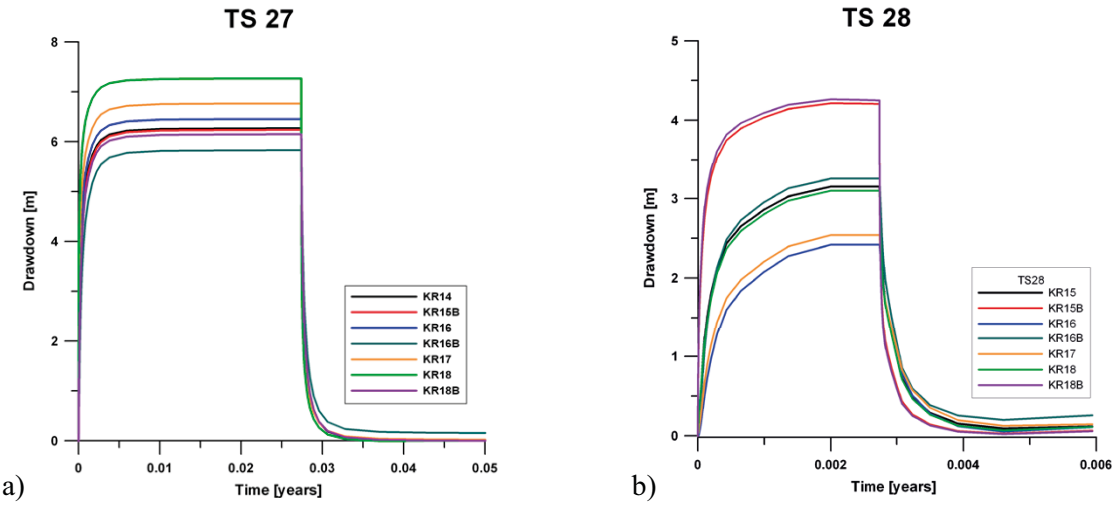

Figure 4-33. *Simulated transient drawdowns for a) 10 days pumping in KR15A (TS27) and b) 1 day pumping in KR14 (TS28).*

Table 4-14. Calculated interval flows in KR15A from transient simulations of pumping in KR14 (TS28).

Selected fracture	Model flow positions	Flow (l/day)	Comment
59 m	60 m	119	Location of HZ19C/Plane-1
72.3 m	70 m	22	Flow from borehole
125 m	120 m	−12	Flow into borehole

Transport simulations

NWMO/Laval performed both advective particle tracking (using TECPLOT) and "life expectancy" calculations (including dispersion and diffusion) for the 9 particle release points. The simulations were repeated for an initial model of undisturbed conditions without boreholes (PA20C) and for the final calibrated model (PA29). The hydraulic conductivities of the facies used in PA29 were the averages of the estimated values from the various flow and pumping simulations (SS21-SS26).

The results from the advective particle tracking (Figure 4-34) are broadly in line with those from the life-expectancy calculations. The PA29 life expectancy probability density functions (PDFs) show lower and slightly later peaks (Figure 4-35) than those from PA20C, which probably reflects the reduced hydraulic conductivity in the calibrated model.

4.5.4 Posiva/VTT

Pumped conditions

Forward models were simulated but the main effort went into model calibration of the open-hole KR14 pumping case (SS23b); the open-hole KR18A pumping case (SS25a) was then simulated using the calibrated model from KR14 pumping. No calibration was performed on the models with packed-off intervals (SS24a/b, SS26a/b) because of the lack of conditioning of fracture locations in the boreholes (resulting in simulated intervals without fracture intersections and therefore without calculated hydraulic heads).

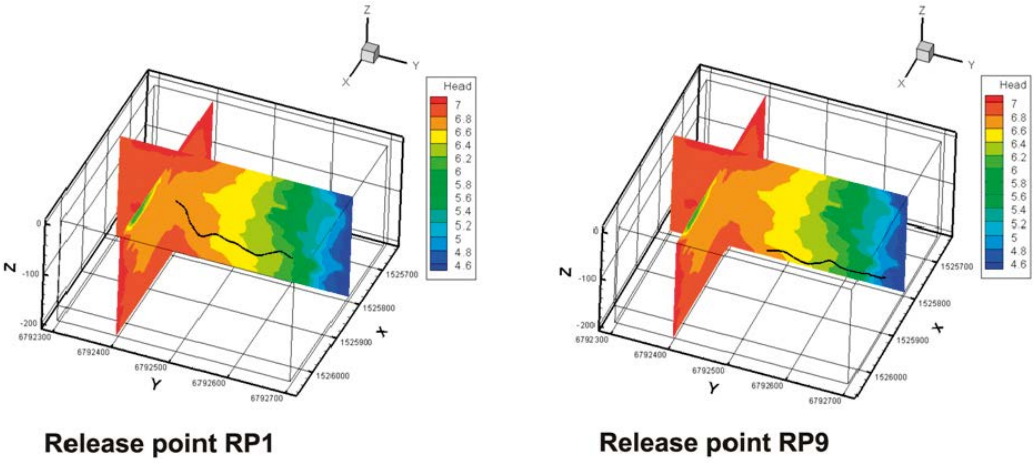

Figure 4-34. *Particles tracks for RP1 and RP9 in the forward calculation in PA conditions (PA20C).*

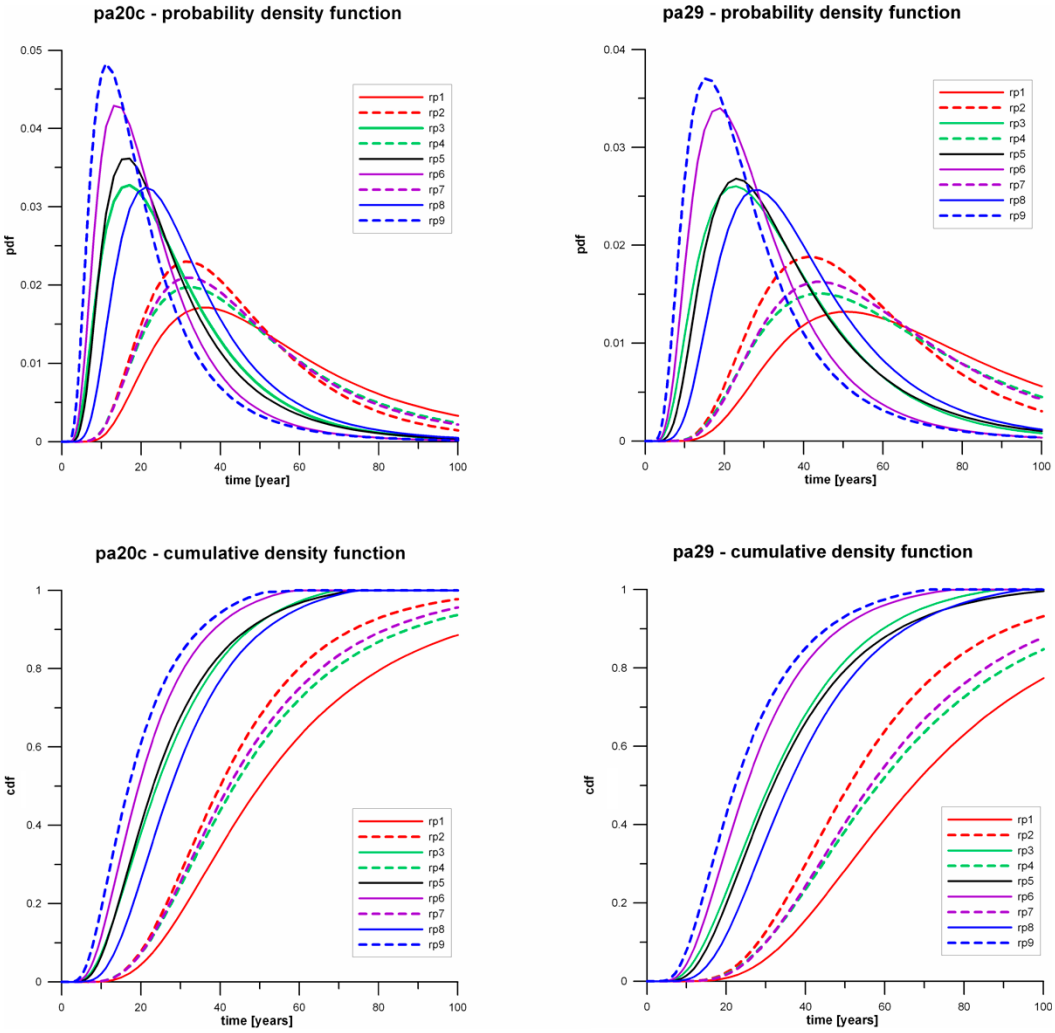

Figure 4-35. *Life expectancy PDFs and cumulative density functions (CDFs) from PA20c and PA29.*

Figure 4-36 shows the simulated flow distributions from the 10 realisations of 3 selected model cases (of the 130 cases considered) together with the observed distribution. The parameters of the 3 model cases are given in Table 4-15. The best-model case (as determined from Flow K-S distance) included sheet joints and excluded high transmissivity background fractures but had a high head RMSD. The calibration procedure identified a small number of model cases with both low Flow K-S distance and Head RMSD.

Figure 4-37 shows the relationship between Flow K-S distance and Head RMSD. The parameters of the best overall model case are given in Table 4-15. Krumenacker et al. (2017) commented that the poor head RMSD scores were obtained in sensitivity cases with low transmissivities (upper truncation $\log_{10}(\text{Tmax}) = -6.5$ m^2/s) that included the two sheet joints (Figure 4-38a), while poor flow K-S distances came from cases with larger fractures (rmax = 100 m) with higher transmissivities (upper truncation $\log_{10}(\text{Tmax}) = -4.0$ m^2/s) and with weak correlation between fracture size and transmissivity (SL ≥ 0.07).

A separate calibration of the sheet joint transmissivity using the EnKF approach resulted in a transmissivity of 2×10^{-5} m^2/s for the upper sheet joint, and a very low transmissivity $\sim 10^{-16}$ m^2/s for the lower joint (Figure 4-38b), suggesting that it was not hydraulically significant and therefore need not be included in the models.

Transient simulations were also performed (Figure 4-39). EPM models produced qualitatively correct results with a fairly large range of specific storage values, but finding a storativity value for the DFN model constituted a problem. The specific storage was set to $S_s = 10^{-6}$ m^{-1}.

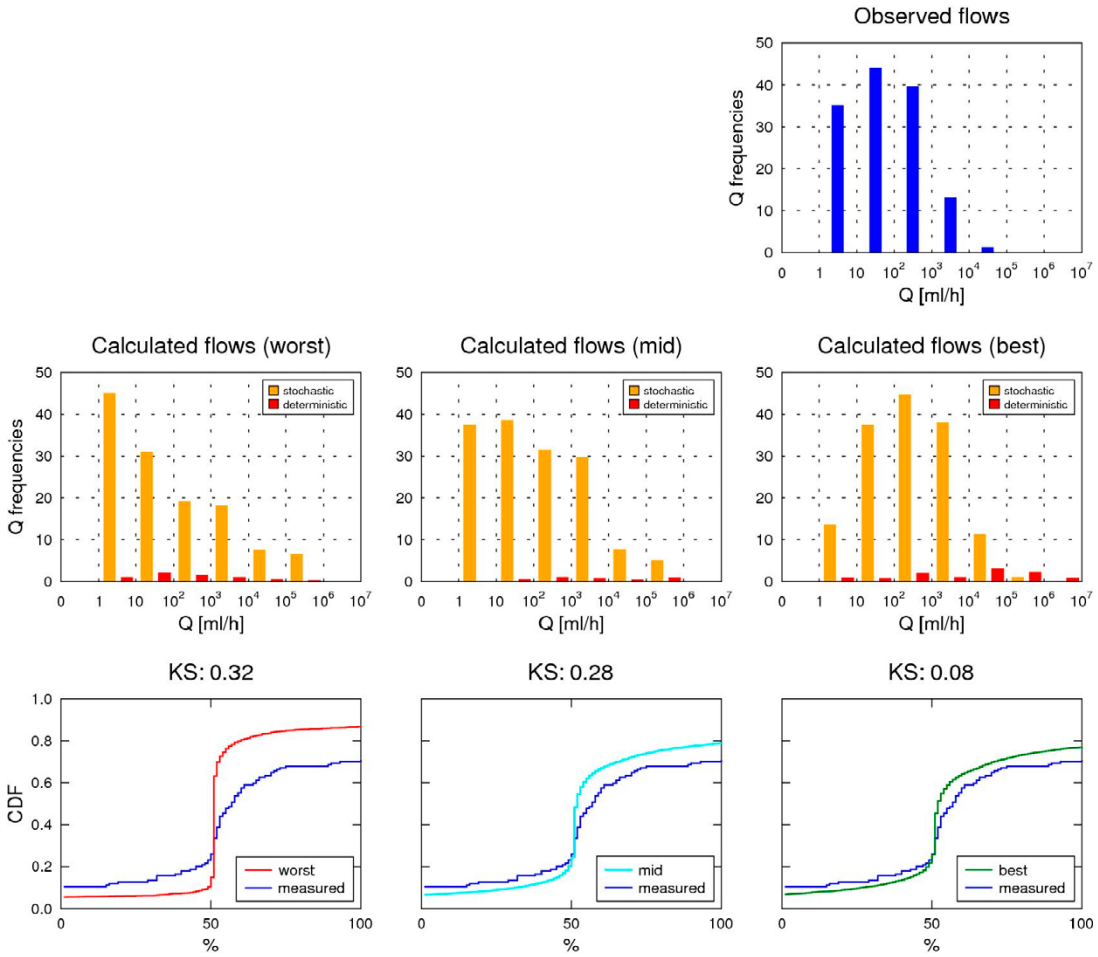

Figure 4-36. *K-S scoring of observed flow frequencies showing worst, mid and best Flow K-S distance scoring model cases.*

Table 4-15. Parameters of worst, mid and best model cases as defined by K-S scoring.

	Worst K-S case	Mid K-S case	Best K-S case	Best overall case
Flow K-S distance	0.32	0.28	0.08	0.097
S_L (-)	0.25	0.15	0.15	0.07
Head RMSD (m)	8.6	8.4	51.2	3.6
σ(Q) (ml/min)	0.6	0.8	1.2	0.8
r_{max} (m)	100	100	50	50
$\log_{10}(T_{max})$ (m^2/s)	−4	−4	−6.5	−5
$\mu(\log_{10}(T))$ (m^2/s)	−8.3	−8.3	−8.3	−8.3
$\sigma(\log_{10}(T))$ (m^2/s)	1.2	1.2	1.8	1.8
Sheet joints	None	None	Upper and lower	None

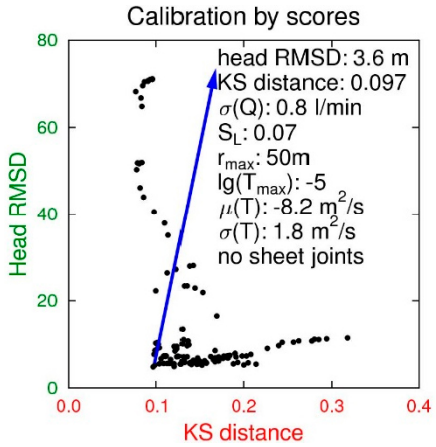

Figure 4-37. *Cross-plot of model case scores for Kolmogorov-Smirnov distance (flows) and Head RMSD. Parameters of lowest score case shown.*

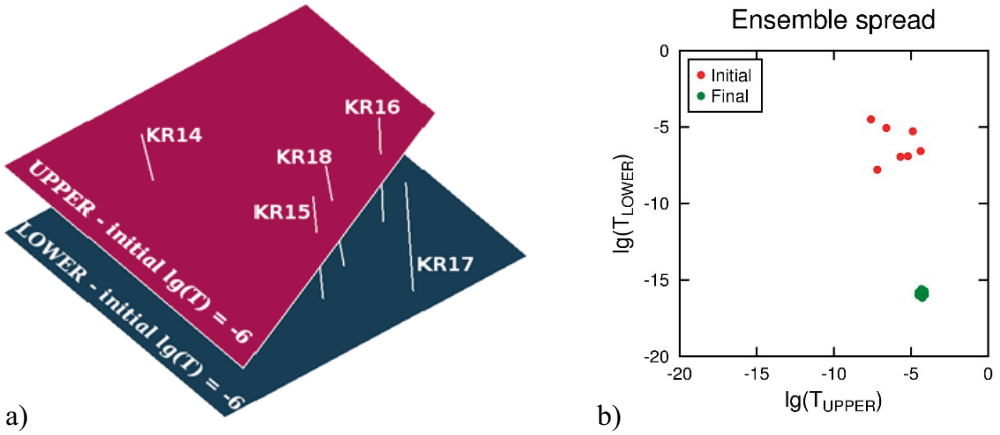

Figure 4-38. *Sheet-joints a) configuration and b) EnKF results for log_{10} transmissivity.*

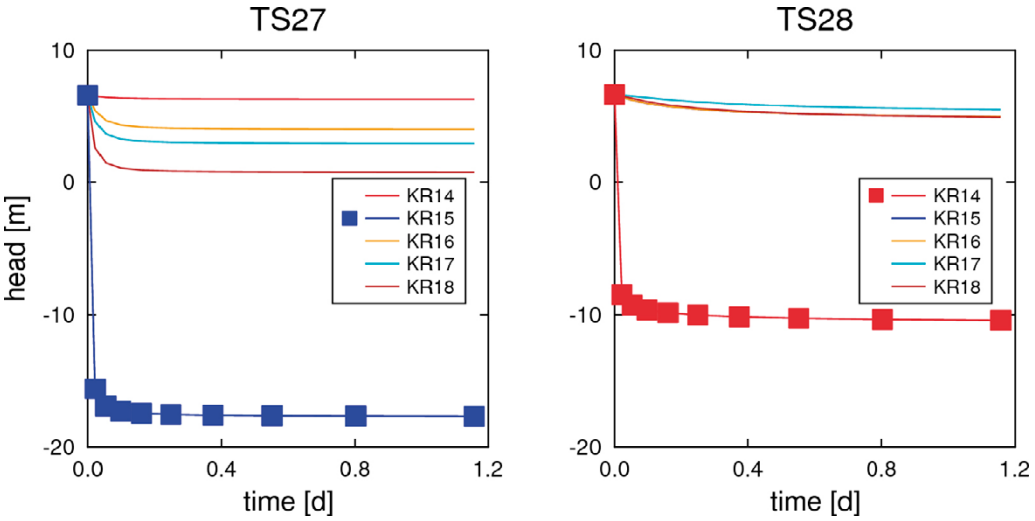

Figure 4-39. *Head histories for the first day of pumping in the KR15A pumping (TS27) and KR14 pumping (TS28) simulation cases.*

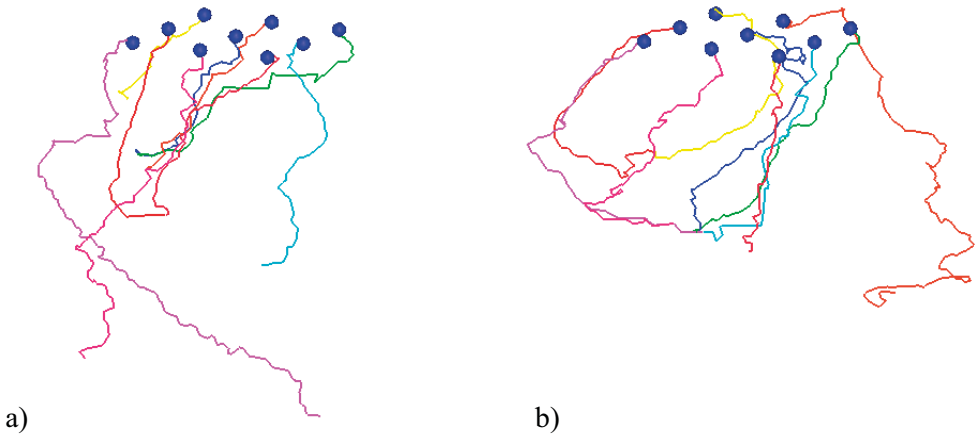

Figure 4-40. *Posiva/VTT particle tracking paths from a) the initial (PA20c) and b) the final (PA29) transport simulations.*

Transport simulations (particle tracking)

Path lines initiated from the nine locations defined in the performance measures are shown for the initial (PA20c) and final (PA29) transport simulations in Figure 4-40. The effect of model calibration produces quite different trajectories for almost all of the starting positions.

4.5.5 SKB/CFE

SKB/CFE performed simulations with models based on both the 2006 hydro-structural model (described as Old Structural Model or OSM) and the updated 2008 hydro-structural model (described as New Structural Model or NSM). Initially calculations were performed on 3 realisations of the background rock DFN. It was found that there were only minor differences between realisations and one realisation was selected as being preferable based on the total drawdowns for pumping in KR14, KR15A and KR18A.

Table 4-16 gives the measured and simulated drawdowns for the two hydro-structural models. For both models the simulated drawdowns show a reasonable match with observation. However, a comparison of the flows along the boreholes shows significant differences between them. In particular the flow along boreholes for "No pumping" conditions changes dramatically. It is possible that this is due to the more uniform head field calculated from the revised model.

Table 4-16 Measured and simulated drawdowns (m), for open hole pumping tests in KR14, KR15A, KR16A, KR17A and KR18A. Measurement in black, 2006 structural model (OSM) simulation in red, 2008 structural model (NSM) simulation in blue.

	KR14			KR15A			KR15B			KR16A			KR16B		
KR14	6.0	6.7	6.8	3.4	3.1	4.0	4.4	4.0	4.9	3.0	3.7	3.9	3.0	4.8	4.7
KR15A	1.0	0.9	1.0	10.0	8.6	14.3	2.0	0.8	1.0	3.5	2.6	3.8	2.4	0.7	0.9
KR16A	0.9	0.9	0.9	3.3	2.4	3.3	1.0	0.8	0.8	10.0	13.7	13.5	1.7	0.8	0.8
KR17A	1.0	1.1	1.1	3.5	3.5	5.2	2.0	1.0	1.0	3.9	5.9	5.6	1.5	0.9	1.0
KR18A	0.8	0.8	0.8	3.5	2.7	3.9	0.9	0.7	0.7	3.5	5.9	3.8	1.5	0.7	0.7

	KR17A			KR17B			KR18A			KR18B		
KR14	3.0	3.5	3.7	0.2	2.6	2.5	3.0	3.7	3.9	5.6	5.0	4.9
KR15A	3.0	3.1	4.5	1.0	0.4	0.5	3.2	2.3	5.0	1.3	0.7	0.9
KR16A	3.4	4.5	4.3	0.4	0.5	0.5	3.7	4.3	4.3	0.9	0.8	0.8
KR17A	11.0	17.5	16.5	0.2	0.6	0.6	3.7	5.9	6.0	0.9	1.0	1.0
KR18A	3.2	4.1	4.1	0.2	0.3	0.4	10.0	10.2	10.0	0.8	0.7	0.7

Simulation of the packer tests was performed without any further calibration. These simulations are therefore forward models based on calibration to the open hole pumping tests. The measured and simulated drawdowns are given in Table 4-17.

Transport simulation (particle tracking)

Particle tracking was based on the results from the "Natural Conditions" simulation (SS20b). The Task Definition (Vidstrand et al. 2015) specified that particles were to be released in a rectangular area at a depth of −100 m.a.s.l. Because the model grid was not continuous at this depth, particles were released in an area with down-going flow at a depth of −10 m.a.s.l. (x: 5 815–5 830 m; y: 2 405–2 420 m). The resulting particle tracks are shown in Figure 4-41. Particles travel north and end below the Baltic Sea. A separate path takes some particles slightly further north than the majority of particle tracks.

Table 4-17. Measured and simulated drawdowns (m), for pumping in KR14 and KR18A.

Borehole	Int	Pumping KR14				Pumping KR18A			
		P_{NAT}	P	ΔH Meas	ΔH Sim	P_{NAT}	P	ΔH Meas	ΔH Sim
KR14	L3	6.9	0.3	6.6	6.8	6.91	6.13	0.8	0.6
	L2					6.92	5.48	1.4	0.7
	L1					6.92	5.05	1.9	2.8
KR15A	L6	6.90	2.88	4.0	5.6	6.89	4.05	2.8	0.9
	L5	6.90	3.04	3.9	3.5	6.89	2.12	4.8	3.6
	L4	6.86	3.52	3.3	3.4	6.82	3.11	3.7	3.5
	L3	-	-	-	1.5	-	--	-	0.3
	L2		-	-	-	-	-	-	-
	L1		-	-	-	-		-	-
KR15B	L2	6.91	3.6	3.3	4.7	6.90	6.31	0.6	0.6
	L1	6.90	2.87	4.0	5.7	6.89	4.12	2.8	0.9
KR16A	L6	6.91	3.05	3.9	3.2	6.86	3.53	3.3	3.3
	L5	6.91	3.11	3.8	3.2	6.90	2.12	4.8	3.7
	L4	6.90	4.06	2.8	2.4	6.89	3.75	3.1	3.9
	L3	6.81	4.02	2.8	2.1	6.89	3.93	3.0	2.2
	L2	-	-	-	0.9	-	-	-	0.5
	L1	-	-	-	0.5	-	-	-	0.3
KR16B	L3	6.94	4.40	2.5	3.3	6.94	6.50	0.4	1.0
	L2	6.92	2.35	4.6	3.3	6.91	6.14	0.8	3.1
	L1	6.91	3.9	3.9		6.85	3.54	3.3	
KR17A	L6	6.86	3.57	3.3	3.2	6.85	3.74	3.1	3.4
	L5	6.88	3.30	3.6	3.2	6.88	2.10	4.8	3.4
	L4	6.86	3.60	3.3	3.3	6.85	2.75	4.1	3.0
	L3	6.85	3.89	3.0	1.3	6.84	3.33	3.5	1.2
	L2	6.84	3.96	2.9	1.3	6.84	3.45	3.4	1.2
	L1		-	-	0.4	-	-	-	-
KR17B	L2	6.88	4.53	2.4	1.7	6.87	6.42	0.5	0.5
	L1	6.86	3.8	3.1	3.3	6.85	4.82	2.0	2.8
KR18A	L5	6.91	2.96	4.0	3.2	6.89	−3.72	10.6	8.1
	L4	6.90	3.08	3.8	3.4	-	-	-	-
	L3	6.90	3.09	3.8	3.4	-	-	-	-
	L2	6.88	3.58	3.3	2.5	-	-	-	-
	L1	6.88	3.68	3.2	2.7	-	-	-	-
KR18B	L2	6.95	6.27	0.7	5.4	6.95	6.80	0.2	0.7
	L1	6.91	2.15	4.8	6.1	6.91	6.10	0.8	0.8
KR14	L3	6.9	0.3	6.6	6.8	6.91	6.13	0.8	0.6
	L2					6.92	5.48	1.4	0.7
	L1					6.92	5.05	1.9	2.8

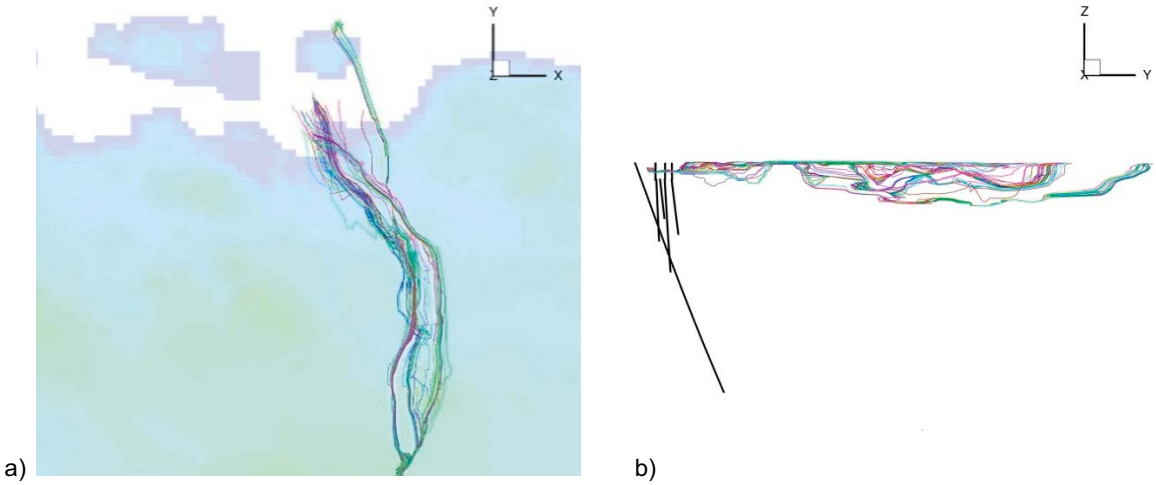

Figure 4-41. *SKB/CFE particle tracking paths from a) plan view; b) S-N vertical section.*

4.5.6 SKB/KTH

SKB/KTH considered only the flow data for the different model variants. Frampton et al. (2015) provide detailed results from all the model variants but only the results from Configurations A (reference case) and B (improved model) are shown in Figure 4-42. to Figure 4-44. The flows in the pumping boreholes are typically better matched by Configuration A and underestimated in Configuration B, while the observation boreholes are better matched in terms of magnitude and direction by Configuration B.

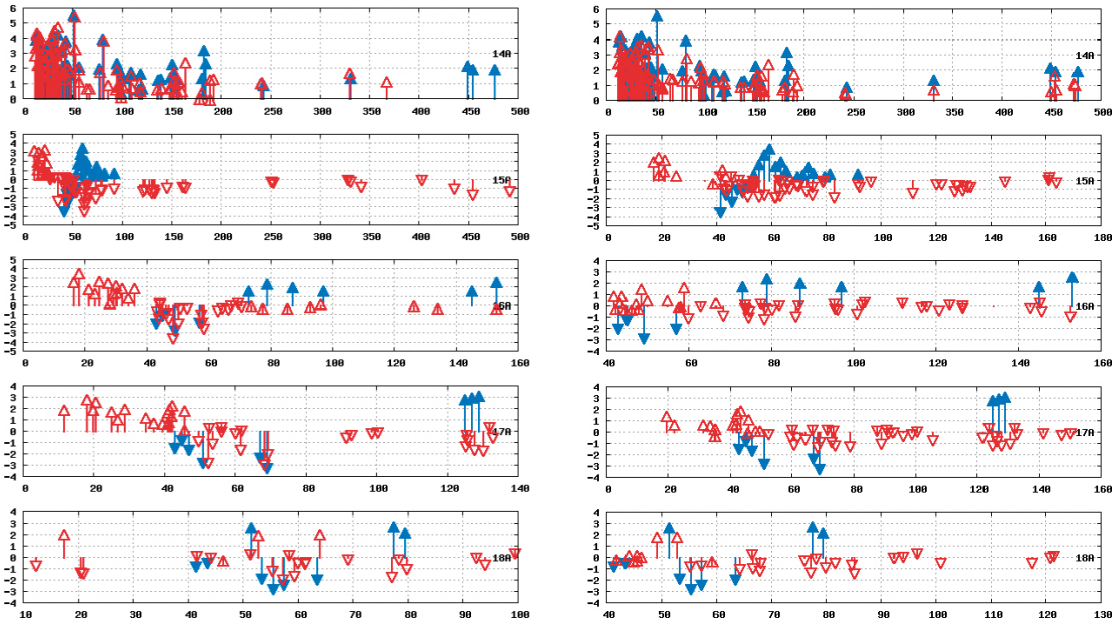

Figure 4-42. *Predicted (red) and measured (blue) flow in/out of boreholes KR14-KR18A for pumping in KR14 for Configuration A (left) and B (right).*

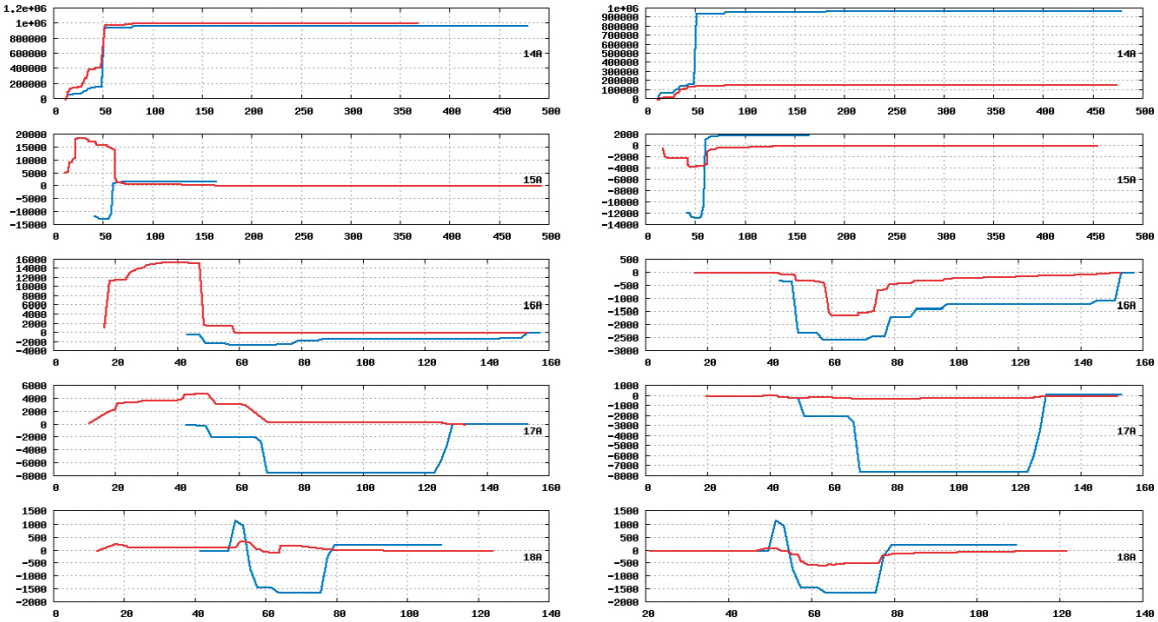

Figure 4-43. *Predicted (red) and measured (blue) flow along boreholes KR14-KR18A for pumping in KR14 for Configuration A (left) and B (right).*

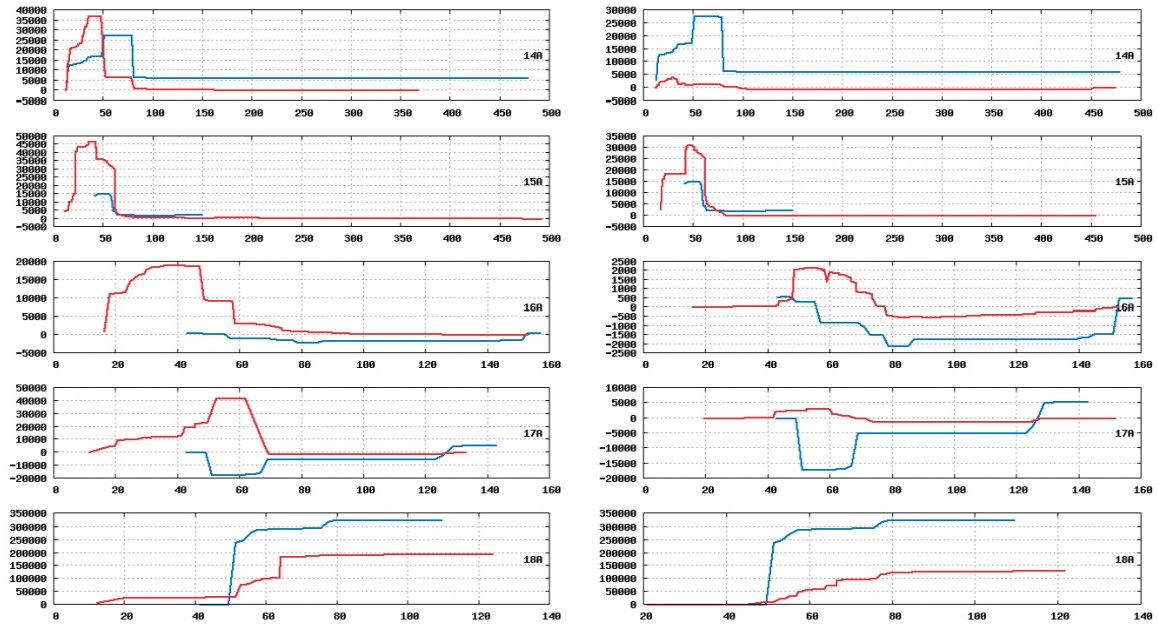

Figure 4-44. *Predicted (red) and measured (blue) flow along boreholes KR14-KR18A for pumping in KR18A for Configuration A (left) and B (right).*

Frampton et al. (2015) note the absence of measured PFL flows in the deep part of KR15A, and that generally there are more simulated fracture flows than are measured for all boreholes, also that cumulative flow-rates are generally over-estimated in observation boreholes. For Configuration B an exception to the overall good match to observation borehole flow is the response in KR17A when pumping in KR14, KR16A and KR18A. Also, the response magnitude in KR14 is generally under-estimated for the upper parts of the borehole for all pumping cases.

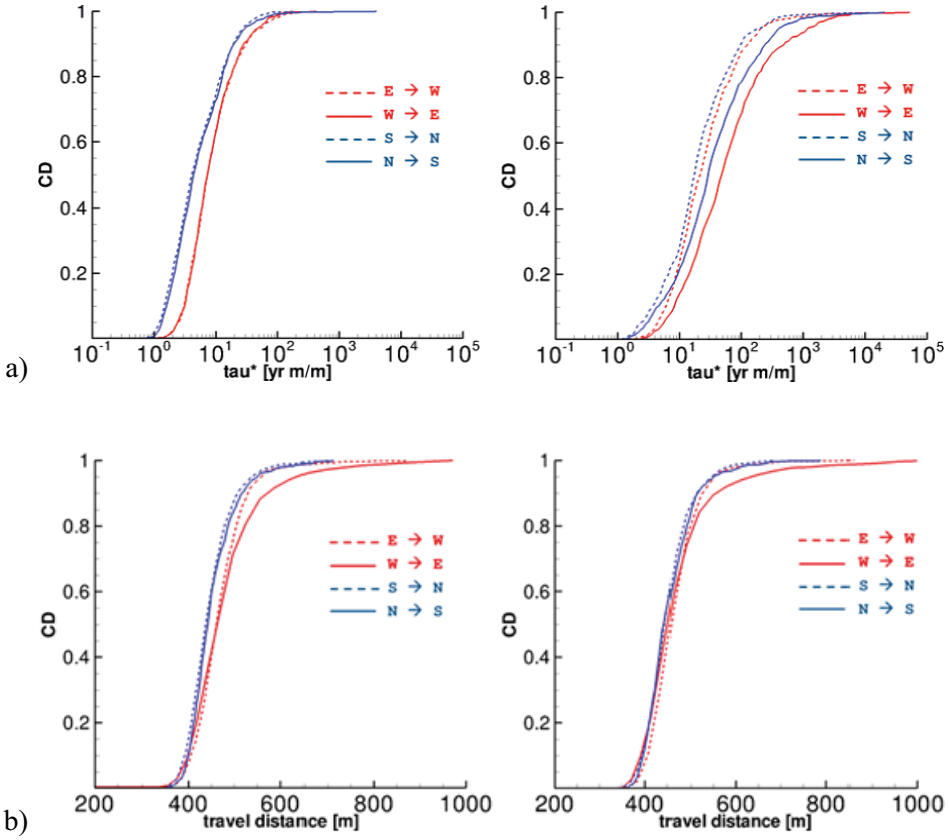

Figure 4-45. *Cumulative distribution of a) total particle travel time normalised by the value of the hydraulic gradient; and b) travel distance for each of the four principle directions. Left: Flux injection mode. Right: Resident injection mode.*

Transport simulations (particle tracking)

Transport simulations were performed for Configuration B model variant. Particle tracking was performed in four directions (North–South, East–West). For each direction a 1 % gradient was applied to the lateral boundaries of the model and 1 000 particles were injected. Particle injection locations were either proportional to the estimated flux ("flux injection") or randomly selected from the fracture interactions ("resident injection"). The simulations considered only advective transport within the fractures[23].

4.6 Model comparison

The modelling groups were asked to submit a range of performance measures as part of the Task Description (Vidstrand et al. 2015). In Task 7B these measures included descriptions of the conceptual model (Task 7B1) and a set of quantitative measures for comparison with measurements and between models. The quantitative performance measures included:

- Hydraulic heads during natural and "undisturbed" conditions.
- Drawdowns and flows during pumped conditions.
- Particle tracks.

These measures have been used as the basis for discussion within this section. While most groups submitted a single set of measures, JAEA provided the results from 5 different model realisations. Although no single realisation was preferred, realisation "02" had relatively larger drawdown for the KR14 and KR18 pumping cases which were not significantly improved by calibration.

[23] CONNECTFLOW assumes "perfect mixing" at fracture intersections.

When comparing heads or drawdowns the evaluation used cross-plots of simulated versus measured data, the calculated Pearson correlation coefficient r and the mean square residual (simulation-measurement). Ahokas et al. (2008) reviews head measurement methods and provides detailed estimates of head uncertainty for the KR1 borehole. Typically, uncertainty in fresh water head varies with depth (in part due to increasing salinity) and for the depths of interest here it ranges between ±0.1 m to ±0.5 m. There is a higher uncertainty ±1 m on the groundwater level in the borehole due to seasonal variations. A comparison between the quiet period heads for the SS22 conditions and the quoted initial heads for SS24 and SS26 (from Klockars et al. 2006) is given in Table 4-18. There are some relatively large differences which may relate to head disturbances during the pumping tests and/or changes in groundwater table. For this reason, modellers were encouraged to match drawdowns rather than measured heads for SS24 and SS26.

Table 4-18. Comparison between the quiet period heads for the SS22 and SS26.

Interval	SS22	SS24	Difference	Interval	SS22	SS26	Difference
KR15:L1	4.4	4.6	−0.2	**KR14:L1**	6.6	6.7	−0.1
KR15:L2	4.9	5.4	−0.5	**KR14:L2**	6.7	6.4	0.3
KR15:L3	5.7	5.0	0.7	**KR14:L3**	6.7	6.6	0.1
KR15:L4	6.5	6.3	0.2	**KR15:L1**	4.4	3.4	1.0
KR15:L5	6.5	6.2	0.3	**KR15:L2**	4.9	5.1	−0.2
KR15:L6	6.6	6.2	0.4	**KR15:L3**	5.7	5.2	0.5
KR15B:L1	6.6	6.3	0.3	**KR15:L4**	6.5	6.4	0.1
KR15B:L2	6.7	6.3	0.4	**KR15:L5**	6.5	6.4	0.1
KR16:L1	5.7	5.3	0.4	**KR15:L6**	6.6	6.6	0.0
KR16:L2	5.7	5.4	0.3	**KR15B:L1**	6.6	6.6	0.0
KR16:L3	6.2	6.0	0.2	**KR15B:L2**	6.7	6.7	0.0
KR16:L4	6.4	6.1	0.3	**KR16:L1**	5.7	5.7	0.0
KR16:L5	6.5	6.2	0.3	**KR16:L2**	5.7	5.2	0.5
KR16:L6	6.5	6.2	0.3	**KR16:L3**	6.2	5.9	0.3
KR16B:L1	6.6	6.2	0.4	**KR16:L4**	6.4	6.3	0.1
KR16B:L2	6.8	6.4	0.4	**KR16:L5**	6.5	6.5	0.0
KR16B:L3	0.0	0.0	0.0	**KR16:L6**	6.5	6.4	0.1
KR17:L1	5.4	4.6	0.8	**KR16B:L1**	6.6	6.5	0.1
KR17:L2	6.0	5.9	0.1	**KR16B:L2**	6.8	6.8	0.0
KR17:L3	6.0	5.9	0.1	**KR16B:L3**	0.0	0	0.0
KR17:L4	6.4	6.1	0.3	**KR17:L1**	5.4	4.8	0.6
KR17:L5	6.5	6.2	0.3	**KR17:L2**	6.0	5.1	0.9
KR17:L6	6.5	6.2	0.3	**KR17:L3**	6.0	5.1	0.9
KR17B:L1	6.5	6.2	0.3	**KR17:L4**	6.4	6.4	0.0
KR17B:L2	7.3	6.8	0.5	**KR17:L5**	6.5	6.5	0.0
				KR17:L6	6.5	6.4	0.1
				KR17B:L1	6.5	6.5	0.0
				KR17B:L2	7.3	7.6	−0.3
Min			−0.5	**Min**			−0.3
Mean			0.3	**Mean**			0.2
Max			0.8	**Max**			1.0
SSQ			0.14	**SSQ**			0.14

4.6.1 Natural conditions (SS20)

4.6.2 Undisturbed conditions (SS21, SS22)

In SS21 the modellers were asked to predict open-hole head and flow for the 9 boreholes (JAEA provided results from 5 realisations of their model). In SS22 the modellers were asked to predict the heads in 31 packed-off intervals. The specific intervals in KR18A related to those used during the HTU pumping tests and no intervals were specified in KR18B.[24]

Head values from the 9 open boreholes showed only a small variation between 6.9 and 8.2 m (KR17b). If we exclude the relatively higher head in KR17B from the comparison, it can be seen that all the simulation sets except those of SKB/KTH (~3 m too low) and to a lesser extent Posiva/VTT (~0.5 m too low) provide a reasonable match to the observed heads. The mean square head difference for most simulation sets is small and comparable to the uncertainty in head due to measurement error and seasonal variations. The KAERI and CRIEPI simulations reproduce the relatively small variability in head relatively well (excluding KR17B). The KR17B value appears to be an outlier either reflecting local groundwater conditions or a measurement problem. The measured and simulated flows up the boreholes for undisturbed conditions are shown in Figure 4-47. Several of the models capture the pattern of cross-flows if not the magnitude. The updated JAEA-3 realisation has much larger cross-flows, in particular along KR18 where a significant outflow is simulated. The cause of this behaviour is unknown. Figure 4-48 shows the cumulative histograms of flows. Several models capture the shape of the distribution in at least some of the boreholes. The SKB/KTH model shows a reasonable match in most boreholes.

For the undisturbed conditions with packed-off intervals (SS22) the data show a wider range of heads as cross-flows along the boreholes no longer act to equalise heads. The SKB/CFE simulation shows too little variability in heads, while the other simulations show a reasonable agreement to the mean values (Mean square difference ~0.2 m2). The KAERI and Posiva/VTT simulations capture more of the observed variability in measured heads, while the NWMO/Laval simulation captures the pattern but not the variability. Overall all the models have somewhat lower variability in head than observed. CRIEPI and JAEA did not predict the undisturbed heads for this case.

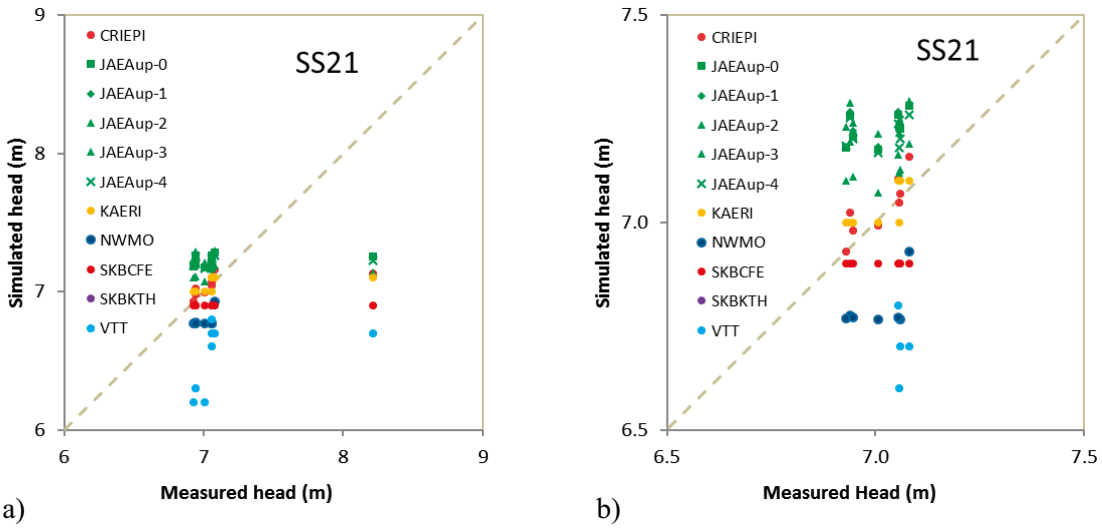

Figure 4-46. *Comparison of simulated and measured head in undisturbed conditions for a) open hole conditions; b) open hole conditions excluding KR17B.*

[24] 33 and 31 intervals are specified for SS24 and SS26. Intervals are slightly different due to changes in completion of the pumping borehole.

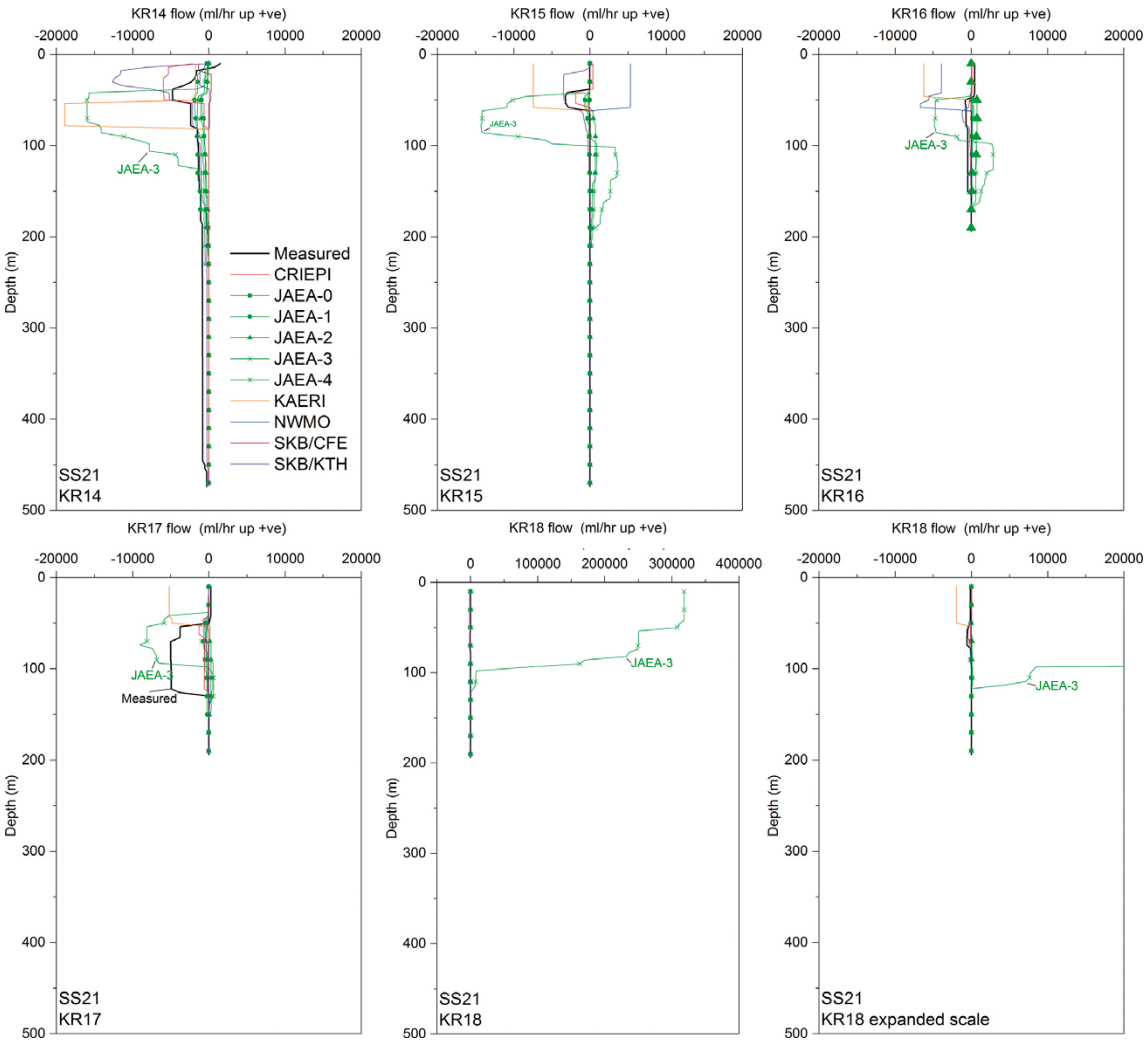

Figure 4-47. *Comparison of simulated and measured flow along open boreholes for undisturbed conditions (SS21). Colour coding as in head/drawdown plots.*

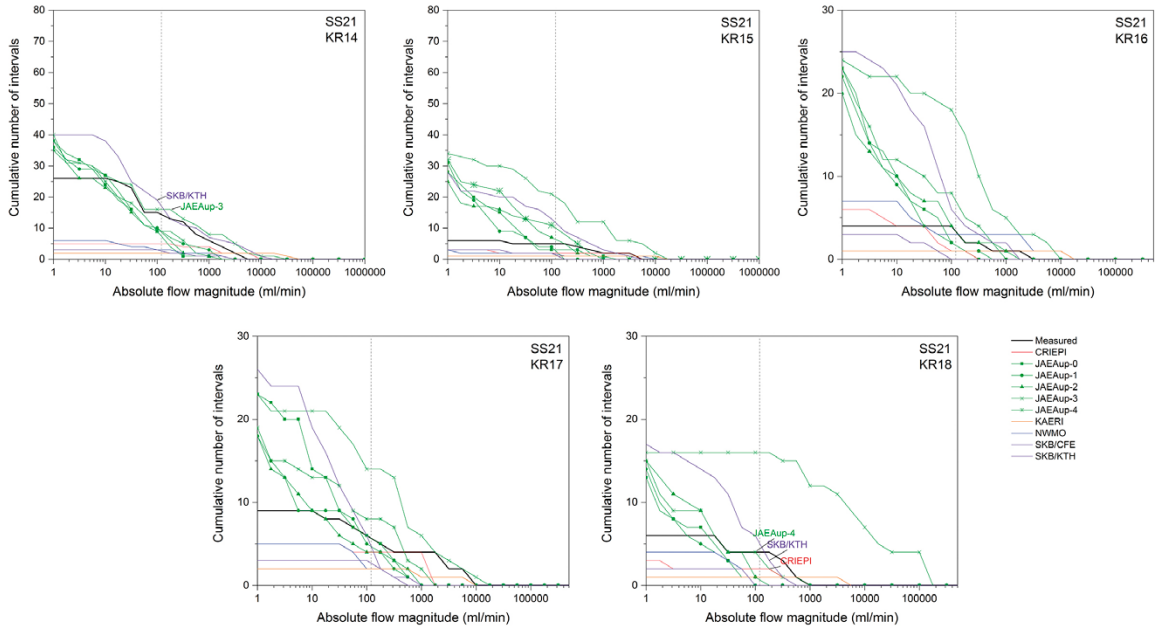

Figure 4-48. *Cumulative histograms of flows to 4 m borehole sections for undisturbed conditions (SS21).*

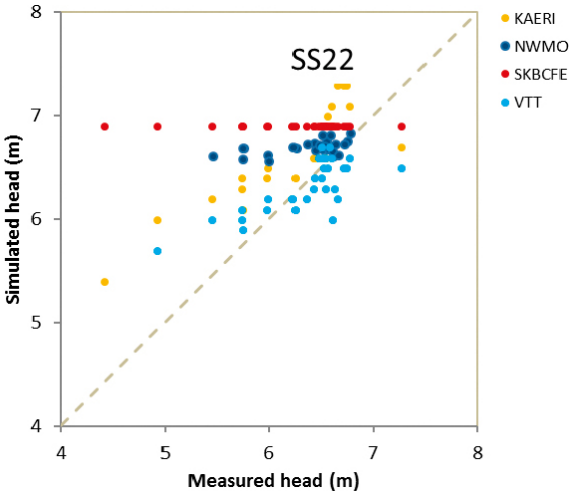

Figure 4-49. *Comparison of simulated and measured head in undisturbed conditions for packed-off conditions.*

4.6.3 Open-hole pumping in KR14 (SS23)

Cross-plots of the simulated and measured drawdowns are shown in Figure 4-50. Overall the NWMO/Laval simulations show very good matches to observed heads with relatively small changes between the forward (A) and calibrated (B) simulations.

The JAEA simulations using specified pumping rates resulted in large predicted drawdowns (15–30 m) at KR14, suggesting that locally the transmissivity of features intersecting KR14 was too low. JAEA also provided some simulations where the borehole boundary condition was set as the observed drawdown resulting in lower flows. Here the imposed flow-rate models have been used as the emphasis is placed on the monitoring drawdowns and flow responses. The simulations for KAERI, SKB/CFE, SKB/KTH and two of the 5 realisations of the updated JAEA model show moderate matches to the monitoring drawdowns.

Figure 4-51 shows the simulated change in flow up the borehole for the A boreholes. While the simulations capture the pumping borehole behaviour and the magnitude of flow responses reasonably well, they often do not capture the flow direction. The JAEA updated models show greater flow in the lower part of the rock than the other simulations or the data but otherwise capture the pattern reasonably well. The JAEA simulations also show the range of realisation dependence from the background rock stochastic network.

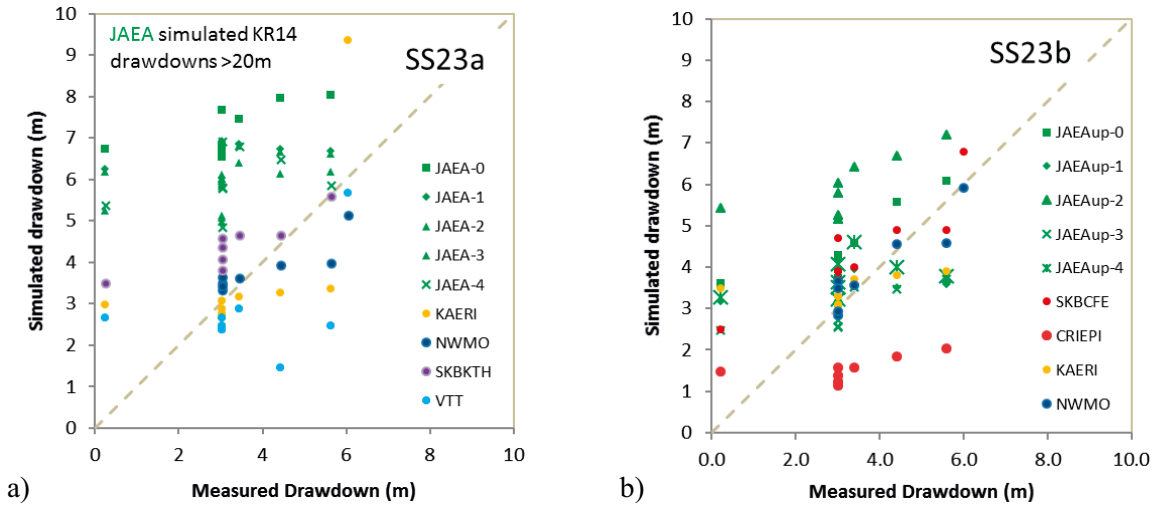

Figure 4-50. *Comparison of simulated and measured drawdown during open-hole pumping of KR14: a) forward models; b) calibrated models.*

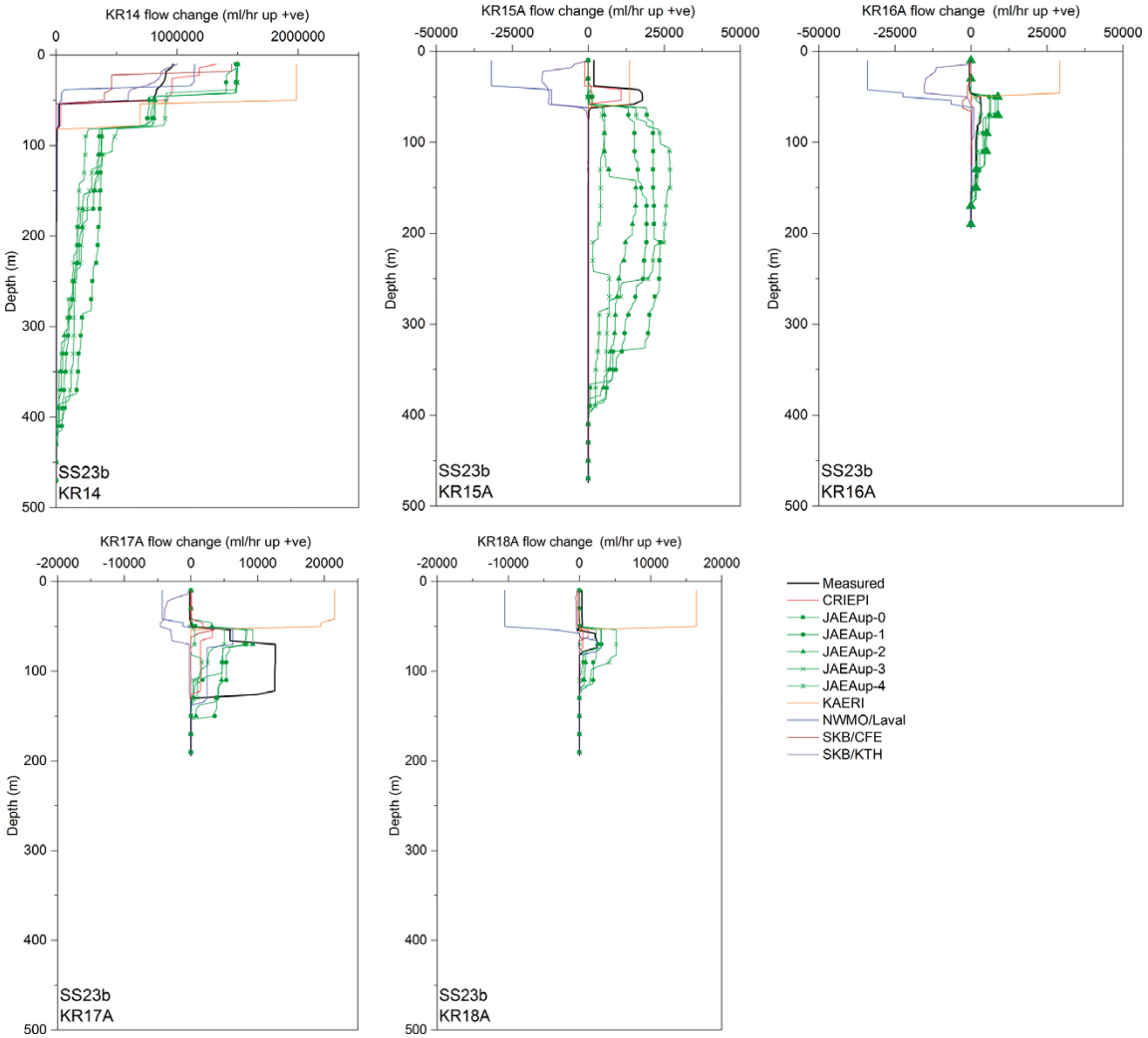

Figure 4-51. *Comparison of simulated and measured flow along open boreholes for pumping in KR14 (SS23b). Colour coding as in head/drawdown plots.*

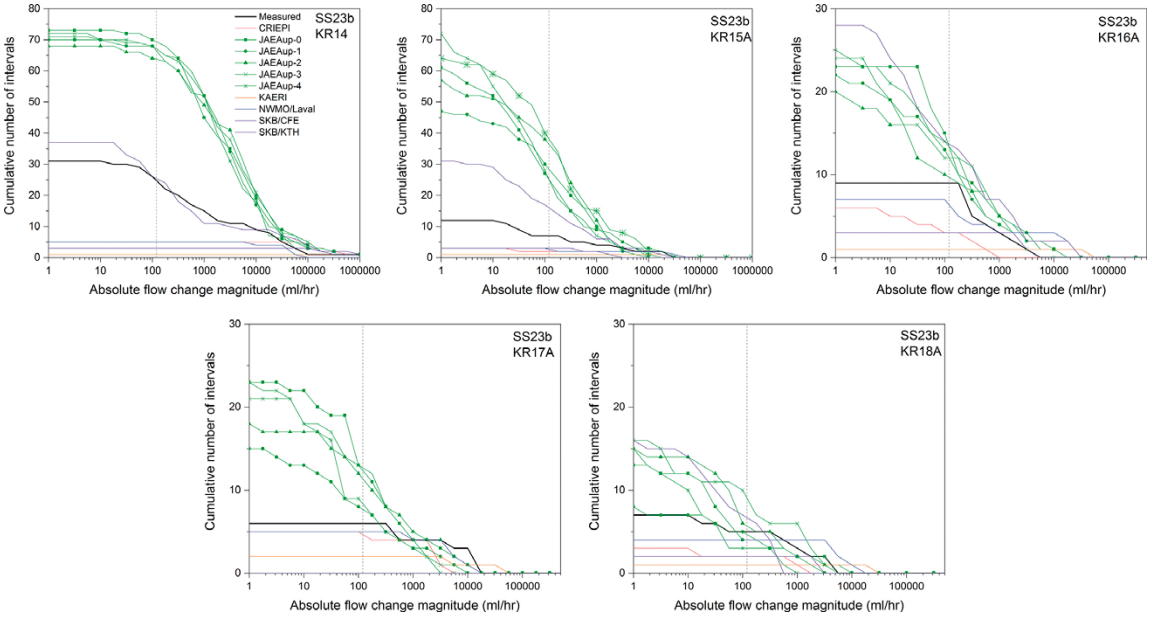

Figure 4-52. *Cumulative histograms of flows to 4 m borehole sections for pumping in KR14 (SS23).*

4.6.4 Packer test pumping in KR14 (SS24a,b)

The simulated and measured drawdowns for packer testing in KR14 are shown in Figure 4-53 and Figure 4-54. The best matches to the overall pattern of drawdown are from the NWMO/ Laval simulations. The NWMO/Laval calibrated simulation in particular reproduces the overall pattern of drawdown in a large number of intervals with a Pearson r = 0.9 and Mean Square Error (MSE) of 0.6 m^2. The SKB/CFE and KAERI simulations also produce a good match (Figure 4-53). The match is much improved for the SKB/CFE simulation if the small simulated drawdown at KR18B:L2 is ignored.

The simulations from JAEA (realisation 0 and 2), KAERI and VTT also show a moderately good match. The JAEA SS24a simulations (run as specified drawdown) typically show too small a drawdown in the monitoring intervals (as would be expected because of the lower pumping flow-rate) while the updated JAEA simulations with specified flow-rates (SS24b) resulted in higher drawdowns than observed. Distance drawdown plots for the two simulations are shown in Figure 4-54.

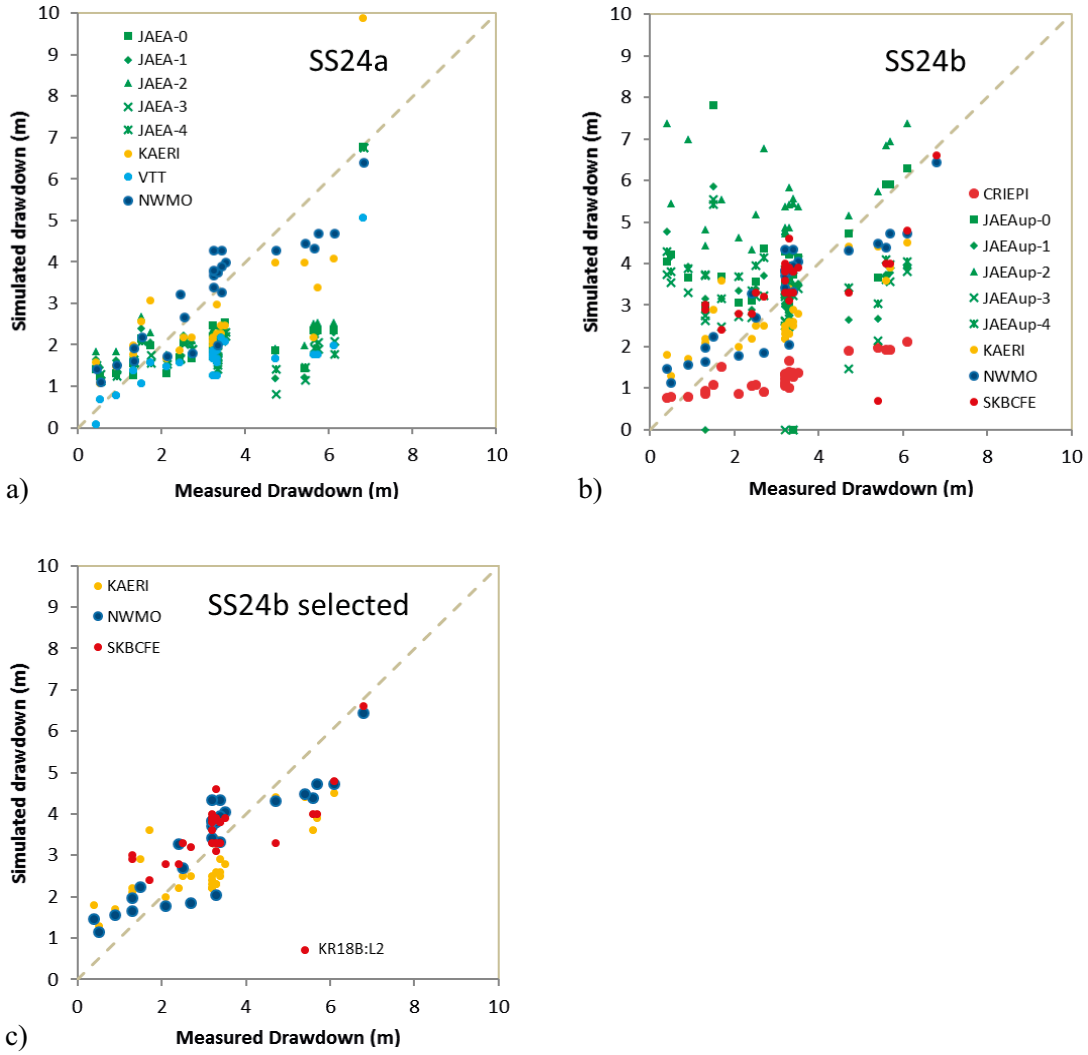

Figure 4-53. *Comparison of simulated and measured drawdown during packer-test pumping of KR14: a) forward simulation; b) calibrated simulations, c) selected calibrated simulations.*

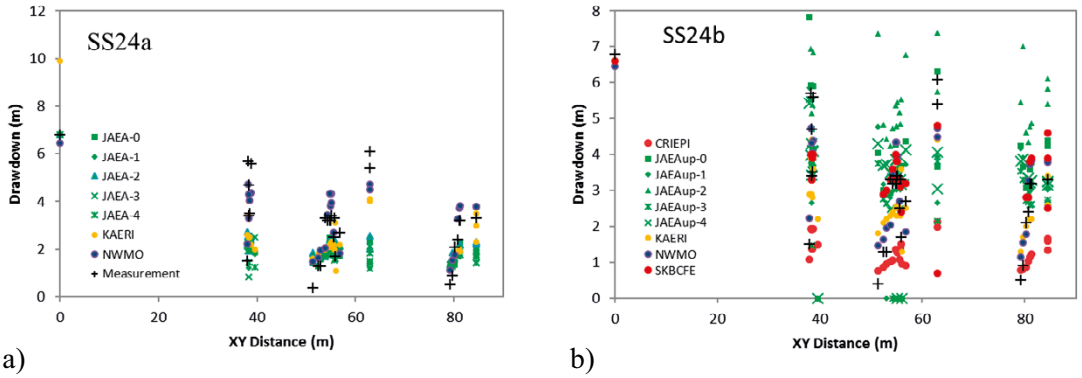

Figure 4-54. *Distance (XY) drawdown plot for packer-test pumping of KR14 a) SS24a and b) SS24b.*

4.6.5 Open-hole pumping in KR18A (SS25)

The simulated and measured drawdowns for open-hole testing in KR18A are shown in Figure 4-55. The best match to the overall pattern of drawdown is from the SKB/CFE simulation which produces an excellent match to the drawdown in the pumped borehole and in the observation boreholes. Realisations of the JAEA SS025a and SS25b simulations also provide a good match to observed heads. The NWMO and Posiva/VTT simulations provide a reasonable match.

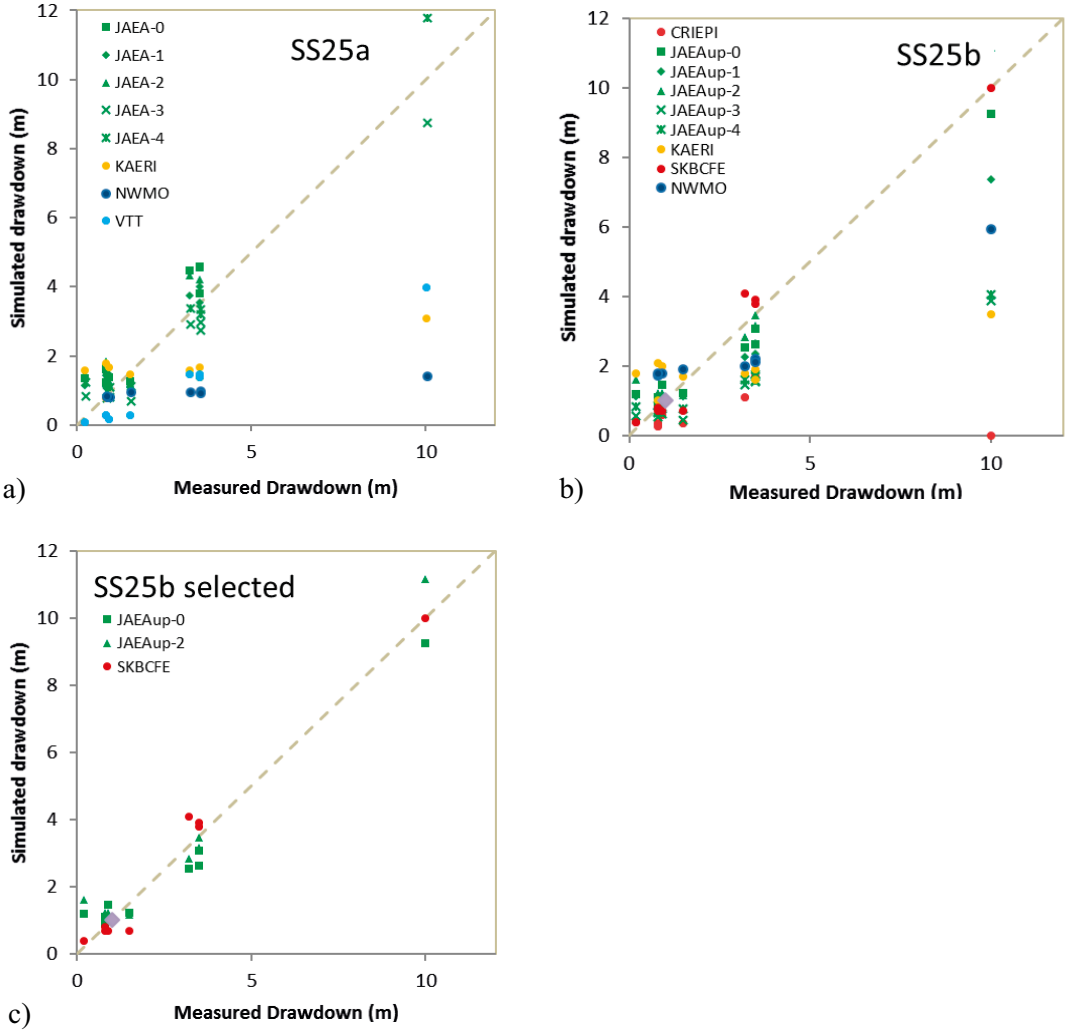

Figure 4-55. *Comparison of simulated and measured drawdown during open-hole pumping of KR18A: a) forward models; b) calibrated models, c) selected calibrated models.*

Figure 4-56 shows the simulated change in flow along the borehole and Figure 4-57 the cumulative distribution of magnitude of flow change. Again, JAEA show more flows in the lower part of the rock. The best matches to flow change in the pumping well are from the CRIEPI, SKB/CFE and JAEA-up2 and JAEA-up4 simulations. In the observation boreholes several simulations show a good match to the magnitude of flow changes (Figure 4-57) if not to the direction.

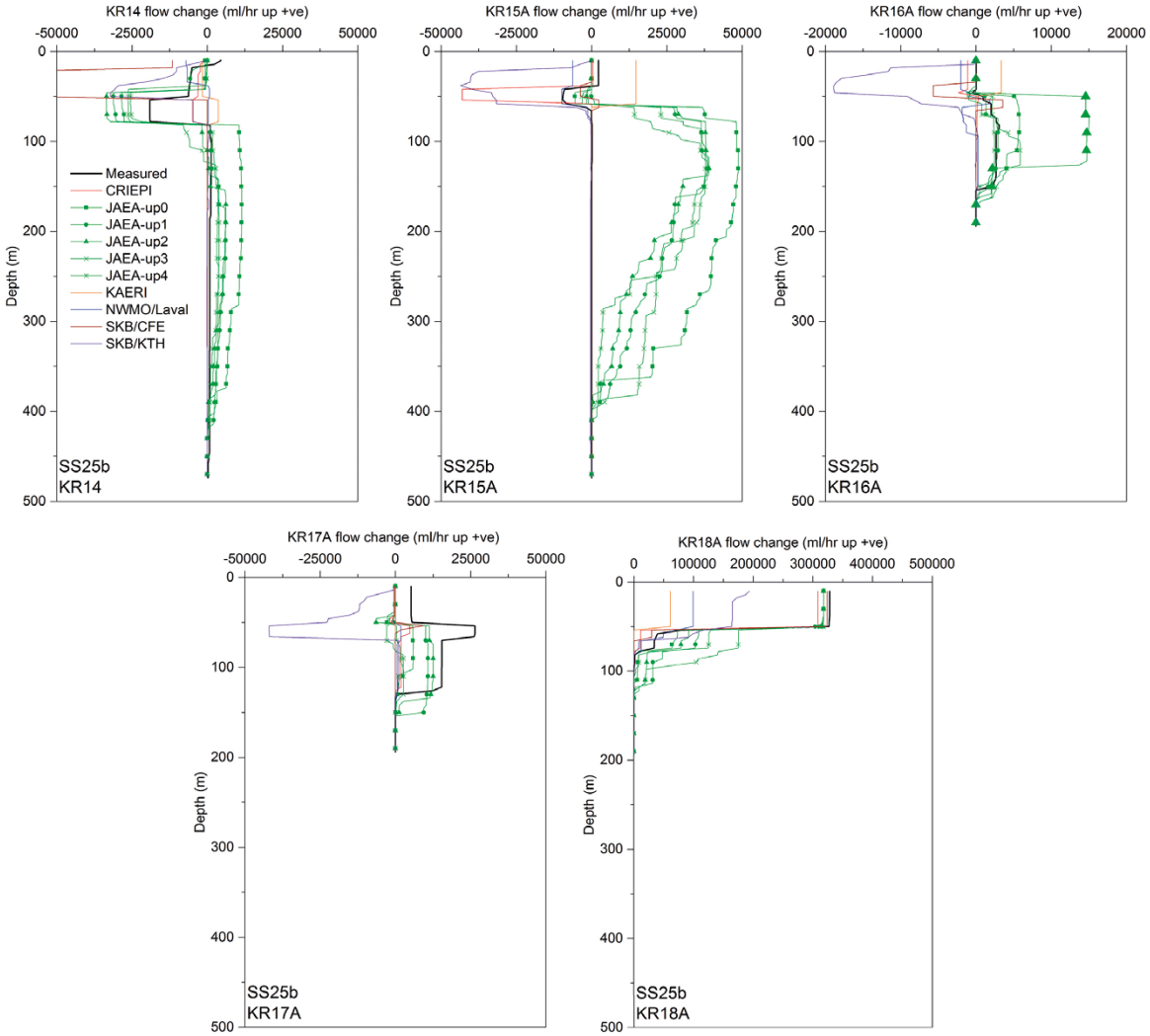

Figure 4-56. *Comparison of simulated and measured flow along open boreholes for pumping in KR18A (SS25). Colour coding as in head/drawdown plots.*

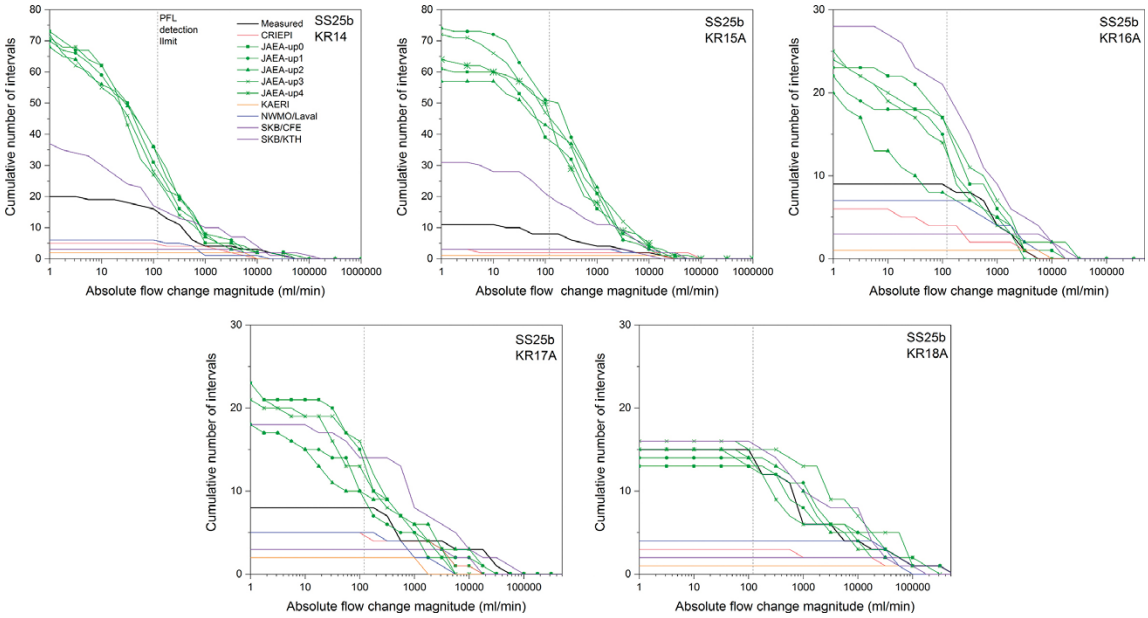

Figure 4-57. *Cumulative histograms of flows to 4 m borehole sections for pumping in KR18A (SS25).*

4.6.6 Packer tests pumping in KR18A (SS26)

The simulated and measured drawdowns for packer testing in KR18A are shown in Figure 4-58. The JAEA SS26a realisations (fixed drawdown) and three realisations of SS26B (fixed flow) provide a good match to drawdowns as does the CRIEPI simulation. The two remaining JAEA SS26b, NWMO, SKB/CFE and VTT simulations provide a reasonable match to observed drawdowns. Most models do a reasonable job at predicting the overall form of the distance drawdown (see Figure 4-59).

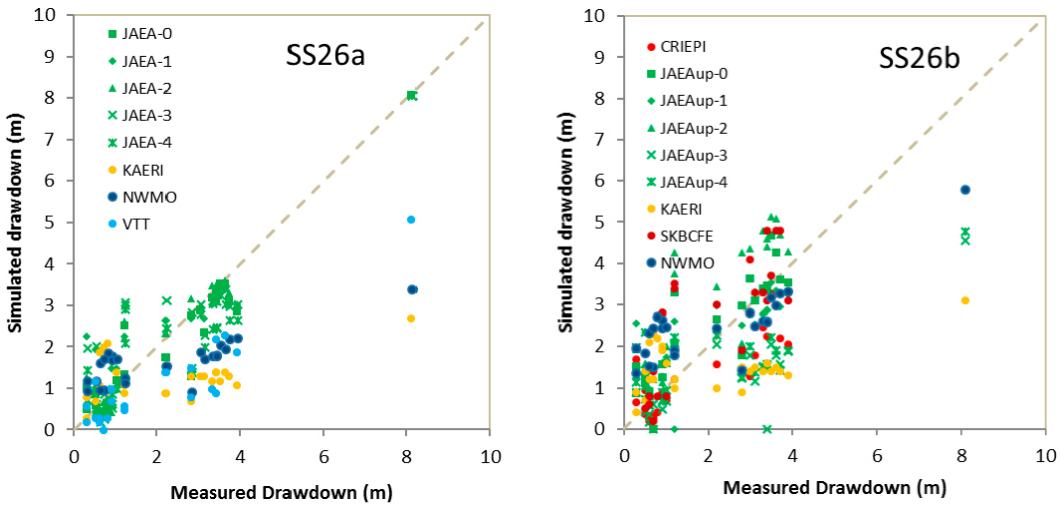

Figure 4-58. *Comparison of simulated and measured drawdown during packer test pumping of KR18A: a) forward models; b) calibrated models.*

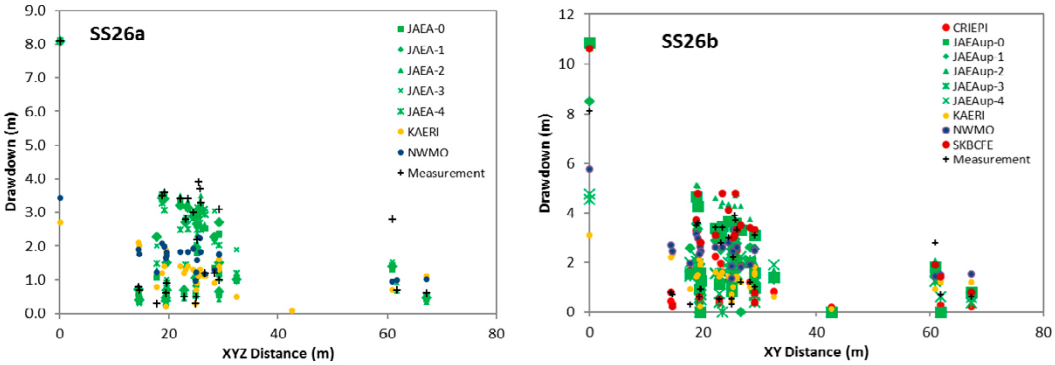

Figure 4-59. *Distance drawdown plot for packer-test pumping of KR14 (SS26a and SS26b).*

4.6.7 Open hole pumping in KR15A (TS27)

The simulated and measured drawdowns at 240 hrs for packer testing in KR18A are shown in Figure 4-60. The best matches are achieved by the JAEA models (both the original and updated). All realisations show a Pearson *r* of ~0.75 and MSE < 1.5 m^{2}. The SKB/CFE model also provides a reasonable match.

Figure 4-61 shows the measured and simulated flow along the boreholes during pumping in KR15A. The 5 JAEA realisations of the updated model used a specified flow-rate (6.7 l/min) for KR15A. In general all the groups capture the major flow at 60 m but the JAEA simulations include more flows from below 100 m in the borehole.

Cross-flows up/down the monitoring boreholes are clearly seen in the measured flows and in the simulations. The direction of flow varies in the different boreholes and simulations. The measured cross-flows vary from ~1 000 to ~30 000 ml/hr, while in one of the JAEA realisations (#3) a down-flow of ~300 000 ml/hr is simulated (a significant fraction of the KR15A outflow). This realisation is also associated with a relatively small drawdown in KR15A.

Given uncertainty on the data (the sum of the PFL inflows was less than the total produced flow), the simulations do a reasonable job of catching the main flows into KR15A but none of the simulations consistently captures the main flows in all the monitoring boreholes. However, the overall pattern of significant flow diversion along the boreholes is reproduced.

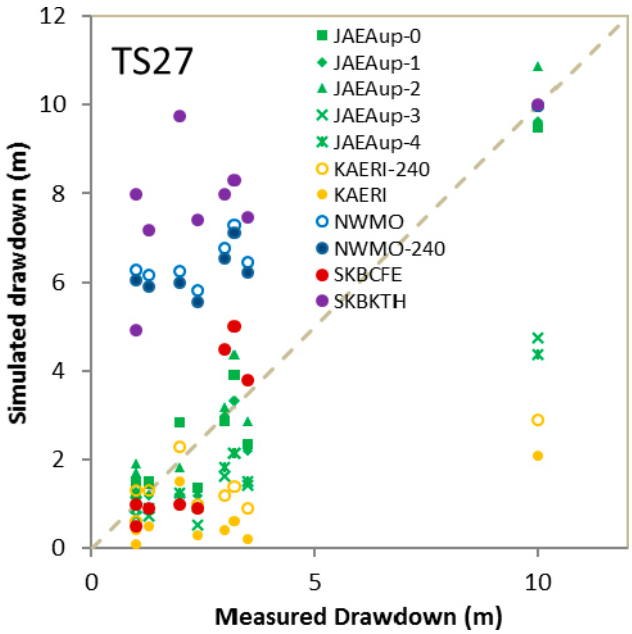

Figure 4-60. *Comparison of simulated and measured head during open-hole pumping of KR15A (TS27).*

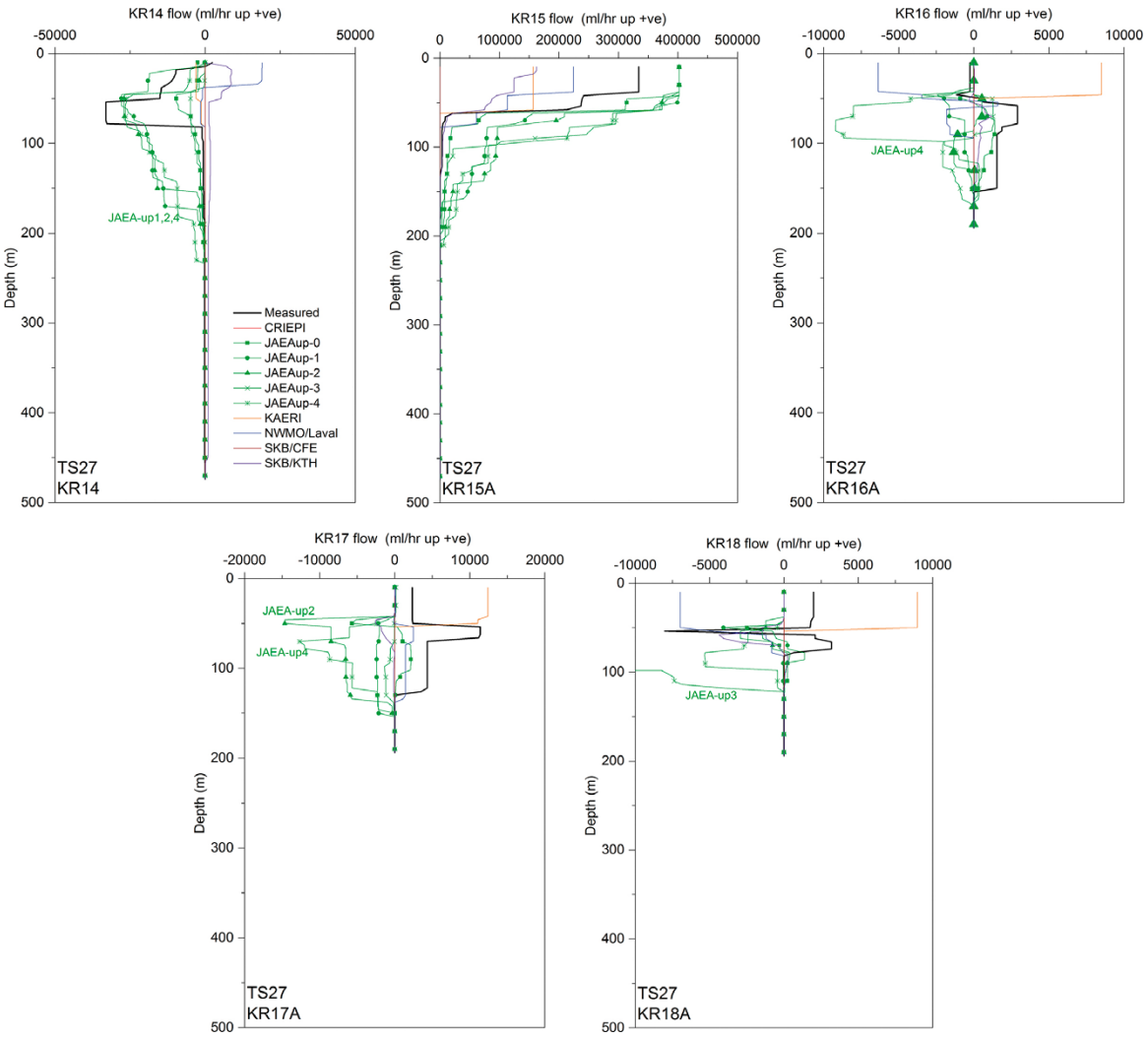

Figure 4-61. *Comparison of simulated and measured flow along open boreholes for pumping in KR15A (TS27). Colour coding as in head/drawdown plots.*

Figure 4-62 shows cumulative histograms of flow for 4 m borehole sections for the measured and simulated flows. The JAEA and SKB/KTH simulations show very similar distributions and provide a match to the distribution of measured flows above the measurement limit, while the KAERI and NWMO/Laval simulations model only the major flow features. In KR15A there appear to be slightly fewer features measured than in the JAEA or SKB/KTH simulations (this might indicate some bias against identifying small flows in the pumping borehole).

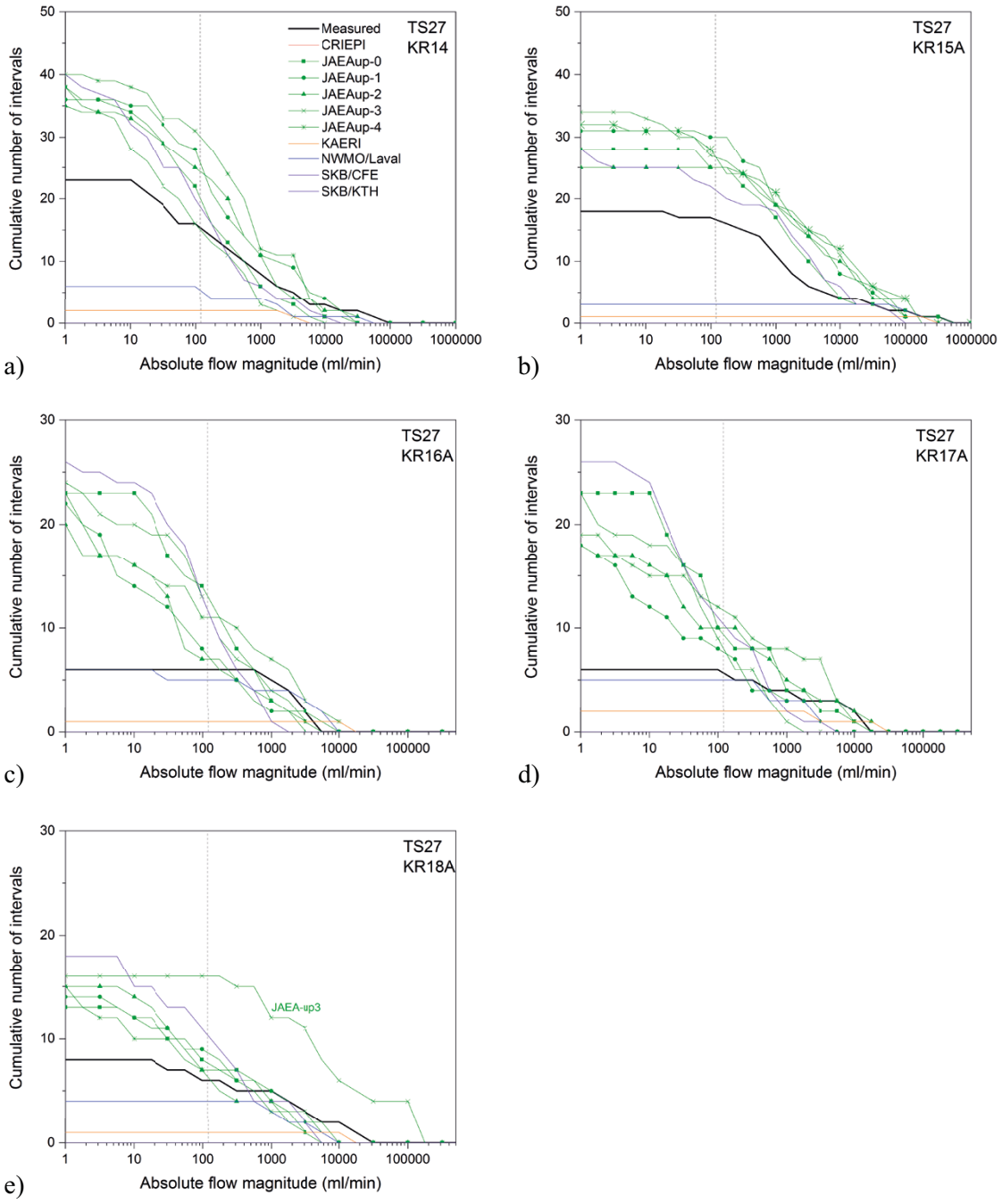

Figure 4-62. *Cumulative histograms of flows to 4 m borehole sections for pumping in KR15A (TS27).*

4.7 Task evaluation

4.7.1 The Task 7B structure and definition

The Task Definition set out a relatively large number of simulations covering undisturbed and pumped conditions for both open boreholes and packed-off boreholes and PA conditions (no boreholes). The simulation structure provided the opportunity to trace the evolution of the models with the inclusion of additional data, any reduction in uncertainty and their subsequent predictive capability.

In general the modelling groups felt that the Task Definition was satisfactory, especially given the complexity of the Task. One group felt that there should have been greater emphasis on understanding the cross-hole pumping tests, while another group suggested that the Task might have been better structured as two different tasks: one related to simulation of the pumping tests and a second to consider reduction of uncertainty in PA conditions.

4.7.2 The Task 7B dataset

The hydro-structural models provided by Posiva and used within the Task are relatively mature, albeit better suited to the larger scale description of the site. The fracture zone descriptions required some local scale updating to better describe the block at the 500 m scale, as performed by several of the modelling groups. In addition, small scale high transmissivity near-surface features (sheet joints) were added by some of the groups on the basis of the hydraulic data (and experience from the Forsmark site).

The ensemble of pumping tests using both open boreholes and packed off intervals for the KR14–KR18 block is an exceptionally complete testing dataset. The use of boreholes for both pumping and monitoring is likely to improve the quality of available information and to reduce the under-determination of the inverse problem (Klepikova et al. 2013). This dataset is augmented by the PFL data from undisturbed conditions. There is some uncertainty about hydraulic heads related to annual variations and possible measurement errors which, given the relatively small variability in head in undisturbed conditions may add to uncertainty, but overall, there are likely to be very few more comprehensive site characterisation datasets of a fractured rock volume at this scale from surface-based investigations.

A summary of the modelling groups' evaluation (from the Task 7B Questionnaire) is given in Table 4-19. In general, the modellers thought there was sufficient (if not too much) data. Some groups felt that additional information was needed to identify minor fault/fracture zones or better characterise the background fracture network.

Table 4-19. Summary of modelling groups' evaluation of Task 7B dataset (from Task 7B questionnaire).

Group	Evaluation of the dataset	Missing information?
JAEA	Sufficient	Discriminate minor zone data from major fault zone and near-surface zones
KAERI		Geophysical survey results that help to conceptualize the background fracture extents or connectivity
NWMO/Laval	Large and detailed dataset.	-
SKB/KTH	Data could have been delivered in a more compact and clearer way. Perhaps too much data. Significant efforts needed to implement sub-sets of the data	-
SKB/CFE	OK.	-
Posiva/VTT	There was a wealth of information with good support from PI	

4.7.3 The work of the modelling groups

Each modelling group had slightly different objectives and placed different emphasis on the different testing phases and data. A summary of the objectives as documented in the Task 7B questionnaire is given in Table 4-20.

Table 4-20. Summary of modelling groups' objectives for Task 7B (from Task 7B questionnaire).

Group	Objectives for modelling Task 7B?
JAEA	To demonstrate modelling methodologies of the major flow structure conceptualization by the derivative analysis of the transient pressure interference tests and the minor fracture network structure modelling for the heterogeneous flow path distribution among the boreholes
KAERI	• Block-scale modelling of the groundwater system of Olkiluoto site and the hydraulic responses by pumping test at KR14 and KR15. • To find factors causing uncertainty of hydrogeologic conditions. • To examine the effect of background fractures on groundwater flow.
NWMO/Laval	Model calibration based on hydraulic heads and PFL measurements. Only hydraulic heads were considered in the first modelling phase. Flow measurements were then included as targets for calibration to assess their influence on model calibration.
SKB/KTH	To improve the conceptual understanding the flow characteristics of the groundwater system in the vicinity of the KR14-KR18 boreholes by studying the cross-hole pump tests and based primarily on using high-resolution PFL flow measurements.
SKB/CFE	The priorities are: develop methods for borehole simulations and simulate the interference tests in KR14-KR18.
Posiva/VTT	Test the applicability of flow data to improve the predictions.

JAEA

JAEA were the only group to perform detailed interpretation of the cross-hole pressure responses to better constrain the hydro-structural model. This allowed a local refinement of the hydro-structural model for the fracture zones which was then integrated with a stochastic DFN model for the background rock.

The stochastic DFN model was then calibrated by

- increasing transmissivity above z = −90 m and removing stochastic fractures below HZ20A,
- hydraulic disconnection at random fracture intersections.

It is notable that in the deep system, calibration required, at least locally, a decrease in connectivity of both zones and the stochastic network.

KAERI

KAERI developed a block-scale model for the KR14-KR18 region based on deterministic zones from the hydro-structural model used in Task 7A and then implemented a stochastic model of the background fractures considering variability using several realisations of this network. This was an overall development of the approach used Task 7A.

KAERI were only able to perform limited model calibration on the ECPM (Equivalent or Effective Continuum Porous Medium) model by adjusting recharge rates.

NWMO/Laval

NWMO/Laval was the only group to use a formal inverse model (PEST) as part of their calibration strategy. This choice was facilitated by the use of the hydrofacies model limiting the number and type of parameters to the hydraulic conductivity of each hydrofacies and the hydraulic aperture of the two deterministic features. The use of formal methods allowed definition of confidence intervals and investigation of parameter correlations. The inverse models also performed reasonably well, achieving consistent matches to the two pumping tests in KR14.

The confidence intervals and correlations allowed NWMO/Laval to investigate the relative importance of head and flow data in the inversion. The observations were weighted to reflect the different magnitudes, with head observations (m) having a weight of 1.0 and flow (m^3/y) a weight of 0.1. They concluded that "including flow observations as targets for calibration allows for a better interpretation of inverse modelling results, since more residuals are analysed and different observation types provide more information about the system behaviour." Further they found that parameter uncertainty was reduced by including PFL measurements as targets for calibration.

NWMO/Laval also developed the only model not directly linked to a geometric fracture network, instead implementing the fracture facies concept developed by Park et al. (2004).

Posiva/VTT

Posiva/VTT's goals included the development of a new method for creating stochastic DFNs (FEFTRA/VINTAGE) and the quantitative assessment of the derived DFNs. This included integration of the EnKF approach with the FEFTRA package. This focus on methodology development allowed several innovative approaches to be considered:

- VINTAGE: DFN mesh generation using an integer space providing computationally efficient and reliable discretisation.
- Extensive sensitivity studies of DFN parameters on flow and head measurements together with methods for ranking/selection of realisations for model conditioning.
- Use of EnKF for model calibration.

FEFTRA/VINTAGE (Virtual INTeger Arithmetic for Generating Elements) acts a pre-processor and allows the incorporation of large deterministic features and smaller stochastic fractures into the same finite element mesh. This allows integration of effective porous medium FEFTRA/OCTREE and DFN representations based on a FEFTRA/VINTAGE mesh. Löfman and Mészáros (2013) provide comparisons of the OCTREE and DFN representations for a set of verification problems. The production of credible, qualitatively correct results from the POSIVA/VTT Task7B simulations using VINTAGE represents a successful outcome. Minor issues with the implementations were also identified and subsequently corrected.

Posiva/VTT's calibration approach used both head/drawdown (via RMSD) and a comparison of the measured and simulated flow distributions via the Kolmogorov-Smirnov test. This was perhaps the most complete method of model comparison used within the manual calibration approaches. In addition to the developments outlined above Posiva/VTT performed a very extensive sensitivity analysis for the background fracture network.

SKB/CFE

SKB/CFE's objectives were to develop methods for borehole simulations and simulate the interference tests in KR14-KR18. The approach did not follow the set of simulations specified in the task description, but resulted in a very efficient model development process that identified the influence of near-surface high permeability features.

SKB/KTH

SKB/KTH's approach was focused on using the hydraulically active fractures (i.e. those identified by PFL logging) to reproduce flow magnitude and direction using the simplest possible approach. They developed a novel DFN generation scheme that ensured that fracture intersection location and orientation was honoured (so flow occurred at the right places) by extrapolating the fractures from the intersection with the borehole into a local partition of the model volume. The partitions associated with each borehole overlapped to ensure connectivity. Fracture transmissivity was initially set to the PFL value (Configuration A) but later adjusted in a series of trial-and-error calibration variants.

This approach maximised use of the integrated PFL dataset and resulted in a semi-deterministic model. However:

1. The generation scheme is dependent on the borehole geometry which is to some extent arbitrary.
2. Hydraulically-active fractures are by definition well-connected within the partitions[25].

The resulting models typically over-estimated flows (for the given pumping head) and did not capture the direction and magnitudes of flow in the observation boreholes.

These results confirm that within the background rock fracture connectivity is a controlling property of the flow system and that knowledge (and honouring) of the borehole fracture intersections and local transmissivity are insufficient to capture the system behaviour.

4.7.4 Overall evaluation

Task 7B presented a significant challenge to the modelling groups, in terms of:

- An extensive characterisation dataset with relatively complex testing protocols.
- The need to simulate multiple borehole interference tests requiring matches to both head/drawdown and flow measurements.

The modelling groups for the most part produced simulations based on:

- Deterministic zones identified within the site-scale hydro-structural model with some local refinement based on observation or well-test analysis.
- A small number of transmissive near-surface features ("sheet joints") not included in the hydro-structural models.
- Stochastic background rock representations.

NWMO/Laval used the fracture facies approach and did not include site-scale zones. Some of the model variants considered by SKB/KTH also excluded the zones. With the exception of NWMO/Laval all the groups relied on manual inverse models to calibrate models. Two common themes within the work are constraining the connectivity of the simulated fracture network and difficulties in conditioning and calibration of the network models.

Matching flow and head measurements

The approach to matching heads and flows in simulations differed between the modelling groups and is summarised in Table 4-21. The definition of either a combined objective function or scoring system varied between the groups. NWMO/Laval were the only group to define an objective function and used a simple form incorporating different weights for the head and flow measurements. Posiva/VTT developed the most sophisticated model scoring system incorporating measures of the model flow distribution and head residuals. Other groups either defined separate measures for head and flow or prioritised one measurement type. This illustrates an important issue regarding flow data in that the limited analysis of cross-hole measurements means that as yet there is no established literature for identifying key measures of flow. In contrast well-established methods for evaluating matches to drawdowns are available for pressure/head data.

[25] Some attempts were made to limit the connectivity of the network by randomly removing parts of the fractures which had been tesselated.

Table 4-21. Approaches to scoring/calibrating models with head/drawdown and flow.

Modelling Group	Approach
JAEA	Pressure derivative analysis used to constrain hydrostructural model. Plausibility scores (Mean Square Error) for pressure and flow
KAERI	Total sum of squared errors for head only
NWMO/Laval	PEST used objective function with different weights for flow and drawdown measurements
Posiva/VTT	Ad hoc “unified score” based on mean square error for heads, Kolmogorov-Smirnov distance for the distribution of flows and variability in flow.
SKB/CFE	Calibration of interference test with open holes based on comparison of drawdowns and max inflow in boreholes,
SKB/KTH	Considered only the flow responses

Fracture network connectivity

Multiple authors have previously commented on the potential over-connection of DFN models:

- Billaux et al. (1989) and Cacas et al. (1990a, b) consider highly interconnected fracture networks derived from mapping at the Fanay-Augeres mine but these models were unable to reproduce the observed lack of hydraulic communication between some of the boreholes.
- Poteri et al. (2002) state that there were problems of over inter-connection between the determined structures in the TRUE Block Scale hydrostructural model.
- Black et al. (2007) comment that compared to sparse channel networks, DFN models are typically too well connected and do not reproduce characteristic behaviours.
- Frampton (2010) comments that the DFN approach may correctly represent geometric or structural connectivity of the fractured media studied, but due to absence of internal heterogeneity may cause flow conduits to be overconnected.
- Follin et al.(2014) conclude that the “flow rate to/from an abstraction/injection borehole in a hydrogeological DFN is probably largely controlled by how well connected the network of open fractures is (i.e. largely determined by size and intensity).” The reduced hydraulic connectivity of channelled flow systems will therefore not be well-reproduced.
- Black and Barker (2018) demonstrate that the connectivity of stochastic DFNs is largely controlled by the fracture length distribution and shape and that therefore assumptions of uniform flow over ”equi-dimensional” features may significantly influence effective properties.

The assumption of uniform transmissivity across the fracture (which runs counter to small-scale measurements on single fractures) ensures hydraulic connection between intersecting fractures, although these may be subject to geometric flow chokes (Öhman and Follin 2010). In channelled flow systems the connectivity between channels in fractures may be limited (although there are suggestions that fracture intersections may themselves act as channels e.g. Cacas et al. 1990a,b).

Within Task 7B several groups considered DFN connectivity, in particular with regard to reducing the connectivity of networks assuming uniform flow across the fractures or zones. Other Task 7B approaches that influenced or represented differences in connectivity included:

- Assuming lack of hydraulic connection between deterministic features and randomly removing fracture intersections (JAEA).
- The fracture growth model (SKB/KTH).
- Randomly removing parts of tesselated features (SKB/KTH).
- Hydrofacies based on fracture density (NWMO/Laval).

The JAEA approach allowed variation of the network connectivity by defining a disconnection probability that could be varied. This probablity can be viewed as the chance that flow channels in a given fracture connect across a fracture intersection into the channels within the intersecting fracture.

Conditioning and calibration of the network models

Manual calibration of the DFN-based models resulted in some improvement in the matches to observation but no model was consistently good and there is little evidence that calibration to one set of tests resulted in either increased predictive power or reduced uncertainty. Difficulties in identifying the key parameters for adjustment (DFN geometry, transmissivity, boundary conditions) and in finding appropriate adjustments hampered the modellers. Further, because formal inverse models were not used in conjunction with DFN models no estimates of parameter uncertainty were derived.

The different approaches taken in Task 7B are listed in Table 4-22. The diversity of approaches used in Task 7B relates more to the relative ease of implementation within the numerical codes rather than to well-established methodologies for calibration of cross-hole tests.

Several groups added additional deterministic features to represent significant flow features at test-scale that were not represented either within the hydrostructural models provided or in the "background rock" representations. The different approaches taken are listed in Table 4-23.

Table 4-22. Model conditioning and calibration approaches used within Task 7B.

Item	DFN Parameter	Evaluation
Network geometry and connectivity	Length-scale (Posiva/VTT)	Only limited control on overall effective conductivity and may bias models if equi-dimensional fractures assumed (Barker and Black 2018)
	Fracture-growth model (SKB/KTH)	Honours borehole local data but with very limited control on the network in the inter-borehole region. Models highly dependent on the spatial distribution of conditioning boreholes
	Random feature disconnection (JAEA)	Likely to require evaluation across multiple realisations and therefore expensive to perform
	Random removal of feature conducting surface area	
	Feature removal (JAEA)	Creates zones of limited connectivity – used by JAEA to represent observed depth dependence.
Addition of deterministic features	JAEA, NWMO/Laval, Posiva/VTT, SKB/CFE, SKB/KTH	Addition of sheet joints/additional zone structures used to represent transmissive structures not well reproduced by the stochastic distributions but too small to be included in the site-scale structures.
Deterministic feature transmissivity	JAEA, SKB/KTH, Posiva/VTT, SKB/CFE	Almost all groups either modified feature transmissivity, either locally at borehole intersections or for individual structures. These provided valuable tools for model conditioning
Stochastic feature transmissivity	JAEA, Posiva/VTT	Straightforward calibration approach to changing effective hydraulic conductivity and magnitude of flows from background rock
Boundary conditions	Recharge rate (KAERI, SKB/KTH)	Significant in undisturbed conditions but limited effect on pumping-induced drawdown or flows

Table 4-23. Additional deterministic features included within the models.

Group	Additional features Transmissivity T (m^2/s)	Comment
KAERI	None	Only deterministic features derive from Hydrostructural model
JAEA	HZ002 added to 2008 Hydro-structural model	Well-test analysis used to revise hydro-structural model
NWMO/Laval	50 mah KR14 T = 1.E−4 60 mah KR15A Plane_1/HZ19C T = 1.E−4	Models were sensitive to feature transmissivity when pumping from KR14 but not when pumping in KR14
Posiva/VTT	−20 m.a.s.l. T = 2.E−5 from EnKf (cut to exclude KR17) −50 m.a.s.l. T-low rom EnKf (rectangular feature)	Adding features improved match to flow distribution but not head and were not included in overall best model
SKB/CFE	−20 m.a.s.l. T = 2.2E−4 (triangular) −50 m.a.s.l. T = 1.E−5 (rectangular)	Added to match heads in calibration step
SKB/KTH	None	Used fracture growth scheme

5 Task 7C Posiva Flow Logging characterisation and analysis of low permeable fractures and assessment of flow distribution pattern at shaft wall sections at Onkalo, Olkiluoto, Finland

Task 7C focused on three individual low-transmissivity fractures within low permeability background rock. The fracture descriptions are derived from the characterisation performed around the three ventilation shafts at Onkalo. The sub-surface location of the boreholes within Onkalo allowed higher drawdowns within the boreholes (~200 m) and hence the PFL characterisation of significantly lower transmissivity features than in the previous subtasks.

Task 7C is documented within the series of SKB P series reports covering Task 7 as listed in Chapter 4. The Task 7C Task Description is included within Vidstrand et al. (2015). CRIEPI participated at the start of the subtask but withdrew prior to reporting their work.

5.1 Task 7C Objectives

The objectives of Task 7C were

- to use PFL to characterise and analyse procedures to quantitatively describe low transmissivity fractures, and
- to demonstrate procedures of characterisation of flow in fractures of transmissivity less than 10^{-9} m^2/s.

These objectives were specified through a set of goals:

1. To advance the understanding of PA relevant single fracture micro-structural models.
2. To use PFL to characterise in-plane fracture heterogeneities.
3. To improve the ability to predict inflow to suitable and unsuitable canister holes.
4. To assess whether data from pilot boreholes has any predictive power with regard to prediction of flow to canister holes.

The low transmissivity of the fractures suggested that they may be representative of the class of structure encountered close to deposition holes in good rock within the repository volume. This provided a particular focus for the study as such fractures represented a class of structure not previously considered.

The intention was to develop near-field single-fracture models incorporating microstructural information in order to assess the flow pattern on a section of shaft wall and to assess the transport characteristics (F-factor) and flow distribution on a larger scale within the fracture.

Task 7C definition and structure

The task was split into four subtasks:

- Task 7C1: Parameterised and justified microstructural model for three fractures.
  Within Task 7C1 each group was to develop and justify a microstructural model for each of the 3 fractures.
- Task 7C2: Simulation of flow patterns in low transmissivity fractures.
  Within Task 7C2 the modelling groups were to simulate hydraulic tests (single hole PFL and cross-hole PFL) and calculate F-factors using the fracture models developed in Task 7C1.
- Task 7C3: Nappy experiment (optional) in Shaft KU2.
  Within Task 7C3 modellers were to simulate the detailed inflow distribution to the shaft for the fractures using the microstructural models developed in 7C1 and 7C2.

- Task 7C4: Uncertainty of flow in single fractures (optional, but recommended).

  Within Task 7C4 the modellers were to consider several sources of uncertainty: parameter uncertainty, phenomenological uncertainty, geological conceptualisation and mathematical implementation and consequences from the shaft-wall boundary conditions.

The Task Definition allowed the fractures to be treated as either

- 3 individual 2D fracture models, or
- a 3D model containing the 3 fractures.

5.1.1 TS28 revision

Within the Task 7C definition an additional simulation TS28 was suggested. The objective was to predict transverse flow measures during a pumping test in the KR14–18 volume considered in Task 7B. Posiva had performed transverse flow measurement (PFL-Trans) in KR15, KR15B, KR16B, KR17B and KR18B while pumping KR14 (Väisäsvaara 2009). The PFL TRANS tool is shown in Figure 5-1a and the measurement sequence is:

- Measuring section (0.5 m) is positioned over a previously identified flowing feature and a first flow measurement is made.
- The packers are inflated isolating the measurement section and the system is allowed to equilibrate.
- Multiple flow measurements (typically 4) are made with the flow channel oriented at multiple angles so that the direction and magnitude of flow across the borehole can be estimated (Figure 5-1b).

Test were performed under multiple flow conditions (undisturbed and with pumping at different rates). The transverse flow measurement limit was 5 ml/hr. During the testing repeat measurements were made to demonstrate consistency.

In the TS28 simulations, boreholes were open and free to cross-flow, with the exception of the PFL TRANS measurement interval. The simulation was originally proposed as a verification of the models developed in Task 7B but was then revised and rescheduled to make use of the Task 7C microstructural models. Not all groups performed TS28. The revised Task Definition required the prediction of the transverse flows at the simulated flowing features in KR15 during pumping in KR14. In particular the transverse flow at 59 m (location of the HZ19C zone in Task 7A) was requested.

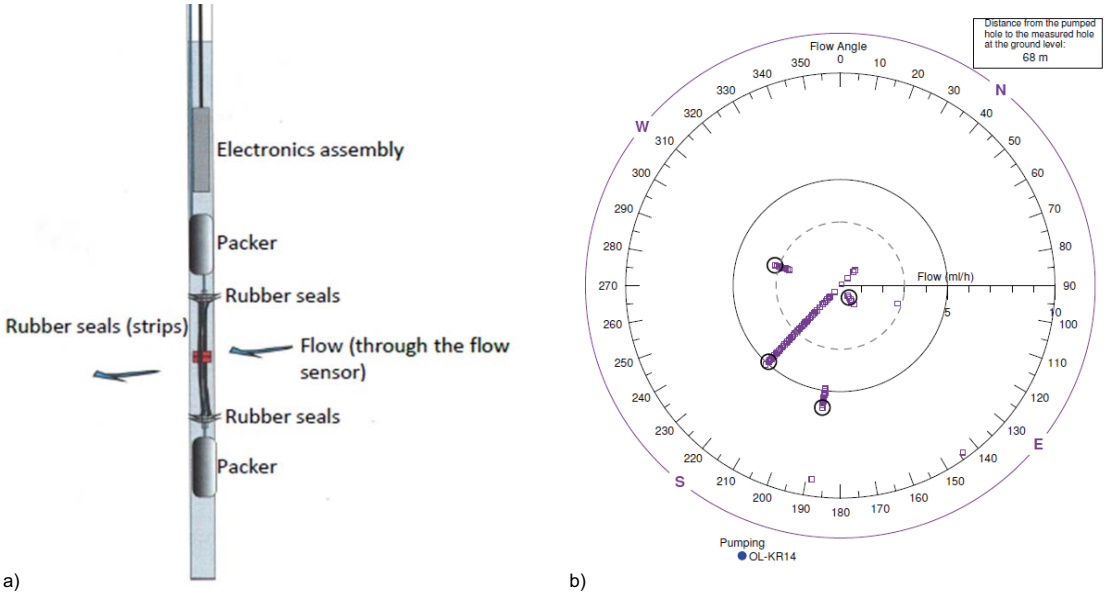

Figure 5-1. *Posiva PFL-Trans a) packer system, b) transverse flow measurement in KR15 during pumping in KR14 (greatest measured flow is approximately towards KR14).*

5.1.2 Task 7C dataset

The three fractures under considerations were:

- FR1-KU: fracture intersected in shaft KU1.
- FR1-KU2: one of 3 fractures mapped in shaft KU2 and the fracture used for Nappy measurements.
- FR1-KU3: fracture intersected in shaft KU3.

The modellers were not expected to consider possible shaft-wall processes: e.g. effects of excavation, two-phase flow or grouting operations and the chosen region containing the three fractures was selected as it was considered to be the least disturbed by such processes. Table 5-1 lists the shafts and associated boreholes.

The three shafts (KU1, KU2 KU3) and an example of the fractures identified in the ONK-PP probe holes are shown in Figure 5-2.

Table 5-1. Onkalo shafts and probe holes used in PFL testing of low transmissivity fractures.

Shaft	Diameter (m)	Deep borehole	Probe holes ONK-PP	Elevation (m.a.s.l.)	PFL testing
KU1/Personnel	4.5	KR24	131, 134, 137	−177.52	March 2008
KU2/Exhaust air	3.5	KR38	122, 123, 124, 126, 128	−181.09	February 2008
KU3/Inlet air	3.5	KR48	125, 127, 129	−176.81	September–October 2008

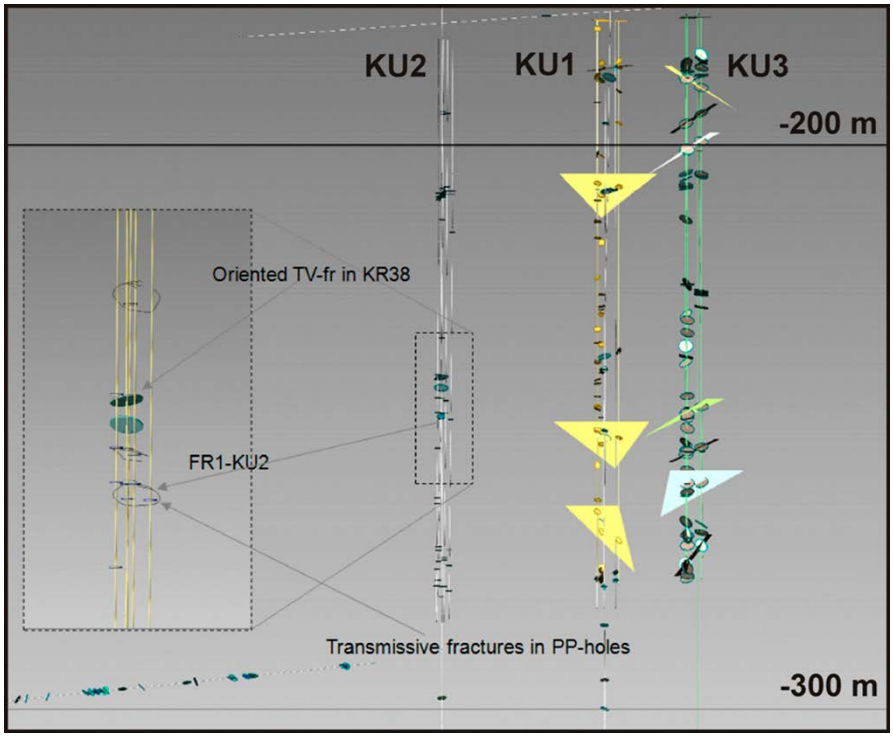

Figure 5-2. *Example of fracture data available along the three shafts: Fracture1 is indicated as FR1 in shaft KU2.*

The probe holes (ONK-PP xxx) were 100 m in length and the PFL measurement interval was chosen as 0.5 m long with a 0.1 m measurement increment so that overlapping sections were measured ("detailed mode"). PFL measurements were performed as:

- Single hole measurements where the nearby boreholes were closed with a packer near the surface (no outflow but potential for cross-flow within the borehole).
- Cross-hole measurements where PFL measurements were performed in ONK-PP125 and ONK-PP127 (KU3) and nearby boreholes were open or closed (with a single packer) in a range of configurations.

When a borehole was open this resulted in a drawdown of approximately 190 m due to the elevation of the borehole mouth (Table 5-1) and an average undisturbed head at surface of 6 m.a.s.l. Transmissivity was estimated in the standard way (see Chapter 2) assuming an R/r_0 of 500. As the actual flow geometry and any skin effects (e.g. groundwater degassing) were unknown, the transmissivity values were considered as an indication of the prevailing orders of magnitude (Pekkanen 2009a).

The testing in the KU1 and KU2 shaft probe holes used a simple protocol whereby the nearby boreholes were closed with a single packer close to the top of the hole while PFL measurements were taking place in the open probe hole (see Table 5-2 and Table 5-3). Cross-hole testing in the KU3 shaft probe holes utilised a more complex sequence of hydraulic boundary conditions as shown in Table 5-4. The pattern of flows for the different tests is shown in Figure 5-3.

Table 5-2. Simulations and probe hole boundary conditions for KU1.[26]

Simulation	State of borehole		
	PP-131	PP-134	PP-137
s-PP131	PFL	Closed	Closed
s-PP134	Closed	PFL	Closed
s-PP137	Closed	Closed	PFL

Table 5-3. Simulations and probe hole boundary conditions for KU2.

Simulation	State of borehole				
	PP-122	PP-123	PP-124	PP-126	PP-128
s-PP122	PFL	Closed	Closed	Closed	Closed
s-PP123	Closed	PFL	Closed	Closed	Closed
s-PP124	Closed	Closed	PFL	Closed	Closed
s-PP126	Closed	Closed	Closed	PFL	Closed
s-PP128	Closed	Closed	Closed	Closed	PFL

Table 5-4. Simulations and probe hole boundary conditions for KU3.

Simulation	State of borehole		
	PP-125	PP-127	PP-129
s-PP125	PFL	Closed	Closed
c-PP125-1	PFL	Open	Open
c-PP125-2	PFL	Open	Closed
c-PP125-3	PFL	Closed	Open repeated
s-PP127	Closed	PFL	Closed
c-PP127-1	Open	PFL	Open
c-PP127-2	Open	PFL	+2bar
s-PP129	Closed	Closed	PFL
c-PP129-1	Open	Open	PFL

[26] Simulation names as test type-PFL logged borehole. Test type s: single with only the logged PFL borehole being open; c: cross-hole with both the PFL and other boreholes being open.

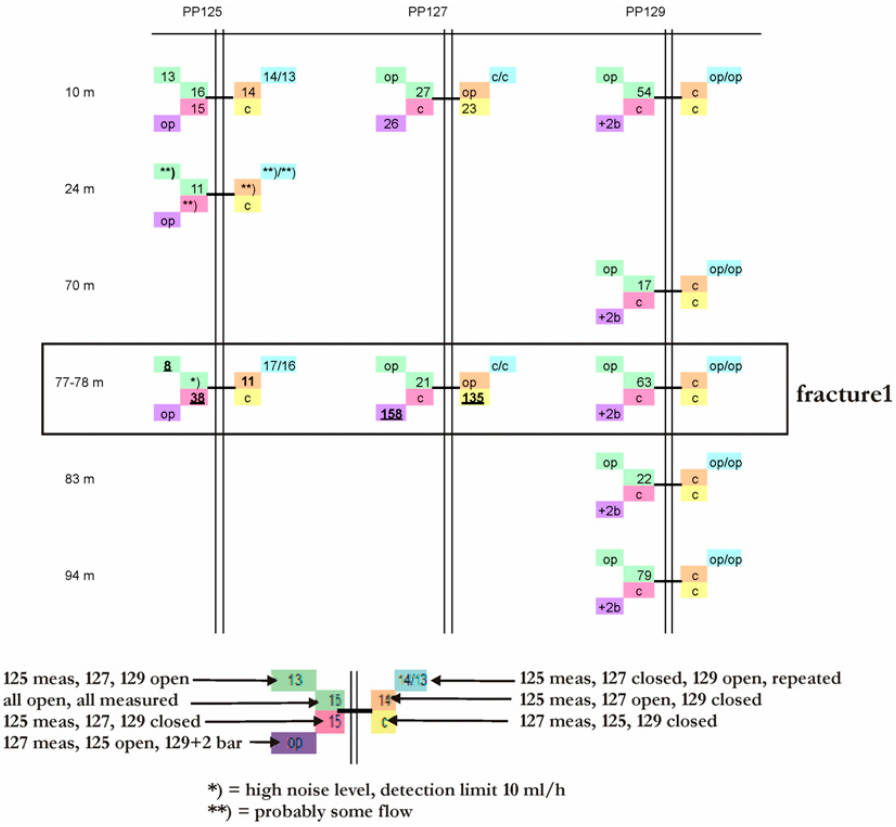

Figure 5-3. *Summary of PFL measurements in ml/h in shaft KU3 (Pekkanen 2009b).*

Each of the three fractures were associated with 4–7 borehole intersections providing an opportunity to address the hydraulic heterogeneity of such fractures. All the boreholes were cored and one fracture had been characterised by cross-borehole PFL interference test measurements. The estimated transmissivity distribution for the different KU2 boreholes is shown in Figure 5-4.

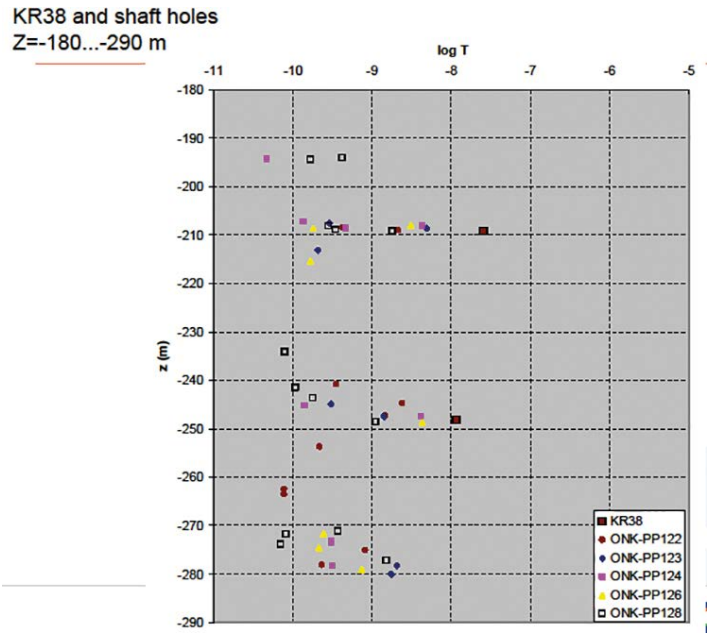

Figure 5-4. *PFL data from the deep borehole KR28 and Onkalo pilot holes PP122–124, PP126, PP128.*

For one fracture in KR38 borehole TV images were available (for location see Figure 5-2). In all three shafts there was trace-line mapping on the walls and detailed surface mapping of the individual fracture intersections. The data provided to the modellers included:

- Borehole geometry (survey data).
- Shaft wall geometry.
- Fracture trace geometries.
- PFL data and fracture identification (performed prior to shaft excavation).
- Detailed mapping, photos and water leakage values.

The “Nappy Test” and fracture mapping were performed in the KU2 shaft. The shaft was being used for ventilation at the time of the experiment. The air current in the shaft resulted in significant drying of the shaft wall. In unventilated conditions spots identified as “damp” under the test conditions might have been identified as “wet”. The sketches of the three approximately parallel fractures (bearing ~320°) mapped are shown in Figure 5-5. The leakage spots have about the same bearing in every fracture.

After mapping, the absorbent nappies (disposable diapers) were individually pressed along the Fracture 1 trace for one minute and the difference in weight (due to water absorption) was measured with a scale. The nappies where protected from drying by the air current by using a cover. Measurements were repeated in few spots to check the results. The first measurement gave higher values due to surface moisture.

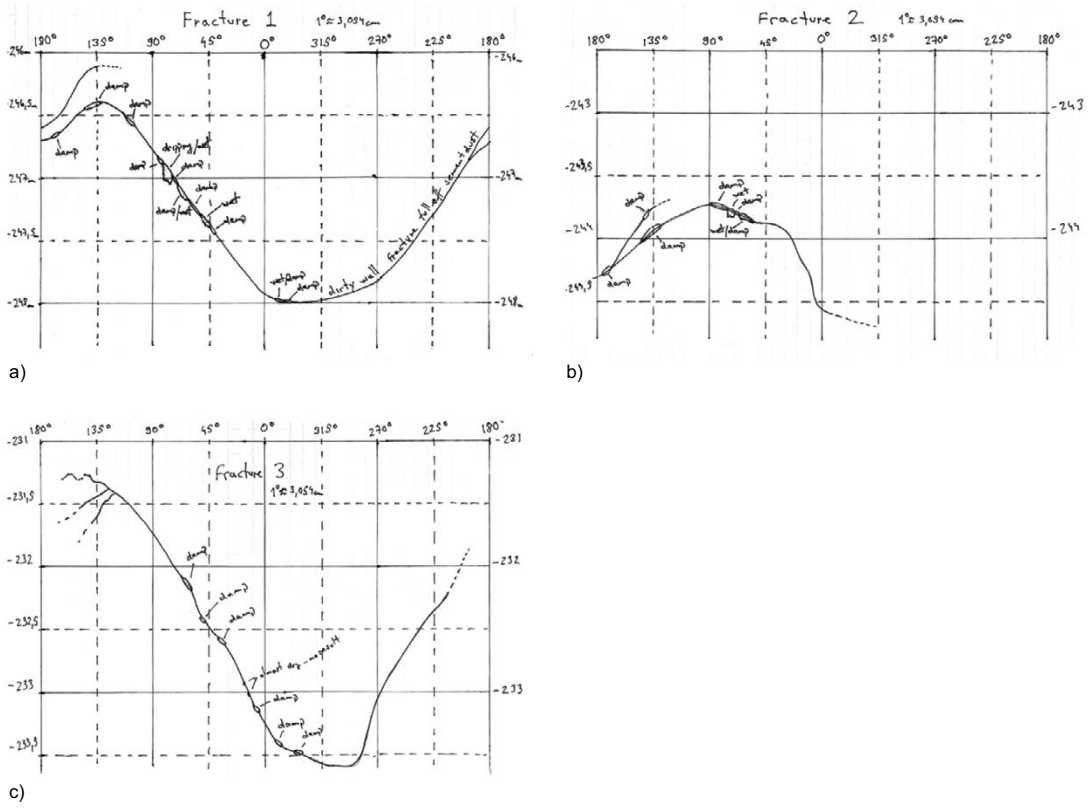

Figure 5-5. *KU2 fracture mapping a) Fracture 1 (−248 to −246m), b) Fracture 2 (−245 to −243) and c) Fracture 3 (−234 to −231).*

5.2 Modelling approaches

5.2.1 JAEA

JAEA aimed to model the in-plane heterogeneous aperture distribution of a single fracture based on the PFL data from pilot boreholes and fracture mapping of the shaft walls. They developed two workflows for modelling of heterogeneous fracture aperture within Task 7C. The first workflow (Figure 5-6a), based on simple variogram models, was found not to reproduce the multi-scale channelling structures observed in the TRUE experiment (Winberg et al. 2003) and the Kamaishi Mine rock sample (Tetsu and Sawada 2010). An alternative model was therefore developed using multiple nested correlation lengths (Figure 5-6b). In the absence of site-specific data the correlation lengths were taken from analysis of the Kamaishi Mine rock sample and the aperture distribution was constrained by the PFL data and Nappy Tests. It was then necessary to scale the aperture data to match the observed geometric mean transmissivity at KU2 and KU3.

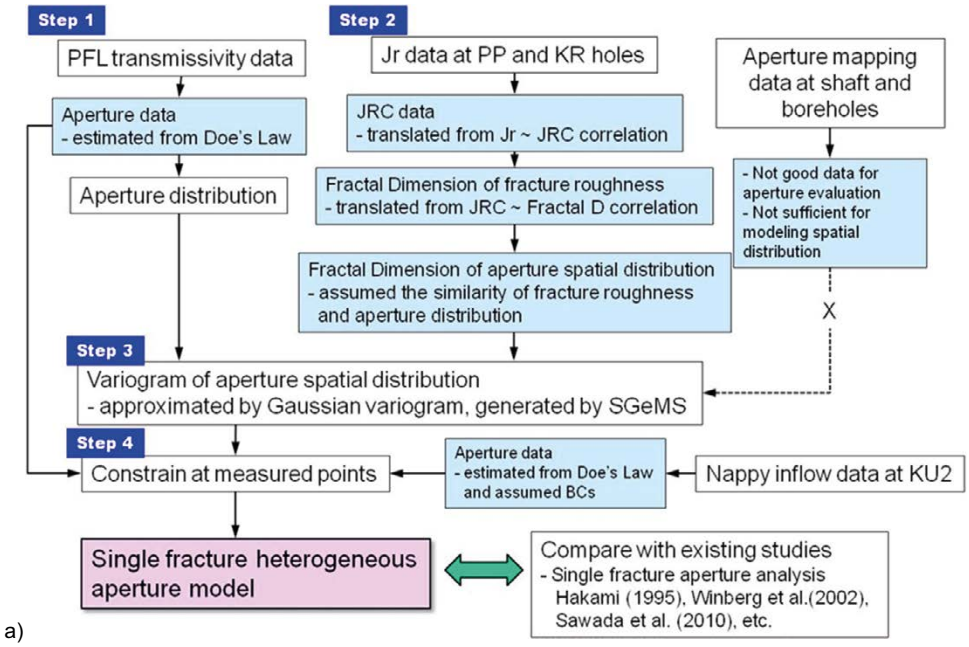

Figure 5-6. *Workflows for modelling a single fracture with heterogeneous aperture: a) original workflow based on PFL and JRC; b) alternative approach using multi-scale correlation length model.*

Transmissivity was related to aperture by an empirical relationship $e = AT^b$, where e is aperture in m and T transmissivity in m^2/s, with $A = b = 0.5$[27]. Apertures derived from the measured PFL transmissivity could be well-fitted to a log-normal distribution. Sample transmissivity realisations are shown in Figure 5-7. In addition to the heterogeneous fracture, a network of very low transmissivity background fractures was included in the simulations. The properties of the background fracture network were based on orientation data from the relevant pilot and deep boreholes and the PFL data (Figure 5-8).

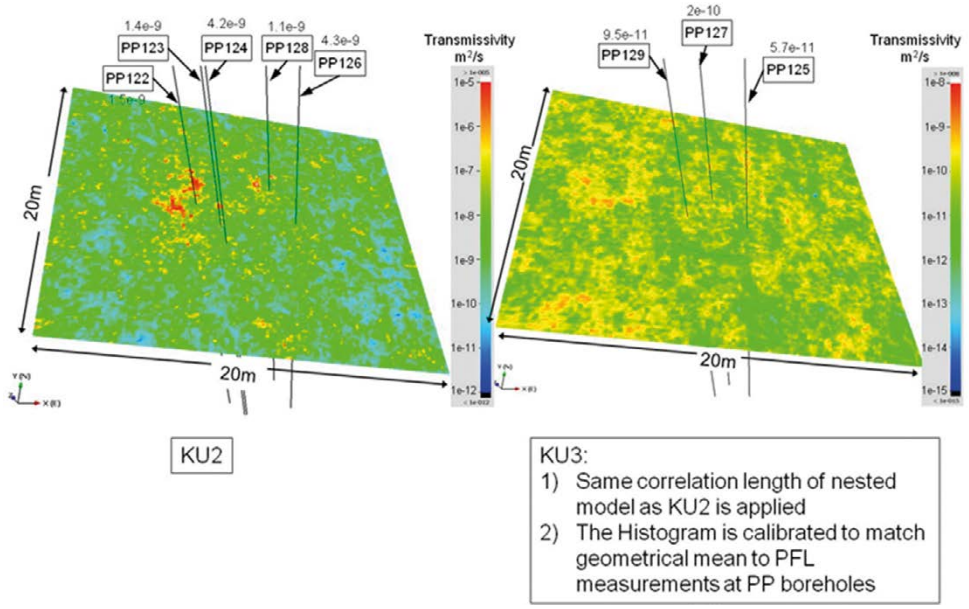

Figure 5-7. *Sample realisations of the fracture heterogeneity models for KU2 and KU3 based on the multi-scale correlation length model.*

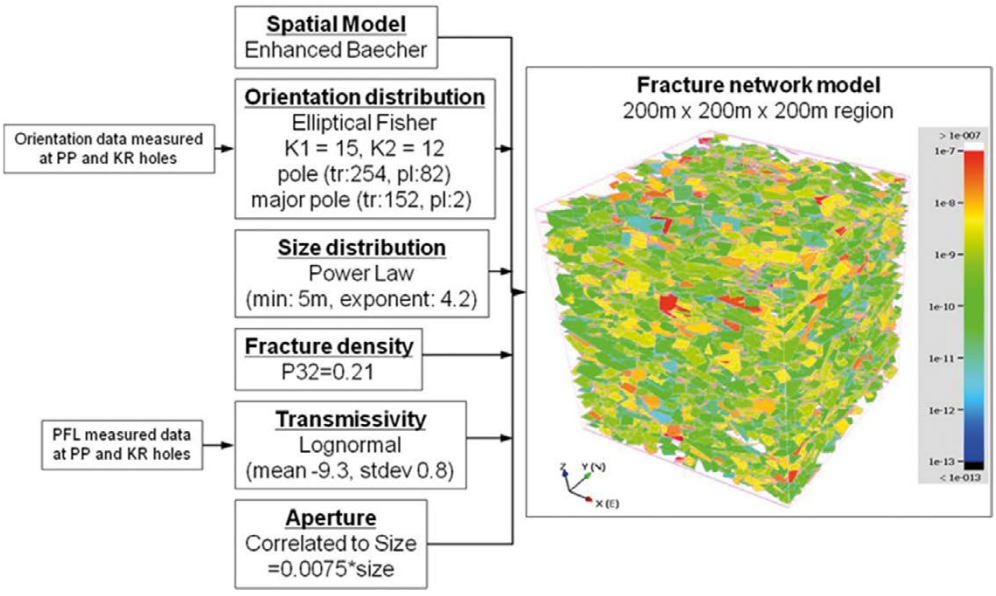

Figure 5-8. *Background fracture network parameters and sample realisation.*

[27] Also known as Doe's Law (see Dershowitz et al. 2003).

The model region used for simulations was a 200 m cube centred on shafts KU2 and KU3 (Figure 5-9). The target heterogeneous fracture FR1 was represented as a 20 m square plane oriented to match the shaft intersections with apertures sampled at 0.05 m resolution and up-scaled to the 0.2 m scale of the finite element mesh. The sides of the model region were set to a constant −60 m head based on the estimated large-scale drawdown around the shafts while the top and bottom faces were treated as no-flow boundaries.

Model conditioning and calibration

The original heterogeneity models (Figure 5-6a) were discarded because they did not reproduce the multi-scale channelling observed at Kamaishi Mine and the TRUE experiment at Äspö. The alternative approach used correlation lengths from the Kamaishi Mine rock sample and PFL data but then required scaling to match the expected feature transmissivity. Forward simulations of tests in PP124 and PP126 (KU2) did not match observation but the model was calibrated to match the observed flow by increasing the local transmissivity.

5.2.2 KAERI

KAERI's objectives in Task 7C were:

- to understand how to characterise the hydraulic properties of a single fracture using field data;
- to find a way to use the characterised single fracture properties to reduce the uncertainty of the safety assessment for a subsurface repository.

Model structure

KAERI modelled a single fracture as a rectangular 2D porous medium with heterogeneous transmissivity. Local transmissivity values were calculated at borehole intersections and analysed using geostatistical approaches (Kriging and conditional simulation[28]) to derive the transmissivity distribution across the feature (Figure 5-10) around KU1 and KU2. For detailed simulations around the KU3 shaft a smaller model domain was used (Figure 5-11).

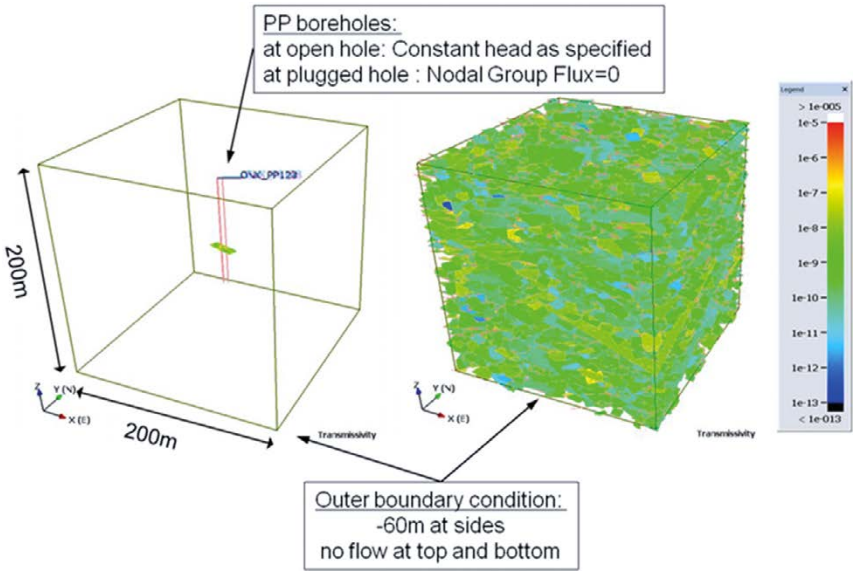

Figure 5-9. *The modelling region (200 m × 200 m × 200 m) and boundary conditions used for Task7C simulations. DFN fractures coloured by transmissivity (m^2/s).*

[28] Ko and Ji (2017) refer to the method as conditional random generation.

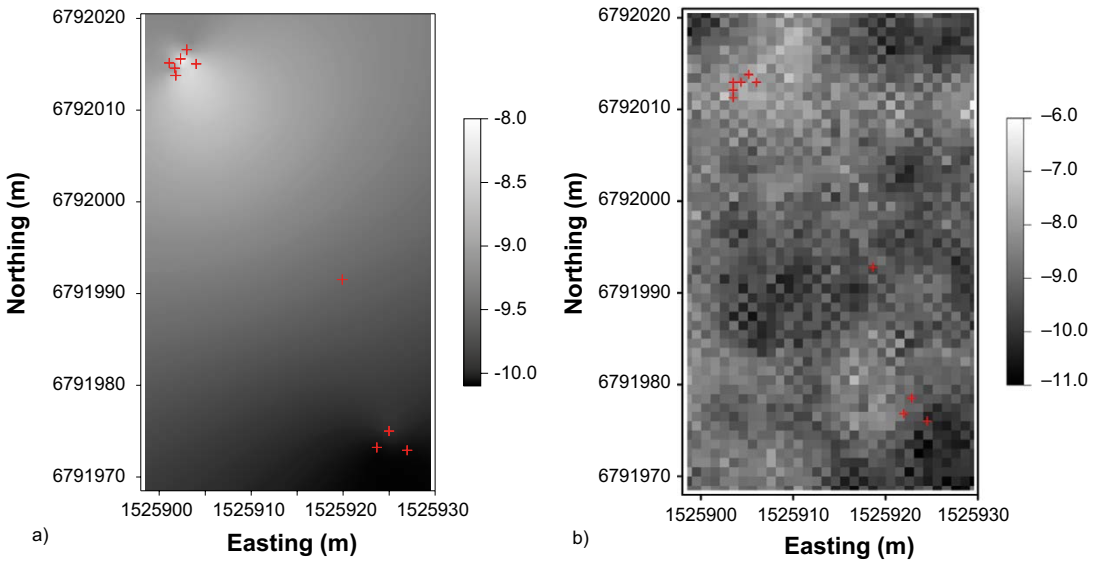

Figure 5-10. *Examples of the transmissivity fields constructed by (a) interpolation by Kriging and (b) conditional simulation.*

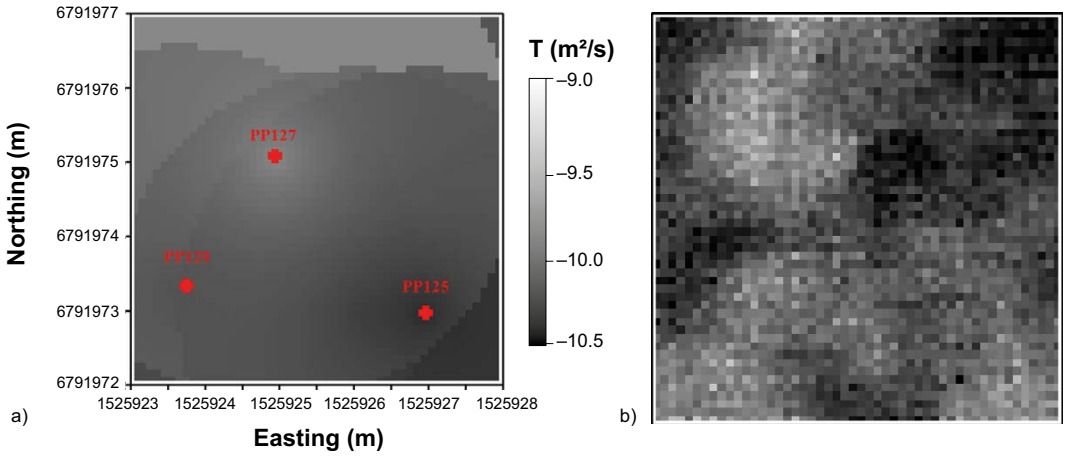

Figure 5-11. *Transmissivity fields constructed by (a) interpolation by Kriging and (b) random generation in the reduced model domain.*

The lateral boundaries of the horizontal fracture were treated as constant head using results from the local and regional groundwater flow models. Borehole boundary conditions were applied based on the elevation of the open boreholes together with any overpressure (e.g. c-PP127-2).

Model conditioning and calibration

Within Task 7C the models were not calibrated but were run as forward "predictive" simulations.

5.2.3 NWMO/Laval

Model structure

NWMO/Laval focused on describing the heterogeneity within Fracture1 using the FGEN (Robin et al. 1993) random field generator. Fracture hydraulic aperture is described by a spatially correlated log-normal distribution parameterised by the mean and standard deviation of natural log aperture and the correlation length. The mean of −11.54 (equivalent to an aperture of 10^{-5} m) and standard deviation of 0.273 were derived from the nine PFL measurements in the PP holes while the range of correlation lengths considered (0.2, 0.35 and 0.5 m) was based on results from literature review (Figure 5-12).

For the simulations of flow to the probe hole arrays, the models included Fracture1, which was assumed to cross all three shafts, together with a small number of discrete fractures identified in Pekkanen (2009a, b). The rock matrix around the fracture was considered as a porous medium with low hydraulic conductivity. The resulting conceptual model is shown in Figure 5-13. Use of the facies approach developed in Task 7B was considered for the background rock and test calculations were made but rejected on the basis of limited data, model discretisation limits and the lack of significant improvement in matches to observation. The outflow from each borehole in the models was set to the total PFL flow plus the relative deviation from the total measured outflow.

For calculations of retention parameters (β), a 30 m × 50 m plane (Fracture1) was modelled embedded within an impermeable matrix resulting in a 2D flow domain. Linear head gradients were imposed on the domain as specified in Vidstrand et al. (2015). The three shafts were represented as internal boundaries for transport. The fracture aperture was generated using the same model and parameters used in the probe hole calculations. To minimise additional dispersion (beyond that due to aperture variation) very small longitudinal and transverse dispersivities were used. Barium and Calcium were selected as sorbing tracers for the calculations.

For the KU2 shaft inflow simulations (Subtask 7C3) the model consisted of Fracture1 embedded in a homogenous porous matrix. The hydraulic conductivity of the matrix was adjusted to derive the best fit to observations.

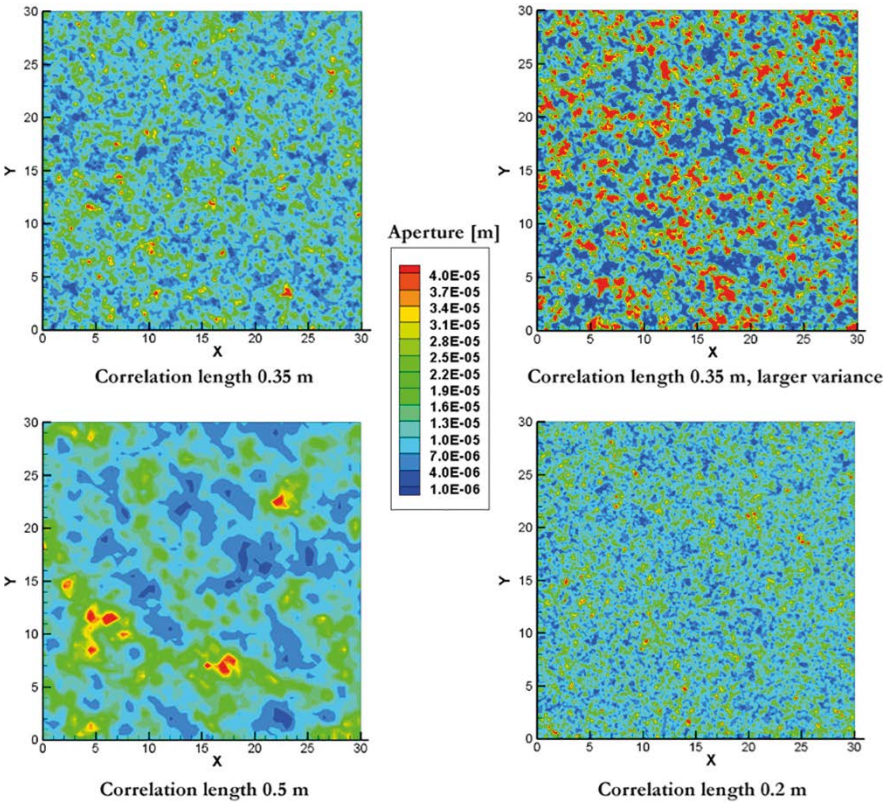

Figure 5-12. *Fracture1 hydraulic aperture fields with varying correlation length.*

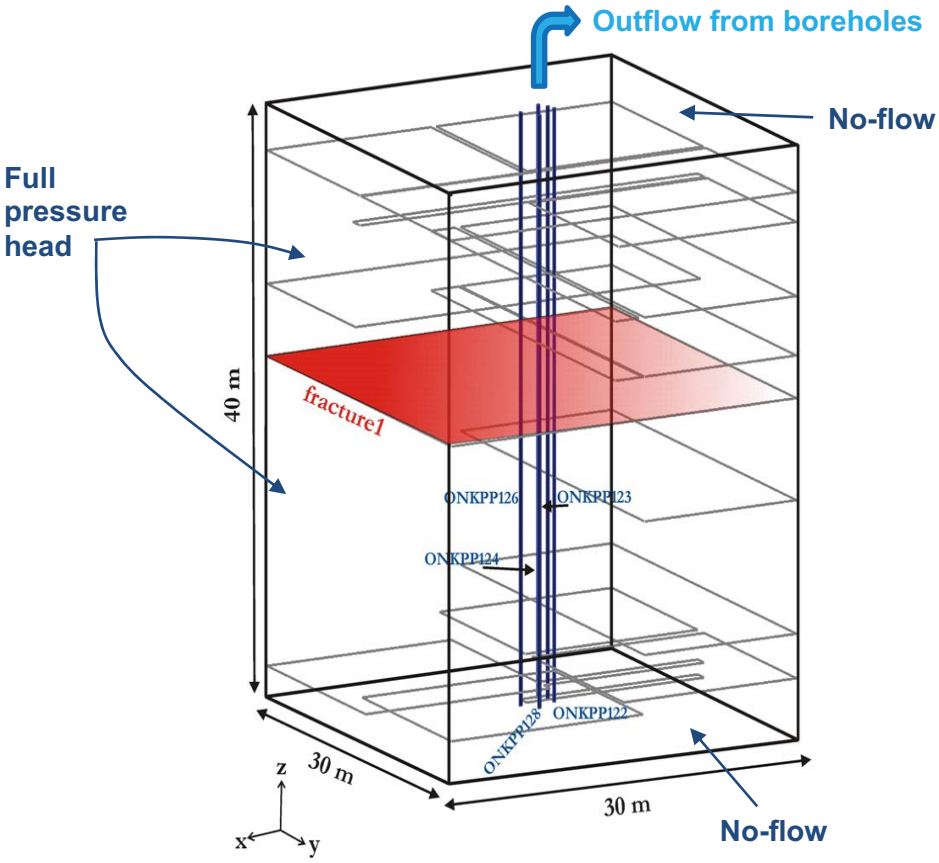

Figure 5-13. Simulation domain for probe hole calculations showing boreholes, fractures and boundary conditions.

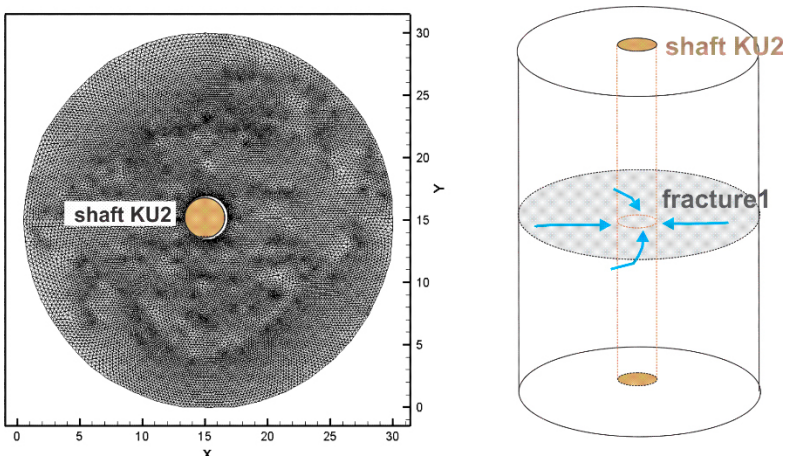

Figure 5-14. Simulation domain for shaft inflow calculations (7C3).

Model conditioning and calibration

The hydraulic conductivity of the porous rock matrix was set by manual calibration. A range of values (between 10^{-9} m/s and 10^{-12} m/s) derived from Task 7A for the matrix hydraulic conductivity were tested and a value of 10^{-11} m/s was selected. Further, a range of correlation lengths were tested. A summary is given in Table 5-5.

Table 5-5. Summary of NWMO/Laval calibration approaches in Task 7C.

Model	Calibration approach
Borehole inflow calculations (7C2)	Comparison of results for different correlation length (only single realisations). The hydraulic conductivity of the porous rock matrix was set by manual calibration.
Shaft inflow (7C3)	Matrix hydraulic conductivity was adjusted to better match the observed inflow (transmissivity of Fracture1 was not changed). Inflow boundary conditions at the shaft were adjusted to match the observed dry (potentially grout affected) region.

5.2.4 Posiva/VTT

Model structure

The model volumes used in Task 7C1,2 were 40 m tall, 15 m radius cylinders (approximated as hexagonal prisms) centred on the intersection of the shafts with the horizontal FR1 fracture. The model radius was based on comments in Vidstrand et al. (2015) that heads at 15 m from the shaft could be considered as undisturbed. For the calculation of retention properties (F-factors), the boundaries and boundary conditions were reset with unit E-W and N-S hydraulic gradients.

The FR1 fracture was represented as a horizontal feature with spatially varying transmissivity. The local FR1 transmissivity was assumed to have a log-normal distribution and be spatially correlated. The transmissivity field was conditioned to the borehole PFL data using the method of Dietrich and Newsam (1996).

For the Task 7C1,2 models a single set of low transmissivity stochastic background fractures was included. The properties common to the different models are listed in Table 5-6. Fracture radius was modelled as a truncated power-law distribution and manually adjusted (via the minimum radius parameter rmin) so that only 5–10 fractures were generated in each model region and that these reached the model boundary. Disconnected fractures were removed from the model. Transmissivity was correlated with fracture size using the same approach as in Task 7B.

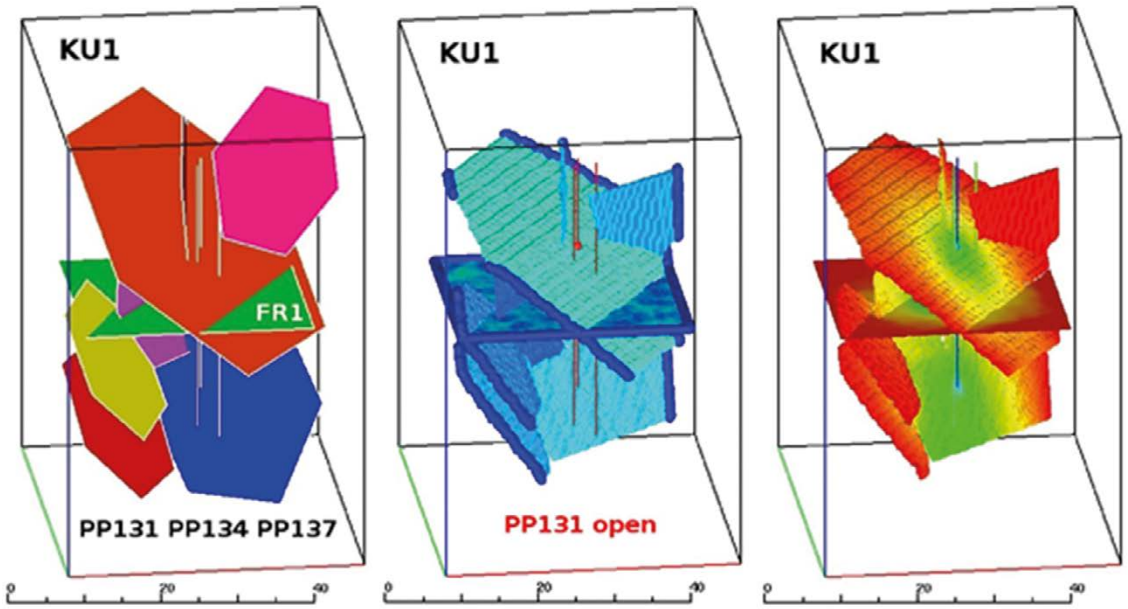

Figure 5-15. *Example realisation of KU1model: left conceptual model, centre numerical model and boundary conditions, right head solution for drawdown in PP131. The horizontal FR1 fracture can be seen at the centre of the model.*

Table 5-6. Common parameters of stochastic background fractures.

Parameter	Distribution	Source
Orientation	26/60° von Mises-Fisher κ = 21.9	KU1 borehole fracture data
Size (L m)	Truncated power-law b = 2.5	Chosen to limit numbers and generate fractures that connect to the boundaries
Fracture density	Homogeneous Poisson Process	From borehole data
Transmissivity (T m^2/s)	Spatially correlated log-normal $\mu = -12.5$, $\sigma = 0.6$, correlation length = 2.9 m	Calibrated μ based on $-13 \leq \log_{10} T \leq -10$
T-L relationship	Correlated $S_L = 0.1$	Sensitivity study in Task 7B

The models for Task 7C3 and 7C4 were essentially two-dimensional considering only the FR1 fracture and its intersection with the shaft without inclusion of any background fractures.

Model conditioning and calibration

In Task 7C1,2 the transmissivity distribution parameters of the FR1 fracture were calculated using the observed PFL transmissivities and the transmissivity field was simulated to honour the local transmissivity at each borehole intersection (Dietrich and Newsam 1996). The correlation length and log standard deviation σ were assumed and the log mean μ was adjusted to match the observed inflow based on a trial and error basis using 20 realisations of each model for each calibration step. The transmissivity distribution of the stochastic background fractures was taken as being the same as that of the local distribution within FR1, in the absence of other information.

Table 5-7. Model region-dependent parameters of FR1 and stochastic background fractures.

Task	Model	FR1 transmissivity		Background fracture properties	
		Correlation length (m)	μ, σ	P_{32} (m^2/m^3)	r_{min} (m)
7C1	KU1	2.9	−10.5, 0.6	0.11	10
7C1	KU2	2.9	−10.5, 0.6	0.11	10
7C1	KU3	2.9	−12.5, 0.6	0.01	8
7C3,4	KU2	Varied	Varied	Not considered	

Revised TS28 model

In a final step the block-scale TS28 simulation of crossflow in HZ19a and HZ19C was revisited using the derived transmissivity heterogeneity models of the FR1 fracture.

5.2.5 SKB/CFE

Model structure

The computational domain was a 15 m radius circle containing a single heterogeneous fracture. Three different methods for generating fracture aperture/transmissivity heterogeneity were evaluated:

- Multivariate log-normal distribution incorporating anisotropy with specified correlation lengths.
- The use of an underlying stochastic DFN to modify feature permeability.
- Fractal surface using a self-affine procedure to generate a surface with specified fractal dimension and correlation length.

For the flow simulations the heterogeneity was generated in a 2-step process:

1. Generation of a spatially-correlated log-normal transmissivity field over the fracture.
2. Generation of a stochastic DFN and modification of the heterogeneous fracture along intersections with the stochastic fractures.

Fixed pressure boundary conditions were used at a) the outer boundary, b) borehole intersections during simulations of pumping tests and c) the shaft boundary for shaft inflow calculations. The permeability, simulated pressure and flow fields for pumping conditions are shown for 2 sample realisations of the KU1 fracture in Figure 5-16.

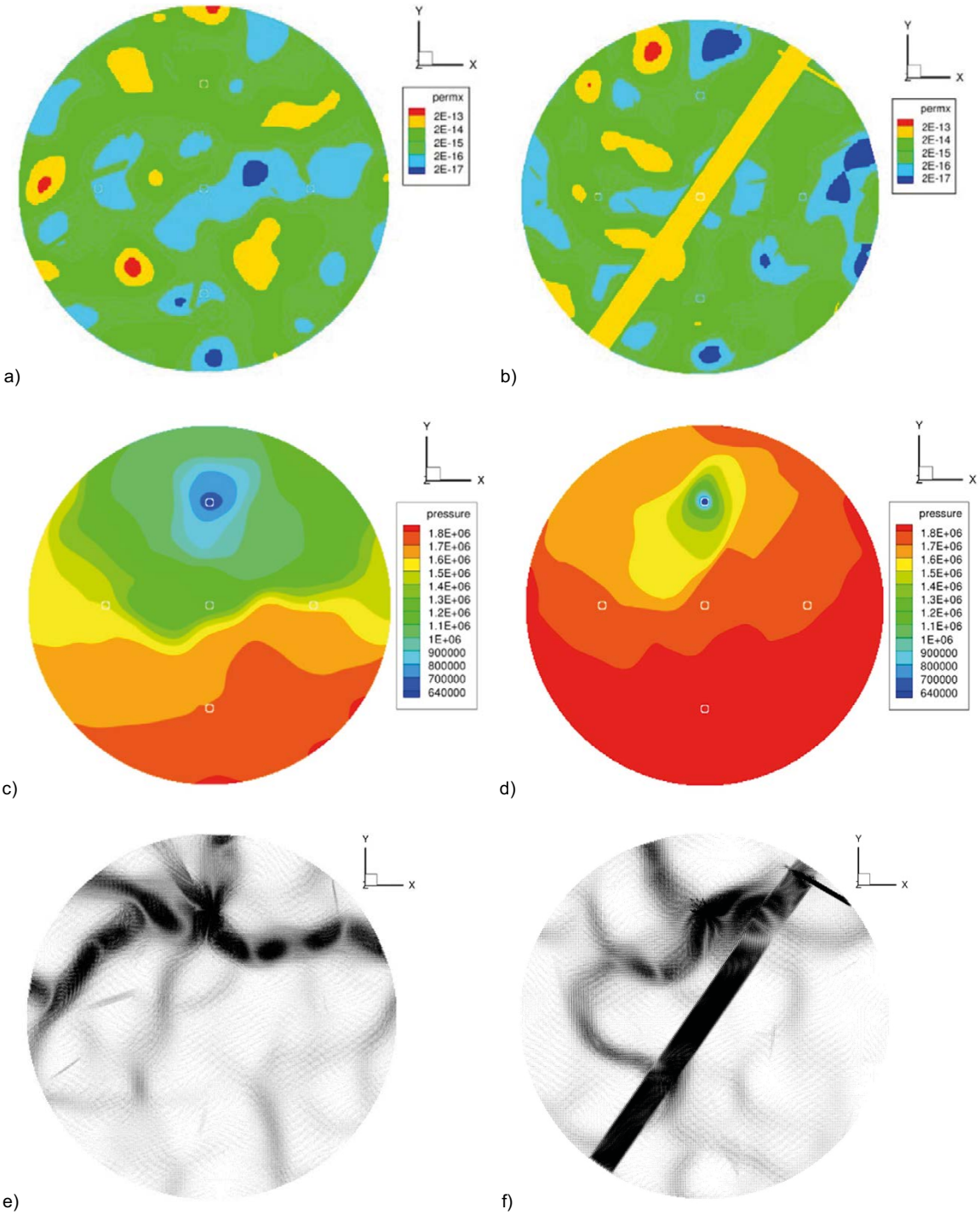

Figure 5-16. *Simulated permeability (m^2), pressure and flow distributions in Fracture 1 around shaft KU1. The feature is assumed to have a thickness of 0.1 m: a, c, e) realisation 1 (no large intersecting stochastic fractures); b, d, f) realisation 2 showing the influence of intersection with a large stochastic fracture.*

Model conditioning and calibration

The single hole pump tests were used to evaluate the mean transmissivity of the fractures crossing KU1, KU2 and KU3. The transmissivity was adjusted to match the measured head and inflow for 3 realisations of the DFN. The resulting mean transmissivities were:

- KU1: 5×10^{-10} m^2/s
- KU2: 2×10^{-10} m^2/s
- KU3: 5×10^{-11} m^2/s

Revised TS28 model

SKB/CFE chose to develop a model for what was called "Task ABC": an integration of the models developed for the 3 main subtasks of Task 7. The ABC model was similar to the model used in Task 7B but with the following modifications:

- The pump tests in the open boreholes KR14–18 were repeated with homogeneous sheet joints and with heterogeneous sheet joints (based on the Task 7C heterogeneity models). Five different realisations of the sheet joints were tested.
- The heterogeneous sheets joints used the same local fracture network used in Task 7C.
- A much finer computational grid was used to resolve the heterogeneous sheet joints with a local cell size of 0.12 m. This resulted in a model with about 8 million cells.

The resulting permeability field at −50 m.a.s.l. (elevation of the deeper sheet joint) is shown at different scales in Figure 5-17. The figure emphasises the fine resolution with which the flowing feature has been described within a regional scale model.

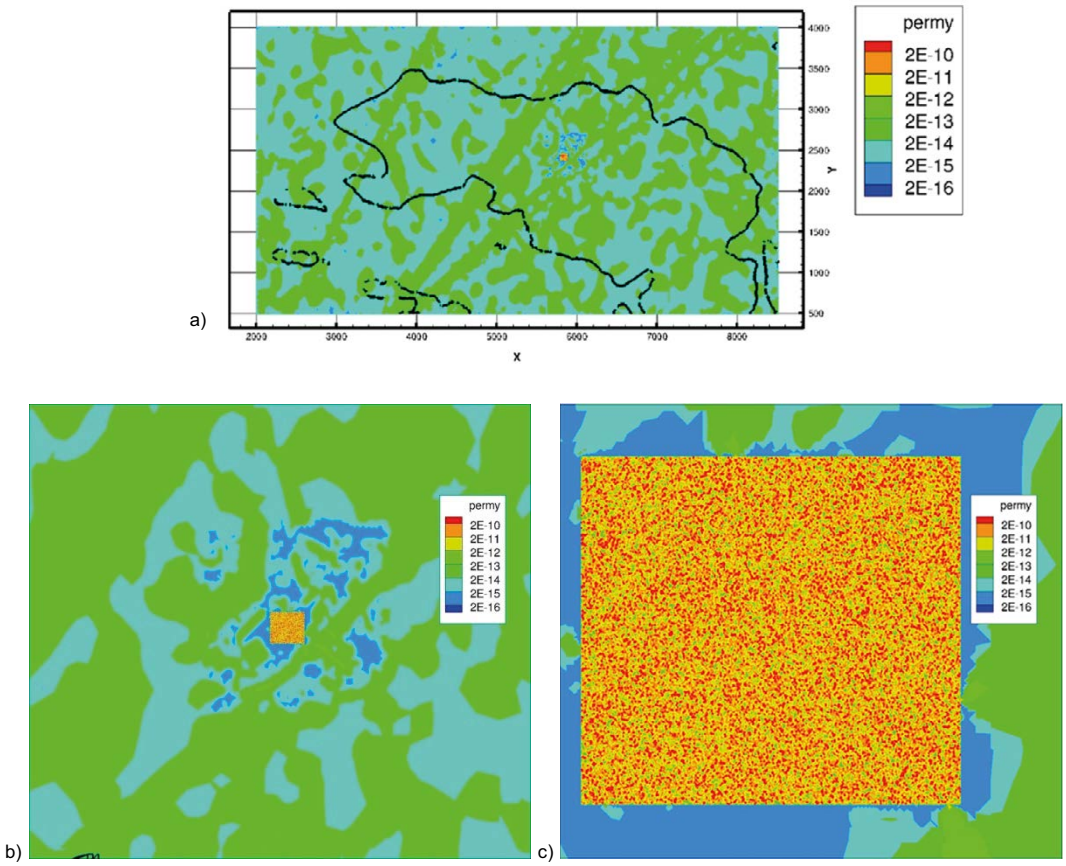

Figure 5-17. *Simulated permeability (m^2) field at −50 m.a.s.l: a) Regional scale showing coastline; b) 500 m × 500 m scale; c) 100 m × 100 m scale.*

5.2.6 SKB/KTH

SKB/KTH's overall aim for Task 7C was to improve the understanding of flow in heterogeneous low-transmissivity fractures. The approach adopted was to attempt to constrain parameters describing fracture plane heterogeneity by comparing simulated flows with field measurements. SKB/KTH also took the opportunity of using an innovative flow solution method capable of producing highly resolved flow fields.

Model structure

SKB/KTH modelled a single fracture plane with heterogeneous hydraulic aperture/ transmissivity. Three different aperture heterogeneity models were considered based on previous studies from Zinn and Harvey (2003) as listed in Table 5-8. All three models use the same underlying log-normal aperture distributions but differ in the connectivity of low and high transmissivity regions. Both quadratic and cubic aperture-transmissivity relationships were considered. Example realisations are shown in Figure 5-18. For simulations of inflow to the shaft, a constant head boundary condition was applied at 16 m radial distance from the shaft axis as shown in Figure 5-19.

Flow in the heterogeneous fracture was solved using an adaptive multi-resolution Fup method (see Frampton et al. 2015). Transport parameters (travel times and F-factor) were calculated from particle tracking. The model region and boundaries for the shaft inflow calculation are shown in Figure 5-19.

Table 5-8. SKB/KTH heterogeneous fracture model parameters.

Model parameter	Values
Aperture structure	MG (Multi-Gaussian) isotropic Gaussian variogram texture DN (Disconnected) non-Gaussian texture with connected low permeable zones CN (Connected) non-Gaussian texture with connected high permeable zones
Transmissivity Aperture relationship	Quadratic or cubic law $T = c_{0m} b^m$, where T is transmissivity, b is aperture and m = 2 or 3
Aperture variability	Effective (mean) fracture transmissivity 4.2×10^{-9} m^2/s (base case m = 2). Effective (mean) fracture transmissivity 2.8×10^{-9} m^2/s (m = 3). Variance of ln(T) = 1, 4, 8, correlation length 0.5 m

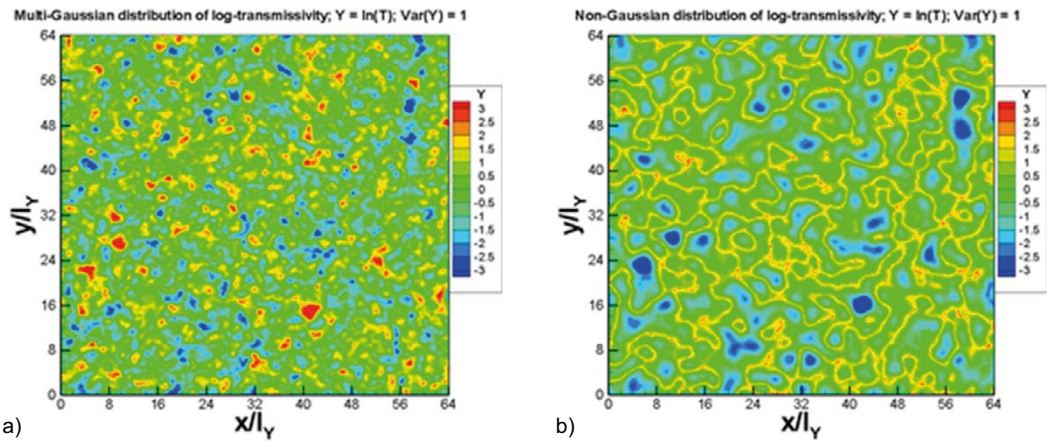

Figure 5-18. *Example realisations of the MG and CN aperture heterogeneity fields for ln(T) variance of 1. Note that the DN field is the complement of the CN field.*

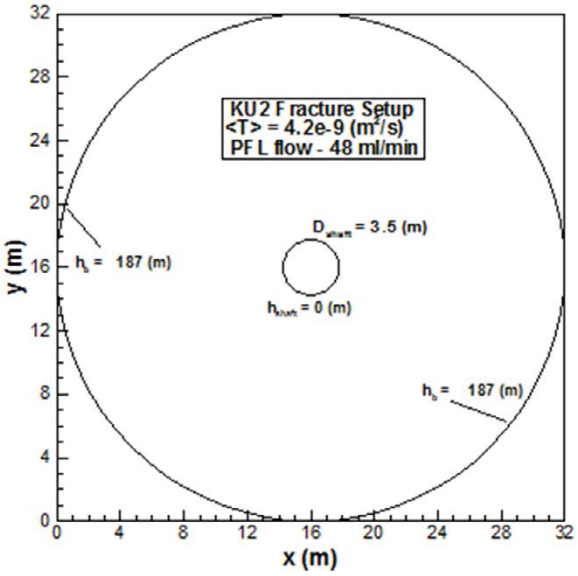

Figure 5-19. *Model setup showing shaft-inflow boundary conditions.*

Model conditioning and calibration

No formal conditioning or calibration procedures were used. Instead, a sensitivity analysis of the different aperture and transmissivity heterogeneity models was used to examine flow variability along the shaft wall, based on comparison with field data (Nappy Test in KU2). In one set of simulations inflow to the shaft was restricted to only part of the shaft wall by setting regions of very low conductivity along segments where cement dust (grouting) had been observed.

Revised TS28 model

A specific objective considered here was to combine the different methodologies and simulation approaches used in Tasks 7A, 7B and 7C, and by combining these to attempt to model effects of small-scale heterogeneity and flow channelling within a larger network.

The models used Configuration B from Task 7B combined with the aperture heterogeneity models used in Task 7C. Boundary conditions for a 10 m × 10 m sub-region centred on KR15A were extracted from the Task 7B model and applied to a single heterogeneous fracture. The mean transmissivity of the fracture was set to 5.15×10^{-5} m^2/s (equal to the constant transmissivity value of the homogeneous fracture in Task 7B) and a spatial correlation length of 0.08 m was assumed. Flow and velocity fields were then calculated for 100 realisations of each of the three structure models (MG, CN, DN) for a ln(T) variance of 1 and 8. The central borehole (KR15A) is represented by a high transmissivity circular region of 76 mm diameter. The flow was simulated on a high-resolution grid (0.02 m × 0.02 m) with significantly increased resolution at the borehole location (below 0.01 m).

5.3 Modelling results

5.3.1 JAEA

Task 7C1

An empirical quadratic relationship ($T = \frac{b^2}{2}$, i.e. Doe's Law, Dershowitz et al. 2003) was used to convert the PFL transmissivity (PP and KR holes) to fracture aperture and fit a log-normal aperture distribution. The transformed flow data from the Nappy Test were also used as aperture measurements and were used to constrain the multi-scale model based on the Kamaishi fracture characterisation implemented using the SGEMS (Stanford Geostatistical Modelling Software; Remy et al. 2009) nested approach.

The use of the detailed correlation structure from the Kamaishi fracture was justified by the lack of equivalent data from Olkiluoto and the expectation that fracture apertures would show a similar multi-scale correlation.

Task 7C2

JAEA focused their modelling on the KU2 and KU3 tests due to the limited amount of data for KU1. JAEA simulated the single hole PFL tests with 10 realisations of the heterogeneous fracture for KU2 and KU3. The normalised RMS error for the six simulated KU2 tests are shown in Figure 5-20a; with the exception of realisation 4 the results are relatively consistent. Sensitivity studies showed that locally (within a 1 m radius of borehole) modifying the fracture transmissivity around the PP124 and PP126 boreholes allowed higher flows and the potential for model calibration. The normalised RMS error for the three KU3 single-hole test simulations is shown in Figure 5-20c. The match is generally less good and realisation 5 shows a significantly larger RMS error.

The F-factors were calculated by particle tracking in the heterogeneous fracture flow field (without the background fracture network). There were no significant differences between the F-factors calculated from the E-W and N-S gradients. The calculated KU2 F-factor was in the range 10^{13}–10^{14} (s/m), while the KU3 F-factor was about a factor of 10^2 higher. This reflects the higher geometric mean transmissivity (calculated from the PP PFL data) of the KU2 fracture (~2.1×10^{-9} m^2/s) than that of KU3 fracture (~10^{-13} m^2/s).

Upscaled effective transmissivity and F-factor were calculated for the 20 m × 20 m target fracture around KU3 with varying spatial resolution. While the transmissivity is relatively insensitive to spatial discretisation[29] (see Figure 5-21a), the F-factor shows an increase of over a factor of 10^2 with the increase in spatial resolution from 0.2 (10 × 10 grid) to 0.02 m (100 × 100 grid). The extent to which this result is dependent on the multi-scale aperture generation method is unclear.

Task 7C3

JAEA incorporated the flow data from the Nappy Test within the Task 7C1 methodology for generating the heterogeneous fracture apertures.

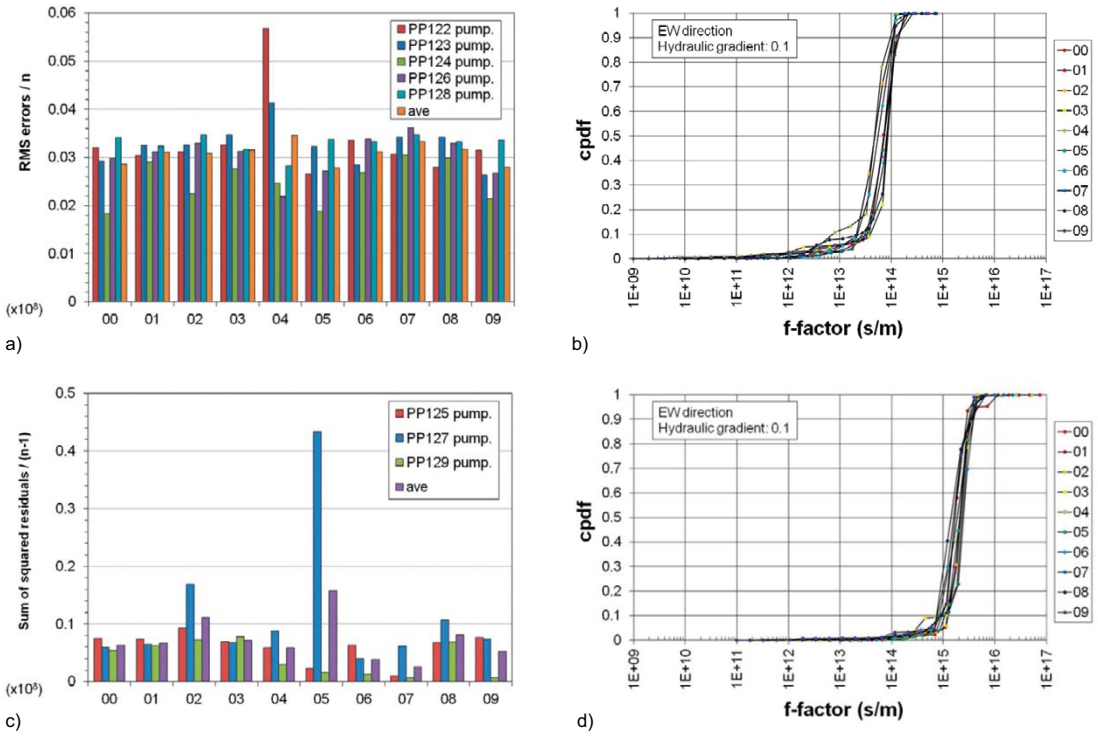

Figure 5-20. *Normalised RMS error (left) and cumulative F-factor (right, gradient of 0.1 m/m in E-W direction) histograms: a, b) KU2, c, d) KU3.*

[29] Consistent with Matheron's analyses that predict the effective transmissivity is controlled only by the geometric mean transmissivity.

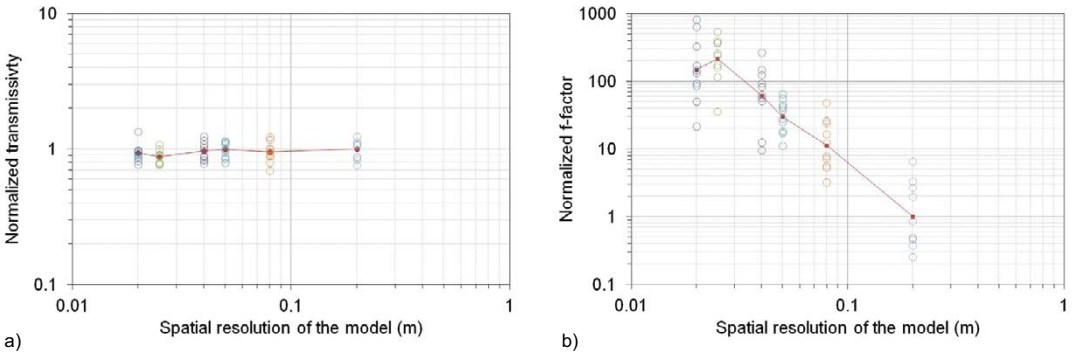

Figure 5-21. *Upscaling simulations: a) normalised transmissivity and b) F-factor. Results normalised to 0.2 m discretisation (i.e. 10 × 10 transmissivity grid).*

5.3.2 KAERI

Task 7C1

The single hole PFL measurements were used to create a semivariogram and fit an exponential model with a range of 15 m and sill of 0.4 (Figure 5-22). The FR1 transmissivity field was then interpolated using a Kriging method and 30 conditional simulation realisations were generated using a simulated annealing method. The transmissivity was assumed to be distributed log-normally with a geometric mean of 10^{-9} m^2/s and $\log_{10}$ standard deviation of 0.63.

For detailed simulations around the KU3 shaft the semi-variogram model was assumed to have a range of 2.55 m and sill of 0.055 and the transmissivity field a geometric mean of 10^{-10} m^2/s and $\log_{10}$ standard deviation of 0.23. The realisations were generated in the same manner as the larger model.

Task 7C2

KAERI only performed simulations for the KU3 shaft probe holes (Table 5-4).

The computed flows shown in Figure 5-23 are on average higher than those measured for the larger domain but show significant realisation-dependence such that for several tests the measurement lies within ± 1 standard deviation (from 30 realisations). The overestimation of flows led to the development of the reduced domain model. For the reduced domain the computed flows show significantly less variability between holes than the measurements. The realisation-dependence is also smaller than those calculated for the larger domain for all the tests. This probably reflects the smaller variance in the transmissivity field.

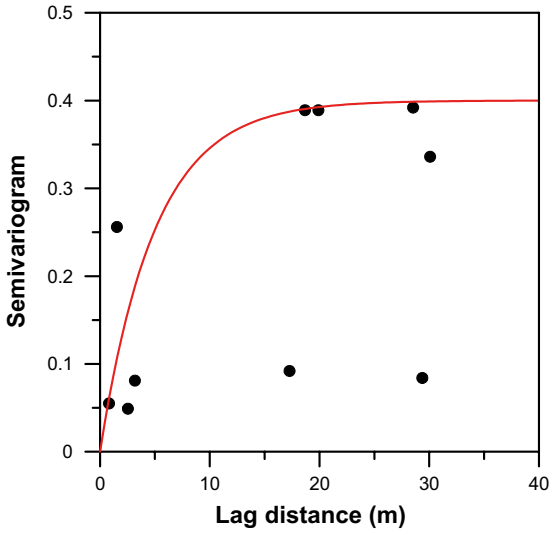

Figure 5-22. *Semi-variogram and fitting exponential model from single-hole PFL.*

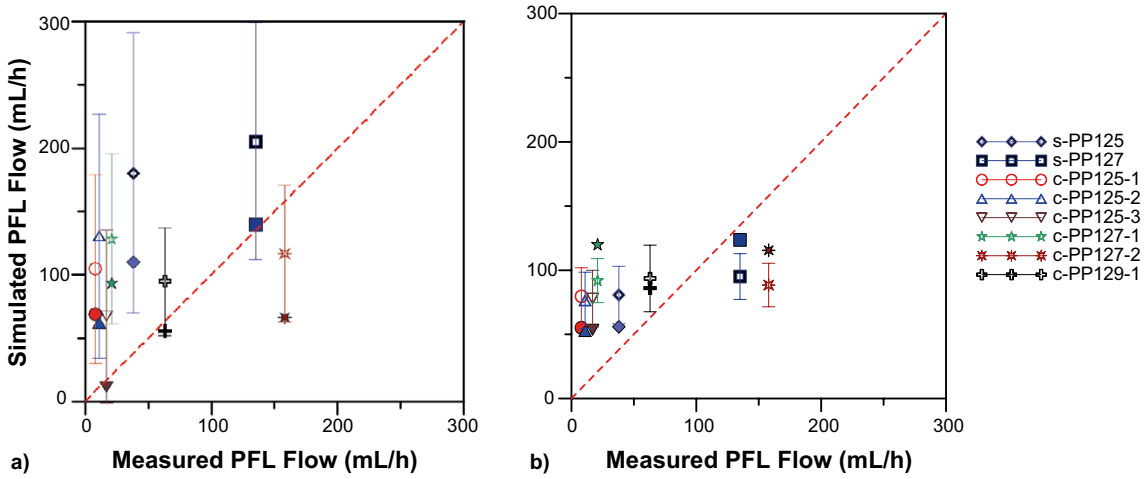

Figure 5-23. *Cross-plots of measured and simulated flow for the KU3 shaft probe holes in a) the larger and b) reduced domains. Simulated flow shown as mean with 1 standard deviation error bars calculated for he realisations.*

5.3.3 NWMO/Laval

Task 7C2

The outflow rates from the boreholes in the simulations were adjusted where possible to account for the observed mismatch between the sum of PFL flows and the measured outflow. A correlation length of $\lambda = 0.35$ m was found to give the best match. In general, the match between measured and simulated PFL flows was good in both shaft KU1 and KU2, although no measured inflows were associated with Fracture1 in ONK-PP131 and ONK-PP137 in shaft KU1. Measured and simulated flow rates are compared in Figure 5-24.

For shaft KU3 there was no measurement of the total outflow so outflow from the model boreholes were set as the sum of the PFL flows. Given the observed discrepancy between the total outflow and PFL flows in the KU1 and KU2 boreholes this assumption results in some uncertainty as to the true flows. Simulations of the single hole tests showed reasonable agreement with measured flows. The mismatch was comparable in magnitude to the uncertainty associated with the total flows from the boreholes.

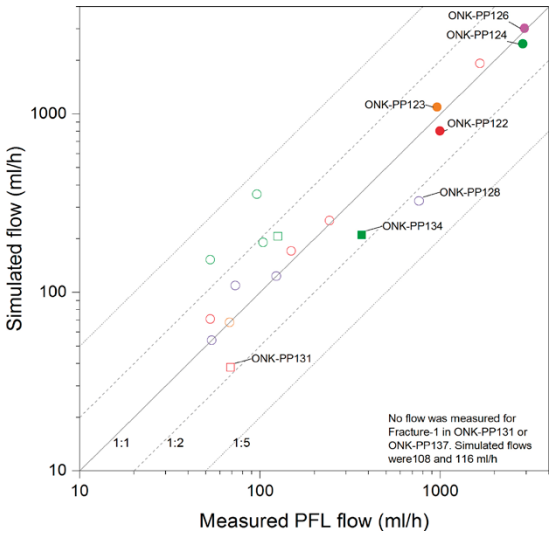

Figure 5-24. *Measured and simulated inflows to KU1 (square symbols) and KU2 (circles) boreholes.*

In the simulations of single-hole tests it was noted that flow directions in/out of ONK-PP125 during pumping of ONK-PP127 were in the opposite sense to that expected. Further investigations showed that flow directions varied with the correlation length[30]. Figure 5-25 shows the measured and simulated flows for the multi-hole tests.

For the transport simulation F-factor (also called β-factor) was calculated based on the simulated breakthrough curves (see Hodgkinson 2007). The F-factor for shaft KU3 was smaller than those from KU1 and KU2, due to the larger simulated Fracture1 aperture (transmissivity) around KU3. This contrasts with other modelling groups who simulated lower transmissivity around KU3. As the aperture is not conditioned at the shaft locations Therrien and Blessent (2017) suggest results should only be considered qualitatively.

Table 5-9. NWMO/Laval comparison of simulated and measured borehole flows.

	Borehole and flow	Flow rates at Fracture1		Flow rates at other identified fractures	
		Measured [ml/h]	Simulated [ml/h]	Measured [ml/h]	Simulated [ml/h]
Shaft KU2	PP122 Q = 3690 ml/h	996	803	53	71
				149	171
				1660	1918
				243	253
	PP123 Q = 1381 ml/h	961	1092	68	68
	PP124 Q = 3801 ml/h	2870	2473	96	355
				53	153
				104	191
	PP126 Q = 3700 ml/h	2930	3022		
	PP128 Q = 1016ml/h	761	325	73	109
				123	123
				54	54
Shaft KU1	PP131* Q = 2.3 m^3/y = ml/h		108	69	38
	s-PP134 Q = 7.2 m^3/y = ml/h	367	210	126	206
	s-PP137 Q = 2 m^3/y = ml/h		166	17	8

* For PP131 and P137 no flow rates were measured at the fracture location.

Task 7C3

The simulations of the Nappy experiment considered two shaft boundary conditions (see Figure 5-27):

- Complete fracture perimeter at atmospheric pressure and open to flow.
- No-flow boundary over area where grouting and dust observed, resulting in no measured flow from this section (inflow only computed for the portion of the shaft covered by nappies).

For the first case, a reasonable match to the total measured inflow was achieved using the 7C2 Fracture1 and matrix conductivity (10^{-11} m/s). The match was improved by increasing the hydraulic conductivity and varying the head on the model boundary. Simulations with inflow along only half the perimeter typically showed ~60 % of the measured inflow.

The flow field in Fracture1 and inflow to shaft KU2 is shown in Figure 5-26.

[30] And presumably realisation – although only single realisations were considered for each correlation length. Realisations of the aperture field were not locally conditioned on borehole data.

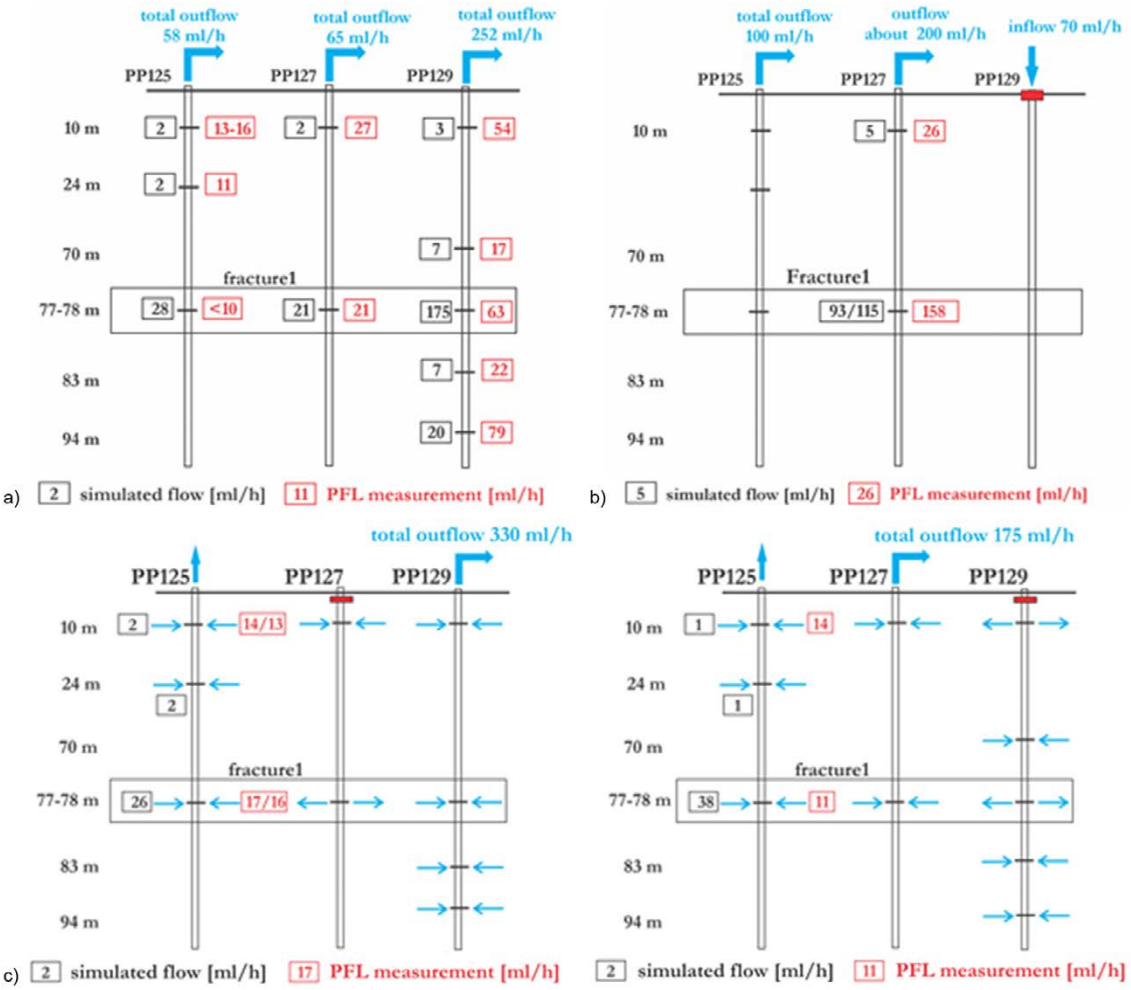

Figure 5-25. *Measured and simulated flows for the KU3 cross-hole tests: a) all three holes open, b) injection inPP129 with outflow from PP125 and PP127, c) PP125 and PP129 open, d) PP125 and PP127 flowing.*

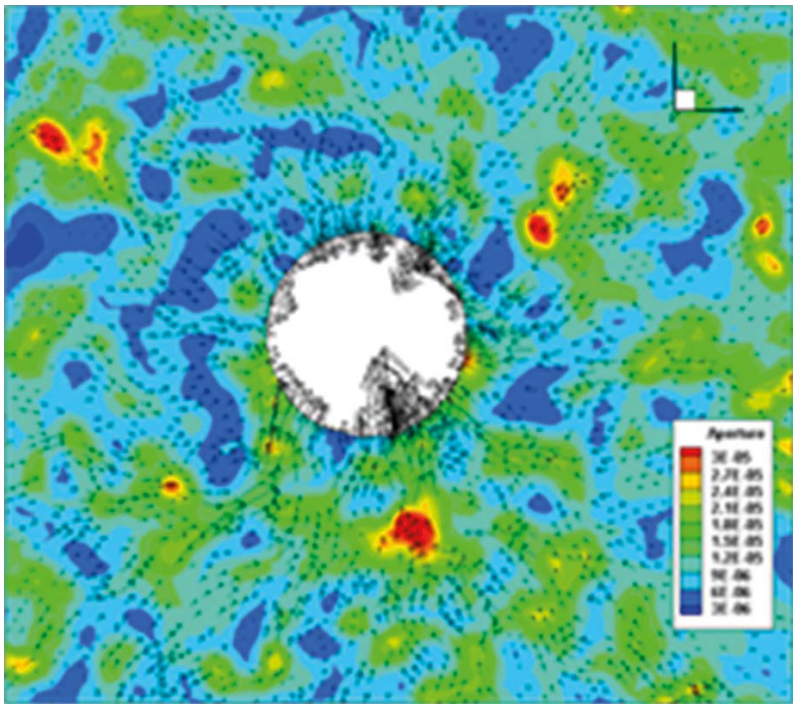

Figure 5-26. *Simulated KU2 Shaft inflow and flow field (as vectors) in Fracture1.*

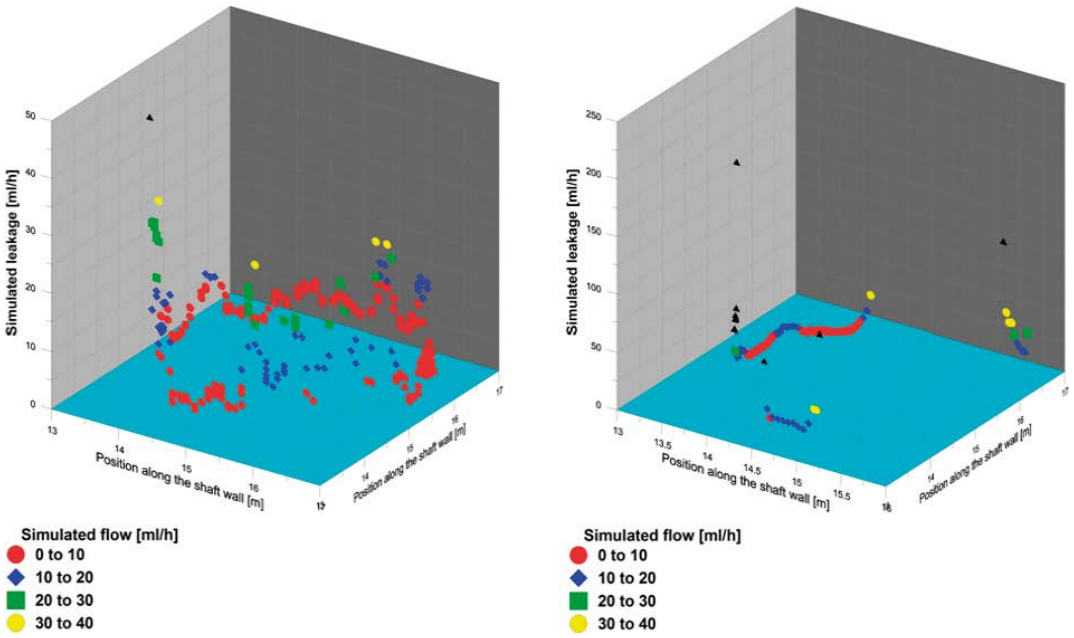

Figure 5-27. *Inflow into the shaft wall. On the left: leakage is simulated through the whole shaft circumference; on the right: leakage is simulated only from the portions of the shaft wall where leakage was measured with nappies.*

5.3.4 Posiva/VTT

Task 7C2

The simulated and observed flow magnitudes calculated for the three different shaft locations are shown in Figure 5-28. The match is generally very good with the exception of PP-129 at Shaft KU3 which shows significantly higher flows than simulated, suggesting a better connection to high transmissivity features than found within the model.

F-factors were also calculated as 2 wl/q using 100 particles in each direction for N-S and E-W hydraulic gradients of 0.1 m/m (total 2 000 particle tracks). The lower transmissivity around KU3 resulted in higher flow related transport resistance (higher F-factor).

Task 7C3,4

The shaft-wall flows were calculated for a range of transmissivity distribution parameters and multiple realisations in Task 7C3 and subsequently as part of the uncertainty estimation in Task 7C4. Figure 5-29 shows one of the best matches to observation while Figure 5-30 shows the effect of different correlation lengths. Although the models clearly show channelization and peaks in the spatial flow distribution it was not possible to identify a conclusive relationship or trend between correlation length and the number of flow peaks[31] observed.

Figure 5-31 shows simulated flow paths from the model boundary to the shaft wall. The effects of varying correlation length and transmissivity variability are shown. Channelling in the fracture seems to increase with greater $\log_{10}T$ standard deviation and correlation length. Correlation lengths significantly greater than the shaft diameter were not simulated. The effects on F-factor are shown in Figure 5-32.

Posiva/VTT also studied the influence of different choices regarding numerical methods including finite element types and discretisation when calculating retention and the arithmetic precision used in particle tracking. It was found that these had a measurable effect on the calculated transport parameters.

[31] where a “peak” is considered to be a local maximum rising above a threshold, e.g. 2 ml/min

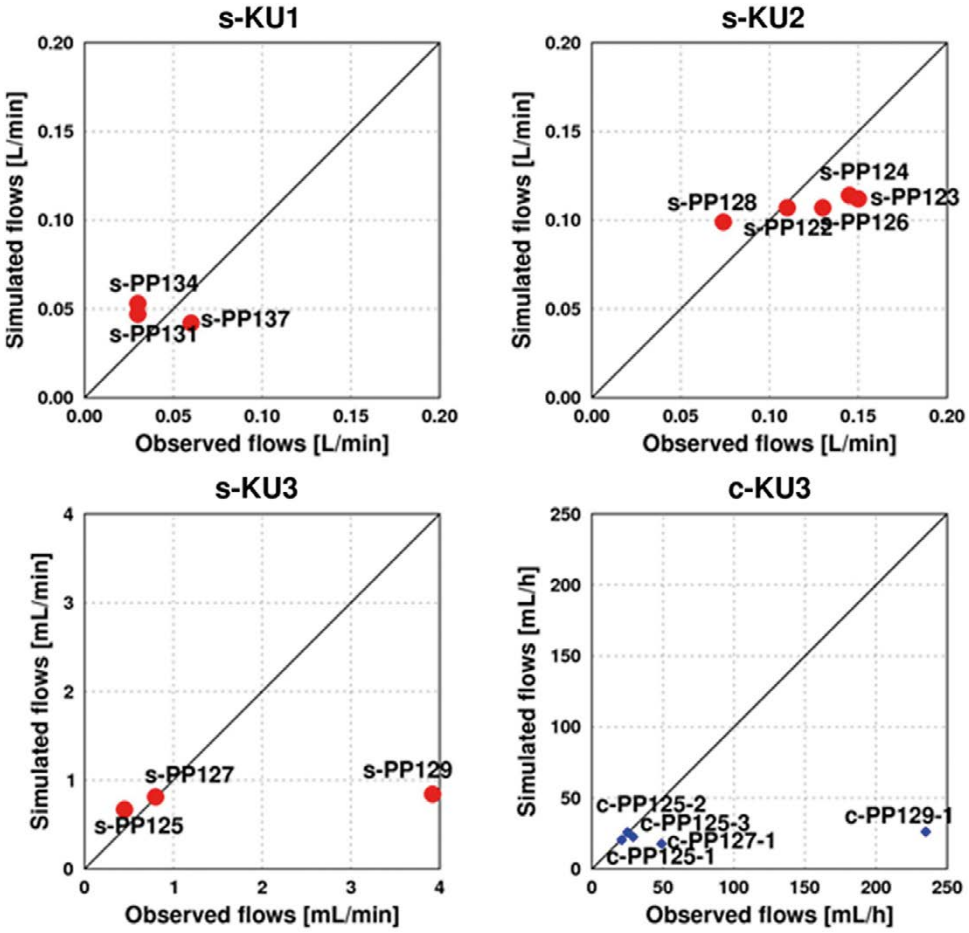

Figure 5-28. *Comparison of observed and simulated flows in the single-hole (s-) and cross-hole (c-) tests.*

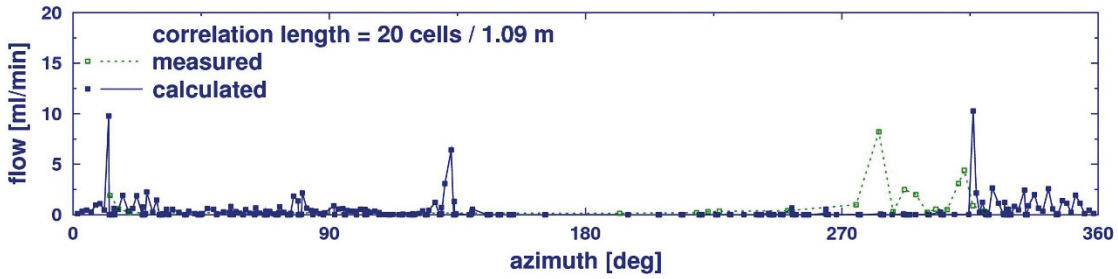

Figure 5-29. *Computed shaft-wall flows at correlation length of 1.09 m for a selected realisation in Task 7C3.*

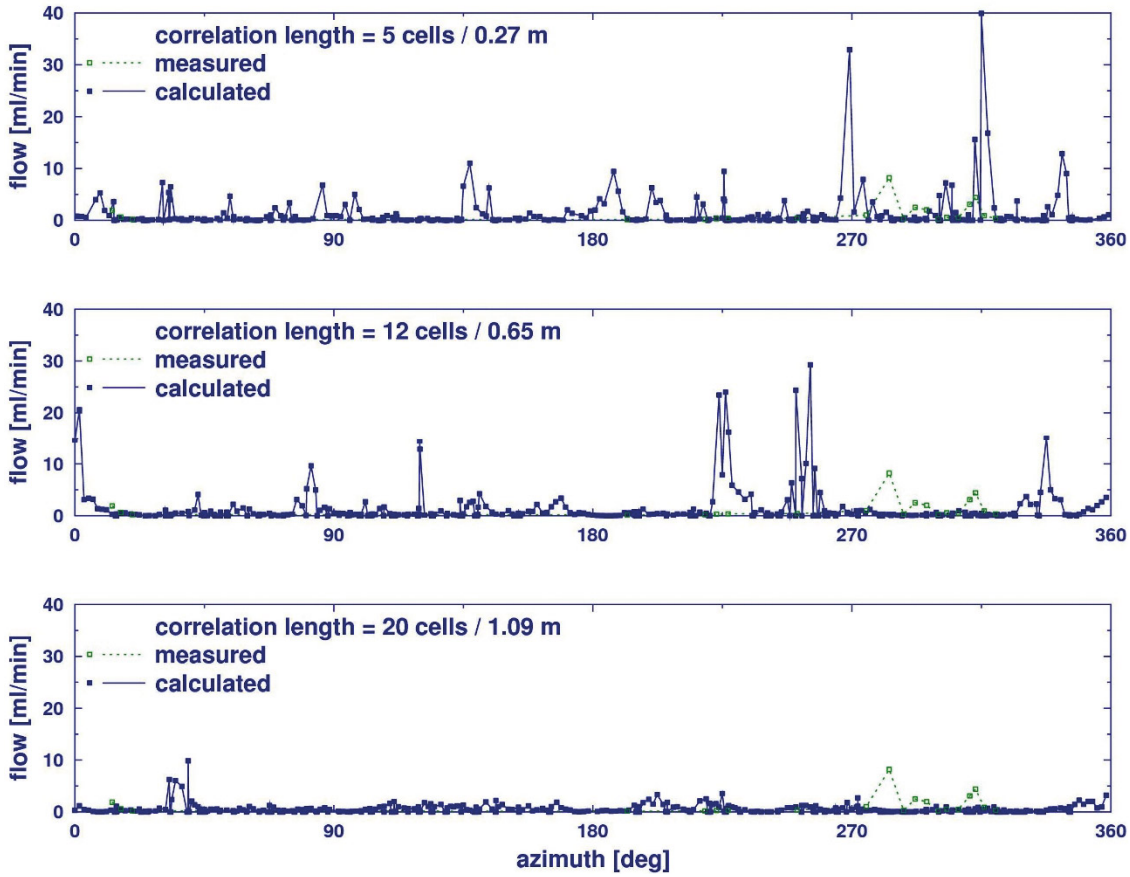

Figure 5-30. *Computed shaft-wall flows at correlation lengths of 0.27, 0.65 and 1.09 m.*

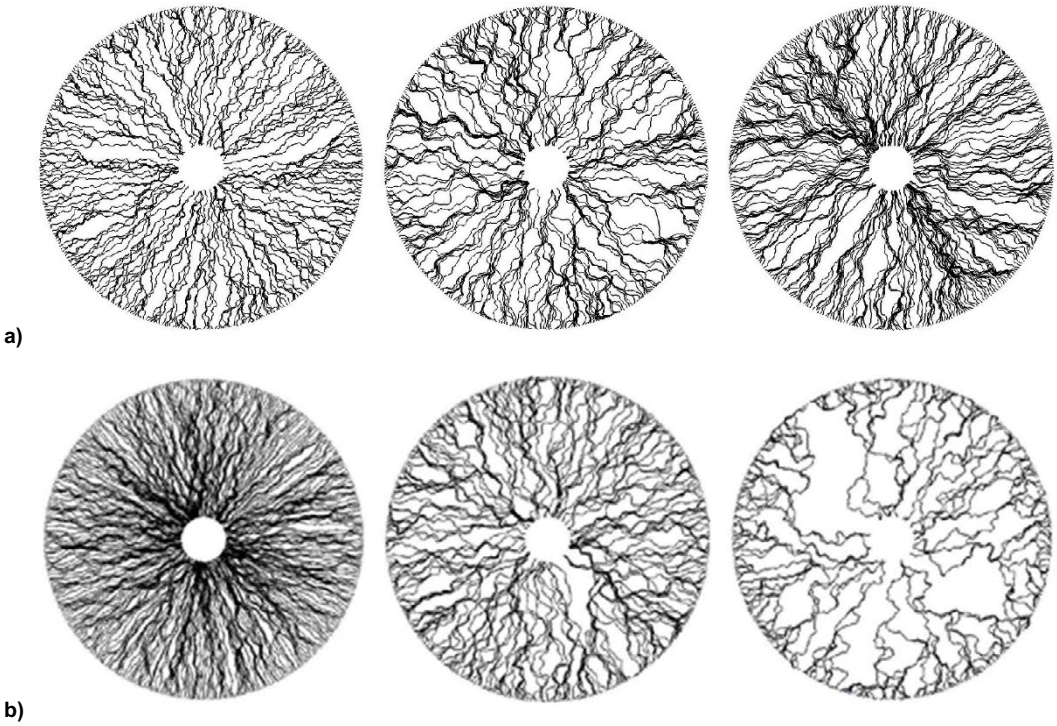

Figure 5-31. *Flow paths to shaft wall: a) for varying correlation lengths of 0.3, 0.6 and 1.2 m. $\sigma(\log_{10}T) = 1.0$ in all three cases, b) for varying $\sigma(\log_{10}T) = 0.4$, 1.0 and 1.8 for correlation length of 0.5 m.*

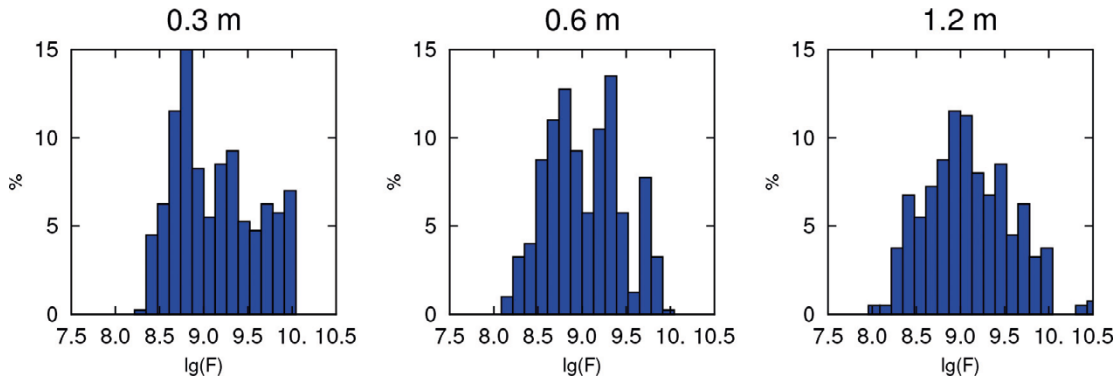

Figure 5-32. *log F = 2 wl/q (yr/m) frequencies for correlation length of 0.3 m, 0.6 m and 1.2 m, respectively. As correlation length increases, the frequencies of smaller F-values grow indicating channelization and lower retention.*

Revised TS28 model

In an attempt to consider the effect of small -scale variability at larger scales the TS28 simulation case was recalculated using both homogeneous and three spatially varying transmissivity models for the HZ19A and HZ19C zones. The models were compared in terms of computed final heads at the pumping and observation boreholes. While there were significant differences in simulated head at the KR14 pumping borehole, differences were smaller at the observation holes suggesting that the use of "skin terms" to represent local transmissivity variability are more important at pumping boreholes than at observation points (at least for late-time/"steady state" drawdown measurements).

5.3.5 SKB/CFE

Task 7C2

The measured and simulated flowrates from the PFL tests are shown in Figure 5-34. The simulations give a wide range of results but measurements typically lie within the range of simulated values. Svensson (2015) concludes that the calibrated mean transmissivities generate the correct magnitude of the inflow and that the spread indicates that the simulated fracture heterogeneity gives a variation of the flow-rate that is in some agreement with data. The model assumes a 0.2 m correlation length and transmissive paths along intersections with stochastic fractures.

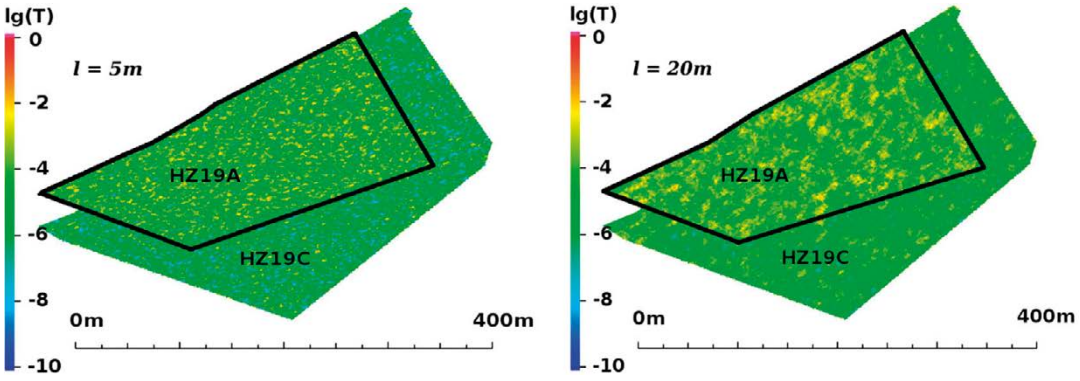

Figure 5-33. *F = 2 wl/q frequencies for correlation length of 0.3 m, 0.6 m and 1.2 m, respectively. As correlation length increases, the frequencies of smaller F-values grow indicating channelization and lower retention.*

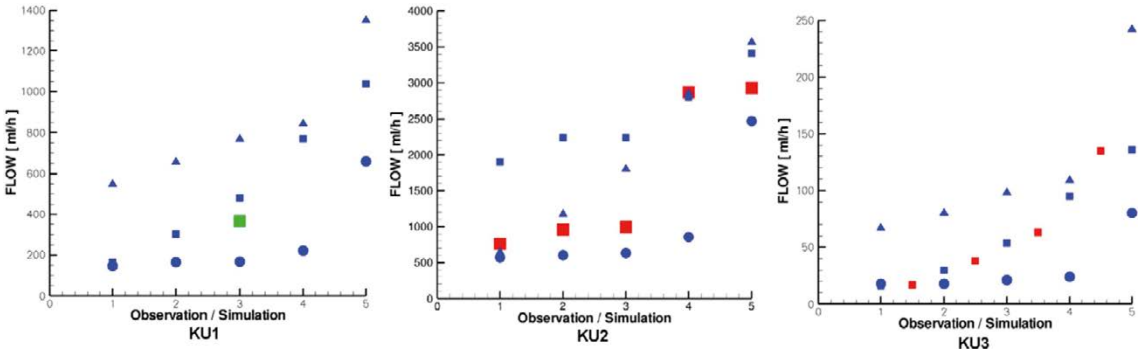

Figure 5-34. *SKB/CFE comparison of measured (squares) and simulated (3 simulations, blue) flowrates for KU1 (1 measurement), KU2 (5 measurements), KU3 (4 measurements). Five measurements were simulated for each shaft.*

Task 7C3

The influence of correlation length was investigated in relation to the results of the Nappy Test. SKB/CFE simulated inflow to the KU2 shaft for two realisations using three different correlation lengths for the variable transmissivity feature. Figure 5-35 shows the flow pattern around the shaft and the inflow distribution to the shaft wall for one realisation of each of the three different correlation lengths.

Task 7ABC

Table 5-10 shows the measured and simulated KR14-KR18 drawdowns for a) homogeneous sheet joints and b) heterogeneous sheet joints. Drawdowns calculated from the homogeneous sheet joint models are typically within the range of drawdowns of those simulated with heterogeneous joins (of the same mean transmissivity). Figure 5-36 shows example flow and pressure distributions in a 20 m square of the heterogeneous sheet joint around KR15A (pumped borehole).

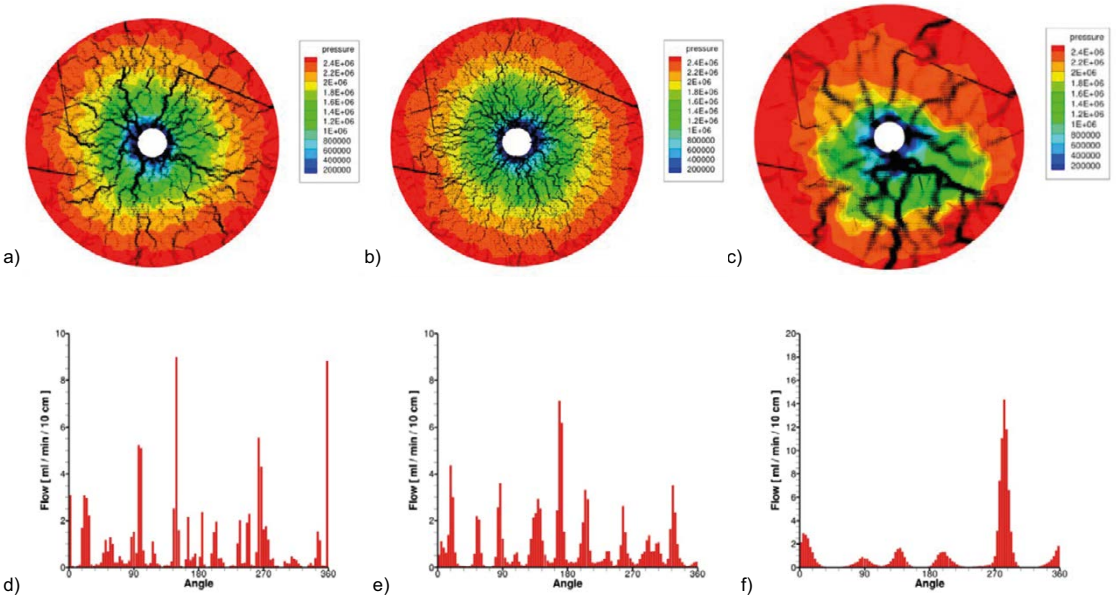

Figure 5-35. *SKB/CFE Pattern of flow and pressure for varying correlation lengths a) 0.1 m, b) 0.2 m, c) 0.6 m and inflow distribution to the shaft wall d) 0.1 m 17 peaks, e) 0.2 m 12 peaks, f) 0.6 m 5 peaks.*

Table 5-10. SKB/CFE Task ABC; measured and simulated drawdowns for homogeneous and heterogeneous sheet joints. Shaded cells indicate the drawdowns from the pumping boreholes; bold indicates the measured values.

Response	Sheet joint model	Pumped borehole				
		KR14	KR15 A	KR16 A	KR17 A	KR18 A
KR14	Measured	6	1	0.9	1	0.8
	Homog.	6.3	1.1	1.2	1.5	1
	Hetero.	5.8–6.6	0.9–1.1	1.1–1.2	1.4–1.8	0.9–1
KR15A	Measured	3.4	10	3.3	3.5	3.5
	Homog	3.4	14.1	3.8	5.9	4.3
	Hetero	3.3–3.5	11–20.2	3.7–3.8	5.3–6.1	3.9–4.4
KR15B	Measured	4.4	2	1	2	0.9
	Homog	4.3	0.9	1.1	1.4	0.9
	Hetero	4.3–4.5	0.9–1	1–1.2	1.3–1.5	0.8–0.9
KR16A	Measured	3	3.5	10	3.9	3.5
	Homog	3.2	4.1	13.8	6.3	4.2
	Hetero	3.1–3.3	3.5–4.3	10.5–18.7	5.5–6.5	3.8–4.3
KR16B	Measured	3	2.4	1.7	1.5	1.5
	Homog	4.2	0.9	1.1	1.4	0.8
	Hetero	2.4–4.3	0.8–0.9	0.9–1.3	1.2–1.4	0.8–0.8
KR17A	Measured	3	3	3.4	11	3.2
	Homog	3.3	4.9	4.8	17.3	4.6
	Hetero	3–3.2	4.4–4.9	4.5–4.9	14.3–24.2	4.2–4.6
KR17B	Measured	0.2	1	0.4	0.2	0.2
	Homog	1.8	0.4	0.5	0.7	0.4
	Hetero	1.8–1.9	0.4–0.4	0.5–0.5	0.6–0.7	0.4–0.4
KR18A	Measured	3	3.2	3.7	3.7	10
	Homog	3.3	5.3	4.7	6.8	10.6
	Hetero	3.2–3.4	4.7–5.3	4.6–4.8	6.1–7.3	9–11.8
KR18B	Measured	5.6	1.3	0.9	0.9	0.8
	Homog	4.4	0.9	1.1	1.4	0.9
	Hetero	4.3–4.5	0.8–0.9	1–1.1	1.2–1.5	0.8–0.9

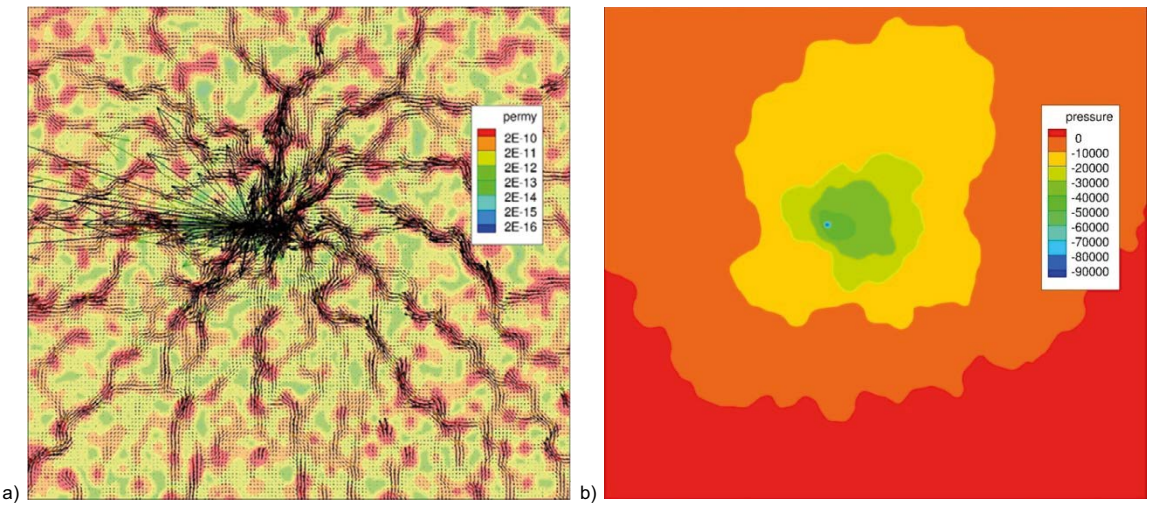

Figure 5-36. *Simulation of a) flow and b) pressure in 20 m × 20 m region of heterogeneous sheet-joint intersecting KR15A.*

Svensson (2015) suggests that "heterogeneous sheet joints will generate large variations in draw downs in pumped boreholes, while a smaller effect is found in observation boreholes". This is confirmed in the summary shown in Table 5-11. Svensson (2015) also points out that the effect on drawdown is asymmetric with 5–6 m above but only 2–3 m below the drawdown from the homogeneous case. This is typically the case for the pumping borehole but the pattern is the opposite for observation boreholes – although the number of realisations is small.

Table 5-11. SKB/CFE Task ABC: Drawdown difference between simulated values for heterogeneous sheet joint and homogeneous sheet joint cases. Range given as percentage of homogenous case drawdown and minimum and maximum values.

Borehole	When pumped borehole			When observation borehole		
	Range	Below (m)	Above(m)	Range	Below (m)	Above (m)
KR14	13 %	0.5	0.3	16 %	0.1	0.1
KR15 A	65 %	3.1	6.1	8 %	0.3	0.1
KR15B				12 %	0.1	0.1
KR16 A	59 %	3.3	4.9	13 %	0.5	0.2
KR16B				21 %	0.5	0.1
KR17 A	57 %	3.0	6.9	8 %	0.4	0.0
KR17B				4 %	0.0	0.0
KR18 A	26 %	1.6	1.2	10 %	0.4	0.2
KR18B				11 %	0.1	0.0

5.3.6 SKB/KTH

SKB/KTH focused on a sensitivity study of inflow to the shaft from a single transmissive plane for comparison with the results of the Nappy Test in KU2 (Task 7C3,4). The influence of transmissivity variance on the head and flow field is clearly seen in Figure 5-37 with significant channelling of flow at higher variance. The Fup approach was able to provide highly resolved flow fields over the highly heterogeneous transmissivity fields.

The flow distribution around the shaft was extracted from the models and compared with the measured data. The flows from the cases where Var(ln(T)) = 1 showed low variability while for the higher variance case, comparison of individual realisations showed inflow peaks comparable to those measured (see Figure 5-38). Multiple realisations of the different model cases were summarised as a histogram of inflow to the shaft as shown in Figure 5-39. At low transmissivity variance the MG models do not show significant numbers of inflow points above the detection limit, while at high variance (Var(ln(T)) = 8) peaks in flow similar to the measurements are seen for all three models.

The models do not show the clustering of inflows seen in the data and a model variant where inflow to part of the shaft wall was restricted due to possible grouting effects was also run and head contours and streamline distributions close to the shaft are shown in Figure 5-40.

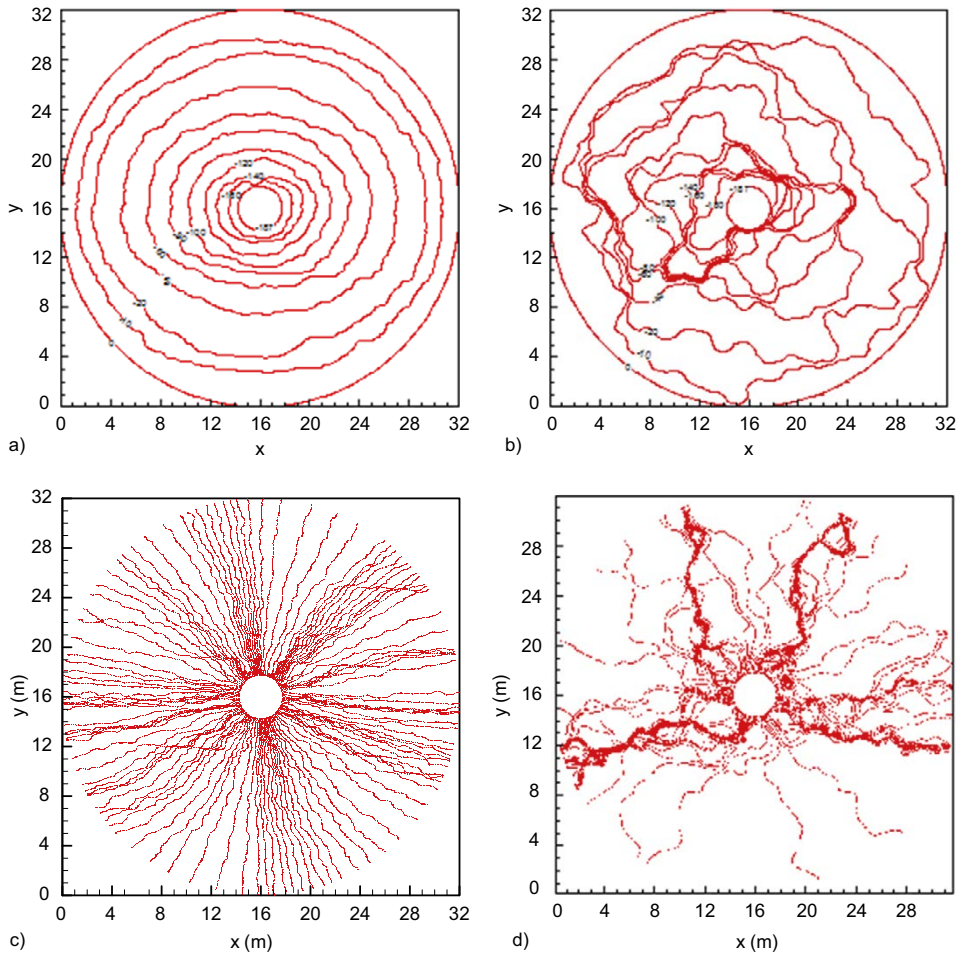

Figure 5-37. *Simulated head contours and streamline distributions for MG (Multi-Gaussian) model with left: Var(ln(T)) = 1; and right: Var(ln(T)) = 8.*

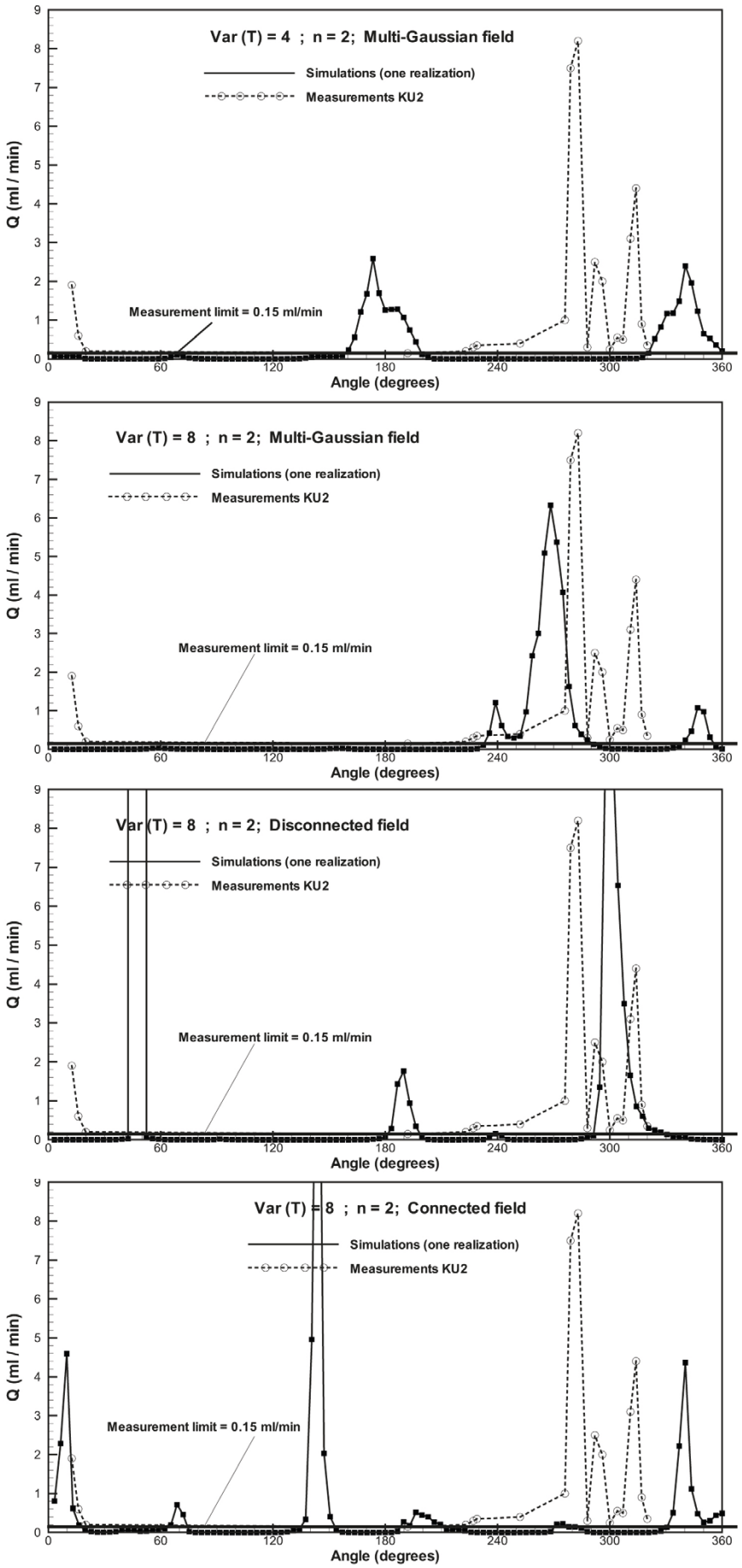

Figure 5-38. *Simulated inflow distribution for varying aperture structure and variance.*

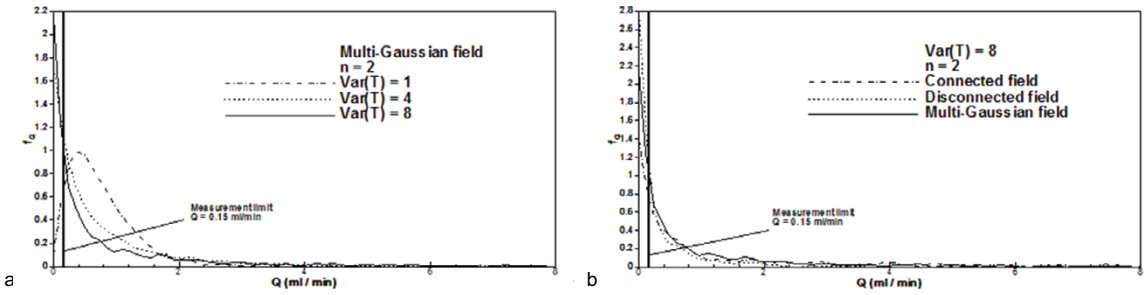

Figure 5-39. *Inflow distribution histogram for a) MG field with different variance; b) the 3 heterogeneity models for Var(ln(T) = 8. The vertical line shows the lower measurement limit from the Nappy Test.*

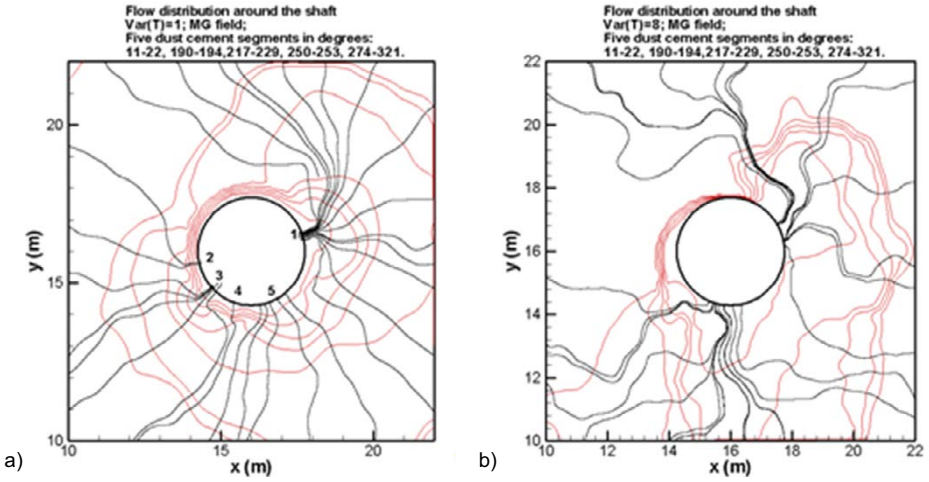

Figure 5-40. *Simulated head contours and streamline distributions for MG model where inflow is restricted to half of shaft with a) Var(ln(T)) = 1; and b) Var(ln(T)) = 8.*

SKB/KTH calculated F factors (yr/m) for multiple realisations of the 3 texture models using 3 values of Var(ln(*T*)) and both the quadratic and cubic flow laws. Figure 5-41 shows the derived F-factor probability distributions for the Multi-Gaussian model for different values of Var(ln(*T*)) and for the three different textures with high variability. The influence of variability can be clearly seen and there are also clear differences between the textures. Modal (most likely) values are in the range 5–50 yr/m (10^8 to 10^9 s/m).

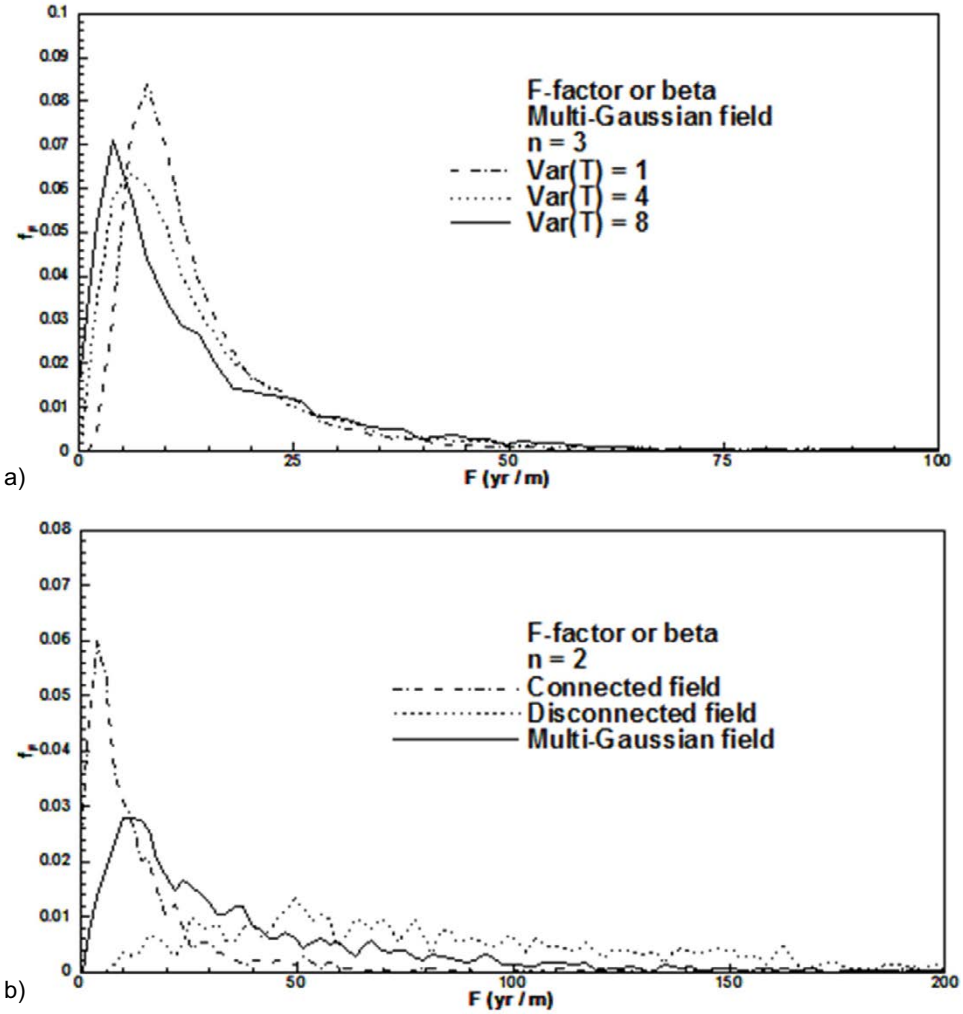

Figure 5-41. *Probability density distribution of β parameter (F-factor) values obtained from particle streamlines from multiple realisations of various simulation cases. a) comparison for the Multi-Gaussian (MG) texture for variance of log aperture = 1, 4, 8, assuming cubic law flow b) comparison for the three textures (CN, DC, MG) for high variability (log aperture variance = 8), assuming quadratic law flow.*

5.3.7 SKB/KTH downscaling calculation

SKB/KTH performed a "downscaling" from the Task 7C single fracture model to compute the detailed flow in a single feature (at 61 m in KR18) from the Task 7B simulation. The simulation was based on the Model B configuration with pressure boundary conditions on a 10.24 m × 10.24 m plane extracted from the DFN model and applied to the detailed scale model. The pressure gradient runs from the north towards the southeast corner of the detailed plane. The mean transmissivity of the heterogeneous fracture was set to the transmissivity of the homogeneous feature within the Model B configuration (5.15×10^{-5} m^2/s) and simulations were made with the three different heterogeneity structures with natural log transmissivity variance of 1 and 8. The heterogeneous fields were simulated with a resolution of 0.02 m with higher resolution (< 0.01 m) around the borehole to allow a detailed consideration of flow at the borehole wall. Two additional sensitivity cases were considered. In total 100 realisations were computed for each model case and ensemble statistics calculated.

Figure 5-42 shows the simulated head contours and streamlines for realisations of the different structure models of the target fracture. Strongly channelled flow and complex head distributions are evident in all the cases where Var(ln(T)) = 8, but especially for the CN structure model.

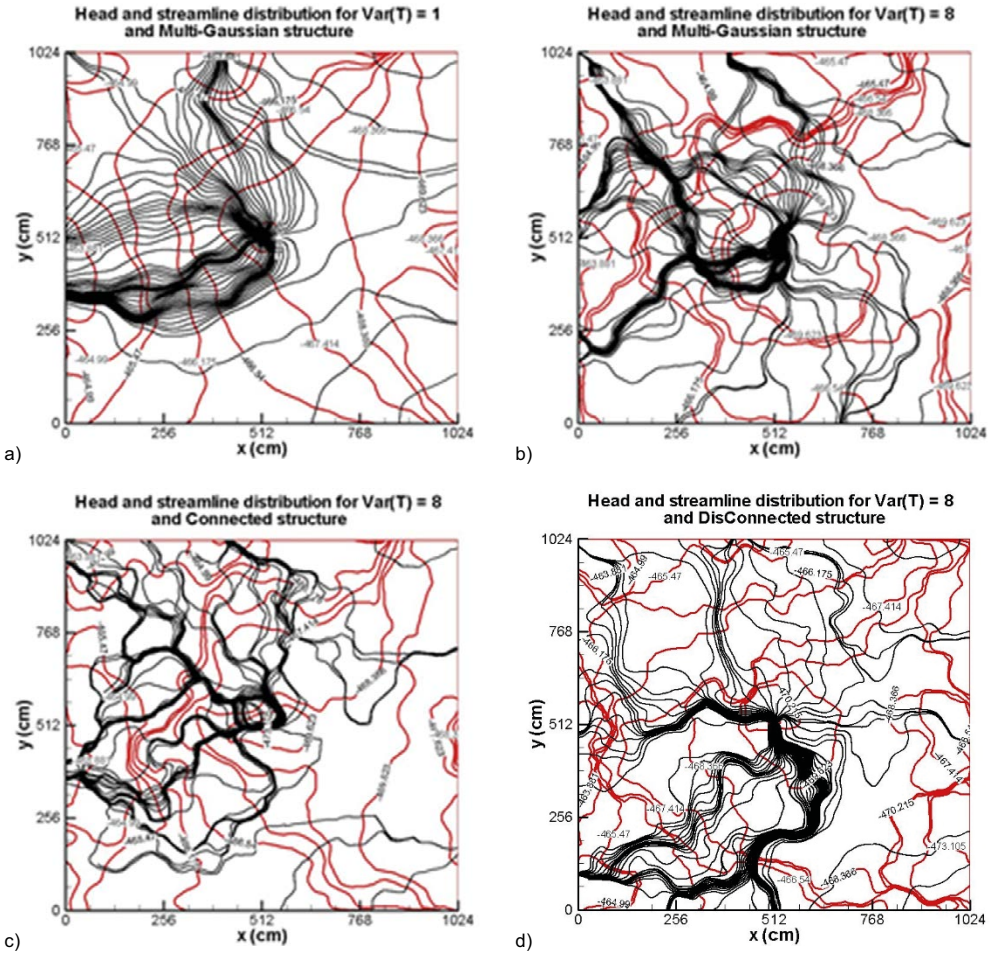

Figure 5-42. *Simulated head contours (red) and streamlines entering the borehole for the MG and CN structure models: a) MG Var(ln(T)) = 1; b) MG Var(ln(T)) = 8, c) CN Var(ln(T)) = 8, d) DN Var(ln(T)) = 8.*

It can be seen that in the high variance case flow is strongly channelled and the flow entering the borehole is concentrated in distinct channels dominated by local heterogeneity. The flow distributions into the borehole were also computed and typically showed greater anisotropy where Var(ln(T)) = 8. The orientation was influenced by the local heterogeneity rather than the fixed head boundary conditions. Figure 5-43 shows simulated flow and velocity distributions at the borehole wall for a single realisation. For the high variance case the main direction of flow varies strongly with realisation suggesting a strong dependence on the local transmissivity field.

The statistics of flow into the borehole were also calculated for the 100 realisations of the different model cases. Mean inflow and variance increase with var(ln(T)) as would be expected. For var(ln(T)) = 8 and the CN model the mean and variance of flows are significantly higher than for DN or MG. No comparison with measurements was made.

Table 5-12. SKB/KTH TS28 mean and variance of total borehole inflow over 100 realisations for the different structural models.

	Var(ln(*T*)	n = 2, mean $T = 5.15 \times 10^{-5}$ m²/s,		n = 3, mean $T = 3.4 \times 10^{-5}$ m²/s	
		Mean total inflow (ml/min)	Variance total inflow (ml/min)	Mean total inflow (ml/min)	Variance total inflow (ml/min)
MG	1	378	33 651	260	15 710
MG	8	512	206 609	354	98 882
CN	8	892	512 059	617	235 703
DN	8	195	14 912	136	6 500

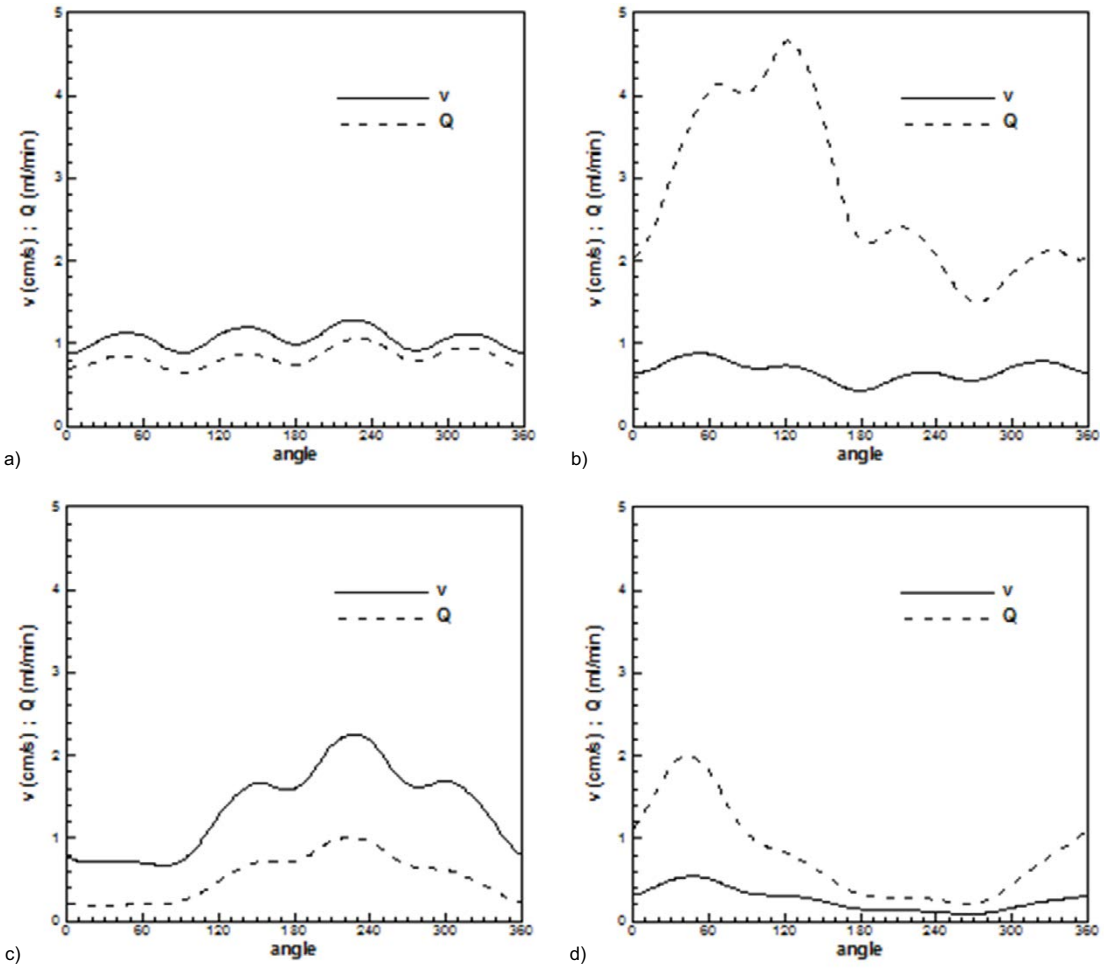

Figure 5-43. *Simulated flow and velocity distribution at borehole wall for one realisation: a) MG Var(ln(T)) = 1; b) MG Var(ln(T)) = 8, c) CN Var(ln(T)) = 8, d) DN Var(ln(T)) = 8.*

5.4 Modelling comparison

5.4.1 7C1

The emphasis within subtask 7C1 was to develop models of the FR1 fracture and the low permeability rock volume around it. The modelling groups used a range of methods to create heterogeneous transmissivity fields for the deterministic FR1 fracture. Most of the models assumed an underlying log-normal transmissivity distribution parameterised by:

- μ: Mean of $\log_{10}T$,
- σ: standard deviation of $\log_{10}T$,
- λ: correlation length (for an exponential semi-variogram the range is 3λ).

The spatial correlation structure varied between the modelling groups (see Table 5-13 below). Both conditioned (honouring local PFL transmissivity measurements) and unconditioned realisation generation methods were used.

The ability to develop site-specific geostatistical models of heterogeneity was limited by the small number of observations. To address this, groups took information for correlation lengths and spatial structure from previous work (e.g. JAEA's Kamaishi fracture characterisation) or from literature. SKB/KTH applied a sensitivity study by using three models of correlation structure based on a log-normal aperture distribution but with quite different connectivity (Zinn and Harvey 2003). SKB/CFE explored a spatial method where intersections with stochastic background fractures influenced the transmissivity within the fracture.

Table 5-13. 7C1 Approaches to generation of heterogeneous transmissivity fields and treatment of background rock.

Group	FR1 heterogeneity	Background rock
JAEA	Application of multi-scale aperture distribution from Kamaishi fracture using SGEMS.	Background DFN of low transmissivity fractures.
KAERI	Spatially correlated log-normal field.	Not considered.
NWMO/Laval	Spatially correlated Gaussian conditioned on PFL data. Sensitivity studies on correlation length and discretisation.	Uniform hydraulic conductivity 10^{-11}m/s (calibration range 10^{-12}–10^{-9} m/s).
Posiva/VTT	Spatially correlated Gaussian conditioned on PFL data. Sensitivity studies on correlation length and discretisation.	Background DFN of low transmissivity fractures.
SKB/CFE	Fracture transmissivity heterogeneity generation method based on spatially correlated log-normal field and transmissive fracture intersections.	Background fracture intersections with the deterministic fracture create channels.
SKB/KTH	Study of different log-normal distributions using 3 different correlation structures. High resolution accurate flow and transport simulations using Fup-based approach.	Not considered.

The effective transmissivity (geometric mean) of the heterogeneous fields was either taken from the average of PFL transmissivity or manually adjusted as part of model calibration (Table 5-14). The estimates from the different modelling groups were largely consistent with the FR1 transmissivity at KU3 showing a lower transmissivity than at KU1 or KU2 (NWMO/Laval used unconditioned modes that resulted in higher transmissivity around KU3). All the heterogeneity models were under-determined and models were typically conditioned on single hole PFL data but with only limited calibration against the PFL cross-hole data. There was an opportunity to compare the inflow distribution at the shaft-wall, but it was difficult to use this information to constrain model parameters (even assuming there was no influence from excavation or grouting).

Table 5-14. Effective transmissivity (m^2/s) of heterogeneous fracture crossing the three shafts.

Modelling group	Approach	KU1	KU2	KU3
JAEA	SGEMS Multi-scale correlated field.		2.1×10^{-9}	10^{-10}
KAERI	Spatially correlated log-normal.	10^{-9} σ = 0.63 15, 0.4	10^{-9} σ = 0.63	10^{-10} σ = 0.23 2.55, 0.055
NWMO/Laval	Spatially correlated log-normal.			
	Background rock facies.	10^{-12}	3.2×10^{-11}	3.2×10^{-10}
Posiva/VTT	Spatially correlated λ = 2.9 m log-normal fracture conditioned on PFL + stochastic DFN.	μ = −10.5, σ = 0.6	μ = −10.5, σ = 0.6	μ = −12.5, σ = 0.6
		Manually adjusted geometric mean transmissivity for 20 realisations. Initial estimate based on geometric mean of observations.		
	Truncated lognormal distribution correlated to length.	−13 ≤ logT < −10 mean and standard deviation same as deterministic fracture. *T* semi-correlated to fracture radius.		
SKB/CFE	Spatially correlated log-normal σ = 1, with transmissive fracture intersections.	5×10^{-10}	2×10^{-9}	5×10^{-11}
SKB/KTH	Spatially correlated log-normal distribution using 3 different correlation structures (MG, CN, DN see Zinn and Harvey 2003).	2.8×10^{-9} σ^2 = 1, 4, 8		

5.4.2 7C2 PFL Single and Cross-hole test simulation

Modelling groups took either a forward, sensitivity or manual calibration approach to simulating the PFL tests. Model fits were assessed by cross-plots of measured flows (JAEA also present RMS error values). Not all groups simulated all the tests: again the testing programme was relatively complex, requiring a significant number of simulations if models for the 3 shafts were considered. Pressure measurements were not generally used other than as model surface boundary conditions because of possible hydraulic connections to the open tunnels.

The different approaches to cross-hole testing and transport simulations (calculation of F-factors) within Subtask 7C2 are summarised in Table 5-15.

Table 5-16 list the reported F-factors from JAEA, NWMO/Laval and Posiva/VTT. SKB/KTH only calculated F-factors for KU2 while KAERI and SKB/CFE did not calculate F-factors. There is no significant difference in the calculated values due to flow orientation. Both JAEA and Posiva/VTT calculate significantly higher F-factors for KU3 where the transmissivity of the conditioned feature was significantly lower, while NWMO/Laval using an unconditioned model calculated a lower F-factor around KU3 as the realisation used had higher aperture/ transmissivity around KU3. SKB/KTH provided β factor probability distributions for KU2 for differing aperture variability, spatial correlation and aperture-transmissivity relationships (see Figure 5-41) the modal values were in the range 10_8 to 10_9 s/m.

It should be noted that Posiva/VTT show that path lines and anticipated retention properties vary with numerical precision at a level comparable in magnitude to realisation dependence. The influence of discretisation was also demonstrated by JAEA.

Table 5-15. Subtask 7C2 approaches to cross-hole testing and transport simulations.

Group	Cross-hole testing	Transport property calculation
JAEA	10 realisations of stochastic model typically showing a reasonable overall match to measured flows.	Particle tracking across 20 m × 20 m heterogeneous fracture (no background rock).
KAERI	Forward models using interpolated (Kriged) and multiple realisations of random field, followed by comparisons to observations.	N/A
NWMO/Laval	Sensitivity studies on assigned outflows and choice of correlation length.	Limited particle tracking capability, so β-factors calculated for Barium and Caesium transport across the shaft.
Posiva/VTT	Adjustment of individual model parameters based on 20 realisations of stochastic models. Comparison of ensemble means with measurements.	Particle tracking of 100 particles through each of the 20 realisations.
SKB/CFE	Comparison of single-hole PFL flows with 3 realisations of stochastic model.	N/A
SKB/KTH	Main focus was Nappy Experiment.	High resolution particle tracking calculations for multiple realisations of the different fields (correlation structure, variance and transmissivity-aperture relationship)/

Table 5-16. Calculated F-factors (s/m).

	JAEA	NWMO/Laval	Posiva/VTT
KU1 E-W		$1–3\times10^{11}$	2×10^{15}
KU1 N-S		$1–2\times10^{11}$	2×10^{15}
KU2 E-W	$10^{14}–10^{13}$	$1–2\times10^{11}$	2×10^{15}
KU2 E-W	$10^{14}–10^{13}$	$1–2\times10^{11}$	2×10^{15}
KU3 E-W	$10^{15}–5\times10^{15}$	$5–8\times10^{9}$	2×10^{17}
KU3 N-S	$10^{15}–5\times10^{15}$	$5–8\times10^{9}$	2×10^{17}
Conditioning	Conditioned model lower T at KU3.	Unconditioned model larger local T at KU3.	Conditioned model lower T at KU3.
Uncertainty treatment	Estimated from 10–90 % CDF plots.	Evaluated at 3 different locations.	Given as log mean and standard deviation from 2000 particles. Log standard deviation ~1 in all cases.

5.4.3 7C3 Nappy test in KU2

The different approaches to modelling the KU2 Nappy Test are listed in Table 5-17. In general the modelling groups could simulate shaft inflows of comparable magnitude to those observed. Qualitative matches to the distribution of flow could also be achieved by assuming a no-flow boundary over part of the shaft intersection. In the sensitivity study performed by SKB/KTH it was possible to exclude models with low aperture variability but it was not possible to identify a robust dependence between model correlation length, aperture variability and the number of observed inflow peaks (defined as a local maximum, rising above a certain threshold, e.g. 2 ml/min). Realistically this is likely to be non-unique and a complex function of the model parameters.

Table 5-17. Subtask 7C3 approaches to Nappy Test simulation. JAEA and KAERI did not perform simulations.

Group	Deterministic fracture	Background rock	Boundaries
NWMO/Laval	Unconditioned 2D heterogeneous fracture. Variant model with no-flow boundary over “grout” zone.	Uniform K (sensitivity $10^{-9}–10^{-11}$ m/s).	Fixed head (270 or 350 m) at r = 15 m.
Posiva/VTT	Conditioned 2D heterogeneous fracture, sensitivity study varying μ, σ, λ, discretisation and numerical precision.	-	Fixed head h = 180 m at r = 15 m.
SKB/CFE	2D heterogeneous fracture geometric mean $T = 2\times10^{-9}$, λ = 0.1, 0.2, 0.6 m.	Intersections with deterministic fracture create channels.	Fixed head at r = 15 m.
SKB/KTH	Conditioned 2D heterogeneous fracture (λ = 0.5 m), sensitivity to correlation structure (MG, DN, CN), μ, σ^2 = 1, 4, 8 over multiple realisations. Model variant with no-flow boundary over “grout” zone.	-	Fixed head h = 187 m at r = 16 m.

5.5 Evaluation

5.5.1 Task 7C definition and structure

The Task Definition allowed the modellers to consider the influence of in-fracture heterogeneity and PFL testing of low transmissivity fractures at high drawdown. The performance measures specified were:

- Task 7C1: fully parameterised conceptual models and microstructural models.
- Task 7C2: pressure and flow data from PFL simulations and calculated F-factors for transport simulations.
- Task 7C3: inflow to the shaft at 10 cm increments.
- Task 7C4: uncertainty bounds (75 % and 95 % bounds) for parameters investigated.

Detailed formats for the performance measures were not specified and they were provided by the modellers within their reports. This resulted in some inconsistencies in reporting of F-factors in terms of units and uncertainty ranges.

5.5.2 Task 7C Dataset

KU2 shaft and Nappy experiment

The PFL transmissivity derived from the higher drawdown tests in the five KU2 probe holes are significantly lower ($1-4\times10^{-9}$ m^2/s) than the PFL logging in KR38 (1.2×10^{-8} m^2/s). This may indicate that the high drawdowns in the probe holes (~180 m) resulted either in closure of the fracture or some near-wellbore flow restriction (turbulent channel flow, or phase obstruction due to degassing). Only in the KU2 dataset is there a feature detected from the normal PFL logging procedure with low drawdown. Further, as pointed out by Therrien and Blessent (2017) the measured inflow to the KU2 shaft during the Nappy experiment of 2 712 ml/h is lower than that to two of the probe holes (ONK-PP124, ONK-PP126), suggesting that excavation effects may be significant. For this reason only approximate matches to observation should be expected from the models.

The dataset focused on data from the shaft probe hole arrays including PFL data (single and cross-hole). Fracture trace-maps from the shaft-wall were also available. Since there were no site-specific data on fracture void-space morphology, the modellers used fracture heterogeneity models from literature.

5.5.3 Modelling groups evaluations

Each modelling group has provided an evaluation of the Task within their report. Selected comments from these sections have been collated here but the reader should refer to the individual reports for a fuller discussion.

JAEA

The dataset was insufficient to support aperture distributions based on complex fracture surface topography seen in previous studies (e.g. Winberg et al. 2003, Tetsu and Sawada 2010). Despite the lack of site-specific data most of the model realisations produced values comparable to measurements (with the exception of the PP124 and PP126 responses), perhaps due to the single-hole PFL and Nappy data constraining the possible flow properties. The PP124 and PP126 responses could be explained by increased transmissivity close to the boreholes.

JAEA suggest that up-scaling methodologies for transmissivity, aperture and F-factor are needed to take the millimetric-scale aperture variation into the model scale (~decameter); further, that the transport behaviour was directly affected by the resolution of the aperture distribution.

KAERI

KAERI also commented that the observations were too limited to develop appropriate geostatistical models that could reproduce the hydraulic system at the site.

NWMO/Laval

NWMO/Laval commented that there was too little data to build a geostatistical model of the FR1 fracture so that the correlation length was arbitrarily defined on the basis of a literature review and model size. Further the FGEN software did not support the generation of conditioned realisations. For the simulation of the single-hole PFL tests there were some problems due to the difference between model height (40 m) and actual borehole length (100 m), however:

- KU1 models matched the measured flows reasonably,
- KU2 models did not perform so well but this may have been due to the overall uncertainty in the data as there was a large deviation between the sum of PFL measurements and measured total outflow,
- KU3 models focused on getting the correct pattern of in/outflow.

The simulations of cross-hole tests showed that local apertures have a significant influence on simulated flow directions. The β-factor (F-factor) was calculated using the method of Hodgkinson (2007), and the calculated values for the different shafts showed an overall relationship to the local fracture aperture (or transmissivity).

The simulated shaft total inflow distribution matched the measured value quite well but this did not account for the observed restriction of flow to only part of the fracture. NWMO/Laval also point out that differences in the observed inflow distribution and the measured PP borehole flow data are unexplained.

Posiva/VTT

Posiva/VTT concluded that the results appear to correctly characterise the behaviour of the flow system in a qualitative manner. The calculated heads and flows were in line with expectations. Uncertainties in the model arose from model assumptions on the form of heterogeneity, uncertainty in the data and from the numerics (discretisation and precision). Retention properties are a function of correlation length with longer correlation lengths resulting in more “channelled” fields. For one model hundreds of realisations were run and the statistical convergence of the F-factor distribution was evaluated.

If excavation-related artefacts are ignored then the observed inflow distribution (Nappy Experiment) points to a relatively large spread in the transmissivities (i.e. significant channelling).

SKB/CFE

SKB/CFE commented that their model based on a heterogeneous fracture with small correlation length and longer flow structures associated with fracture intersections could be calibrated to reproduce the single hole pump tests performed prior to excavation. While the inflow distribution in KU2 was found to be sensitive to the correlation length it was difficult to estimate the correlation length from the inflow distribution with any certainty although the length used was not inconsistent with the measurements.

SKB/KTH

SKB/KTH considered that the low variability case ($\sigma(\ln T) = 1$) was a poor representation of the heterogeneity of the KU2 and that higher variability cases (particularly the CN and DN textures) provided a better match to the Nappy Test data. However, it had not been possible to examine the effects of different correlation lengths and uncertainties associated with grouting would also affect the results. It was therefore concluded that it may be difficult to determine an optimal heterogeneity structure from the available dataset.

5.5.4 Overall evaluation

Fine-scale aperture/transmissivity models

All the modelling groups were able to develop heterogeneous flow models based on the high-drawdown low-transmissivity PFL data. Several modelling groups commented that the site-specific data was insufficient to characterise the small-scale aperture/transmissivity variation. The modellers adopted a variety of models from literature where the aperture/transmissivity textures used correspond to different assumptions (conceptual models) of fracture aperture heterogeneity. All models were based on a log-normal distribution of aperture. SKB/CFE developed a hybrid aperture variation model based on a spatially correlated log-normal distribution and preferential paths along fracture intersections. Aperture was linked to transmissivity by either a cubic (Witherspoon et al. 1980) or quadratic law (Dershowitz et al. 2003).

The limited amount of data (PFL data, Nappy test and trace maps) were insufficient to identify particular heterogeneity models so the range of models developed in Task 7 gives some indication of the bandwidth possible. While some of the models could produce reasonable matches to the observed flow responses the transport properties were found to be dependent on the details of the small-scale aperture distributions (i.e. not just aperture distribution and correlation length- see Zinn and Harvey 2003) but also various aspects of the numerical implementation (see the work by Posiva/VTT, Krumenacker et al. 2017).

A wide range of heterogeneity models were developed (Table 5-18) that could match the observed transmissivity range. The limited amount of data (PFL data, Nappy test and trace maps) were insufficient to identify particular heterogeneity models so the range of models developed in Task 7 gives some indication of the bandwidth possible. SKB/KTH specifically chose models from literature that, although characterised by similar distributions of aperture/transmissivity had quite different connectivity.

Table 5-18. Aperture structure models.

Group	Description	Σ(ln(*T* [m^2/s]))	*L* (m)	Justification
JAEA	Simple semivariogram model.	-	-	Not used because it did not reproduce multi-scale structure.
	Multiple nested correlation model.		0.06, 0.1, 6.15	Observed aperture structure of Kamaishi Mine rock sample.
KAERI	Spatially correlated log-normal distribution.			
NWMO/Laval	Spatially correlated log-normal distribution.			
Posiva/VTT	Spatially correlated and conditioned Gaussian.	0–2.8	0.1–3	No data support for any other model.
SKB/CFE	Spatially correlated log-normal distribution with small correlation length plus paths along intersections.	1	0.2	Three models initially evaluated: multivariate normal distributions, random fracture network, fractal surface.
SKB/ KTH	MG Multi-Gaussian.	1.8	0.5	Minimum information assumption (see Gómez-Hernández and Wen 1998).
	CN Connected high permeability.	1.8	0.5	Shear deformation and normal stress seal most of the fracture and permeability is localised in “islands”.
	DN Disconnected high permeability.	1.8	0.5	Fracture contains connected conduits e.g. connected void space along fracture intersections.

The calculated F-factors from the different groups show a wide-range (5×10^9–2×10^{17} s/m), largely controlled by differences in the underlying aperture models and to some extent by computational methods and choice of discretisation (see discussion of work by JAEA and Posiva/VTT). The high resolution Fup-based simulations of SKB/KTH show wide probability distributions for the F-factor for the different paths over multiple realisations (Figure 5-39), but also the influence of the different spatial correlation models with "fast" paths being more common in the CN model.

5.5.5 TS28 simulations

None of the modelling groups performed a predictive simulation of the PFL TRANS measurements but instead adapted their models to consider the effect of microstructural models[32] as shown in Table 5-19.

Table 5-19. Modelling group approaches to TS28.

Group	Approach to revised TS28 simulation
Posiva/VTT	Modelled change in drawdown due to inclusion of heterogeneous fracture zone representations and compared with homogeneous zones.
SKB/CFE	Integrated heterogeneous representation of transmissive feature (sheet joint) into large scale simulation and determined effect on drawdown.
SKB/KTH	Downscaling calculation where pressure boundary conditions for fine-scale model taken from Task 7B homogeneous fracture zone DFN simulation. In total 100 realisations of different heterogeneity models were simulated. The pattern of borehole inflow was extracted.

Both Posiva/VTT and SKB/CFE calculated the changes in drawdown due to inclusion of microstructural models for major zones. They both showed that the changes are largest at the pumping borehole and that drawdown changes at the monitoring boreholes are small. This can be explained by the expected "logarithmic" drawdown profile around a pumping well such that near borehole heterogeneity can result in significant "skin" effects. The effect of local heterogeneity at the monitoring holes is small as might be expected.

SKB/KTH were the only group to calculate detailed flow distributions around a monitoring borehole in such a way as to be comparable with the PFL TRANS measurements. The simulations demonstrate the influence of local transmissivity variation and show that at high variance this dominates the flow directions rather than the larger-scale flow direction due to pumping. This suggests that the PFL TRANS can be used to identify the extent of flow channelling within a feature by comparison of the local and "regional" flow directions.

[32] NWMO/Laval calculated flow at the Plane 1 feature in KR15 in Task 7B but no microstructural heterogeneity was considered.

6 Task 7 Overall Evaluation

6.1 Task 7 Aims and Objectives

Task 7 aimed at providing a bridge between site characterisation (SC) and performance assessment (PA) approaches to pumping tests and measurement from borehole flow logging. Task 7 also aimed to develop an understanding of the effects of open boreholes on the groundwater system and the use of data from such boreholes in site characterisation and performance assessment. These overall aims were translated into a series of objectives in each Subtask following on from the initial pre-studies, the aims of which focused on the modelling of open boreholes during site characterisation (Table 6-1).

The Subtask objectives related to consideration of both site characterisation activities (PFL logging in open boreholes and more generally cross-hole testing) and the reduction of uncertainty in performance assessment. The connection to performance assessment followed on from work within Task 6 concerning the ability of tracer and flow data to constrain PA parameters, which included the design of site characterisation activities to optimise the value to performance assessment calculations.

The relationship between the modelling of cross-hole testing and uncertainty in performance assessment is a complex one involving significant abstractions of results from site characterisation to radionuclide transport calculations within performance assessment. The different requirements to model complex cross-hole testing sequences and to reduce uncertainty in PA were not easy to balance and within the Subtasks consideration of PA goals was generally limited to simplified transport calculations for conservative tracers (typically via particle tracking), although other possible approaches were investigated in additional studies.

A more extensive consideration of uncertainty in PA would have been difficult to include within the Task given the other objectives and the scope of the cross-hole testing (3 different cross-hole testing campaigns). Some modelling groups felt that it would have been better to focus exclusively on the analysis of the cross-hole tests as this was the bulk of the work performed within the Task.

One aspect of the early Task Definition that was not addressed during later considerations was the "Identification of necessary and sufficient site data". In particular "Will anything ever be enough?".

An overview of the site characterisation process and how it feeds into performance assessment (and disposal system design) would have been needed to answer this. The question was never explicitly addressed during Task 7, although the Task Force might have been a good forum to explore it. Perhaps as a result of this, while modellers were encouraged to calibrate models, only limited emphasis was placed on what a "good enough" model would be.

Information on data uncertainty and possible biases were provided but the question "What is the required level of detail?' (Berkowitz 2002) was never answered. So, while useful performance measures were specified, in hindsight the failure to specify metrics for acceptable model matches both within simulations and across simulations[33] should have been identified early in the Task[34].

[33] Should we expect a "good model" to provide matches to pump tests performed in different boreholes?

[34] Perhaps by the reviewer?

Table 6-1. Task 7 Subtask objectives.

	Objectives
Pre-studies	1. To determine means of incorporating open boreholes in numerical groundwater flow models. 2. To implement results corresponding to flow logging measurements in numerical models. 3. To address the need for transient modelling. 4. To become acquainted with the available data set and to determine the model data needs.
7A	1. To understand the major features of the groundwater system. 2. To understand the consequences of the tests and measurement systems used, e.g. the open boreholes. 3. To understand how to model open boreholes within site characterisation studies and for the provision of parameters for PA. 4. To understand how PFL measurements could reduce uncertainty in models as compared to models calibrated with only head measurements. 5. To increase understanding of compartmentalisation and connectivity at the Olkiluoto site and more generally in fractured crystalline rock. 6. To evaluate how uncertainty in PA can be reduced based on the analysis of the Olkiluoto dataset.
7B	1. To understand how major features could be used as boundary conditions. 2. To understand the minor features of the groundwater system, (background rock). 3. To understand the consequences of the tests and measurement systems used, e.g. the open boreholes (as 7A 2). 4. To understand how to model open boreholes within site characterisation studies and for the provision of parameters for PA (as 7A 3). 5. To understand how PFL measurements could reduce uncertainty in models as compared to models calibrated with only head measurements as 7A 4. 6. To increase understanding of compartmentalisation and connectivity at the block scale. 7. To evaluate how uncertainty in PA can be reduced based on the analysis of the Olkiluoto dataset as 7A 6.
7C	1. To advance the understanding of PA-relevant single fracture micro-structural models. 2. To use PFL to characterise in-plane fracture heterogeneities. 3. To improve the ability to predict inflow to suitable and unsuitable canister holes. 4. To assess whether data from pilot boreholes has any predictive power with regard to prediction of flow to canister holes.

6.2 Task definition and structure

Significant efforts were made to provide detailed Task Definitions documenting the objectives, dataset, required simulations and performance measures. These were updated throughout the task and the final versions summarised in Vidstrand et al. (2015). Most of the modelling groups felt these were at least satisfactory, especially considering the complexity of the tasks.

The Task was structured into four main elements:

- Preliminary simulations on flow along boreholes.
- Task 7A: KR24 pumping test.
- Task 7B: KR14-KR18 pump tests.
- Task 7C: Testing in the shaft probe boreholes.

In hindsight, the inclusion of 3 significant Subtasks each with its own extensive supporting dataset was ambitious and resulted in a longer Task than had originally been intended. The idea of modelling at three different scales: site, block and single feature was appealing and resulted in work to develop integrated models across the scales (see discussion of TS28 and related work in Chapter 5). However, the overall workload in integrating data, performing and interpreting simulations and then reporting all the tasks may have prevented the groups from performing more complete investigations of the individual subtasks, so that while interesting tools and approaches were developed, there were not always fully investigated and evaluated.

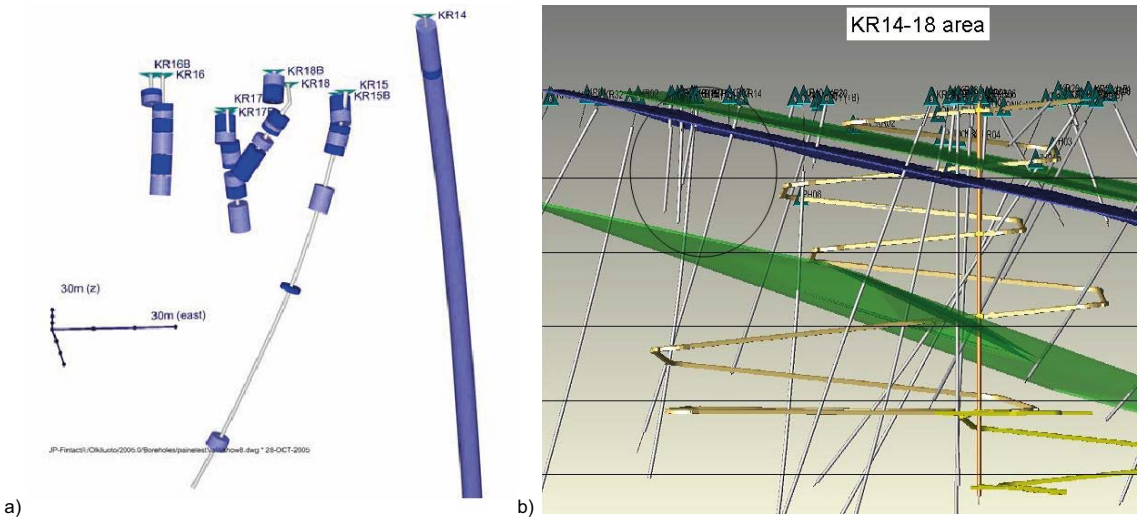

a) b)

Figure 6-1. *KR14-KR18 boreholes: a) monitored sections and b) the three major fracture zones of significance for the model domain. Structure HZ19A located at top (Site Model 2006).*

6.3 Task 7 dataset

The datasets provided by Posiva and managed by the Principal Investigators were extensive and of high quality. The PIs were active in supporting the modellers by providing clarifications or additional data where needed. The volume of data did however require significant effort to manage and integrate within the models.

The dataset from Task7B was particularly rich (Figure 6-1), with multiple hydraulic testing campaigns using both PFL and packer testing approaches. There are very few borehole-based site characterisation datasets in fractured rock of comparable quality. Having said that, two groups thought more data on background fracture length-scale or connectivity would have been useful.

Handling the PFL flow data was generally more complex than head or drawdown data, due to its high spatial resolution and large dynamic range. Also, analysis methods for flow were typically less well developed than those for heads.

6.4 Modelling approaches

6.4.1 DFN Models

The majority of the models used within Task 7A and 7B[35] used a Discrete Fracture Network approach, although the numerical methods and final implementation (discrete features or equivalent continuum) varied between the groups. Once the model objectives and volume/scale have been defined DFN modelling requires the following steps:

- Identification of relevant deterministic features and classes of stochastic features (structural model).
- Determination of geometric descriptions of features.
- Determination of spatial distribution of features (generation of multiple realisations).
- Assignment of hydraulic properties to features.
- Modification of connectivity between features.
- Treatment of connections to model boundaries.
- Generation of a numerical mesh for simulation (discrete elements of effective medium).
- Solution for flow and transport.

These steps are commonly part of an iterative approach for model calibration.

[35] And some models in Task 7C

Identification of relevant features and classes of features

Hydraulically relevant features are usually assumed to relate to geological structures (fractures, fracture zones, faults, dykes etc.) that can be identified in geophysical data, boreholes or outcrop. Evidence from hydraulic testing and literature allows the identification of the potentially hydraulically significant features.

Individual features may be associated with specific classes of structure. Classes may relate to geomechanical mechanisms (e.g. extension fracture or shear fracture), geological terminology (e.g. joints, faults, dykes) or some assessment of size or significance (e.g. major fracture zones). Only a fraction of any class of feature, and only a fraction of the surface area (or volume) of any individual feature may be sufficiently water-conducting to be relevant for a specific application.

Within Task 7, PFL data was the primary basis for identification of flowing features. The site-scale structural models were used to identify "major fracture zones"; these structures having been identified from the integration of geological, geophysical and hydraulic data (including PFL). These two datasets resulted in essentially two classes of features:

- Stochastic background rock fractures taken from the integrated PFL dataset.
- Deterministic fracture zones taken from the structural model.

Additional deterministic features were then added on the basis of alternative structural models or experience from other sites, usually as part of model calibration driven by features of the flow and pressure response. These features represented structures intermediate between the site-scale structures within the structural model and the background rock.

Geometric description of features

Individual features may be sufficiently well-characterised that their geometry can be described deterministically (sometimes with an associated uncertainty). Where it is necessary to deal with multiple features whose geometry is uncertain and may vary, stochastic approaches are used and it is assumed that suitable probability distributions can be found to describe the features' shape, length-scale, and orientation.

Shape: Feature shape is typically assumed to be a relatively simple geometric primitive: rectangle (square), ellipse (circle) or occasionally a triangular mesh common to all features of a particular class. In general, there is little data to characterise fracture shape, and shapes requiring the minimum information (squares or circles) have been used. Information on the aspect ratios of features is rarely available although the impact of aspect ratio on feature connectivity can be significant (Barker 2018). Within Task 7 stochastic features were either represented as squares or simplified circular disks.

Length-scale: While feature length-scale (or a projection of it e.g. trace-length) can be observed in outcrop or lineaments, and surface and borehole geophysics can identify the extent of major structures, for most features intersected by boreholes it is not possible to determine the length-scale of the feature and it is necessary to make assumptions about the length-scale distribution for each feature class.

Within Task 7 most modelling groups assumed that the length-scale of stochastic features followed a truncated power-law, parameterised by

- r_{min} – the minimum length-scale of any feature,
- r_{max} – the maximum length-scale of any feature,
- a – the power-law exponent.

The use of power-laws to describe empirical data is widespread in modern science and power-laws have been used extensively to describe scaling in fracture systems including fault and fracture length scales (Bonnet et al. 2001) over a large range of scales (10^{-3} to 10^{5} m) with a range of estimated exponents from $a = 0.8$ to 3.5 with a peak at about 2-2.1. A key argument for power-law or fractal scaling is the absence of "characteristic length" in the fracture growth process (Bonnet et al. 2001) although power-laws may also arise by the mixing of multiple "heavy-tailed" distributions (Stumpf and Porter 2012). Alternative distributions such as log-normal distributions have also been used to describe fracture/fault length but have a characteristic length-scale. There is usually relatively little

data to constrain the parameters for a specific site or model application and literature values plus arguments on identification of deterministic features (constraining maximum length) and model practicality[36] (constraining minimum length) have typically been used.

Within Task 7 the use of power-law length distributions for stochastic features was assumed, but not tested. The values of the distribution parameters were either assumed or calibrated although they were within geologically-defendable ranges. Within Task 7B Posiva/VTT performed sensitivity studies on background fracture length-scale to support calibration and understand the influence of length-scale on connectivity.

Orientation of features: The orientation of geological features can be derived from core or geophysical imagery but is subject to orientation bias such that the distribution derived from borehole or scan-line data is a biased version of that in the volume of interest. For boreholes this geometric bias is normally addressed by weighting fracture observations by $1/\cos(\alpha)$ where α is the angle between the feature normal and the local borehole direction (Terzaghi 1965). When the feature and borehole are parallel this weighting is infinite and Priest (1993) advises a maximum weighting of ~10 (equivalent to ~6° between the fracture normal and borehole direction) to avoid over-correction (e.g. due to errors in borehole or fracture orientation).

Within Task 7 the modelling groups generally used orientation distributions based on Terzaghi-weighted borehole statistics (from the integrated PFL data set). An exception is the fracture growth model of SKB/KTH based on extrapolation from the boreholes. This model does not account for orientation bias and could result in a significant underestimate in sub-vertical features (where the boreholes themselves are vertical).

Spatial distribution of features: The spatial distribution of stochastic feature centres has typically been described by a Poisson Process. The homogeneous Poisson process is characterised by a mean area density (single-sided macroscopic area per volume m^2/m^3 or P_{32} Dershowitz and Herda 1992). The Poisson distribution is equivalent to assuming that features are positioned independently of each other. Although Poisson models result in no preferential clustering as feature centres are equally likely to occur in any location, there is typically some degree of clustering observed (e.g. intersection spacing along a sampling line follows a negative exponential distribution). Alternative models to the Poisson approach might result in situations where:

- Features preferentially cluster together such that the presence of a feature results in an increased likelihood of a nearby feature.
- Features “avoid” each other such that the presence of a feature results in a reduced likelihood of a nearby feature (e.g. Ackermann and Schlische 1997).

Bour and Davy (1999) suggest that fault size distribution is related to the spatial distribution (clustering) of the faults. In particular they relate the power-law slope of the length distribution *a* to the fractal dimension D of the fault network. Studies of the Forsmark Site (Darcel et al. 2013) include methodologies for testing the applicability of Poisson models to the observed spatial variability. Darcel et al. (2013) suggest that the data from Forsmark supports a “weakly fractal” DFN model rather than a pure Poisson model. Alternative DFN growth models aiming to replicate fracture network topology (Sanderson and Nixon 2015) are currently under development (Libby et al. 2019).

Within Task 7 most modelling groups have assumed homogeneous Poisson processes characterised by a single P_{32} for stochastic features. An exception is the fracture growth model of SKB/KTH, where fractures “grow” outwards from borehole intersections within volumes defined by the relative borehole locations, although only limited testing of this model has been possible.

Assignment of hydraulic properties to individual features

The hydraulic properties of individual features are usually determined from hydraulic testing. In Task 7 this is either from PFL logging or packer testing and the derived transmissivity (or equivalently hydraulic aperture) is ascribed to an individual feature. While, transient analyses can determine

[36] Small values of the power-law exponent may result in very large numbers of small fractures resulting in high computational costs.

changes in property with the radius of investigation of the test (related to the elapsed time), flow properties derived from steady state analyses are likely to be a composite of any near-wellbore resistance, the spatially varying properties of the feature intersected and of the network of features to which it connects.

In Task 7A most groups assumed a uniform effective transmissivity for the major zones based on the geometric mean of the PFL derived transmissivity for each feature (see Vidstrand et al. 2015). Several groups (CRIEPI, SKB/CFE) assigned different properties around borehole intersections (skins) to represent the effect of local variability of the zone properties on the measured borehole flows. One group also considered differences between the deep and near-surface parts of fracture zones (Posiva/VTT).

With regard to background fractures in Task 7B, most modellers assumed that the transmissivity derived from PFL logging corresponded to an estimate of the uniform effective transmissivity for the feature identified at the borehole intersection, and that flow across the feature could be described by this transmissivity. These feature transmissivities were then be used to condition fractures intersecting the boreholes and to derive probability distributions for the transmissivity of the population of background fractures.

Within Task 7C the heterogeneous nature of the target fracture was considered by all the modelling groups.

Hydraulic connectivity between features

Where it is assumed that the whole of a feature is uniformly capable of flow (homogenous isotropic transmissivity within the feature), the hydraulic connectivity is dictated by the geometry of features and their intersections. Even in such a case, flow will be hydrodynamically channelled. The geometric connectivity of the network is largely controlled by the feature densities, chosen length-scale distribution and assumptions about aspect ratios and orientation[37]. Where there is significant variability of flow properties within features then hydraulic connectivity will be influenced by how the channels and barriers within the features are connected at the feature intersections. Two cases can be considered:

- Channels (high transmissivity regions) of features are spatially correlated across intersections.
- No spatial correlation between channels in intersecting features.

It is also possible that fracture intersections themselves have special properties, they may be either preferential flow paths (perhaps due to the presence of a more open pore space potentially related to deformation) or barriers. There is little site-specific information on the hydraulic properties of fracture intersections[38].

In Task 7 for the most part modellers assumed that the connectivity between channels within fractures was sufficiently good that the hydraulic connectivity was controlled by the geometric connectivity of the features. Within Task 7B, JAEA, even though they represented fractures as uniformly transmissive planes, ascribed a connection probability to represent the possible effects of channel connectivity. Within Task 7C SKB/CFE considered a model where intersections between a larger deterministic feature with stochastic background fractures formed preferential flow paths in the deterministic feature.

Hydraulic connectivity with model boundaries

The connectivity of major zones with model upper boundaries representing the near-surface soils (regolith) or the sea-bed were typically treated as constant head boundaries without any significant flow restrictions. It is possible that clogging by soils or sediments can limit flow at such boundaries. Alternatively, lower stresses near the surface may result in more open and permeable fractures and

[37] Unless the orientation distribution results in many sub-parallel features, orientation is likely to have a lesser effect on connectivity than density and length-scale.

[38] Schneeberger et al. (2018) analysed the spatial distribution of tunnel inflows at the Grimsel Test Site in central Switzerland and and suggest that feature intersections may be associated with preferential flow paths.

near-surface exfoliation (or sheet) joints result in higher connectivity (although potentially more anisotropic if sheet joints are not well-connected to sub-vertical features).

Across Task 7 modellers generally assumed that surface-connections were not affected by such processes, although within Task 7A Posiva/VTT considered splitting the major zones to allow for different connectivity to the boundary conditions and SKB/CFE incorporated an exponential permeability dependence in the near surface.

DFN model summary

As discussed above, the development of DFN models of a rock volume requires a significant number of choices (essentially assumptions) regarding the representation of the network of water conducting features. The modelling groups have been able to develop a range of DFN models based on the integrated PFL dataset but have not always tested or quantified the uncertainties associated with these choices. Useful sensitivity work has been performed within the task (e.g. Posiva/VTT Task 7B sensitivity studies) but more work is needed to fully understand the implications of all the assumptions.

6.4.2 Alternate models

While most models in Task 7A and 7B were based on an underlying discrete fracture network, the fracture facies model of NWMO/Laval used in Task 7B represented a different conceptual model for the background rock where the effective hydraulic conductivity is controlled by fracture density (see Park et al. 2004), assuming that the effect of variation in individual fracture transmissivity or length scale are of lesser importance.

This model was supported by a comparison of fracture density with transmissivity for the 7B PFL dataset, although this comparison did not account for the observed trend of decreasing density and transmissivity with depth. There is therefore some uncertainty whether the observed correlation of transmissivity with fracture density can be applied to the rock volume as a whole.

The facies model provided a useful alternative model which, when combined with deterministic representations of key features (the sheet joints), provided results that performed comparably to the DFN-based models and were well-suited to calibration using PEST.

Park et al. (2004) demonstrated that the model could successfully characterise and reasonably predict solute migration behaviour in moderately fractured rock at the URL in the Lac du Bonnet granite. Park et al. (2004) found a power-law relationship between fracture density in core and interval log hydraulic conductivity ($r^2 = 0.83$). It should be noted that the MFR (Moderately Fractured Rock) experimental volume had a relatively homogeneous fracture distribution and had been well characterised. A significant correlation of fracture density with hydraulic conductivity might arise where:

- fracture hydraulic properties do not vary significantly between features (e.g. no major fracture zones),
- fractures are not highly channelled and the fracture density is close to the percolation threshold, or
- fractures are channelled such that the effective properties are dominated by the connectivity of the channels and the channel network is close to the percolation threshold.

Approaches to model conditioning and calibration are discussed in the next sections.

6.5 Interpretation of cross-hole tests – flow and pressure

All three of the Subtasks involved the interpretation and modelling of cross-hole tests. In Task 7A and 7C this was largely concerned with cross-hole flow measurements in open boreholes, while in Task 7B there were both tests with cross-hole flow measurements and corresponding tests where boreholes intervals were isolated and pressure response was monitored.

6.5.1 Interpretation approaches to cross-hole tests

Analysis of cross-hole test responses has been studied extensively for many years. Initial work was based on the radial flow solutions of Theis (1935) and Cooper and Jacob (1946), although subsequent work by Black and Kipp (1977) explicitly considered responses within observation wells and studies on observation well response in heterogeneous aquifers were made by Butler and Liu (1993) and Oliver (1993). Since then a range of approaches have been developed and cross-hole testing has become more sophisticated with the development of multi-level packer systems (Black et al. 1986). Options for cross-hole test analysis approaches include:

- Effective property (transmissivity and storativity) determination (e.g. Sánchez-Vila et al. 1999).
- Inverse approaches based on definition of a structural model and estimation of effective properties of the different units or structures within the model (Day-Lewis et al. 2000, Illman et al. 2009).
- Geostatistical inverse models (e.g. Meier et al. 1998, 2001, Alcolea et al. 2006).
- Scaling analyses (Le Borgne at al. 2004) to derive scaling laws and parameters for a given network volume or structure.
- Apparent diffusivity approaches based on identifying preferential connections within the observations (Meier et al. 2001, Knudby and Carrera 2006).

The majority of studies have concerned pressure responses, but flow, pressure, temperature and tracer concentration data have all been used and all of these approaches may be integrated with information from structural geology and geophysics to refine interpretations or to relate to specific aspects of site characterisation.

Recent developments include “flow tomography”. Klepikova et al. (2013) present a “flow tomography” approach using synthetic model cases with a pumping and observation borehole. Flow along the borehole and drawdown are measured and used in the model inversion. Two of the simple networks considered are shown in Figure 6-2. For the simple model case Kelpikova et al. (2013) suggest that:

- Observed well drawdown increases with T_u or T_l connection transmissivity and is insensitive to the interconnection transmissivity T_i.
- The magnitude of the vertical borehole flow velocity increases with the difference between the T_u and T_l and decreases with the interconnection transmissivity T_i.
- The direction of the vertical borehole flow velocity is toward the largest connection transmissivity.

Klepikova et al. (2013) present uncertainty calculations and inverse models for the six different cases. In general, including both flow and drawdown in the fitting objection function results in a better match to input parameters and results in an objective function with fewer local minima and a better-defined global minimum. However, they also identify situations where measurements are insensitive to model parameters. These observations are consistent with the cross-correlation analyses of Zha et al. (2014) who showed that flow information contained “non-redundant” information (see Wen et al. 2020) about the spatial distribution of heterogeneous hydraulic properties. They found that permeability fields derived from the joint inversion of flux (with or without considering its direction) and head data yielded the most satisfactory head field prediction and the best unbiased flux field prediction. Further, the improvement due to adding more observation boreholes was greater when using both head and flow and sensitivity to boundary condition assumptions was lower. Similar conclusions are reported by Tso et al. (2016) who also consider the influence of geological/structural prior information.

The work of Klepikova (2013) can be compared with the interpretation scheme suggested by Keto and Koskinen (2009) for the KR24 pump test.

One important issue with flow data that requires further work is the sensitivity to near-borehole heterogeneity where any local low transmissivity may significantly influence the measured flow in/out and along the borehole, resulting in additional uncertainty on the rock mass hydraulic properties and dependence on properties in the immediate vicinity of the borehole.

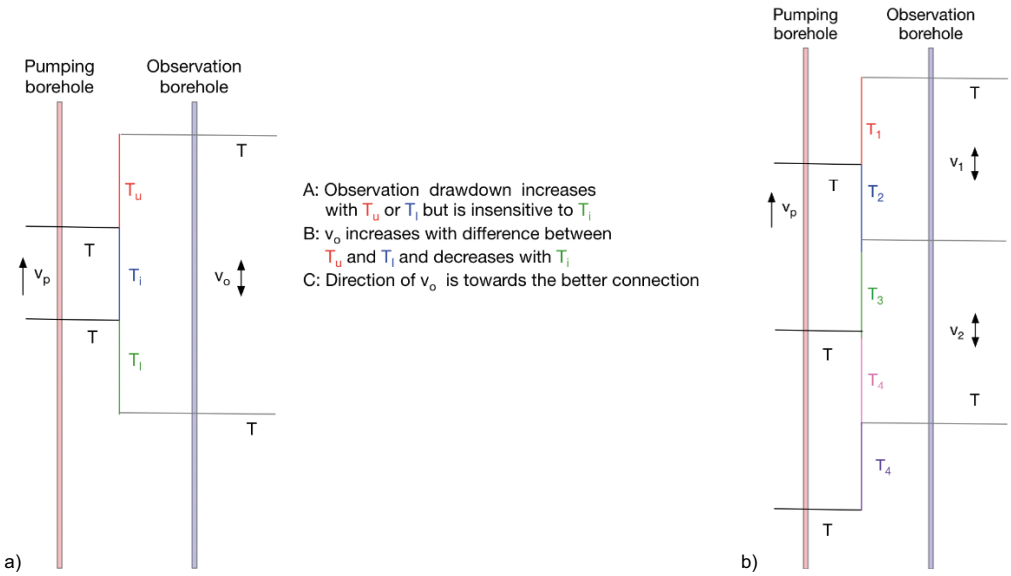

Figure 6-2. *Synthetic fracture networks studies by Klepikova (2013): a) simple model used for sensitivity analysis, b) complex model studied by inverse simulation.*

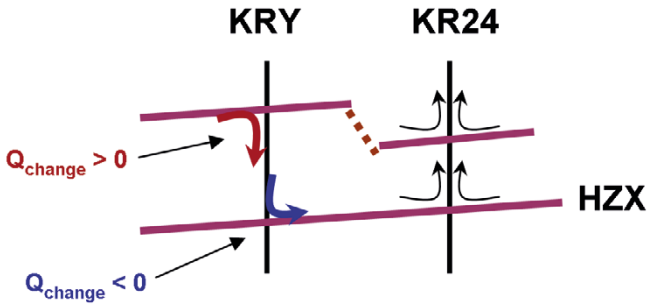

$Q_{change} < 0$	Flow from HZX to KRY decreases when pumping at KR24	There is a good connection from point KRY_HZX to KR24
$Q_{change} > 0$	Flow from HZX to KRY increases when pumping at KR24	There is a more conductive route from KRY_HZX to KR24 than through HZX

Figure 6-3. *Guidelines to interpret the observed changes in PFL measurements.*

6.6 Inverse models of cross-hole tests in fractured rock

Much of Task 7 has been taken up with inverse modelling (calibration) of cross-hole tests to constrain models of the fracture network. Inverse modelling in hydrology is discussed by Carrera et al. (2005) and more recently by Zhou et al. (2014). However, neither specifically addresses fracture networks. Carrera et al. (2005) comment that

- Point values of hydraulic conductivity and transmissivity are prone to error. Moreover they may be of little use when modelling at scales much larger than the pumping test in which they are based. These measurements need to be put into the related geological context.
- Dominant features (i.e. conductive fractured zones, paleochannels, or the like) must be included in the model even if they are not known accurately.
- Much information about aquifer behaviour is contained in discrete events (floods, big rainfalls). Taking full advantage of these requires transient simulations.
- Model calibration is rarely unique (i.e., different model structures may fit hard data satisfactorily). This uncertainty ought to be acknowledged when performing model predictions. Reducing it often requires the use of complementary data.

There has been recent work on inverse DFN models which is summarised in Table 5-10. For the most part studies have been in 2D or have considered relatively simple synthetic networks and there is little experience in using cross-hole data to calibrate DFN models at the scales of Task 7B. Kosack et al. (2010) report a comparative study of inverse modelling of flow and tracer data from the 3 wells at the Soultz-Sous-Forets Enhanced Geothermal System using: Ensemble Kalman Filter, Bayesian Inversion and massive Monte Carlo approaches.

Table 6-2. Inverse modelling of pump tests in fractured or channelled rock.

Reference	Method	Application	Evaluation
Jódar et al. (2000)	Geostatistical inverse models of flow and transport.	Inversion of hydraulic and tracer tests in a highly heterogeneous shear zone at Grimsel Test Site.	Two-dimensional heterogeneous structure (analogous to aquifer models) that does not address networks of features.
Donaldo et al. (2006)	Calibration of a set of DFN realisations to hydraulic and tracer tests. The fitted parameters were transmissivity and storativity for flow; and dispersivity, matrix and fracture set porosity for transport.	Pumping test and tracer test data from 600 m × 600 m × 300 m volume at el Berrocal site.	30 % of realisations achieved an excellent fit to pump test draw-downs. Selected realisations were manually calibrated to tracer test data.
Mardia et al. (2007)	Reversible jump Markov Chain Monte Carlo (rjMCMC). Change fracture slope, intersection, swap fractures, split and join fractures	Synthetic model and 1 m cube jointed granite with 11 × 12 boreholes.	Approach provides a viable method for geometric reconstruction but application used high data density.
Almeida and Barbosa (2008)	Fracture growth model with simulated annealing to condition to location and orientation of fracture intersections and local density index. Simulated annealing with operations to add or delete triangular elements to existing fracture meshes, add a new randomly located fracture.	Match to ~300 m of scan line data from underground marble quarrying and derivation of block-size distribution and associated uncertainty.	Geometric approach capable of generating multiple realisations consistent with scan line data.
Le Goc et al. (2010)	Identification of main flow channels from head and geometric information using “hierarchical” simulated annealing process based on stepwise inclusion of features.	Steady state flow in synthetic 2D channel/fracture networks models with borehole arrays (point head measurements).	Steady state head data was sufficient for only relatively simple cases, more complex cases required geometric information (distance to channel) and a clear “hierarchy” of channels.
Cliffe et al. (2011)	1. Basis Vector Conditioning Method using adjoint solution. 2. Bayesian method using information from the prior distribution of fracture transmissivities and pressure observations.	DFN models of the Olkiluoto site using 11 fracture sets (similar to Task 7A and 7B).	See Chapter 6.
Dorn et al. (2012)	Hierarchical rejection sampling algorithm used to draw realisations from the posterior probability density function at different conditioning levels.	Two boreholes 6 m apart with GPR and cross-hole hydraulic and tracer data for conditioning.	Strong requirement on prior data – availability of GPR data made approach feasible.
Somogyvári et al. (2017)	Trans-dimensional Bayesian Inversion using reversible jump Markov Chain Monte Carlo (rjMCMC). Method allows addition, deletion and shifting of fractures resulting in changes in problem dimensionality.	Inversion of tracer transport in synthetic 2D networks with constant aperture based on two fracture sets with fixed “discretisation length”.	The approach appears attractive but has only been applied within 2D models assuming constant uniform hydraulic apertures for the fractures. Inclusion of aperture variability and extension to 3D is likely to add significant computational overheads and reduction in convergence.
Fischer et al. (2018)	Discrete Network Deterministic Inversion (DNDI): iterative scheme based on sequential updating of network on fixed grid.	Three 2D synthetic study cases with increasing complexity.	The approach has only been used on synthetic networks. The model also relies on refinement of an initial model.

6.6.1 Inverse modelling within Task 7

All the Subtasks involved development of initial forward models of cross-hole flow tests and subsequent calibration using a variety of approaches. The lack of well-developed tools for DFN model calibration during the task[39] was evident in the adoption of largely ad-hoc manual approaches based on:

- Scaling of fracture transmissivity (SKB/KTH, JAEA).
- Local transmissivity modification (skins) at feature/borehole intersections (CRIEPI, SKB/CFE).
- Development of model variants (SKB/KTH).
- Adjustment of model boundary conditions (e.g. recharge KAERI).

As a result of the adoption of manual tools it was difficult to comment on parametric uncertainty or uniqueness. The use of EnKF by Posiva/VTT in Task 7A4 showed promise and the parameterisation selected considered the log transmissivity of the major zones and the surface connections of the zones. This resulted in typically lower transmissivity connections to the surface than the zone itself. The calibration also demonstrated that inclusion of PFL data resulted in a greater reduction of the variance (uncertainty) than a calibration based on the head data alone. The EnKF approach was also used by Posiva/VTT in Task 7B to constrain the transmissivity of the two sheet joints – typically producing consistent results across a range of realisations.

The fracture facies model of NWMO/Laval in Task 7B was able to use the PEST tool (after some initial problems) to constrain the estimates of hydraulic conductivity for each facies and derive uncertainties for these using different datasets (head, flow, head+flow and prior information).

While the modelling groups tried a range of approaches the parameterisation and identification of a suitable objective function to minimise and subsequent manual optimisation was time-consuming and often did not result in significant improvements in the match to observations.

Further work on approaches and methods for automatic calibration of DFNs is needed.

6.7 DFN model conditioning

Within Task 7 several groups conditioned the local properties of large-scale zones (CRIEPI in Task 7A) and the transmissivity of background rock fractures (SKB/KTH in Task 7B). Other groups similarly adjusted transmissivity local to boreholes as part of model calibration. This is equivalent to adding a borehole "skin" term to account for the effect of small-scale heterogeneity of flow in/out of the borehole. When modelling cross-hole flow tests the influence of the near-borehole properties of flow features is of great importance and such approaches are typically required to achieve reasonable matches.

Recently more extensive approaches to conditioning have been developed that provide a stochastic approach to conditioning. Chiles (1987) sets out a method for geometric conditioning of 3D DFN simulations using borehole intersection data based on "libraries" of simulated intersections; this approach was further developed by Lanyon et al. (1998). Appleyard et al. (2018) and Bym and Hermanson (2018) present conditioning methodologies for conditioning fracture geometry, connectivity and flow together with example applications to a synthetic rock block "Hyposite" based on expected conditions at repository level in Forsmark. The local conditioning methods developed by Appleyard et al. (2018) were used to show that predictions made using models conditioned to both geometric and flow data were more accurate than those conditioned to geometric data alone and much more accurate than the predictions made with unconditioned models.

[39] The methods of Cliffe et al. (2011) were under development in the CONNECTFLOW code during Task 7 and SKB/KTH had plans to use them, but they were not fully implemented until after the completion of the Task.

While the methods described by Bym and Hermanson (2018) were also successful in conditioning individual fractures, problems arose when predicting inflow due to differences in connectivity of the conditioned fractures and those from the Hyposite realisation. In addition, predictions of flow to other deposition holes based on conditioning to simulated flow in the main tunnel and two deposition holes showed little predictive power. It should be remembered that the Hyposite synthetic fracture network shared many of the assumptions about fracture geometry and flow with the models used to predict Hyposite results. In this way the results should be considered more as a verification of the methods than validation as key assumptions about flow in the rock were not tested.

7 Conclusions and recommendations

7.1 Conclusions

7.1.1 PFL data

Single hole PFL data provides a robust description of flowing features intersecting the borehole where the local transmissivity is $>\sim 10^{-9}$ m^2/s. The data is well suited to parameterising background fracture properties. For larger scale fracture zones the PFL data gave local properties (~10s of metres) that could be averaged to estimate large-scale effective properties of the zones and which could also be used to locally condition the properties of the fracture zones.

PFL data from cross-hole tests provided a cost-effective characterisation of the flow system response to pumping across borehole arrays. Model developments early in Task 7 allowed accurate and detailed simulation of flows in, out of and along the boreholes, allowing direct comparison with PFL data. The PFL data was more complex to deal with than pressure/drawdown data however, as:

1. The influence of open boreholes needed to be included within the interpretation.
2. There were typically larger numbers of measured responses.
3. The PFL data is sensitive to multiple features intersecting the open hole section.
4. The measured PFL flow response is more sensitive to local low transmissivity regions around the borehole than pressure/drawdown responses.
5. Flow in the undisturbed (no pumping) state is sensitive to small head differences between feature intersections which may be difficult to model, resulting in problems when calculating flow changes due to pumping[40].

7.1.2 Open Boreholes

The influence of open boreholes on measured heads and responses to cross-hole testing was considered within Task 7A. The models suggested that:

- the head field is significantly altered by the open boreholes and that, locally at least, flow paths are significantly changed.
- the boreholes play a significant role in groundwater flow during pumping where water may "short-circuit" along the boreholes to connect to the most transmissive paths into the pumping borehole.
- analyses of large-scale pump tests that do not include the effect of the open boreholes are likely to overestimate the connectivity and effective hydraulic properties of the rock.

In addition, open boreholes may induce longer term transients by mixing waters from the surface with deeper waters. The simplified hydrostructural model used was likely to exaggerate the significance of the boreholes as conduits for vertical flow, but the relatively good performance of some of the calibrated models and (more directly) the PFL measurements from the site suggest that the boreholes play a significant part in the deep groundwater flow system at the site.

7.1.3 Reduction in uncertainty

While it was possible to develop and calibrate a wide range of models in both Task 7B and 7C, only qualitative reductions in uncertainty could be demonstrated and uncertainties associated with model assumptions were not quantified. A strength of the Task Force is that modellers are encouraged to use a range of conceptual models with common data and objectives. This provides the opportunity to consider both conceptual and parametric uncertainty. However only limited links to PA were made within the Task (particle tracking calculations) and a significantly greater effort would have been necessary to provide a robust demonstration of uncertainty reduction, beyond the development of "improved" models.

[40] Compare with drawdown estimation for pumping tests where undisturbed head variation is likely to be relative small.

Calibration of the models (e.g. inclusion of near-borehole skin terms or deterministic features) based on the PFL data generally improved the match to observation but it is not clear that it significantly reduced uncertainty in PA. Within the Task, particle tracking and effective transport parameters (F-Factors) were used as proxies for performance assessment calculations, using initial forward models or calibrated models. As the uncertainties in the initial and calibrated model PA proxies were limited (e.g. values from multiple release points and/or realisations) it is difficult to estimate the true uncertainty reduction. NWMO/Laval used a formal inverse model that was able to provide some evidence of reduction of uncertainty in effective hydraulic properties of fractured rock facies.

The limited success in demonstrating uncertainty reduction is in part due to the additional work required when modelling groups were already stretched by the complex nature of the testing and the large datasets. Uncertainty reduction was also limited by:

- Lack of available tools (e.g. formal inverse facilities for DFN models).
- Limited experience with uncertainty quantification for multiple conceptual models.

An attempt to address the second issue was made within Task 8 and is documented in Finsterle et al. (2018).

7.1.4 Calibration of DFN models

DFN model calibration remains a challenge, despite significant efforts during the Task. The appropriate parametrisation and efficient optimisation methods are not yet established.

Conditioning approaches for major (relative to model scale) deterministic features are reasonably well developed and conditioning of background rock features where they intersect boreholes or excavations have been developed. However, uncertainties regarding the connectivity of the hydraulically significant features beyond those directly observed limit what can be achieved.

7.2 Recommendations

7.2.1 Modelling approaches

DFN models provide a direct representation of the fracture system but are difficult to calibrate. In part this is due to the limited controls on fracture heterogeneity (channels) and hydraulic connectivity provided by the DFN models in contrast to their ability to describe the geometric aspects of the fracture system. The complexity of the models developed and of their outputs sometimes seems to have limited the number of realisations used. Even though many of the models developed were stochastic typically only a small number of realisations were used.

Often, well-characterised volumes (i.e. near the boreholes) are represented in the models in a similar manner to poorly characterised model volumes (away from the boreholes). When simulating pumping tests that are highly dependent on near-borehole properties either multiple realisations of conditioned models or "hybrid" models allowing conditioning on the well characterised volumes with more "schematic" representation of the poorly known volumes (e.g. equivalent continua, pipe or polygon networks) might be appropriate options[41].

7.2.2 Task Force process

Task 7 evolved from an initial study of how best to model flow along open boreholes and of Posiva Flow Log data, to an extensive study of a series of single and cross-hole flow tests performed at a range of scales. During this evolution the early objectives were supplemented by an additional objective relating to uncertainty reduction in performance assessment.

[41] Such hybrids were used within Task 8 (Finsterle et al. 2018) and have the advantage that they provide a clear demarcation of the different levels of knowledge about the rock volume.

Within the Subtasks relatively complex sequences of simulations were specified as a guide in order to facilitate comparison of results between the modelling groups and to track the evolution of the models with the aim of demonstrating uncertainty reduction associated with integration of different data. These simulation sequences were not always followed and to some extent the imposed modelling structure may have removed responsibility for developing overall approaches to meeting the Task objectives from the modelling groups.

During the Task the modelling groups were well-motivated, enthusiastic and innovative and the Task Force Secretariat endeavoured to facilitate the modelling groups' work. However, Subtasks typically took longer to perform than initially planned. In part this was due to the extensive dataset provided by Posiva, but was also due to the relatively large number of simulations required for the complex testing protocols. Many modelling groups were keen to integrate additional data and to perform simulations but the time necessary to do this was usually underestimated. More realistic estimation of effort may have allowed better focus on key aspects of the Task.

Reporting of Task 7A was relatively efficient with all the modelling groups producing reports[42], together with production of the evaluation report in 2009. The reporting of Task 7B, Task 7C and additional studies was deferred until the end of the Task. This resulted in the reporting period extending from 2010 to 2015 for the modelling groups (final publication of some reports extended to 2017). In hindsight the decision to postpone compilation of this evaluation report until all the modelling reports were finalised may have been unwise as it resulted in a further significant delay. Ideally, reporting of significant pieces of work should not be delayed until the end of a Task.

[42] KAERI did not produce a report as they did not join the Task Force until the end of Task 7A, but a short summary of their Task 7A modelling is given in the Task 7A evaluation report (Lanyon, 2009).

Acknowledgements

This report is based on the work of the seven modelling groups, the PIs and the Task Force Secretariat. During Task 7 the modelling groups consistently worked enthusiastically to develop better models of flow in fractured rock within the framework established by the Task Force Secretariat.

Thanks are also due to Björn Gylling and Aimo Hautojärvi for their helpful and careful reviews of the report.

I would like to thank everyone involved in the Task Force for their enthusiasm, hard work, and participation in lively but civilised discussions. Thanks, are also due to SKB and Posiva for managing the Task Force and to the participating organisations in Task 7: ANDRA, CRIEPI JAEA, KAERI and NWMO.

Glossary

ANDRA	Agence nationale pour la gestion des déchets radioactifs
Background rock	Rock matrix and fractures not described by deterministic features
BRIE	Bentonite Rock Interaction Experiment
CEA	Commissariat à l'Energie Atomique, Paris
CFE	Computer-aided Fluid Engineering AB
Channel	Part of the open fracture void space associated with the potential for significant advective flow.
CONNECTFLOW	Groundwater flow modelling tool: Hartley and Holton 2008
CPM	Continuum Porous Medium
CRIEPI	Central Research Institute of Electric Power Industry, Japan
DarcyTools	Numerical tool: Svensson 2010
DFE	Discrete Fracture Element
DFN	Discrete Fracture Network
EnkF	Ensemble Kalman Filter; Evensen 1994
EPM	Equivalent Porous Medium
FEFLOW	Groundwater flow modelling tool: Diersch 2005a, b
FEFTRA	Groundwater flow modelling tool: Löfman and Mészáros 2013
FEGM	Groundwater flow modelling tool: Kawanishi et al. 1994
FEM	Finite Element Method
Fracman	Groundwater flow DFN modelling tool: Dershowitz et al. 2007
Fracture network	The interconnected system of fractures within the rock
Fracture system	The fracture network and the rock that contains it
Fup model	Multi-resolution methodology for flow in single heterogeneous fractures
HI test	Head controlled Injection test
HW test	Head controlled Withdrawal test
Hydrogeosphere	Control-volume finite element groudwtaer flow simulator: Graf and Therrien 2007
JAEA	Japan Atomic Energy Agency
K-S	Kolmogorov-Smirnov statistic
KAERI	Korean Atomic Energy Research Institute
KBS-3	Kärnbränslesäkerhet −3 disposal concept for HLW developed by SKB
KTH	Royal Institute of Technology, Stockholm
LPT2	Large-scale Pumping and Tracer test 2
LTDE-SD	Long Term Sorption Diffusion Experiment (Aspo Hard Rock Laboratory)
mah	metres along hole
m.a.s.l.	metres above sea level
mbgl	metres below ground level
NWMO	Nuclear Waste Management Organization, Canada
OCTREE	Data structure linking each node to eight "child" nodes
PA	Performance Assessment
PA conditions	Undisturbed hydraulic conditions without boreholes
PASC	Performance Assessment Modelling Using Site Characterisation Data

PEST	Model-Independent Parameter Estimation and Uncertainty Analysis tool: Doherty 2004
PFL	Posiva Flowmeter Log
PI	Principal Investigators
PI test	Pulse Injection test
PW test	Pulse Withdrawal test
RI test	Rate controlled Injection test
RW test	Rate controlled Withdrawal test
SC	Site Characterisation
SKB	Svensk Kärnbränslehantering AB
TF	Task Force
T-PROGS	Transition probability geostatisticsl model: Carle 1999
Undisturbed conditions	Hydraulic conditions without pumping
URF	Underground Rock characterisation Facility
VTT	Technical Research Centre of Finland
WCA	Well Characterised Area
WCF	Water ConductingFeatures
TRUE	Tracer Retention and Understanding Experiments

References

SKB's (Svensk Kärnbränslehantering AB) publications can be found at www.skb.com/publications. SKBdoc documents will be submitted upon request to document@skb.se.

Abelin H, Birgersson L, Gidlund J, Moreno L, Neretnieks I, Widén H, Ågren T, 1987. 3-D migration experiment – Report 3, Part I: Performed experiments, results and evaluation. SKB Stripa Project SKB TR 87-21, Svensk Kärnbränslehantering AB.

Ackermann R V, Schlische R W, 1997. Anticlustering of small normal faults around larger faults. Geology 25, 1127–1130.

Acuna J A, Yortsos Y C, 1995. Application of fractal geometry to the study of networks of fractures and their pressure transient. Water Resources Research 31, 527–540.

Ahokas H, Tammisto E, Lehtimäli T, 2008. Baseline head in Olkiluoto. Posiva Working Report 2008-69, Posiva Oy, Finland.

Alcolea A, Carrera J, Medina A, 2006. Pilot points method incorporating prior information for solving the groundwater flow inverse problem. Advances in Water Resources 29, 1678–1689.

Almeida J A, Barbosa S, 2008. 3D stochastic simulation of fracture networks conditioned both to field observations and a linear fracture density. In Ortiz J M; Emery X (eds). Proceedings of The Eighth International Geostatistics Congress, Santiago do Chile. Santiago, Chile: Gecamin, Vol. 1, 129–136.

Andersson J-E, Nordqvist R, Nyberg G, Smellie J, Tiren S, 1991. Hydrogeological conditions in the Finnsjön area. Compilation of data and conceptual model. SKB TR 91-24, Svensk Kärnbränslehantering AB.

Andersson P, Andersson J E, Gustafson E, Nordqvist R, Voss C, 1993. Site characterization in fractured crystalline rock: A critical review of geohydraulic measurement methods. SKI Technical Report 93:23, Swedish Nuclear Power Inspectorate.

Anttila P, Ahokas H, Front K, Hinkkanen H, Johansson E, Paulamäki S, Riekkola R, Saari J, Saksa P, Snellman M, Wikström L, Öhberg A, 1999. Final disposal of spent nuclear fuel in Finnish bedrock – Olkiluoto site report. Posiva 99-10, Posiva Oy, Finland.

Appleyard P, Jackson P, Joyce S, Hartley L, 2018. Conditioning discrete fracture network models on intersection, connectivity and flow data. SKB R-17-11, Svensk Kärnbränslehantering AB.

Barker J A, 1988. A generalized radial flow model for hydraulic tests in fractured rock. Water Resources Research 24, 1796–1804.

Barker J A, 2018. Intersection statistics and percolation criteria for fractures of mixed shapes and sizes. Computers & Geosciences 112, 47–53.

Berkowitz B, 2002. Characterizing flow and transport in fractured geological media: A review. Advances in Water Resources 25, 861–884.

Billaux D, Chiles J P, Hestir K, Long J, 1989. Three-dimensional statistical modelling of a fractured rock mass—an example from the Fanay-Augères mine. International Journal of Rock Mechanics and Mining Sciences & Geomechanics Abstracts 26, 281–299.

Black J H, Barker J A, 2018. An alternative approach to understanding groundwater flow in sparse channel networks supported by evidence from 'background' fractured crystalline rocks. Hydrogeology Journal 26, 2707–2723.

Black J H, Kipp K L, 1977. The significance and prediction of observation well response delay in semiconfined aquifer-test analysis. Groundwater 15, 446–451.

Black J H, Barker J A, Woodman N, 2007. An investigation of 'sparse channel networks': Characteristic behaviours and their causes. SKB R-07-35, Svensk Kärnbränslehantering AB.

Black W H, Smith H R, Patton F D, 1986. Multiple-level ground water monitoring with the MP system. In Proceedings of the Surface and Borehole Geophysical Methods and Ground Water Instrumentation Conference and Exposition, NWWA, Denver, Colorado, 41–61.

Bonnet E, Bour O, Odlin N E, Davy P, Main I, Cowie P, Berkowitz B, 2001. Scaling of fracture systems in geological media. Reviews of Geophysics 39, 347–383.

Bour O, Davy P, 1999. Clustering and size distributions of fault patterns: Theory and measurements. Geophysical Research Letters 26, 2001–2004.

Butler J J, 1991. A stochastic analysis of pumping test in laterally nonuniform media. Water Resources Research 27, 2401–2414.

Butler J J, Liu W, 1993. Pumping tests in nonuniform aquifers: The radially asymmetric case. Water Resources Research 29, 259–269.

Bym T, Hermanson J, 2018. Methods and workflow for geometric and hydraulic conditioning. SKB R-17-12, Svensk Kärnbränslehantering AB.

Cacas M C, Ledoux E, de Marsily G, Tillie B, Barbreau A, Durand E, Feuga B, Peaudecerf P, 1990a. Modeling fracture flow with a stochastic discrete fracture network: calibration and validation: 1. The flow model. Water Resources Research 26, 479–489.

Cacas M C, Ledoux E, Marsily G, Barbreau A, Calmels P, Gaillard B, Margritta R, 1990b. Modeling fracture flow with a stochastic discrete fracture network: Calibration and validation: 2. The transport model. Water Resources Research 26, 491–500.

Carle S F, 1996. A transition probability-based approach to geostatistical characterization of hydrostratigraphic architecture. PhD thesis. University of California.

Carle S F, 1999. T-PROGS: Transition Probability Geostatistical Software. Version 2.1. Davis, CA: University of California, Hydrologic Sciences Graduate Group.

Carrera J, Alcolea A, Medina A, Hidalgo J, Slooten L J, 2005. Inverse problem in hydrogeology. Hydrogeology Journal 13, 206–222.

Chiles P, 1987. Three dimensional geometric modelling of a fracture network. In Buxton, B E (ed) Geostatistical sensitivity and uncertainty methods for groundwater flow and radionuclide transport modeling conference; San Francisco, California, 15–17 September 1987. Columbus, OH: Battelle Memorial Institute, 361–385.

Cliffe K, Holton D, Houston P, Jackson C, Joyce S, Milne A, 2011. Conditioning discrete fracture network models of groundwater flow. International Journal of Numerical Analysis and Modelling 8, 543–565.

Cooper H H, Jacob C E, 1946. A generalised graphical method for evaluating formation constants and summarizing well-field history. Transactions of the American Geophysical Union 27, 526–534.

Copty N K, Trinchero P, Sanchez-Vila X, 2011. Inferring spatial distribution of the radially integrated transmissivity from pumping tests in heterogeneous confined aquifers. Water Resources Research 47. doi:10.1029/2010WR009877|

Cornaton F J, Park Y J, Normani S D, Sudicky E A, Sykes J F, 2008. Use of groundwater lifetime expectancy for the performance assessment of a deep geologic waste repository: 1. Theory, illustrations, and implications. Water Resources Research. 44, W04407. doi:10.1029/2007WR006212

Darcel C, Le Goc R, Davy P, 2013. Development of the statistical fracture domain methodology – application to the Forsmark site. SKB R-13-54, Svensk Kärnbränslehantering AB.

Day-Lewis F D, Hsieh P A, Gorelick S M, 2000. Identifying fracture-zone geometry using simulated annealing and hydraulic-connection data. Water Resources Research 36, 1707–1721.

Dershowitz W S, Herda H H, 1992. Interpretation of fracture spacing and intensity. In Tillerson J R, Wawersik W (eds). Proceedings of the 33th U.S. Symposium on Rock (USRMS), Santa Fe, New Mexico, 3–5 June 1992. Rotterdam: Balkema, 757–766.

Dershowitz W, Doe T, Uchida U, Hermanson J, 2003. Correlations between fracture size, transmissivity, and aperture. In Culligan P, Einstein H, Whittle A (eds). Soil Rock America: Proceedings of the 39th US Rock Mechanics Symposium. VGE, Essen, 887–891.

Dershowitz W, Lee G, Josephson N, 2007. FracMan interactive discrete feature data analysis, geometric modeling,and exploration simulation. User documentation, Version 7. Seattle: Golder Associates Inc.

Diersch H-J G, 2005a. FEFLOW: finite element subsurface flow and transport simulation system. Reference manual. Berlin: WASY GmbH Institute for Water Resources Planning and Systems Research.

Diersch H-J G, 2005b. Discrete feature modeling of flow, mass and heat transport processes by using FEFLOW. In FEFLOW: finite element subsurface flow and transport simulation system. White Papers, Vol. 1. Berlin: WASY GmbH, 149–196.

Dietrich C R, Newsam G N, 1996. A fast and exact method for multidimensional Gaussian stochastic simulations: extension to realizations conditioned on direct and indirect measurements. Water Resources Research 32, 1643–1652.

Doherty J, 2004. PEST: Model-Independent Parameter Estimation, user manual. 5th ed. Brisbane: Watermark Numerical Computing.

Donaldo L D, Sánchez-Vila X, Ruiz E, Elorza F J, Bajos C, Vela-Guzman A, 2006. Calibration of hydraulic and tracer tests in fractured media represented by a DFN model. IAHS-AISH Publication 304, 87–92.

Dorn C, Linde N, Le Borgne T, Bour O, Klepikova M, 2012. Inferring transport characteristics in a fractured rock aquifer by combining single-hole ground-penetrating radar reflection monitoring and tracer test data. Water Resources Research 48. doi:10.1029/2011WR011739

Doughty C, Uchida M, 2003. Äspö Hard Rock Laboratory. Äspö Task Force. PA calculations for feature A with third-dimension structure 654 based on tracer test calibration. SKB IPR-04-33, Svensk Kärnbränslehantering AB.

Doughty C, Takeuchi S, Amano K, Shimo M, 2004. Application of Multi-rate Flowing Fluid Electric Conductivity Logging Method to Well DH-2, Tono Site, Japan. Water Resources Research 41. doi:10.1029/2004WR003708

Dyke C G, Wu B, Milton-Tayler D, 1995. Advances in characterising natural fracture permeability from mud log data. Society of Petroleum Engineers, SPE-25022-PA. doi:10.2118/25022-PA

Elsworth D, Doe T W, 1986. Application of non-linear flow laws in determining rock fissure geometry from single borehole pumping tests. International Journal of Rock Mechanics and Mining Sciences & Geomechanics Abstracts 23, 245–254.

Enachescu C, Frieg B, Wozniewicz J, 2004. A new visual synthesis tool for transient test data. In Proceedings of NGWA Conference, Portland, Maine 13–15 September,. 173–184.

Evensen G, 1994. Sequential data assimilation with a nonlinear quasi-geostrophic model using Monte-Carlo methods to forecast error statistics. Journal of Geophysical Research 99, 10143–10162.

Finsterle S, Lanyon B, Åkesson M, Baxter S, Bergström M, Bockgård N, Dershowitz W, Dessirier B, Frampton A, Frannson Å, Gens A, Gylling B, Hančilová I, Holton D, Jarsjö J, Kim J-S, Kröhn K-P, Malmberg D, Pulkkanen V M, Sawada A, Sjöland A, Svensson U, Vidstrand P, Viswanathan H, 2018. Conceptual uncertainties in modelling the interaction between engineered and natural barriers of nuclear waste repositories in crystalline rocks. London: Geological Society. (Special Publications 482)

Fischer P, Jardani A, Lecoq N, 2018. Hydraulic tomography of discrete networks of conduits and fractures in a karstic aquifer by using a deterministic inversion algorithm. Advances in Water Resources 112, 83–94.

Follin S, Levén J, Hartley L, Jackson P, Joyce S, Roberts D, Swift B, 2007. Hydrogeological characterisation and modelling of deformation zones and fracture domains, Forsmark modelling stage 2.2. SKB R-07-48, Svensk Kärnbränslehantering AB.

Follin S, Hartley L, Rhén I, Jackson P, Joyce S, Roberts D, Swift B, 2014. A methodology to constrain the parameters of a hydrogeological discrete fracture network model for sparsely fractured crystalline rock, exemplified by data from the proposed high-level nuclear waste repository site at Forsmark, Sweden. Hydrogeology Journal, 22, 313–331.

Frampton A, 2010. Stochastic analysis of fluid flow and tracer pathways in crystalline fracture networks. PhD thesis. KTH Royal Institute of Technology, Stockholm.

Frampton A, Cvetkovic V, 2007. Upscaling particle transport in discrete fracture networks: 2. Reactive tracers. Water Resources Research 43, W10429. doi:10.1029/m 2006WR005336

Frampton A, Gotovac C, Holton D, Cvetkovic V, 2015. Äspö Task Force on modelling of groundwater flow and transport of solutes. Task 7 – Subsurface flow and transport modelling of hydraulic tests and in situ borehole flow measurements conducted at Olkiluoto Island. SKB P-13-42, Svensk Kärnbränslehantering AB.

Fransson Å, Tsang C-F, Rutqvist J, Gustafson G, 2010. Estimation of de-formation and stiffness of fractures close to tunnels using data from single-hole hydraulic testing and grouting. International Journal of Rock Mechanics and Mining Sciences 47, 887–893.

Gascoyne M, Ross D, Watson R L, 1988. Geochemical and isotopic characterisation of flow in fractured plutonic rocks: Examples from the Canadian Shield. In Hitchon B, Bachu S (eds). Fluid flow, heat transfer and mass transport in fractured rocks: proceedings of 4th Canadian-American Conference on Hydrogeology, Banff, Canada, 21–24 June, 1988. National Water Well Association.

Gómez-Hernández J J, Wen X-H, 1998. To be or not to be multi-Gaussian? A reflection on stochastic hydrogeology. Advances in Water Resources 21, 47–61.

Gotovac H, 2009. A multi-resolution approach for modeling flow and solute transport in heterogeneous porous media. PhD thesis. KTH Royal Institute of Technology, Stockholm.

Gotovac H, Cvetkovic V, Andričević R, 2009a. Adaptive Fup multi-resolution approach to flow and advective transport in highly heterogeneous porous media: Methodology, accuracy and convergence. Advances in Water Resources 32, 885–905

Gotovac H, Cvetkovic V, Andričević R, 2009b. Flow and travel time statistics in highly heterogeneous porous media. Water Resources Research 45. doi:10.1029/2008WR007168

Graf T, Therrien R, 2007. A method to discretize non-planar fractures for 3D subsurface flow and transport simulations. International Journal for Numerical Methods in Fluids 56, 2069–2090.

Gustafson G, 2012. Hydrogeology for rock engineers. Stockholm: BeFo.

Gustafson G, Gylling B, Selroos J-O, 2009. The Äspö Task Force on groundwater flow and transport of solutes: bridging the gap between site characterization and performance assessment for radioactive waste disposal in fractured rocks. Hydrogeology Journal 17, 1031–1033.

Hartley L, Holton D, 2008. CONNECTFLOW Release 9.5, Technical summary document. Didcot, UK: Harwell IBC.

Hill M C, 2000. Methods and guidelines for effective model calibration. In Hotchkiss R H (ed). Proceedings of 2000 Joint Conference on Water Resource Engineering and Water Resources Planning and Management. American Society of Civil Engineers.

Hodgkinson D, 2007. Äspö Task Force on modelling of groundwater flow and transport of solutes. Review of Tasks 6D, 6E, 6F and 6F2. SKB TR-07-03, Svensk Kärnbränslehantering AB.

Illman W, Liu X, Takeuchi S, Yeh T-C J, Ando K, Saegusa H, 2009. Hydraulic tomography in fractured granite: Mizunami Underground Research site, Japan. Water Resources Research 45. doi:10.1029/2007WR006715

Ji S, Ko N, Koh Y, Choi J, 2010. The influence of boreholes on the regional scale groundwater flow in a fractured rock. AGU Fall Meeting Abstracts, 1074.

Jódar J, Alcolea A, Medina A, 2000. Geostatistical inversion of flow and transport parameters. The Grimsel Test Site. In Bjerg P L, Engesgaard P, Krom T D (eds). Groundwater 2000: proceedings of the International Conference on Groundwater Research, Copenhagen, Denmark, 6–8 June 2000. Rotterdam: Balkema.

Juhlin C S, Wallroth T, Smellie J, Eliasson T, Ljunggren C, Leijon B, Beswick J, 1998. The very deep hole concept – geoscientific appraisal of conditions at great depth. SKB TR 98-05, Svensk Kärnbränslehantering AB.

Keto V, Koskinen L, 2009. Äspö Hard Rock Laboratory. Äspö Task Force on modelling of groundwater flow and transport of solutes – Task 7A: Subtask 7A1. SKB ITD-09-06, Svensk Kärnbränslehantering AB.

Kawanishi M, Tanaka Y, Igarashi T, 1994. Development of performance assessment method on natural barrier system for geological disposal of HLW(I): Analysis model for groundwater flow in fractured rocks. CRIEPI Report U93054. (In Japanese.)

Klepikova M V, Le Borgne T, Bour O, De Dreuzy J-R, 2013. Inverse modeling of flow tomography experiments in fractured media. Water Resources Research 49, 7255–7265.

Klockars J, Vaittinen T, Ahokas H, 2006. Hydraulic crosshole interference tests at Olkiluoto, Eurajoki in 2004 boreholes KR14–KR18 and KR15B–KR18B. Posiva Working Report 2006-01, Posiva Oy, Finland.

Knudby C, Carrera J, 2006. On the use of apparent hydraulic diffusivity as an indicator of connectivity. Journal of Hydrology 329, 377–389.

Ko N-K, Ji S-H, Koh Y-K, 2010. Evaluation of groundwater flow modeling including background fractures in a fractured rock domain. Abstracts of proceeding of the Korean Radioactive Waste Society (Spring) 8, 141–142. (In Korean).

Ko N Y, Ji S H, 2017. Äspö Task Force on modelling of groundwater flow and transport of solutes. Hierarchical modelling of groundwater flow at Okiluoto site by KAERI: Uncertainty and lessons. SKB P-13-47, Svensk Kärnbränslehantering AB.

Ko N-Y, Ji S-H, Koh Y-K, Choi J-W, 2012. Consideration of boreholes in modeling of the regional-scale groundwater flow in a fractured rock. Engineering Geology 149–150, 13–21.

Kosack C, Vogt C, Rath V, Marquart G, 2010. Stochastic estimates of the permeability field of the Soultz-sous-Forêts Geothermal Reservoir – Comparison of Bayesian Inversion , MC Geostatistics, and EnKF Assimilation. EGU General Assembly Conference Abstracts 2010.

Koskinen L, Rouhiainen P, 2007. Interconnected flow measurement between boreholes using a borehole flowmeter. In Krásný J, Sharp J (eds). Groundwater in fractured rocks: selected papers from the Groundwater in Fractured Rocks International Conference, Prague, 2003. London: Taylor & Francis, 423.

Krumenacker F M, Keto V, Koskinen L, 2017. Äspö Task Force on modelling of groundwater flow and transport of solutes Task 7 – Assessing the significance of flow data in Model Structure Identification. SKB P-13-45, Svensk Kärnbränslehantering AB.

Lambe T W, 1973. Prediction in soil engineering. Géotechnique 23, 151–202.

Lanyon G W, Marschall P, Vomvoris S, Jaquet O, Mazurek M, 1998. Effective property determination for input to a geostatistical model of regional groundwater flow: Wellenberg T–K. In Characterization and evaluation of sites for deep geological disposal of radioactive waste in fractured rocks. Proceedings from The 3rd ÄSPÖ International Seminar Oskarshamn, June 10–12, 1998. SKB TR-98-10, Svensk Kärnbränslehantering AB, 201–212.

Larsson M, Niemi A, Tsang C-F, 2012. A study of flow-wetted surface area in a single fracture as a function of its hydraulic conductivity distribution. Water Resources Research, 48. doi:10.1029/2011WR010686

Le Borgne T, Bour O, de Dreuzy J R, Davy P, Touchard F, 2004. Equivalent mean flow models for fractured aquifers: Insights from a pumping test scaling interpretation. Water Resources Research 40. doi:10.1029/2003WR002436

Le Borgne T, Bour O, Paillet F L, Caudal J-P, 2006. Assessment of preferential flow path connectivity and hydraulic properties at single-borehole and cross-borehole scales in a fractured aquifer. Journal of Hydrology 328, 347–359.

Le Borgne T, Bour O, Riley M, Gouze P, Pezard P A, Belgouhl A, Lods G, Le Provost R, Greswell R, Ellis P A, Isakov E, Last B, 2007. Comparison of alternative methodologies for identifying and characterizing preferential flow paths in heterogeneous aquifers. Journal of Hydrology 345, 134–148.

Lee H S, Cho T F, 2002. Hydraulic characteristics of rough fractures in linear flow under normal and shear load. Rock Mechanics and Rock Engineering 35, 299–318.

Le Goc R, de Dreuzy J R, Davy P, 2010. Statistical characteristics of flow as indicators of channeling in heterogeneous porous and fractured media. Advances in Water Resources 33, 257–269.

Leskinen N, Ronneteg U, 2011. Tillverkning av kapselkomponenter. SKBdoc 1175208 ver 5.0, Svensk Kärnbränslehantering AB. (In Swedish.)

Libby S, Hartley L, Turnbull R, Cottrell M, Bym T, Josephson N, Munier R, Selroos J-O, Mas Ivars D, 2019. Grown Discrete Fracture Networks: a new method for generating fractures according to their deformation history. In 53rd US Rock Mechanics/Geomechanics Symposium. New York, June 2019.

Ludvigson J-E, Hansson K, Rouihainen P, 2002. Methodology study of Posiva difference flow meter in borehole KLX02 at Laxemar. SKB R-01-52, Svensk Kärnbränslehantering AB.

Lusczynski N J, 1961. Head and flow of ground water of variable density. Journal of Geophysical Research 66, 4247–4256.

Löfman J, Mészáros F, 2013. FEFTRA™. Verification – Update 2013. Posiva Working Report 2013-60, Posiva Oy, Finland.

Mardia K V, Nyirongo V B, Walder A N, Xu C, Dowd P A, Fowell R J, Kent J T, 2007. Markov Chain Monte Carlo implementation of rock fracture modelling, Mathematical. Geology 39, 355–381.

Marschall P, Lunati I (eds), 2006. GAM – Gas migration experiments in a heterogeneous shear zone of the Grimsel Test Site. Nagra Technical Report 03-11, Nagra, Switzerland..

Matthäi S K, Belayneh M, 2004. Fluid flow partitioning between fractures and a permeable rock matrix. Geophysical Research Letters 31. doi:10.1029/2003GL019027

Meier P M, Sánchez-Vila X, Carrera J, 1997. Study of transient constant rate pumping tests in heterogeneous media. In Pointet T (ed). Hard rock hydrosystems. Wallingford: International Association of Hydrological Sciences. (IAHS Publication 241), 135–142.

Meier P M, Carrera J, Sanchez-Vila X, 1998. An evaluation of Jacob's method for the interpretation of pumping tests in heterogeneous formations. Water Resources Research 34, 1011–1025.

Meier P M, Medina A, Carrera J, 2001. Geostatistical inversion of cross-hole pumping tests for identifying preferential flow channels within a shear zone. Groundwater 39, 10–17.

Molz F J, Morin R H, Hess A E, Melville J G, Güven O, 1989. The Impeller Meter for measuring aquifer permeability variations: Evaluation and comparison with other tests. Water Resources Research 25, 1677–1683.

Mourzenko V V, Thovert J-F, Adler P M, 2009. Macroscopic properties of polydisperse, anisotropic and/or heterogeneous fracture networks. In Proceedings of the International Conference on Rock Joints and Jointed Rock Masses, Tucson, Arizona, 7–8 January 2009.

National Research Council, 1996. Rock fractures and fluid flow: contemporary understanding and applications. Washington, DC:National Academy.

Nordqvist A W, Tsang Y W, Tsang C-F, Dverstorp B, Andersson J, 1992. A variable aperture fracture network model for flow and transport in fractured rocks. Water Resources Research 28, 1703–1713.

Oda M, 1985. Permeability tensor for discontinuous rock masses. Géotechnique 35, 483–495.

Oliver D S, 1993. The influence of nonuniform transmissivity and storativity on drawdown. Water Resources Research 29, 169–178.

Paillet F L, 1995. Using borehole flow logging to optimize hydraulic-test procedures in heterogeneous fractured aquifers. Hydrogeology Journal 3, 4–20.

Paillet F L, 1998. Flow modeling and permeability estimation using borehole flow logs in heterogeneous fractured formations. Water Resources Research 34, 997–1010.

Paillet F L, 2000. A field technique for estimating aquifer parameters using flow log data. Groundwater 38, 510–521.

Paillet F L, 2004. Geophysical characterization of fractured rock aquifers : Accounting for scale effects and putting hydrology in the geophysics. In Proceedings of U.S. EPA/NGWA Fractured Rock Conference: State of the Science and Measuring Success in Remediation, Portland, Maine, 13–15September 2004, 14–26.

Park Y-J, Sudicky E A, McLaren R G, Sykes J F, 2004. Analysis of hydraulic tracer response tests within moderately fractured rock based on a transition probability approach. Water Resources Research 48. doi:10.1029/2004WR003188

Pekkanen J, 2009a. difference flow measurements in ONKALO at Olkiluoto, drillholes ONK-PP122–ONK-PP124, ONK-PP126, ONK-PP128, ONK-PP131, ONK-PP134 and ONK-PP137. Posiva Working Report 2009-04, Posiva Oy, Finland.

Pekkanen J, 2009b. Difference flow measurements and hydraulic interference test in ONKALO at Olkiluoto, drillholes ONK-PP125, ONK-PP127 and ONK-PP129. Posivs Working Report 2009-40, Posiva Oy, Finland.

Pekkanen J, Pöllänen J, 2008. Flow and electrical conductivity measurements during long-term pumping of drillhole OL-KR6 at Olkiluoto, Results from the time period between May 2006 and April 2007. Posiva Working Report 2008-20, Posiva Oy, Finland.

Pickens J-F, Grisak G E, Avis J D, Belanger D W, Thury M, 1987. Analysis and interpretation of borehole hydraulic tests in deep boreholes: Principles, model development, and applications. Water Resources Research 23, 1341–1375.

Posiva, 2012. Olkiluoto site description 2011. Posiva 2011-02, Posiva Oy Finland.

Poteri A, Billaux D, Dershowitz B, Gómez-Hernández J J, Cvetkovic V, Hautojärvi A, Holton D, Medina A, Winberg A (ed), 2002. Final report TRUE Block Scale project. 3. Modelling of flow and transport. SKB TR-02-15, Svensk Kärnbränslehantering AB.

Priest S D, 1993. Discontinuity analysis for rock engineering. London: Chapman & Hall.

Pöllänen J, Rouhiainen P, 2002a. Difference flow and electric conductivity measurements at the Olkiluoto site in Eurajoki, boreholes KR13 and KR14. Posiva Working Report 2001-42, Posiva Oy, Finland.

Pöllänen J, Rouhiainen P, 2002b. Difference flow and electric conductivity measurements at the Olkiluoto site in Eurajoki, boreholes KR15–KR18 and KR15B–KR18B. Posiva Working Report 2002-29, Posiva Oy, Finland.

Rasmussen T C, Haborak K G, Young M H, 2003. Estimating aquifer hydraulic properties using sinusoidal pumping at the Savannah River site, South Carolina, USA. Hydrogeology Journal 11, 466–482.

Raven K G, Gale J E, 1986. A study of the surface and subsurface structural and groundwater conditions at selected underground mines and excavations. Atomic Energy of Canada Technical Report TR-17, Whiteshell Laboratories: Pinnawa, Manitoba.

Remy N, Boucher A, Wu J, 2009. Applied geostatistics with SGeMS: a user's guide. Cambridge: Cambridge University Press.

RETROCK, 2005. Treatment of radionuclide transport in geosphere within safety assessments (RETROCK). Final report.. EUR 21230, European Commission.

Robin M J L, Gutjahr A L, Sudicky E A, Wilson J L, 1993. Cross-correlated random field generation with the direct Fourier transform method. Water Resources Research 29, 2385–2397.

Rouhiainen P, 2001. Posiva groundwater flow measuring techniques. In Seiler K-P; Wohnlich S (eds). New approaches characterizing groundwater flow: proceedings of the XXXI International Association of Hydrogeologists Congress, Munich, Germany, 10–14 September 2001. Lisse: A. A. Balkema, Volume 2.

Rouhiainen P, Pöllänen J, 2003. Hydraulic crosshole interference tests at the Olkiluoto site in Eurajoki, boreholes KR14–KR18 and KR15B–KR18B. Eurajoki, Finland. Posiva Working Report 2003-30, Posiva Oy, Finland.

Rutqvist J, 2016. Fractured rock stress–permeability relationships from in situ data and effects of temperature and chemical-mechanical couplings. In Gleeson T, Ingerbritse S E (eds). Crustal permeability. Wiley, 65–82.

Sánchez-Vila X, Meier P M, Carrera J, 1999. Pumping tests in heterogeneous aquifers: An analytical study of what can be obtained from their interpretation using Jacob's method. Water Resources Research 35, 943–952.

Sanderson D J, Nixon C W, 2015. The use of topology in fracture network characterization. Journal of Structural Geology 72, 55–66.

Sawada A, Skamoto K, Dershowitz W S, 2015. Äspö Task Force on modelling of groundwater flow and transport of solutes. Task 7 – Groundwater flow and transport modelling of fracture system at regional, block, and single-fracture scale flow and transport, Olkiluoto. SKB P-13-46, Svensk Kärnbränslehantering AB.

Schneeberger R, Egli D, Lanyon G W, Mäder U K, Berger A, Kober F, Herwegh M, 2018. Structural-permeability favorability in crystalline rocks and implications for groundwater flow paths: a case study from the Aar Massif (central Switzerland). Hydrogeology Journal 26, 2725–2738.

Sena C, Grandia F, Arcos D, Molinero J, Duro L, 2008. Complementary modelling of radionuclide retention in the near-surface system at Forsmark. Development of a reactive transport model using Forsmark 1.2 data. SKB R-08-107, Svensk Kärnbränslehantering AB.

Somogyvári M, Jalali M, Jimenez Parras S, Bayer P, 2017. Synthetic fracture network characterization with transdimensional inversion. Water Resources Research 53, 5104–5123.

Streltsova T D, 1987. Well testing in heterogeneous formations. New York: Wiley.

Stober I, 1996. Researchers study conductivity of crystalline rock in proposed radioactive waste site. Eos 77, 93–94.

Stumpf M P H, Porter M A, 2012. Critical truths about power laws. Science 335, 665–666.

Svensson U, 2010. DarcyTools version 3.4 – Verification, validation and demonstration. SKB R-10-71, Svensk Kärnbränslehantering AB.

Svensson U, 2015. Äspö Task Force on modelling of groundwater flow and transport of solutes. Task 7 – The numerical modelling of pump tests at the Olkiluoto site. SKB P-13-43, Svensk Kärnbränslehantering AB.

Svensson U, Ferry M, Kuylenstierna H-O, 2010. DarcyTools version 3.4 – Concepts, methods and equations. SKB R-07-38, Svensk Kärnbränslehantering AB.

Terzaghi R D, 1965. Sources of error in joint surveys. Géotechnique 15, 287–304.

Tetsu K, Sawada A, 2010. Study of natural fracture topography and fracture aperture distribution in 50 cm scale granitic rock block measured by a precision grinder. JAEA-Research 2010-041, Japan Atomic Energy Agency. (In Japanese.)

Theis C V, 1935. The relation between the lowering of the Piezometric surface and the rate and duration of discharge of a well using ground water storage. Eos, Transactions American Geophysical Union 16, 519–524.

Therrien R, Blessent D, 2017. Äspö Task Force on modelling of groundwater flow and transport of solutes: Task 7 – Reduction of performance assessment uncertainty through modelling of hydraulic tests at Olkiluoto. SKB P-13-44, Svensk Kärnbränslehantering AB.

Therrien R, Sudicky E A, McLaren R G, Panday S M, 2005. HydroGeoSphere: a three-dimensional numerical model describing fully-integrated subsurface and surface flow and solute transport. User's guide. Waterloo, Canada: Groundwater Simulations Group.

Therrien R, Sudicky E A, McLaren R G, Panday S M, 2009. HydroGeoSphere: a three-dimensional numerical model describing fully-integrated subsurface and surface flow and solute transport. User's guide. Waterloo, Canada: Groundwater Simulations Group.

Thury M, Gautchi A, Müller W H, Vomvoris S, Mazurek M, Naef H, Pearson F J, Wilson W, 1994. Geology and hydrogeology of the crystalline basement of Northern Switzerland. Synthesis of regional investigations 1981–1993 with the Nagra radioactive waste disposal programme. Nagra 93-01, Nagra, Switzerland.

Trinchero P, Sánchez-Vila X, Fernàndez-Garcia D, 2008. Point-to-point connectivity, an abstract concept or a key issue for risk assessment studies? Advances in Water Resources 31, 1742–1753.

Tsai C-S, Yeh H-D, 2012. Wellbore flow-rate solution for a constant-head test in two-zone finite confined aquifers. Hydrological Processes 26, 3216–3224.

Tsang C-F, Hufschmied P, Hale F V, 1990. Determination of fracture inflow parameters with a borehole fluid conductivity logging method. Water Resources Research 26, 561–578.

Tsang C-F, Neretnieks I, Tsang Y, 2015. Hydrologic issues associated with nuclear waste repositories Chin-Fu. Water Resources Research 51, 6923–6972.

Tso C-H M, Zha Y, Yeh T-C J, Wen J-C, 2016. The relative importance of head, flux, and prior information in hydraulic tomography analysis. Water Resources Research 52, 3–20.

Vaittinen T, Ahokas H, Heikkinen E, Hellä P, Nummela J, Saksa P, Tammisto E, Paulamäki S, Paananen M, Front K, Kärki A, 2003. Bedrock model of the Olkiluoto site, version 2003/1. Posiva Working Report 2003-43, Posiva Oy, Finland.

Vaittinen T, Ahokas H, Nummela J, 2009. Hydrogeological structure model of the Olkiluoto site – Update in 2008. Posiva Working Report 2009-15, Posiva Oy, Finland.

Vidstrand P (ed), Ahokas H, Bockgård N, Dershowitz B, Holton D, Lanyon B, Poteri A, Koskinen L, 2015. SKB Task Force GWFTS – Task 7. Descriptions for hydrogeological modelling of Olkiluoto, Finland. Compilation of all task descriptions assessed within the Task 7 of the SKB Task Force on modelling of groundwater flow and transport of solutes. SKB P-12-21, Svensk Kärnbränslehantering AB.

Vilarrasa V, Koyama T, Neretnieks I, Jing L, 2010. Shear-induced flow channels in a single rock fracture and their effect on solute transport. Transport in Porous Media 87, 503–523.

Väisäsvaara J, 2009. Transverse flow measurements at the Olkiluoto site in Eurajoki, drillholes OL-KR15, -KR15B, -KR16B, -KR17B, and -KR18. Posiva Working Report 2009-23, Posiva Oy, Finland.

Walker D D, Roberts R M, 2003. Flow dimensions corresponding to hydrogeologic conditions. Water Resources Research 39. doi:10.1029/2002WR001511

Walker D D, Cello P A, Valocchi A J, Loftis B, 2006. Flow dimensions corresponding to stochastic models of heterogeneous transmissivity. Geophysical Research Letters 33. doi:10.1029/2006GL025695

Wang X, 2005. Stereological interpretation of rock fracture traces on borehole walls and other cylindrical surfaces. PhD thesis. Virginia Polytechnic Institute and State University.

Wen J-C, Chen J-L, Yeh T-C J, Wang Y-L, Huang S-Y, Tian Z, Yu C-Y, 2020. Redundant and non-redundant information for model calibration or hydraulic tomography. Groundwater 58, 79–92.

Williams J H, Paillet F L, 2002. Using flowmeter pulse tests to define hydraulic connections in the subsurface: a fractured shale example. Journal of Hydrology 265, 100–117.

Winberg A, Andersson P, Byegård J, Poteri A, Cvetkovic V, Dershowitz B, Doe T, Hermanson J, Gómez-Hernández J J, Hautojärvi A, Billaux D, Tullborg E-L, Holton D, Meier P, Medina A, 2003. Final report of the TRUE Block Scale Project. 4. Synthesis of flow, transport and retention in the block scale. SKB TR-02-16, Svensk Kärnbränslehantering AB.

Witherspoon P A, Wang J S, Iwai K, Gale J E, 1980. Validity of cubic law for fluid flow in a deformable rock fracture. Water Resources Research 16, 1016–1024.

Wu C-M, Yeh T-C J, Zhu J, Lee T H, Hsu N-S, Chen C-H, Sancho A F, 2005. Traditional analysis of aquifer tests: Comparing apples to oranges? Water Resources Research 41. doi:10.1029/2004WR003717

Yeh H-D, Wang C-T, 2007. Large-time solutions for groundwater flow problems using the relationship of small *p* versus large *t*. Water Resources Research 43. doi:10.1029/2006WR005472

Yeo I W, de Freitas M H, Zimmerman R, 1998. Effect of shear displacement on the aperture and permeability of a rock fracture. International Journal of Rock Mechanics and Mining Sciences 35, 1051–1070.

Zha Y, Yeh T-C J, Mao D, Yang J, Lu W, 2014. Usefulness of flux measurements during hydraulic tomographic survey for mapping hydraulic conductivity distribution in a fractured medium. Advances in Water Resources 71, 162–176.

Zhou H, Gómez-Hernández J J, Li L, 2014. Inverse methods in hydrogeology: Evolution and recent trends. Advances in Water Resources 63, 22–37.

Zimmerman R W, Al-Yaarubi A, Pain C C, Grattoni C A, 2004. Non-linear regimes of fluid flow in rock fractures. International Journal of Rock Mechanics and Mining Sciences 41 Suppl. 1, 163–169.

Zinn B, Harvey C F, 2003. When good statistical models of aquifer heterogeneity go bad: a comparison of flow, dispersion, and mass transfer in connected and multivariate Gaussian hydraulic conductivity fields. Water Resources Research 39. doi:10.1029/2001WR001146

Öhman J, Follin S, 2010. Site investigation SFR. Hydrogeological modelling of SFR Model version 0.2. SKB R-10-03, Svensk Kärnbränslehantering AB.

Appendix A

Modellers' task evaluation taken from questionnaires distributed to all modelling groups

	CRIEPI	JAEA/Golder	NWMO/Laval	SKB/CFE	SKB/KTH	Posiva/VTT
Numerical codes used (name and version)	FegmB_II,version 0.11	FracMan/MAFIC	HydroGeoSphere, revision 587M (extended version of the FRAC3DVS model)	DarcyTools	Napsac v9.3 and v9.4	FEFTRA
Answers provided by (name, phone, e-mail)	Yasuharu Tanaka	Atsushi Sawada	Rene Therrien	Urban Svensson	Andrew Frampton	Vesa Keto,

Table A-1. Boundary conditions.

	CRIEPI	JAEA/Golder	NWMO/Laval	SKB/CFE	SKB/KTH	Posiva/VTT
How did you treat the model top surface boundary?	Land: specified head (in SS01 and SS02a), seepage-face type boundary (in other simulation cases) Sea: static pressure Groundwater recharge was assumed to be 5 mm/year in the simulations of SS03 and SS04a and 80 mm/year in the simulations of SS02b, SS02c, SS04b, TR01, TR02a and PA01.	Infiltration at the ground surface, constant head = 0 (EL) at Baltic sea	The elevation of the top of the model is the interpolated surface topography. A 1st-type boundary condition is used for the top nodes, with the head equal to the interpolated groundwater table.	Free surface with net recharge (P-E)	Head = elevation (using surface topography file topo2.zip).	For natural conditions, the long term mean of the gw-table was specified as fixed head boundary condition. When solving for drawdown, no-flow boundary condition was set over the land area of the surface, which implies that the natural recharge rate and spatial distribution of recharge through the surface must not change due to pumping.
How did you treat the model side boundaries?	Specified head boundaries, sea elevation	No flow	A 1st-type boundary condition is used for the side boundaries. The head (h) is equal to the interpolated groundwater table at the boundaries, which is equal to 0 (sea elevation)	Hydrostatic	Head = 0 metres	Fixed head boundary condition/no drawdown boundary condition.
How did you treat the model bottom boundary?	Impermeable boundary	No flow	No flow	Zero flux	No flow	No-flow boundary condition (impermeable)
How did you treat the KR24 pumping borehole?	Option 1 in ”Task description for Task 7A Version 3.0”. We used 5.5E−6 m^3/s as the hydraulic conductance of the by-pass pipe in the simulation of SS02a, SS03, SS04a, SS04b, TR01 and TR02a. But we used 6.1E−5 m^3/s as the hydraulic conductance in the simulations of SS02b and SS02c. The value of 5.5E−6 m^3/s was recommended in Data Delivery Task 7/8d. On the other hand, the value of 6.1E−5 m^3/s was estimated on the basis of Poiseuille’s formula.	Model as constant flux boundary at pumping rate	For the upper part (ground surface to z = −75 m) we impose a flow rate Q = 12.5 l/min. For the lower part (−541.32 m < z < −75 m), we impose a flow rate Q = 5.5 l/min	Prescribed flow in two sections	Two approaches: (1) KR24 as three connected BHs with 2 mm radius for centre section, pumping then applied to top part only with Q = 18 l/min; (2) KR24 as two disconnected Bhs, two pumping rates then applied, top part Q = 12.5 l/min, bottom part Q = 5.5 l/min	Specified outflow rate of 5.5 l/min at the lower section KR24_L1 and 12.5 l/min at KR24_L2 (Option 2). During calibration phase the flowrate at KR24_L2 was altered.

	CRIEPI	JAEA/Golder	NWMO/Laval	SKB/CFE	SKB/KTH	Posiva/VTT
How did you use the salinity information?	We used the salinity information to correct the data in ”fresh water head table.xls”.	Not modeled (considered)	The salinity information is currently not used. We assume constant density for the simulations and haven’t simulated solute transport.	Not used	Have not used in current models.	neglected
How did you use the groundwater table information?	We used ”fresh water head table.xls” to compare with calculated results and calibrate input data.	Compare with steady state flow simulation results, qualitatively.	Interpolated groundwater table used to specify 1st-type boundary conditions for all nodes at the top of the model.	Only qualitative comparison	Have not used in current models.	The long term mean was used as boundary condition over the land area of the surface when calculating the steady-state flow field of the natural conditions.

Table A-2. Data usage: structures.

	CRIEPI	JAEA/Golder	NWMO/Laval	SKB/CFE	SKB/KTH	Posiva/VTT
How did you define the fracture zone geometry and what input did you use? Fracture zone positions (.sat, 3dface and dxf files)	3dface		We incorporated the following 13 fracture zones HZ001, HZ002, HZ003, HZ004, HZ19A, HZ008, HZ19C, HZ20A, HZ20AE, HZ20B_ALT, HZ21, HZ21B, BFZ099. We used the triangulated data provided in the Data Deliveries to represent the geometry of the fracture zones. We developed a method to import the triangulated geometry data into the model, to represent the fracture zones are series of 2D triangular and rectangular elements.	Large scale fractures. Input file for positions used as given. Fracture zones assumed very thin.	Used the files “largeFaces.txt” (= 3dface) when large version exist, and “smallFaces.txt” when only small versions exist. The given format is a CAD format which defines the fracture zones as collections of triangular features. Wrote a code which translates these into the Gocad Tsurf format which can be used by Napsac, as a ”transmissive feature”. Then converted the transmissive features to internal Napsac format (using the soft-ware’s built-in capabilities) which defined fractures as rectangles. That is, the fractures used are rectangular approximations of the given triangular format.	Extracted the information from .sat files.
Which documents did you use in building the structural model? (Bedrockmodel_2003-1, structure-memo…)	Nothing special	LargeFace4.dfx (HZ004, 008, 19A, 19C, 20A, 20B_ ALT, 21, 21B, BFZ099,) and SmallFace4.dxf (HZ001, 002, 003, 20AE) files were used directly	We used a combination of the Task Description documents, geometry of the zones (zones. zip – Data Delivery 8) and bedrock model.	Promemoria 2007-01-31 and Task 7A Version 2.2b	Current (preliminary) model setup is without additional structurs/features. However, have defined the lateral sides of the model domain using the structures known as “hydraulic conductors in contact with the Baltic Sea”, ie the files ”boundaries.txt”.	structure-memo

Table A-3. Data usage: boreholes.

	CRIEPI	JAEA/Golder	NWMO/Laval	SKB/CFE	SKB/KTH	Posiva/VTT
What data source did you use for borehole positions and properties (borehole-xyz /*.pth files?)	We used borehole-xyz/*.pth files for borehole positions and estimated the hydraulic conductance of boreholes on the basis of Poiseuille's formula.		We used the *.pth files. We model the boreholes as 1D line elements and included open boreholes KR04, KR06, KR07, KR08, KR10, KR14, KR22, KR24, KR27, KR28 (upper and lower parts) and packed-off intervals for boreholes KR09 (3 intervals), KR12 (1 interval), KR23 (1 interval), KR25 (4 intervals)	*.pth files	Combination of .pth files and Table 6 in PDF document "Task 7A version 2.2b". Table 6 gives the distance along the borehole to the packed off sections (section up and down) or to the bottom of the borehole caseings. The .pth files give borehole (x,y,z) coordinates as well as the borehole distance at each such coordinate. Thus, to obtain the correct coordinates corresponding to "section up" and "section down" for each borehole or borehole section, I interpolated between the two nearest (x,y,z) coordinates in the corresponding .pth file (one interpolation for "section up" and another for "section down"). Only additional property used to define simulated boreholes is the borehole radius, this was obtained in file "OL_borehole_info_240305_kf-rev-090605.xls" (data delivery 4a).	Positions from the *.pth -files. The conductance of the bar elements was set to K=1.0m^3/s (increasing still did not change results).

Table A-4. Data usage: Hydraulic and transport.

	CRIEPI	JAEA/Golder	NWMO/Laval	SKB/CFE	SKB/KTH	Posiva/VTT
How did you assign transmissivity to the fracture zones? Please give data source.	Geometric mean in Table 2 of ”Task description for Task 7A Version 3.0” and transmissivities measured at intersections of the fracture zones with the boreholes in the tables of ”layot-and-flow-model-memo-draft-21-6-2006.doc”	Borehole-xyz	We used the geometric mean transmissivities for the zones, listed in the Promemoria (2007-01-31). We represent the fracture zones with 2D elements in our model and need to specify aperture rather than transmissivity. We computed the aperture by applying the cubic law with the geometric mean transmissivity.	Promemoria 2007-01-31	Constant transmissivity, using column ”Geometric mean” in Table 3 of PDF document ”Task 7A version 2.2b”.	
How did you assign storativity to the fracture zones? Please give data source.	In the simulations of TR01 and TR02a, storativities were assumed to be twice transmissivities according to ”PM_technicalsession_tf#22.doc”.		We compute the specific storage (Ss) of the fracture zones by using Ss = rho x g x beta (rho = density, g = gravity, beta = fluid compressibility). We use a value of beta = 4.4e−10 m^2/N, which is typical for fresh water and calculate Ss = 3.52e−6 m−1.	Uniform value 1.E−6 used	For transient simulations used two models: (1) S = 2T and (2) S = $0.25T^{0.74}$	S = 1e−6 and 1e−7 as an educated guess for initial simulation.
How did you assign transport properties to the fracture zones? Please give data source.	The transport aperture of each fracture zone was estimated by Doe’s law. Dispersion was not taken into consideration.		We haven’t simulated solute transport yet	Thickness = 0.01 m and given apertures define the porosity.	Used model $a\_t = 2\ T^{0.5}$, where a_t is the transport aperture and T is the fracture transmissivity.	NA
Were fracture zones treated as homogeneous or heterogeneous in terms of their hydraulic and transport properties?	In the simulations of SS01, SS02a, SS03 and SS04a, fracture zones were treated as homogeneous. On the other hand, in the simulations of SS02b, SS02c, SS04b, TR01, TR02a and PA01, transmissivities around the intersection points of the fracture zones with the boreholes were assigned on the basis of measured transmissivities in ”layot-and-flow-model-memo-draft-21-6-2006.doc”. Transmissivities of #L-zones outside the actual zones were assumed to be geometric mean in all the simulation cases.	Defined by Task 7A; Part 1 Version 3.0, table2,	We have currently assumed that the hydraulic properties are homogeneous for a given fracture zone.	Homogeneous	Homogeneous in current model	Homogeneous

	CRIEPI	JAEA/Golder	NWMO/Laval	SKB/CFE	SKB/KTH	Posiva/VTT
How did you treat the background rock within the surface layer?	Option 2 in ”Task description for Task 7A Version 3.0”. We used 2E−7 m/s as the hydraulic conductivity of the surface layer.	Not conducted transient simulations	For elevation z > −70 m, the rock matrix is discretized with 3D elements and is assumed homogeneous with K = 1e−7 m/s	A DFN was defined for the upper 80 m	As a random DFN with a constant transmissivity and an homogeneous areal density (P32 density) , such that the effective hydraulic conductivity = 1e−7 m/s. The spatial extent of the near-surface DFN is it extends horisontally over the entire domain and vertically down to a depth z > = −70 m.	Set a highly permeable layer at depths 0–80 m with unfirom conductivity K = 2e−7m/s
How did you treat the deeper background rock (absent, homogeneous, heterogeneous)?	absent	Defined by Task 7A; Part 1 Version 3.0, aperture = 2*trans-missivity$^{0.5}$	For elevation z < −70 m, the rock matrix is discretized with 3D elements and is assumed homogeneous with K = 1e−12 m/s	absent	Absent in current model	Homogeneous with low hydraulic conductivity K = 1e−11m/s.
What was the source of properties for the deeper background rock?	-	Homogeneous as basic model	No source to cite. We assume a very low hydraulic conductivity, which is practically equivalent to an impermeable matrix in the model	NA	n/a	In the Task Definition special focus on major hydraulic conductors was proposed. Hence the background was set a very low permebility.
Have you (and if so how) used the 2m test data (K2m-values-summary-rev1.xls)?	We have not used the 2m test data.	Surface is modeled as continuum block as defined by Task7ADescrip-tion_20061101. doc	No	No	No	Yes. To check that the boreholes of the model intersect zones correctly, and to construct a local zone between KR24_T2 and KR04 during calibration

Table A-5. Data usage: Measurements.

	CRIEPI	JAEA/Golder	NWMO/Laval	SKB/CFE	SKB/KTH	Posiva/VTT
Which and how did you use the head data from open boreholes (e.g. OL-KR4, KR7 etc)?	We used ”fresh water head table.xls” and the drawdown data in Table 6 of Task description for sub-task 7A Version 2.2b to compare with calculated results and calibrate input data. On this occasion, the data in ”fresh water head table.xls” was corrected on the basis of the salinity information.	NA	We used the file Open_KR_all_KRB.xls from DataDelivery 6[1] and used the hydraulic heads from before pumping (08.03.2004) to compare to simulated heads for steady-state simulations.	Only qualitative comparison, no calibration	Used these files to compare heads in each borehole which was simulated.	To check how the model matches with the field observations and as a calibration target.
Which and how did you use the head data from packed off boreholes (e.g. OL-KR1, KR23, KR25)?	We used ”fresh water head table.xls” and the drawdown data in Table 6 of Task description for sub-task 7A Version 2.2b to compare with calculated results and calibrate input data. On this occasion, the data in ”fresh water head table.xls” was corrected on the basis of the salinity information.	NA	We haven’t yet compared simulated heads with heads in the packed off boreholes	See above	Used all three files. Compared heads in each borehole section T8, T7, ..., T1 with corresponding simulated borehole sections.	To check how the model matches with the field observations and as a calibration target.
Which and how did you use the open borehole flow data (KR4,KR14,KR22 etc)?	We used the open borehole flow data (KR4, KR22 and KR28) in Table 7 and 8 of Task description for sub-task 7A Version 2.2b not to calibrate input data but just to compare with calculated results.		We have done very limited and preliminary comparison of flow rates.	See above	Used all five files. Note that these files have both head and flow measurements. (Slightly confusing is the fact that head varies with depth in these open boreholes, even for the measurements without pumping.) To compare simulation SS02a, I used the time periods given in column 1 of each of these files, which is supposed to correspond to measurements before pumping in KR24. To compare simulation SS04a I used the columns with date stamps closest to the end of the pumping period.	For comparison and as a calibration target at KR04, KR22 and KR28. It should be emphasized, that the whole calibration exercise is masked by the uncertainty at KR24: there are no flow measurements at the pumped drillhole.

Table A-6. Consistency/ model verification.

	CRIEPI	JAEA/Golder	NWMO/Laval	SKB/CFE	SKB/KTH	Posiva/VTT
How have you checked the consistency of your model structure?	We have checked the intersections of the fracture zones with the boreholes.	For checking model to compare with openhole conditions	We used the various checking options included into our model (for example, detection of zero-volume elements) as well as visually checked the 3D grid and examined the output files from our pre-processor to detect any error in data input.	Realistic groundwater table. Realistic draw-downs for pumped conditions	Fracture zone geometry visual check with dxf files in CAD program. Fracture intersections with boreholes checked with Table 6.	The model structure is used as given, but most simulations were performed using both the extended (large) zones and with the local (small) zones and during calibration an addi-tional zone between KR24_T2 and KR04 was constructed.
How have you checked the consistency of your model surface boundary conditions?	We have compared the calculated heads in the boreholes under the natural condition with the measured ones, ”fresh water head table.xls”. On this occasion, the data in ”fresh water head table.xls” was corrected on the basis of the salinity information.	For checking model to compare with packed and/or non-open borehole conditions	We checked the output file generated by the model after reading the input data to ensure that the data was correctly read. We also checked the quality of the interpolated data by contouring the surface heads in a 2D mesh generator (GridBuilder) independently of our 3D simulation. Finally, we visualized the simulated heads at ground surface and visually compared with the interpolated data contoured in Gridbuilder as well as available figures (such as figure 5 – version 2.2b of the task description).	See above	The applied top surface BC is the reference case scenario. No other Bcs attempted yet.	Yes. The recharge rate of the model is approximately 4 mm/a which is close to the assumed value of 5 mm/a
How have you checked the consistency of your model borehole boundary conditions?	We have compared the calculated heads in KR24 under the natural condition and during the pumping test with the measured ones.	For checking model to compare with openhole conditions	We can check the model output where we write in detail the input data (geometry, flow rate, number of 1D line elements) and results (heads, nodal flow rates) for all the 1D line elements as well as the mass balance for these elements.	Comparisons with analytical solutions. See appendix in report	Tested two variants of implementing pumping in KR24. Please see draft report for details.	Yes. The (small) correction caused by using linear shape functions close to strong sinks is included in the results.
How have you checked the numerical accuracy (convergence) of your models?	We have calculated draw-down in KR24 using a model with only one fracture zone intersecting with KR24 and compared the theoretical solution.		We can check the mass balance for the flow simulation to ensure that it is correct (typically on the order of the iterative matrix solution, which means that (Flow in – Flow out) is approximately 1.0e−5 for a steady-state simulation. We also checked results for refined grids, although a rigorous grid refinement study is difficult to conduct because the exact geometry of the fracture zones changes as the grid is refined, because of the method we use to discretize them.	Convergence assured but no grid indepedence test have been done	Used iterative GMRES solver. Numerical convergence criteria for solver is 1E−6. All simulations have a mass flux balance (absolute error) in vicinity of 1E−8 (m^3/s) and a normalised mass flux balance (residual error) in vicinity of 1E−6.	Yes. I found it as an imperative to use double accuracy arithmetics with very strict tolerance for linear solvers. The mass balance at open boreholes is extremely sensitive to rounding errors.

Table A-7. Model evaluation.

	CRIEPI	JAEA/Golder	NWMO/Laval	SKB/CFE	SKB/KTH	Posiva/VTT
What aspects of the groundwater flow system do you believe are well represented in the model	The hydraulic heads under the natural condition and the steady-state drawdowns and the changes of groundwater flow into observation boreholes caused by pumping in KR24 are well represented in our model.	Model structure data was directly used from dxf file.	The geometry of fracture zones appears to be well represented in the model, including the intersections between the zones. In our model, the triangulated fracture data is directly imported. Therefore, fracture zones are represented as inclined non-planar surfaces. The geometry of model domain is also fairly well represented. In the model, the topography is represented as an irregular surface and the model ground plan is represented with an irregular boundary.	The upper 80 meters and the deterministic zones below this level. Also the resolution of boreholes	Flow in fracture zones (geometry of all structures are essentially as exact as they can be using rectangular approximations).	After calibration, the local effects close to KR24 and at the calibration points are represented reasonably. Regional features (drawdown at more distant parts of the model) are more problematic.
What aspects of the groundwater flow system do you believe are poorly represented in the model	The drawdown in the lower section of KR24 is over-estimated in our model.	Infiltration rate was calibrated to 5mm/y as specified.	Although the geometry is our discretized fracture zones is consistent with the data delivery, we feel that the model is perhaps overly connected based on the transient flow simulation results we presented at previous meetings.	An improved treatment of the free groundwater table may be important. Requires information about streams	Background flow is not included in the model yet. In-fracture zone heterogeneity is not modelled yet.	After calibration, the model produces very homogeneous response throughout the modelled domain, which might indicate that transient effects are important at the distant parts of the model.
If you have used different model variants within your work – which model variant do you think best represents the groundwater flow systen at the site and why?		NA	We are currently exploring different combinations of parameters to see if we get a better match to observed heads. We have created an interface to use PEST with our model, for inverse simulations, but with little success up to now.	Only one variant used	Assuming homogenous zones with no background fractures it seems to me that using the geometric mean of the transmissivities produces flow results which are often too low compared with the measurements; therefore I would advise to increase the T's for such a simulation scenario (see draft report, section on calibration attempt 5).	I have altered the extension of the fracture zones. When using the large version of the zones, the large observed drawdowns (e.g. in KR4, KR8 and KR25) are not produced by the model, because of too good connections to the boundaries of the model. The high drawdown values are produced when using the smaller local version of the zones, but then the drawdowns at more distant parts of the model are too strong. The thruth lies somewhere between, and the best model depends on what we want to model: to model the local effects close to KR24 during pumping, the Small/Local zones provide better response.

	CRIEPI	JAEA/Golder	NWMO/Laval	SKB/CFE	SKB/KTH	Posiva/VTT
What would you most like to improve within the model?	We would like to change transmissivity distribution in the fracture zones to reproduce the measured drawdown and the flow logging results better.	Mainly, maximum head change per iteration to single iterative solution is used as tolerance of convergence.	Varying the hydraulic properties of the fractures would very likely improve the model, but it's a non-unique and time-consuming task. We would like to incorporate uncertainly in fracture zone properties to provide confidence intervals for results (of great interest to NWMO). We also need to further refine our representation of the 1D wells, which is more a discretization issue than a numerical modelling issue.	First more comparisons with field data and then decide depending on the outcome of the comparisons.	a) Representation of the near surface and BC. b) Representation of the zones (variability). c) Background DFN to represent the details of the flows.	Refine the description of the region around the upper section of KR24 and about the surface layer. I have now included a small zone connecting KR24_T2 and KR04 in order to be able to include also pumping at the upper section. However, there are indications in the data that there might be larger horizontal zones above HZ19-area and understanding these might be important to model the pumping at the upper section of KR24.

Table A-8. Evaluation of task definition and dataset.

	CRIEPI	JAEA/Golder	NWMO/Laval	SKB/CFE	SKB/KTH	Posiva/VTT
What is your evaluation of the task definition? (Good, satisfactory, poor?)	The task definition is satisfactory.		The task definition has evolved with time, in response to input from all involved, such that the description is now clearer. The simulations to perform and location and availability of input data are more clearly described now and makes it easier for the modelling group to focus on the work needed. It is still not clear how useful calibration will be, since we appear to be moving along with some PA issues after Task 7A1 and 7A2 (how will we carry forward any model improvement made by calibration for sub-tasks 7A3–7A5?).	Satisfactory. I did not like the change to PA-issues. The first definition is what we should have stayed with	Satisfactory.	Satisfactory.
What is your evaluation of the performance measures? (Good, satisfactory, poor?)	The performance measures are satisfactory.	The hydraulic connectivity among the larger scale fault zone in Olukiluoto site was well represented as honor to the task specifications	Good.	Good.	Satisfactory.	Satisfactory.
What is your evaluation of the dataset? E.g. What information was missing?	As a whole, the dataset is satisfactory. But the data volume is too large. Consequently, it was very difficult for us to select important information.	The heterogeneous hydraulic connectivity vicinity of KR24 shallower zone around HZ19 series fault zones intersections were poorly represented, although the specified region (whole Olukiluoto) was relatively larger than the target zone (ONKALO region).	Good.	Nothing missing, but could have been presented more clearly.	Unnecessary amount of time has been dedicated sifting through data files. The various file formats used and the lack of applying a consistent file naming convention and directory structure is frustrating. A lot of time was spent extracting data from Word or PDF documents. Also, I am wondering if there may occasionally be some inconsistency with the data (eg locations of borehole intersections). KR06 was not listed in Task Description but then was required in the PMs. A well-defined data set at least for the reference / base case scenario could perhaps have been defined at the start of the Task, it would then perhaps have been easier to identify modelling setup errors and implement model variations.	

	CRIEPI	JAEA/Golder	NWMO/Laval	SKB/CFE	SKB/KTH	Posiva/VTT
What is your evaluation of this questionnaire!?	Good	Dual permeability model might be useful. Because, DFN is one of extreme hypothetical model, in order to compare with scatterly distributed measured data, moderate and/or lesser permeability might be important.	Useful: PA should be quantifiable to objectively compare different approaches	Good.	Good	Good
What is your evaluation of the scope and objectives of the task? (in relation to the original scope, personal preferences, and to the goals of your funding organisations)	We expect that the preliminary site investigation for HLW disposal will be conducted in Japan in the near future. Therefore we are very interested in to what extent we can understand the characteristics of the underground through the survey with surface boreholes.	The heterogeneous hydraulic connectivity vicinity of KR24 shallower zone around HZ19 series fault zones intersections would be interested.	See Q29. NWMO (and OPG) has less interest in PA issues compared to site characterization (SC), but feel there is room within the task to explore in more detail some SC specific issues, like quantification of uncertainty.	As said, simulations of boreholes of various kind are important, novel and interesting. We should focus on this.	There are very significant exciting challenges remaining to realistically manage to deliver the overall objectives of this task. In particular, the demonstration of uncertainty reduction.	The task has evolved quite far from the original scope and seems to be driven towards a data-analysis task rather than a task for (numerical) modellers. I will put more emphasis on developing our modelling and calibration methodologies during Task 7B, and less emphasis on 7A2–7A5.

Appendix B

Modelling groups questionnaires Task 7B

During Task 7B two questionnaires were completed by the modelling groups to support the evaluation. The first questionnaire (Data Delivery 31) covered a range of topics while the second (Data Delivery 35) focussed on the approaches to model calibration used by the groups.

The responses to the questionnaires are presented below.

Table B-1. Task 7B Questionnaire 1: Tools, objectives and approach.

Modelling Group	Numerical codes used (name and version?)	Answers provided by (name, phone, e-mail)	Date	What are your objectives for modelling Task 7B?	What approaches, tools have you used to address ”uncertainty reduction” within the subtask
CRIEPI	FegmB_II, version 0.11	Yasuharu Tanaka	21/04/10	My objectives are to learn and improve how to model groundwater flow system at block scale and to confirm whether the PFL measurement is useful to modelling the flow system or not.	I have checked the validity of my model by using the data on groundwater inflow to boreholes as well as the drawdown data.
JAEA/ Golder	FracMan, version 7.20	Atsushi Sawada	21/10/09	To demonstrate modeling methodologies of the major flow structure conceptualization by the derivative analysis of the transient pressure interference tests and the minor fracture network structure modeling for the heterogeneous flow path distribution among the boreholes	Basically the root mean square of residuals is used for checking the model applicability
KAERI	FeFlow (v5.20)	Sung-Hun Ji	1/10/09	• Block-scale modeling of the groundwater system of Olkiluoto site and the hydraulic responses by pumping test at KR14 and KR15 • To find factors causing uncertainty of hydrogeologic conditions • To examine the effect of background fractures on groundwater flow	• We tried to consider the background fractures to match the field data with modeling results in natural conditions with boreholes and hydraulic responses by pumping tests, but it is not finished yet.
NWMO/ Laval	T-PROGS 2.1 (Carle 1999)/HydroGeoSphere (Therrien et al. 2009)/ PEST (Doherty 2004)	René Therrien	14/12/09	Model calibration based on hydraulic heads and PFL measurements. Only hydraulic heads were considered in the first modeling phase. Flow measurements were then included as targets for calibration to assess their influence on model calibration.	Calibration output information, such as the estimated parameter confidence intervals and parameter correlation coefficients, was provided by PEST and was used to analyze model uncertainty. By including PFL measurements as targets for calibration, a reduction of uncertainty on estimated hydraulic conductivity values has been observed.
SKB / KTH	ConnectFlow/Napsac v9.6	Andrew Frampton,	07/10/09	To improve the conceptual understanding the flow characteristics of the groundwater system in the vicinity of the KR14-KR18 boreholes by studying the cross-hole pump tests and based primarily on using high-resolution PFL flow measurements.	An improved understanding should enable a reduction in the uncertainty of the characteristics of this particular groundwater system, thereby indicating suitable and feasible approaches for characterisation of similar systems. Thus the idea of the approach undertaken is that improving a conceptual understanding of a system can reduce uncertainty in the knowledge of the behaviour of a system. Ultimately, this can be linked to uncertainty in long term safety assessment of a flow system, since long term safetly relies on site characterisation knowledge.
SKB/CFE	DarcyTools v3.2, v3.3	Urban Svensson	23/09/09	My objective is to carry out the task according to the priorities given by SKB. The priorities are: develope methods for borehole simulations and simulate the interference tests in KR14-KR18.	No systematic approach or specific tool. My method can be called ”trial and error” or ”building an understanding of the site through sensitivity studies”.
VTT	FEFTRA v4.2 (pre-processors: octree and vintage module, FEA module solvit, various postprocessing utilities)	Ferenc Mészáros	09/10/09	Test the applicability of flow data to improve the predictions.	Manual calibration.

Table B-2. Task 7B Questionnaire 1: Data sources.

Modelling Group	What data sources did you use for fracture zone representations? (positions and properties)	What data sources did you use for the model representation of the background rock?	What data sources did you use for model boundary conditions?	What data sources did you use for borehole boundary conditions? (specified rates/head)	Have you used the salinity information in any way?
CRIEPI	HZ-08_faces_rev_20080312.txt HZ-model 2008 borehole intersections.xls K2m-values-summary-rev1.xls KR**_Fractures.xls	KR**_Fractures.xls	GW-table-long-term-mean.txt	summary of head and pumping-rev2(without KR15).xls Pumpings and overpressures-rev1.xls	No
JAEA/ Golder	2006 model and 2007 model provided by Posiva is used for the deterministic fault zone modeling	The water conducting fracture data above HZ20 was used OL-KR14–18 All Fractures.zip	arbitrary defined by constant head for fixing ground surface	For both open borehole and fixed packer intervals, ”nodal group boundary flux = 0, the net flux at the boundary group” was defined. For flow response tests, measured pumping flow rate is applied as the boundary condition and for the pressure response tests both of measured pumping rate and drawdown is applied at the pumping boreholes.	no
KAERI	• The properties of the fracture zone are from DD_24.	• The minimum values of the properties of the background rock in the DD_24 are used.	• The result of the Task 7A in natural condition with boreholes	• Flow conduits with very high hydraulic conductivity in the natural condition without pumping • Constant rate of flux boundary in case of the pumping tests	• No use of information for variable density flow caused by salinity
NWMO/ Laval	The information presented on WR 2006-01 (Klockars et al. 2006) was used. Planar hydraulic features were identified to explain the observed responses during the crosshole interference tests.	The conductive fractures (those that were above the detection limit of the PFL tool) were considered to define a transitional probability model of fractured rock facies using TPROGS. Fracture transmissivity was related to fracture density to define the facies distribution. Fracture density was calculated from the number of conductive fracture per borehole interval length (a length of 5 m was considered).	The long term mean water-table at Olkiluoto was used to define the boundary conditions.	WR 2006-01, WR 2003-30 and the measured drawdown.	No, salinity variation was neglected.

Modelling Group	What data sources did you use for fracture zone representations? (positions and properties)	What data sources did you use for the model representation of the background rock?	What data sources did you use for model boundary conditions?	What data sources did you use for borehole boundary conditions? (specified rates/head)	Have you used the salinity information in any way?
SKB/KTH	The use of HZs only applies to preliminary simulations and the forward case model. Geometries obtained from file: DD25 / HZ-08_faces_ rev_20080312.txt Transmissivities obtained from T7A, Table 3 in file: DD8 / Task7a_definition_v2_2b. pdf	From files: DD25 / OL-KR14–18 All Fractures / KR*_Fractures.xls using columns describing location (coordinates) of observation in bore-hole, together with measured angles (dir, dip) and measured transmissivity (Tmin, Tmax). Note only observations with existing transmissivity are used, as these are interpreted as being PFL flowing fractures.	For cases where a top surface BC is used, then head = ground surface elevation. The ground surface elevation (topography) is obtained from the file: DD9 / topo2.dat	Applied pumping in bhs 14A, 15A, 16A, 17A, 18A with drawdowns (as a negative head value). Measured drawdowns taken from graphs in Working report 2003-30, appendix 41, pp 214 (approx error perhaps +/- 0.5m): KR14A 6.5 m KR15A 10.0 m KR16A 10.5 m KR17A 10.5 m KR18A 10.5 m	No
SKB/CFE	The fracture zones were kept from Task 7A, i.e. the old structural model. Later a modification was introduced to account for the new structural model (see Report).	The background fracture network was specified according to experiences from Äspö and tested for HPF statis-tics (High Permeability Features).	Only a net precipitation of 100 mm/year and hydrostatic pressure on vertical bounda-ries. Zero flux at bottom boundary. Below the Baltic a fixed pressure condition was used.	For pumped boreholes I used the given rate. For other boreholes, or sections, inflow = outflow was the condition.	No.
VTT	Posiva flow model as of 2008 was used for the geometries of the zones. As for the propertes, the measured transmissivity distribution was “kriged” onto the set of finite elements which represented the zone.	The sparsely fractured rock was represented by a DFN model, of which parameters were derived from the material found in OL-KR14–18 All Fractures.zip. Some of the coordinates were corrected in a later update obtained from Henry in April 2009 (Summary-of-orientated-hydro-fractures-KR14–18-rev1.xls). The stochastic DFN part and the deterministic zones were combined in a single finite element mesh accom-panied by a property lookup table.	Top boundaries: (1) over the perimeter of the HZ19A zone the hydraulic head field obtained from a larger, EPM model was interpolated (here HZ19A also confines the model), and (2) beyond HZ19A the watertable was set. The model is confined by the HZ20A zone from below, for the perimeter of which constant head obtained from the EPM model was set. No-flow was set along the vertical boundaries of the model.	For the pumped boreholes the specified flow rates were set. Unpumped boreholes were carefully disconnected from the constant head boundaries.	No.

Table B-3. Task 7B Questionnaire 1: Calibration and model consistency.

Modelling Group	What aspects of the model have you calibrated/adjusted to improve match to observation?	How have you checked the consistency of your model's representation of the fracture zones?	How have you checked the consistency of your model's representation of the background rock?	How have you checked the consistency of your model boundary conditions?	How have you checked the numerical accuracy (convergence) of your models?
CRIEPI	Effective precipitation. Transmissivities of major fracture zones. Size distribution of background fractures. Relationship between size and transmissivity of background fractures. Transmissivities of several fractures observed at boreholes and their intersection with the other boreholes.	I have checked the drawdowns and groundwater inflow to the boreholes.	I have checked the number of the intersections of background fractures with boreholes. I have also checked the drawdowns at the packed-off sections and groundwater inflow to the boreholes.	The calculated heads at the boreholes were compared with the measured ones under natural conditions.	The drawdown at the borehole was calculated using the model which considered only HZ19A or HZ19C. And the calculated drawdown was compared with the theoretical one.
JAEA/ Golder	Major fault zone model was checked by the conceptual model from the derivative analysis and compared the model applicability. For the background fracture, an average hydraulic conductivity and heterogeneous flow path is calibrated.	Major fault zone model was checked by the conceptual model from the derivative analysis and compared the model applicability.	Average hydraulic conductivity and the reproductivity of the heterogeneous flow paths among the boreholes.	no	Mainly, maximum head change and flux change per iteration to single iterative solution is used as tolerance of convergence.
KAERI	• Primarily, the head values at the boreholes were used in order to calibrate the model. Secondly, the flow rates at the monitoring position in each borehole were employed.	• We used an equivalent porous model with heterogeneous hydraulic conductivity assigned by the transimissivity of the fracture zones. Therefore, we checked the fracture zones by identifying the distribution of hydraulic conductivity values.	• We checked the background rock by identifying the hydraulic conductivity distribution in the domain.	• We used constant head boundary on the model boundary by introducing the result of Task 7A at same locations. The boundary conditions were maintained in all of the modeling tasks.	• The convergence features were checked in all modeling tasks. The termination criterion of the preconditioned conjugate gradient solver used in modeling was less than 10–8.
NWMO/ Laval	To improve match of observation, the hydraulic conductivity of the fractured rock facies and the apertures of the discrete fractures were estimated through an iterative parameter optimization process. Moreover, boundary conditions were adjusted to simulate the pumping in boreholes KR14 and KR18. Finally, to attempt a better match of SS25 and SS26, it was also tried to increase the pumping rate in borehole KR18.	The consistency has been checked by varying the fracture apertures and by observing the corresponding simulated drawdown at the pumping wells and neighboring boreholes. Moreover, a different number of discrete fractures (1 to 4) have also been tested.	The consistency has been checked by executing different facies realizations, keeping the model conditioned by the same facies distribution along boreholes KR14-KR18.	The consistency has been checked by evaluating the simulated drawdown with different boundary conditions for the top of the domain (first-type versus no flow boundary condition).	To ensure an appropriate parameter optimization with PEST, the HydroGeoSphere flow solver convergence criteria was lowered to 1 × 10–12.

Modelling Group	What aspects of the model have you calibrated/adjusted to improve match to observation?	How have you checked the consistency of your model's representation of the fracture zones?	How have you checked the consistency of your model's representation of the background rock?	How have you checked the consistency of your model boundary conditions?	How have you checked the numerical accuracy (convergence) of your models?
SKB/KTH	Target has been to match measured detailed/discrete PFL flow values in open boreholes conducted during the cross-hole KR14--KR18 pump tests. Target flow values are obtained from files: DD24/package2 / flow response tests 2002 data without KR15/FDOL*-final.xls using columns containing measured flows in boreholes both without pumping as well as responses during pumping. Then, model variations have included: • Generation of fractures into compartments associated with boreholes. • Sensitivity of the resolution of fractures in these compartments. • Sensitivity of the the fractures density / connectivity. • Choice of model boundary conditions (top, lateral sides). • Modifying (increasing) fracture T for entire domain. • Modifying (increasing) fracture T in vicinity of borehole. • Modifying (increasing/decreasing) fracture T in horizontal slices through domain.	For the case where zones have been used the zones where taken from T7A, so relying on previous consistency checks.	First, provided borehole fracture data has been applied to generate background fractures. Then, in simulations, the resulting geometry of fractures in boreholes has been checked and verified agains the provided borehole fracture data, thus reducing input errors (eg units, angles etc).	The lateral side BC for most cases is head = 0. This has been evaluated with respect to the size of the model domain. Starting with the model domain from 7A which encompasses the entire island, and hence has head = 0 on the hydraulic conductors which are in contact with the Baltic Sea, then reducing scale to the 300 m × 300 m domain, and also smaller domains such as 200 m × 200 m and 150 m × 200 m have been tested. Since results are reasonably consistent between cases, the assumption that head = 0 for the domain mainly used (300 m × 300 m) seems sufficiently consistent. The top BC is evaluated in terms of (1) head = elevation and (2) no-flow. Here there are significant differences in results, as would be expected. For the case (1), visual comparison of provided surface elevation maps has been checked against the numerical implementation, and the numerical implementation seems perfectly reasonable for the resolution of the topography data used. The bottom BC is no-flow, this is assumed to be a reasonable conjecture.	The PCCG solver converges to the assigned criteria (1e-12, dimensionless), and in all cases provides very small mass-balance errors, both in terms of global absolute and relative volumetric flow conservation. The worst case abs mass-flux balance is ~1E−13 m^3/s, and worst case rel mass-flux balance is ~1E−09 (dimensionless).
SKB/CFE	I introduced two sheet joints (see Report) and calibrated the transmissivities of these to match the pump test with open boreholes. Different realizations of the background DFN was used as a "fine-tuning".	Only visually.	The HPF statistics, see question 4.	In principle not. However if we include the top few meters of the model in the boundary condition, I checked that the conductivity in the top layer gives a realistic large scale distribution of lakes and wetlands.	By several measures like: decreasing residuals, steady values in points, steady pressures in boreholes, etc.

Modelling Group	What aspects of the model have you calibrated/adjusted to improve match to observation?	How have you checked the consistency of your model's representation of the fracture zones?	How have you checked the consistency of your model's representation of the background rock?	How have you checked the consistency of your model boundary conditions?	How have you checked the numerical accuracy (convergence) of your models?
VTT	The measured head responses were targeted to match by adjusting (1) the size distribution's parameters, (2) the correlation between the size and the transmissivity distribution of the DFN model characterising the background fracturing and (3) the transmissivities of the introduced deterministic sheet joints.	Special care was excersised to faithfully model the deterministic fracture zones in terms of both their geometry and the transmissivity distribution over them. The geometry of each zone consisting of several triangles and quadrangles and their finite element representations were visually compared and in case of discrepancies the discretisation algorithm in the preprocessor was improved.	When deriving the statistical parameters that defined the DFN model, the resulting fracture sets' orientation distribution was visually compared to the data. Also the transmissivity-size correlation was defined and checked several times by plotting these quantities against each other etc.	Several boundary conditions were tested. The appropriate distance of the bounding surfaces (thus the boundary conditions) was identified in the first phase of the modelling. It was also found that modelling the hydraulic tests the modelled volume can be confined by the conductive zones HZ19A from the top and HZ20A from below. Constant head for the external boundaries of the model were derived from EPM models with similar hydraulic disturbances.	We believe that numerical accuracy of all converged runs are not an issue. On the other hand, poor convergence is a decisive sign in assessing a model's integrity (eg, erroneously set boundary conditions, etc). In this project probably the only (otherwise correct) input which may have caused numerical problems was the spread of the transmissivity in the DFN model – but eventually, it did not. Experience showed that using higher arithmetic precision (REAL*8 in Fortran or double in C) leads to faster convergence, albeit at the expense of computer memory.

Table B-4. Task 7B Questionnaire 1: Model evaluation.

Modelling Group	What aspects of the groundwater flow system do you believe are well represented in the model	What aspects of the groundwater flow system do you believe are poorly represented in the model	If you have used different model variants within your work – which model variant do you think best represents the groundwater flow systen at the site and why?	What would you most like to improve within the model?
CRIEPI	I believe that I represent transmissivity distribution in HZ19A and HZ19C and the water-conductive fractures intersecting with the boreholes well.	I do not believe that I represent the distribution of size of the background fractures and the hydraulic connection between the boreholes well.	0	I would most like to improve the distribution of size of the background fractures and the hydraulic connection between the boreholes.
JAEA/Golder	Deterministically defined fault zones, location and hydraulic conductivity	Heterogeneous distribution of flow path among the target boreholes at minor background fracture zone between the deterministically defined fault zones	??	more minor heterogeneous flow path among the boreholes
KAERI	• The hydraulic heads in open and packed-off boreholes without the pumping well if pumping tests were implemented.	• The flow rate of groundwater into and out of boreholes	• The fracture zones and network constructed by them. The background fractures and fracture network representing such a local anomaly can help show the local difference which cannot be described by only the large-scale fracture zones.	• Implementing the local background fractures in the fracture network and following hydraulic conductivity values.
NWMO/Laval	The global response to pumping in borehole KR14 (both heads and flows are quite well reproduced).	The facies distribution/fractures intersecting borehole KR18.	The model with two discrete fractures intersecting the KR14–18 boreholes allows for a better match between observed and simulated hydraulic responses, especially for pumping in borehole KR14	The hydraulic response of the pumping in borehole KR18
SKB/KTH	Background fractures. Since the background fractures are grouped into compartments associated with boreholes, the background fracture population has a somewhat complex geometry, which is believed to be slightly more realistic than perfectly planar, rectangual features. Most importantly however, the background fractures are essentially perfectly consistent with borehole observations, thus simplifying and enabling direct comparisons with PFL flow measurements; both flow magnitudes and directions (in/out of borehole).	There seems to be some 'anisotropy' in the responses of the cross-hole pump tests, and this seems difficult to capture in simulation. It is believed that connections between compartments (boreholes) have to be modified. In all current simulation cases/variants, there exists connections between all compartments/boreholes. Thus the 'heterogeneity' of connectivity between compartments, both vertically and horizontally, needs to be further investigated. It is beleived this could be achieved through a combination of greater heterogeneity in transmissivity as well as modified connectivity.	Apparently the model case where the top BC is changed to a no-flow condition produces better flow responses, both in terms of magnitude and direction. Conceptually however the top surface GW level should clearly have an impact. This may be partially explained by the absence of highly conductive zones (eg HZ19A, 19C, 20A), and a relatively small domain (horizontal cross-sectional area 300 m × 300 m). Thus the top no-flow BC may simply be replicating the absence of a highly conductive zone(s) close to the surface of the domain. Also, in general it seems PFL T is somewhat under-estimated, even when using the provided 'Tmax' values.	The connectivity and transmissivity of the background fractures could be further investigated. In particular, the connectivity between 'fracture compartments' could be modified, in order to better explain the flow responses, especially concerning the directions of flows at various depths in KR17 and KR18.

Modelling Group	What aspects of the groundwater flow system do you believe are well represented in the model	What aspects of the groundwater flow system do you believe are poorly represented in the model	If you have used different model variants within your work – which model variant do you think best represents the groundwater flow systen at the site and why?	What would you most like to improve within the model?
SKB/CFE	I have only worked with flow and pressure and believe that this part is well represented. Implicity this means that the conductive structures are ok, even if other alternative structures could give similar results (i.e. no uniqueness).	Aspects that I have not worked with for example porosity and storativity.	NA	I should like to validate the flow along boreholes in more detail.
VTT	Deterministic zones, boundary conditions.	Connectivity of the DFN model in its numerical representation (ie the finite element mesh) is believed to be higher than in its geometry due to inherent discretisation errors. This may call for some improvements.	Introducing two sheet joints at the boreholes' location appeared to be a fruitful move. The model was only slightly sensitive to the DFN size distribution (around the sensible values).	The aforementioned overconnectivity of the DFN model (geometry vs. FEM). A formal calibration tool of stochastic models is needed too.

Table B-5. Task 7B Questionnaire 1: Task evaluation.

Modelling Group	What is your evaluation of the task definition? (Good, satisfactory, poor?)	What is your evaluation of the performance measures? (Good, satisfactory, poor?)	What is your evaluation of the dataset? E.g. What information was missing?	What is your evaluation of this questionnaire?	What is your evaluation of the scope and objectives of the task? (in relation to the original scope, personal preferences, and to the goals of your funding organisations)
CRIEPI	Satisfactory	Good	We are short of the information on the distribution of size of the background fractures, though there is fracture trace data.	Good	I could confirm the usefulness of the data of the PFL measurement. And I have found through this task that it is an important issue how to estimate precisely distribution of size of background fractures and the relationship between fracture size and transmissivity.
JAEA/ Golder	Satisfactory	Satisfactory	Enough! It is better to discriminate minor zone data from major fault zone and near-gourndsurface zone	Good	Good data set would be helpful for satisfying the original scope. This should be transfer to the next step/phase of the site investigation programs, in future at any site.
KAERI	• Satisfactory	• Satisfactory	• Geophysical survey results that help to conceptualize the background fracture extents or connectivity	• Well…	• Satisfactory
NWMO/ Laval	Good	Good	Large and detailed dataset.	The questionnaire was useful to summarize the most important modeling aspects.	0

Modelling Group	What is your evaluation of the task definition? (Good, satisfactory, poor?)	What is your evaluation of the performance measures? (Good, satisfactory, poor?)	What is your evaluation of the dataset? E.g. What information was missing?	What is your evaluation of this questionnaire?	What is your evaluation of the scope and objectives of the task? (in relation to the original scope, personal preferences, and to the goals of your funding organisations)
SKB/KTH	Satisfactory, though I believe more emphasis should have been placed on understanding the cross-hole pumping tests with associated PFL flow responses. In the task definition only the pump tests KR14 and KR18 (as well as the 'blind' prediction pumping in KR15) are required. However, pump tests where conducted in all five boreholes thus constituting a permutation of pumping and response measurements. This soley produces a large data set which I believe has not been thoroughly/ sufficiently investigated.	Satisfactory, although PFL flows are perhaps over-simplified since they are grouped into 'flowing features', and the actual measurements are numerous 'discrete' flow values and are generally associated to core-log observations of fractures. Since my understanding of Task 7B is that focus should be on 'background fractures', as opposed to hydraulic zones, I believe this has not been adequatly reflected by the PMs. That is, I would have prefered to see PMs suitable for detailed (background) flow measurements, rather than for grouped 'flowing features' (which could in principle be an interpretation of hydraulic zones). Also on the technical side, perhaps the use of Excel sheets could be simplified – personally I would prefer regular text files as this would reduce 'cut and paste' efforts, although perhaps spreadsheets are used to reduce inconsistencies.	The 7B data set has been clearer, but I still believe data could have been delivered in a more compact and clearer way / lighter. Again, much time has been spent searching for appropriate data delivered in numerous packages containing sometimes unclear sub-directories. Again there might have been too much data, a lot of which was not entirely necessary for hydrogeological/numerical modelling. Just the effort to implement sub-sets of the data has been quite significant, and is not really part of the task objectives.	Good and necessary. Perhaps the use of Excel is not optimal for text – alot of cut and paste from regular word-processor.	The scope and objectives are very reasonable and clear, and sufficiently general to be applied to several conceptual/numerical modelling approaches. Perhaps the concept of model calibration/ inversion should not be emphasised as much, since this is of course not possible for under-determined models such as any GW modelling in general. I believe the emphasis on more general 'uncertainty reduction' is reasonable. Also, perhaps the range of the task scope is too broad, ie there is a large spectrum of assignments. The data delivery is almost at a 'raw data' level (eg borehole fracture data) and the final assignment is to make transport predictions.
SKB/CFE	Poor. I think (as I said many times) that there are two tasks that are mixed "simulation of pumptests" and "reduction of uncertainty in PA".	Satisfactory.	The data sets are OK.	Good.	My view (which I think SKB shares) is that it has been very valuable to develope methods to simulate boreholes (open, packed-off, pumped) and to compare simulations with data from the interfernce tests. More work should be done on flow along boreholes.
VTT	Considering the complexity of the task, I believe it would have been difficult to make the task definition much simpler. Good.	Also good. They were straightforward to grasp and create – even if getting them out of these models required the development of numerous auxiliary programs.	There was a wealth of information and Henry was always very helpful in explaining everything.	I hope it's gonna serve the purpose it was conceived for. As this task was a major DFN calibration exercise for several groups, I may have requested more detailed elaboration on the DFN and on the calibration parts. But these topics may better fit the scale of a report, not a questionnaire indeed.	I believe the objective (improving predictions using flow data) was clear enough. Approaching the conclusion of the task, we might also say it was more ambitious than it originally appeared.

Table B-6. Task 7B Questionnaire 1: Task evaluation.

Modelling Group	Describe the steps in model calibration/ development you have used in Task 7B	How has head data been used in the different calibration steps?	How has PFL data been used in the different calibration steps?	Describe your understanding of model sensitivity	Describe sensitivity to model boundary conditions
CRIEPI	The first step is the calibration of the effective precipitation was calibrated. The second step is the calibration of transmissivities of major fracture zones, size distribution of background fractures and the relationship between size and transmissivity of background fractures. The third step is the calibration of transmissivities of several fractures observed at boreholes and their intersection with the other boreholes.	In the first step, the head data under natural conditions was used to calibrate the effective precipitation. In the second step, the drawdown data was used to calibrate transmissivities of major fracture zones, size distribution of background fractures and the relationship between size and transmissivity of background fractures. In the third step, no head data was used.	PFL data was used in the second and third steps to calibrate transmissivities of major fracture zones and several fractures observed at boreholes and their intersection with the other boreholes.	Drawdowns and Dflow are most sensitive to transmissivities of major fracture zones, moderately sensitive to size and transmissivity of background fractures and less sensitive to the precipitation.	I have not perform any sensitivity analyses as for boundary conditions.
JAEA/ Golder	1. A deterministic fault zone model was developed based on the derivative analysis of transient cross hole interference test data. 2. Three deterministic fault zone models were constructed and compared model plausibility, model 1 (2006 model), model 2 (2008 model), model 3 (2008 model with additional zone HZ002) 3. Stochastic background fractures, with five stochastic realizations, were added to “model 3: modified 2008 model ” and check model plausibility for reproducing minor pressure and flow response 4. The background fracture model was improved by correcting background fracture transmissivity with considering depth dependency and reducing connectivity between KR14 and HZ19C, HZ002 5. To reduce over connectivity of background fractures, the final stage of calibration (currently in process) reduces network connectivity to reproduce heterogeneous flow path.	Simulated pressure responses (head difference between stady state and pumping phase) were compared with measured pressure responses. The RMS error was also used to check the model plausibility.	Simulated flow responses (flow rate difference between stady state and pumping phase) were compared with measured flow responses. The RMS error was also used to evaluate model plausibility. We didn’t discriminate flow response data from pressure response data in the process of calibration, explicitly. However, we found that the heterogeneous connectivity among the boreholes should be modified in order to reproduce the minor flow responses observed by PFL.	Analyses clearly demonstrated that the highest priority needs to be the development of an accurate and defensible hydrostructural model of larger structures (Major Water Conducting Features). The derivative analysis of pressure interference tests was found to be a useful tool to assist the conceptualization of major water conducting features.	No sensitivity study for the model boundary condition was performed, in our study. So, we decided to use the response (the difference between steady state and pumping phase) as one of measures for the calibrations.

Modelling Group	Describe the steps in model calibration/ development you have used in Task 7B	How has head data been used in the different calibration steps?	How has PFL data been used in the different calibration steps?	Describe your understanding of model sensitivity	Describe sensitivity to model boundary conditions
KAERI	First, we conceptualized the groundwater flow model and simulated it with a fracture network consisted of only the identified fracture zones such as HZ19A or HZ19C. After calibrating the model and checking its results, it was modified by adding the background fractures.The revised model was calibrated by sequential simulations and the calibrated parameter was the recharge rate. The open and packed-off borehole conditions without pumping were simulated and the recharge rates of those two conditions were calibrated. Then, the pumping at KR14 and KR18 were simulated, and the recharge rates were also calibrated. Eventually, we selected the recharge rate, which shows the minimum root-mean-squared-errors (RMSEs) among the whole simulation cases, as a final calibrated one.	The head data were used in calibration of the recharge rate for each step, and thus we could get some recharge rates which show the minimum RMSE in each step. Then, we chose the recharge rate as a final one, that shows the minimum RMSE among the whole calibrated recharge rates.	Although the simulated flow rate at the concerned intervals in some boreholes were compared with the PFL data, the PFL data were not directly used to calibrate other hydraulic parameters including the recharge rate. In other word, we used only the head data for calibration works.	The sensitivity of the fractured zones such as HZ19A and 19C is much larger than that of the background fractures on the groundwater flow system. However, the background fractures seriously affect the calculated migration paths and times that are essential as input parameters for the safety assessment of a HLW repository.	For the simulations of the pumping tests, the constant head conditions of lateral and bottom boundaries had little influence on the simulated heads in the deep boreholes as well as the pumping wells such as KR14 and KR18. However, their effects on the simulations were strong when no pumping stress was assigned in the model.
NWMO/ Laval	During the first step, only hydraulic heads were used as targets for calibration. Then, PFL measurements were included to better characterize the system behavior. Finally, some inverse modeling tests (based on simulation SS23) used only PFL measurements as targets for calibration, to investigate calibration suing only flow measurements. The conceptual model was adjusted by varying the top boundary condition and by adding discrete fractures to better capture the observed hydraulic response.	Head data were always used as targets for calibration, except in the last run where only PFL measurements were considered. Optimization iterations are performed by PEST to find the optimal parameters (hydraulic conductivity) that reproduce the measured heads at pumping and observation boreholes	At first, PFL data were only compared to the simulated flow values, because of numerical model limitations. Further work allowed to use PFL data as targets for calibration. Note that there is some difference between the spatial mesh resolution chosen for the model (5 m) and the spatial distribution of PFL measurements (2 m section).	First sensitivity analysis was carried out before starting with inverse modeling. Different combinations of facies hydraulic conductivities were tested to analyze their influence on the simulated hydraulic response. Simulations showed that the response was sensitive to the isotropy/anisotropy of the SFB rock facies. Some indications on model sensitivity are also automatically provided by PEST. Observation sensitivity show how simulated head and flow values are sensitive to parameter variations, while parameter sensitivity gives a measure of the changes in model outputs (heads and flows) that are incurred by a fractional change in the value of the parameter. In general, simulated heads and flow are less sensitive to the aperture of discrete fractures added to the model than the hydraulic conductivity of the fractured rock facies.	The model was quite sensitive to the top boundary condition. Fixed heads were not appropriate to simulate the drawdown during pumping at this block-scale. Thus, a no-flow boundary is preferred.

Modelling Group	Describe the steps in model calibration/ development you have used in Task 7B	How has head data been used in the different calibration steps?	How has PFL data been used in the different calibration steps?	Describe your understanding of model sensitivity	Describe sensitivity to model boundary conditions
SKB, CFE	1. a) My first goal was to simulate the pump test by Koskinen and Rouhianen (2007). After the introduction of two sheet joints it was quite easy to find suitable T-values for the sheet joints and a background DFN. b) Next the flow along boreholes was studied. It was found that the structural model needed an update (KR14 and KR15A). The pump test was recalibrated and a fair agreement for both draw downs and flow along boreholes was achieved. c) The recalibrated model was the "final model".	The pump test by Koskinen and Rouhanen was the main goal, as said, and it was decided that a good simulation of these head data is the most important step in Task 7B.	a) The positions (z-value) of the two sheet joints was found from transmissivity data. b). The HPF analyses (Table 4-3 in my report) is based on transmissivity data. c) Flow along boreholes (Table 4-6).	a) See my report pp 15→19. The model is not very sensitive to different DFN realizations. b) It is interesting to note that the need to update the structural model was pointed out by the comparisons of flow along boreholes. c) On pp21–22 in my report it is suggested that the flow along boreholes is sensitive to the variations in the ground water table. If this is right it points to a high sensitivity of flow along boreholes to detailed features in the system.	a) Vertical boundaries are far away from the area of interest and for this reason not influential. b) Top boundary may need higher resolution, see point 4C.
SKB/KTH	Focus has been on model development through several steps. The overall idea has been to evaluate the model by comparing simulated borehole flows against PFL flows. Model development has included the following features: (i) Changing fracture structure/geometry (ii) Changing model boundary conditions (iii) Changing fracture transmissivity The overall idea/conceptual model has been to try to reproduce PFL flows through simulation of pump tests by constructing a DFN-only model of the KR14–18 region. See further details after this table.	The primary aim and focus has been to analyse and try to make best use of the PFL flow data. Therefore in this initial work, for simplicity and to reduce the complexity of the problem, head data has not been used. An improved model could make use of the pressure data, which might also reveal insight into connected and disconnected regions between the boreholes. Thereby it may be possibly to incorporate this type of information into the fracture partitioning scheme to improve flow responses. Also, the pressure distribution may give insight into why the flow magnitudes during pumping are often too low in the current model.	PFL data has been extensively used in primarily three different ways. • For 'conditioning': PFL flows have been used to check the consistency of the simulations/ model with field data. That is, the borehole flows obtained from simulation have been compared against PFL flows, both in terms of flow directions entering or leaving the borehole, as well as flow magnitudes. This has been the underlying use of the PFL data throughout all modifications and model changes/developments. • As input data: PFL transmissivities form the basis for assigning fracture transmissivity. • As a data filter: Only fractures deemed to be hydraulically active through a measurable PFL flow value are used.	The sensitivity of a model which consists of parameters will in general be subject to the sensitivity of the values of the parameters used. Therefore it may be of interest to understand the significance of changes in the (input/dependency) parameters have on the model output/results. Eg a stable system may be characterised by it bnehaving such that small changes in parameters poduce small changes in results, but an unstable system may produce large/significant changes in results for small changes in parameters.	Through this work it has been discovered that this particular model is sensitive to boundary conditions, in particular to the type of BC used for the top of the surface domain. Since the BC with no-flow through the top surface seems to provide better results (more consistent with PFL flow directions) than the top BC with head equal to surface elevation, it seems the type of boundary conditions play a significant roll in this scale of the KR14–18 borehole region, at least when only assuming a DFN.

Modelling Group	Describe the steps in model calibration/ development you have used in Task 7B	How has head data been used in the different calibration steps?	How has PFL data been used in the different calibration steps?	Describe your understanding of model sensitivity	Describe sensitivity to model boundary conditions
VTT	Having set the conceptual model with all of its attributes (geometry, properties, boundary conditions) a long series of scoping calculations was performed. Calibration was not really successful whe assuming natural conditions – some disturbance had to be present. Then, head was extracted (and averaged across the different realisations) at the observations' locations to calculate the Root Mean Square Deviation (RMSD) and the flows were calculated along the pumped hole and along the observation holes. Special care was exercised to obtain correct flows from each fracture that intersected the boreholes. Frequency distributions were created from all the collected flow magnitudes and compared to the measured frequency distribution with the Kolmogorov-Smirnov statistical test. Successful cases were considered to exhibit low head RMSD, low flow K-S and low flow variance. Calibration "steps" were not used in the strict sense of the manual calibration in that the different statistical descriptions were not followed from each other but chosen upon some independent considerations. Some steps were taken to find similarly successful statistical description with the Ensemble Kalman Filter approach.	(See 1 above) Head RMSD was calculated at the location of the observations.	(See 1 above) In some contrast with the head RMSD approach, not the calculated flow values were compared to the measured ones, but their distribution with a statistical test. It was very interesting to see that either head RMSD or flow K-S alone would not have guided well the decision over the selection of the succesful cases: models providing the closest head results to the observations showed rather poor flow distribution and also the other way round. When both head RMSD and flow K-S were low, cases with the smallest flow variance won. Thus successful cases were selected as head+flow optima.	Sensitive models exhibit some variations in their output when their input is perturbed. Our models did not prove particularly sensitive under natural conditions. With some disturbance inserted, however, the model responses in terms of head and flow distributions appeared to be sensitive to the following elements of the statistical description of the fracture network: (1) truncation limit of the size distribution, (2) truncation limit of the transmissivity distribution, (3) variance of the transmissivity distribution, (4) correlation between the size and the transmissivity distributions and (5) the presence of the assumed sheet joints. These parameters gave rise to heterogenic connectivities different to the extent that was apparent in the calculated performance measures.	One of the objectives of the preliminary modelling was to find a set of boundary conditions which are adequate and to which the model is not sensitive. These included (1) the transfer of head values over the vertical bounding faces of the model from a larger EPM model (2) no-flow on the top surface and at the bottom and (3) applied nodal flow in place of the disturbances. The size of the model (i.e. the distance of the bounding faces from the disturbance) was experimented and set such that the inherent uncertainty over the external boundaries would not affect the relevant responses.

Additional information provided by SKB/KTH

Further, since the scale is relatively small (of the order of approx 10 m to 100 m distance between boreholes) the idea has been to try to replicate the region with a single, semi-deterministic DFN model. That is, the fracture structure or the DFN is not stochastic in the approach used. This has been achieved by using fracture data from core-logs to describe the center (x,y,z) locations of fractures in the domain as well as vectors describing orientations (strike and dip) of fractures. Then, the concept is that the fractures stemming from each borehole are allowed to 'grow' along the vector directions until they intersect fractures from one of the neighbouring boreholes, and/or reach the model domain boundaries. Further, only fracture observations which contain measurable PFL flow are used; ie other fracture observations are not used (such as from core logs, surface outcrops, be it open or closed, etc). This way a connected network consisting of fractures which are known to be hydraulically active is constructed.

The steps in model development include how the conceptual idea of 'growing fractures' ie fracture regions/compartments are technically implemented in the simulation model (feature (i)), as well as how transmissivity is assigned to fractures (feature (iii)), and combined with what boundary conditions are assigned on model boundaries (feature (ii)). For (i), at first a 'radius' was assigned for fractures, such that they were allowed to extend along the strike and dip directions for a given length. These lengths are chosen to ensure fractures between boreholes actually connect, and so are dependent on how close boreholes are to each other. Then to make connections with the boundaries, the hydraulic zones HZ19A/C and HZ20A (from task 7A) are used. Thereafter, (i) was improved by defining partitions and allowing fractures to grow within their respective regions. This way fractures extended all the way to the model domain boundaries, and so the use of HZs was not needed. It should be noted that this is in one sense more consistent with data, since the PFL fractures include fractures deemed to be part of the HZs, thus the HZs are included directly based on the PFL data.

In general it seems that certain regions are either over-connected or under-connected. It might be possible to improve response directions further by altering connections between borehole regions (partitions/compartments), either at selected lateral or vertical parts between regions.

For (ii), the top surface BC was modified, from the reference case of head = elevation, to the case with no-flow along the top surface. This resulted in better flow directions in the response boreholes for most pumping cases, even though there is currently no a priori underlying conceptual motivation for the no-flow BC.

For (iii), the reference case fracture transmissivity is based on PFL T. Also homogenous fractures are used, ie assuming the PFL T is a suitable effective value for each fracture. Thereafter, T of certain selected sub-regions of fractures are altered. This means that the individual fractures become (slightly) heterogenous, ie T may change spatially for given fractures in the affected regions.

There were two underlying motivations for altering T:

- The range of PFL T is limited and slightly smaller for both low and high T values when compared with other methods (e.g. HTU T's).
- The simulated flow responses were generally too low, indicating higher T is needed (for this model configuration).

It was modified in several ways, eg increasing/decreasing T of the entire system, or restricted to certain spatial regions.

It was observed that if all fracture T is increased, the flow magnitudes in the pumping boreholes may be better matched, but then generally the flow rates in the response boreholes are much too high. Thus it is concluded that a global increase in T will not directly improve the model, instead target regions may be necessary. Therefore it was attempted to increase T in the near vicinity of the boreholes by up to a facture of 10, which seemed to give some improvement.

Also, an attempt at increasing a slice through a layer near the top surface of the domain was attempted, with the motivation that the HZs might be under-represented in terms of T. This also seemed to improve the response magnitudes of the affected depth layer (but not directions).

Table B-7. Task 7B Questionnaire 1: PFL measurements, transport properties and uncertainty.

Modelling Group	What influence has the PFL measurement method (limit of detection, boundary conditions...) had on your modelling?	Describe the concepts you have used for transport calculations	Describe how model and parameter uncertainty has been treated and how it has evolved in your modelling	Have you any other comments about Task 7B modelling?
CRIEPI	The PFL measurement method was very effective to determine transmissivities of background fractures and their intersection with boreholes.	I have not perform any transport calculations yet.	Sensitivity analyses was performed and the parameter values which could reproduce the measured drawdowns and groundwater inflow to boreholes best were selected.	It was a very tough sub-Task. It was very difficult to reproduce measured drawdown and groundwater inflow to boreholes at the same time. We need more information on the distribution of size of background fractures and the relationship between fracture size and transmissivity.
JAEA/ Golder	In general, site investigation is required to discriminate the effects of major water conducting features when testing at minor zones. However, both of measurement and modeling of PFL method could not distinguish between heads in open boreholes. Major features with higher transmissivity have the most significant influence on flow response. This makes it difficult to calibrate the properties of minor features	Particle tracking (FracMan 7.2) was used for all transport calculations.	Transport parameter uncertainty was not studied.	There is a need to develop improved measures for comparing complex, heterogeneously connected fractured rock mass models to interference test results. JAEA has proposed the use of RMS (residual sum of squared errors) as one of performance indices; however, this measure is not sufficient to fully understand the differences between models and measurements. The larger structures were the most important aspect to understand to match pressure and flow responses from hydraulic interference tests. While effective fracture hydrogeologic properties are sufficient for hydraulic interference tests, heterogeneous connectivity of minor fractures and/or in-plane heterogeneity of the larger structures need to be modelled with greater accuracy to match the minor flow responses measured by PFL.
KAERI	The PFL data could be certainly used in the reliability of the conceptualized groundwater flow model especially when we need to consider the background fractures. However, we are still thinking about how we can use it with the head data simultaneously at the calibration works.	A transport modeling was not conducted. Performance assessments for PA20c and PA29 were executed by a method of particle tracking which calculated the moving path and elapsed time of a imaginary particle with the heads of each node and flow rates through adjacent elements.	We think the background fractures were one of the most basic reasons of the uncertainty in the model and considered it through Monte Carlo approach. Several realizations of the fracture network model, where the FZs were inputted deterministically and the background fractures stochasticlly, were generated and flow modelings were conducted with them.	We think that the modeling procedure in Task7B is very interesting and good trial to characterize a deep groundwater system under fractured media.
NWMO/ Laval	The main influence of the measurement method is constituted by the length of the PFL test section (2 m), which is different from the mesh resolution of the numerical model. A smaller mesh size (2 m) would have been less appropriate for the evaluation of borehole core fracture density, which constitutes the basis of the fractured rock conceptual model adopted (based on facies).	The HydroGeoSphere travel time probability package, which allows simulating groundwater life expectancy for the release points, was used.	Uncertainty has been analyzed by using the parameter confidence intervals calculated by PEST. Its evolution was analyzed by varying the number and type of observations included as targets for calibration during the inverse modeling.	

Modelling Group	What influence has the PFL measurement method (limit of detection, boundary conditions...) had on your modelling?	Describe the concepts you have used for transport calculations	Describe how model and parameter uncertainty has been treated and how it has evolved in your modelling	Have you any other comments about Task 7B modelling?
SKB, CFE	I have not questioned the method at all, only used the outcome.	7. As we know very little about porosity and properties of the matrix, the basic concept is that “we can only determine the flow paths, not transport times or dispersion”.	Not considered, see 7.	An interesting and valuable task.
SKB/KTH	The model development relies on comparing against the measured flow rates. The set of fractures used in the model is based on flowing PFL fractures observed during pumping. However in the PFL data not all flowing fractures are consistently observed; this is clear from the data,’ since a greater number of flowing fractures exist when a borehole is being pumped, and generally fewer are observed when the borehole is acting as a response/observation borehole. This this somewhat complicates the model development when comparing responses, since the simulated fractures are of course always there and produce some flow magnitude. However, the target is then to try to maintain the simulated near the detection limit. Also, the PFL flows are not always conserved (the total sum of flow in and out of a response borehole is not always close to zero) and in some cases there seems to be evidence of ’circular flows’ (flow with similar magnitudes but opposite directions in close proximity in the borehole). Furthermore, the range of PFL measurable flows restricts the range of inferrable transmissivities. It seems likely that the least transmissive features are not well represented in the model. In principle it may also be possible that transmissivities above the upper limit are not seen, though this seems unlikely for the Olkiluoto case.	Boundary conditions assigned as weak hydraulic gradient along the four principle directions, resulting in four linear, unidirectional flow simulations (see readme file in particle_tracking.zip file, which contains results from pt). Full mixing at fracture intersections. This means several pathlines are obtainable from a single injection point, where the density of pathlines reflects the flow rates/velocities through the system. Velocity is obtained from the flow rate by assuming the cubic/parallell plate relationship. The quantity denoted as ’F-factor’ refers to a hydrodynamic characterisation of retention along the advective flow path. The definition used here is F = 2WL/Q, but can also be obtained from a ’microscale’ perspective by integrating length over velocity and half-aperture, ie beta = sum_i[l/(v*2b)] where the sum is over each step i along the particle path. F-factor = beta whenever aperture 2b and flow Q is constant along the ’flow channel’. Also, it can be noted that advective travel time ’tau’ along a path can be obtained similarly, but without aperture, ie as tau = sum_i[l/v]. Note that in the RP files containing particle trajectory data, travel times and F-factor values, the values provided are at the step or segment level ’i’, ie the summation is not carried out.	Parameter uncertainty has only been considered for certain aspects. For example, the sensitivity of the overall connectivity of the system has been studied for the improved structural representation (partitioned regions), ie for the final case simulations (the b-series), by randomly removing sub-fractures, and it is observed that if the total fracture density is reduced by 10 % there is little/insignificant change in responses, but if it is reduced by 25 % then there is hardly no flow responses, ie the system becomes disconnected. Thus the fracture density cannot be much lower that which is used in the final case. Also, a brief analysis of the overall sensitivity to fracture T was conducted. It was observed that if all fracture T is increased (by a constant factor), such that the simulated flow rates in the pumped boreholes match the measured flow rates, then the responses in the non-pumped boreholes are much too high. Thus it is concluded that a global increase in T will not directly improve the model, instead target regions may be necessary, and/or modifications to the connectivity structure of the system.	The flexibility in the Task Description, allowing modellers certain freedom in conceptual modelling approaches has been greatly appreciated! I am perhaps slightly sceptical to the long and exhaustive lists of required simulations, but perhaps this is necessary to provide some consistent basis of comparison of results between groups.

Modelling Group	What influence has the PFL measurement method (limit of detection, boundary conditions...) had on your modelling?	Describe the concepts you have used for transport calculations	Describe how model and parameter uncertainty has been treated and how it has evolved in your modelling	Have you any other comments about Task 7B modelling?
VTT	Flow measurements and the corresponding calculated flow distributions provided another aspect for assessing the model responses as well as heads. In the light of the head+flow optimum mentioned above there may be a ground to believe that the inclusion of the PFL data in the modelling led to more accurate statistical description of the hydraulic connectivities.	No transport calculations were performed.	(1) The DFN approach inherently includes parameter uncertainty when it statistically describes the fracture network. (2) The ensemble Kalman Filter requires (a priori) distributions in place of the initial parameters. The method updates these in the course of the assimilation cycles and when successful, considerably decreases the variance of the output variables.	Very instructive and interesting task.

Appendix C

PFL bias due to near-borehole heterogeneity

Fractures in crystalline rock typically show significant heterogeneity in terms of local aperture and transmissivity. This is often described as channelling (Tsang et al. 2015)[43].

Variability in local transmissivity within fractures and fracture zones can be large. Marschall and Lunati (2006) describe local transmissivity variation over 3 orders of magnitude (10^{-8} to 10^{-11} m^2/s) from 7 borehole intersections with a small shear zone at the Grimsel Test Site (GTS). Meier et al. (1997) presents results from a comprehensive set of hydraulic tests from the MI Shear Zone at GTS. Pulse tests and longer cross-hole tests were performed in the shear zone intervals of 8 boreholes (BOMI 86.004 to BOMI 87.011). Local transmissivity ranged from greater than 10^{-5} to less than 10^{-10} m^2/s. The larger scale transmissivity was ~10^{-6} m^2/s. Similarly, Doughty and Uchida (2003) suggest a long normal transmissivity distribution with geometric mean transmissivity ~10^{-6} m^2/s and standard deviation $\log_{10}$ transmissivity of 1.35 for a fracture zone in Äspö. Larsson et al. (2012) suggest a range of hydraulic conductivity variability in fractures up to $s_{ln} = 4.6$ (equivalent to $s_{log10} = 2$).

Borehole intersections with low transmissivity parts of larger transmissive structures (i.e. outside the channels) will show significantly lower flow than intersection with the channels. Analyses of packer tests can potentially identify changes in fracture transmissivity over time as the radius of investigation increases (Copty et al. 2011, Walker and Roberts 2003, Enachescu et al. 2004) however the influence of wellbore storage or other phenomena (e.g. response to packer inflation) may dominate response in low transmissivity intervals (e.g. Black and Kipp 1977, Pickens et al. 1987).

C.1 Effect of hydraulic skin on estimated transmissivity

The PFL analysis method uses only the quasi-steady flow during long interval (or open-hole) tests. PFL transmissivity is estimated using the Thiem equation for steady state radial flow:

$$Q = \frac{2\pi T \Delta h}{\ln\left(r_2 / r_0\right)}$$

If we consider flow to a borehole from a feature with transmissivity T_1 for $r_0 \leq r < r_1$; where r is the radial distance from the borehole axis, r_0 the borehole radius and r_1 the outer radius of the borehole "skin zone" and transmissivity T_2 for $r_1 \leq r < r_2$ where r_2 is the distance to the assumed constant head – either intersection with a more transmissive feature or the radius of investigation of the pumping test. For PFL analyses r_2 is commonly assumed to be 500 r_0 (Pekkanen and Pöllänen 2008). If the transmissivity is calculated directly from the steady flow and the assumed distance to a constant head boundary then the transmissivity estimate T_{PFL} is related to T_1 and T_2 by:

$$T_{PFL} = \frac{\ln(500) T_2}{\ln\left(500/n\right) + \ln(n)\frac{T_2}{T_1}}$$

Where $r_1 = n.r_0$ (i.e. the skin zone extends n borehole radii from the axis). In cases where n is very small or $T_1 \sim T_2$ the estimated transmissivity T_{PFL} is close to the large-scale transmissivity T_2. However, where $T_2 >> T_1$.TPFL may be significantly smaller than T_2 even for moderate n e.g. 5–10 radii.

Figure C-1 shows contour plot of T_{PFL}/T_2 for varying T_2/T_1 and r_1/r_0. The asymmetric effect of a low transmissivity zone close to the borehole is clearly seen. A higher transmissivity zone clos to the borehole results in only a minor over-estimate of T_2 – less than a factor of 2 for a zone extending ~20 times the borehole radius while a locally low transmissivity interval of similar size result in underestimate by much greater factors.

[43] The initial fracture local aperture distribution is typically modified by normal and shear deformation (Yeo et al. 1998, Lee and Cho 2002, Vilarrasa 2010) and the development of fracture filling material through fine particle transport or chemical reaction.

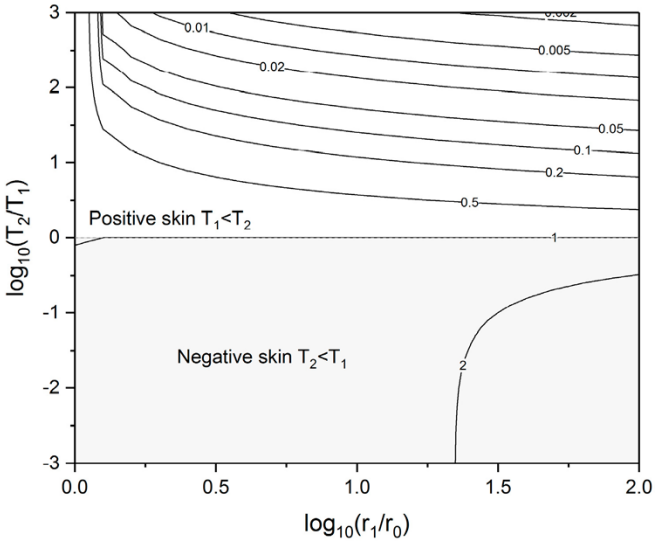

Figure C-1. *Contour plot of ratio T_{PFL}/T_2 for varying T_2/T_1 and r_1/r_0.*

If the local transmissivity T_1 is assumed to follow a log-normal distribution with mean of T_2 (the large-scale transmissivity) and $\log_{10}$ standard deviation s_{T1}, the distribution of T_{PFL}/T_2 can be calculated for any given skin radius. Figure C-2 shows the cumulative distribution of T_{PFL}/T_2 for $r_1 = 5r_0$ (for a borehole diameter of 76mm equivalent to 19cm radius). It can be seen that for $s_{T1} = 3$, T_{PFL} would show a transmissivity of less than 1 % of the large-scale value (T_2) in approximately 20 % of intersections.

More general steady state and transient solutions for radial two-zone models can be found in Yeh and Wang (2007) and Tsai and Yeh (2012).

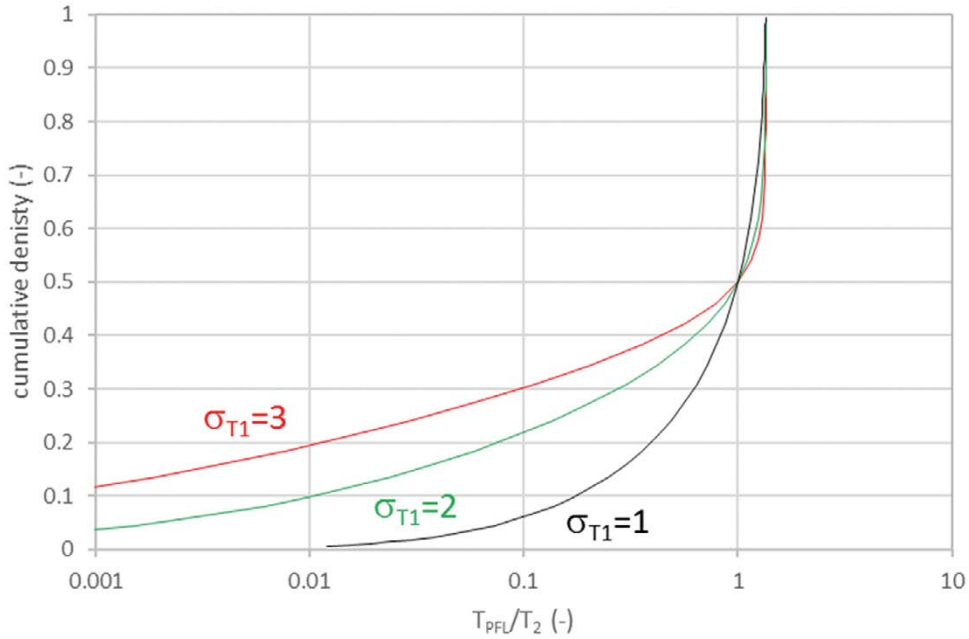

Figure C-2. *Cumulative density function for T_{PFL}/T_2 for varying $\log_{10}$ standard deviation s_{T1} assuming $r_1 = 5r_0$.*

C.2 Conclusions

Small-scale transmissivity variation close to borehole intersections will bias PFL-based estimates of transmissivity. Where the borehole intersection is more transmissive than the larger scale properties of the feature, this will typically result in a small over-estimate of transmissivity (<2 see Figure C-1). However, where the borehole intersects a lower transmissivity part of the feature, the transmissivity may be significantly underestimated or the inflow point may go undetected.

In DFN calibration approaches based on the measured quasi-steady flow (Q) rather than estimated transmissivity a similar bias will be induced if variation in small scale transmissivity is not considered.

Table C-1. Model parameters.

Parameter	Description
T_1	Local transmissivity around borehole (m^2/s)
σ_{T1}	Log_{10} standard deviation of T_1
T_2	Undisturbed “larger scale” transmissivity (m^2/s)
Q	Flow in/out of borehole (m^3/s)
Δh	Head (m) difference between borehole and r_2 due to flow
r_0	Borehole radius (m)
r_1	Radius of skin zone (m)
r_2	Radius to constant head boundary (m). Assumed $500 \times r_0$ in PFL method
h_0,h_1,h_2	Head at r_0,r_1,r_2

Appendix D

DFN model data usage and assumptions in Task 7B

Figure D-1 illustrates an idealised dataflow for site characterisation DFN models from input data to model outputs. The modelling groups' approaches to Task 7B have been used to illustrate the parameterisations used and some of the assumptions behind them.

A – WCF orientation

Within Task 7B modellers either fitted orientation distributions to the integrated PFL dataset, bootstrapped from it or assumed generic distributions. Studies of network percolation and effective permeability show that orientation typically has little effect on percolation density and only results in significant permeability anisotropy when orientations are highly clustered in a single set (Mourzhenko et al. 2009). Feature orientation will however affect the estimated feature density when correcting for borehole bias (Terzaghi 1965) which will affect the effective permeability of the network (particularly when close to percolation threshold).

Table D-1. WCF orientation distributions.

Modelling group	Orientation distribution for stochastic features
JAEA	A single Fisher orientation distribution was assumed
KAERI	Derived from borehole data (integrated PFL dataset)
NWMO/Laval	N/A
Posiva/VTT	A single orientation distribution was assumed
SKB/CFE	A generic (Äspö) background DFN model was used
SKB/KTH	Feature orientation was taken directly from the integrated PFL dataset.

B – WCF spatial distributions

The deterministic fracture zones were derived from the geometries provided within the data deliveries and were largely unaltered. Several groups added features (sheet joints) to match the observed hydraulic responses (calibration) or developed variants of the deterministic structures using the two structural models provided.

With the exception of SKB/KTH and NWMO/Laval all the modelling groups assumed the background rock WCFs were distributed according to a homogeneous Poisson Process. The line density of the features was derived from the integrated PFL dataset and corrected using Terzaghi weighting. The assumption of a homogeneous Poisson Process was not tested by the groups. The uniform Poisson Process requires the least information (P_{32} value and length distribution) to generate the fracture centres.

The use of a homogeneous Poisson Process is equivalent to assuming that fractures are positioned independently of each other. Although such a model results in no preferential clustering as fracture centres are equally likely to occur in any location, it does not result in uniform distributions of features and there is some degree of clustering observed (i.e. intersection spacing along a sampling line is negative exponentially distributed).

C – WCF length scale and shape

Table D-2. Representation of water conducting features in the background rock.

Modelling group	Geometry of water conducting features in the background rock
JAEA	Derived fracture lengths from the transmissivity using a correlation derived in Task 6C (Dershowitz et al. 2003).
KAERI	Derived from borehole data (see Ko et al. 2010).
NWMO/Laval	N/A
Posiva/VTT	Sensitivity studies using a truncated power-law with a fixed lower size and exponent but varying the maximum length.
SKB/CFE **SKB/KTH**	A generic (Äspö) background DFN model was used. Fracture-growth model based on borehole intersections and a partitioning of the volume. The resulting length distribution was not reported.

Stochastic fractures were assumed to be square or a regular polygon approximating a circular disk (both aspect ratio 1). Barker (2018) and Black and Barker (2018) show the influence of feature aspect ratio on the connectivity of networks. Typically networks of high aspect ratio features are better connected than networks of circular or square features at the same area density.

D – Cross-hole test constraints

The purpose of the task was to investigate the constraints resulting from the different types of cross-hole testing performed. Model calibration resulted in:

1. Inclusion of deterministic features to match key aspects of the observed responses.
2. Variation of stochastic DFN parameters.
3. Modifications in the connectivity of features.
4. Modifications to boundary conditions.

For the deterministic fracture zones within the structural model, cross-hole testing had been used to identify the existence, extent and large-scale effective transmissivity of the features.

E – WCF Connectivity

For most of the modelling groups WCF connectivity was controlled by the deterministic features and the length-scales chosen for the stochastic features (there is a small influence of orientation) based purely on the geometric considerations. JAEA/Golder varied the hydraulic connectivity between features using a random process. SKB/KTH determined the connectivity by the choice of fracture growth model (at compartment boundaries).

Within NWMO/Laval's model, connectivity between WCFs was conceptually "lumped" within the facies definitions (i.e. the higher fracture density facies were associated with higher effective hydraulic conductivity).

F – Pump test analysis

Most modelling groups used the PFL derived transmissivity directly. The assumptions underlying this analysis include steady radial flow in a homogeneous feature with a constant head boundary at 500 × borehole radius. Uncertainties in the PFL analyses were typically not considered (presumably on the basis that these were small relative to the overall variability in feature transmissivity).

JAEA used pressure derivative analysis methods to refine their structural model at the scale of the pumping tests.

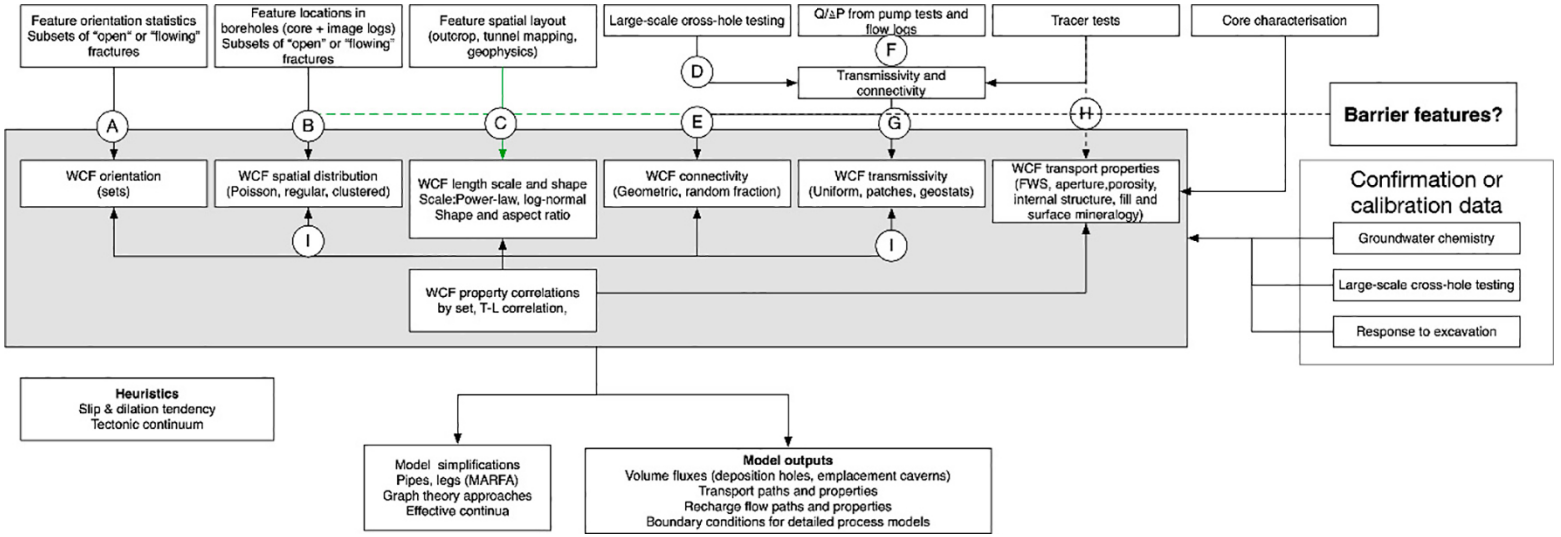

Figure D-1. *Site characterisation DFN data flow.*

G – WCF transmissivity

All DFN models assumed that small scale features were uniformly transmissive across their surface (Task 7C addressed small-scale transmissivity variation). Transmissivity distribution was either taken from the PFL data or subject to calibration.

Large scale feature transmissivity was derived from cross-hole testing or the geometric mean of multiple PFL measurements. JAEA performed some transient well-test analyses to inform their modelling. Locally some modelling groups applied "skin" terms to address the effects of small-scale heterogeneity close to the boreholes.

H – WCF Transport properties

Modellers assumed transport porosities based on scaling of the feature transmissivity, most commonly using "Doe's Law". Although advective transport time performance measures were derived for some model runs, the emphasis was on comparison with measured heads and flows so modelling groups used simplified approaches (as facilitated by their numerical codes) for the transport analyses.

I – WCF property correlations

Several groups assumed that feature length-scale was correlated with transmissivity.

The effects of length-transmissivity correlations were investigated by Posiva/VTT.

Summary

A summary of the different datasets or assumptions used is given in Table D-3. It can be seen that the modellers made a range of choices to populate the DFN driven by the data available supplemented by literature assumptions. Some sensitivity studies were performed by individual groups.

Table D-3. Derivation of DFN properties used within Task 7B.

	Derivation	Test
Orientation	Generic or based on integrated PFL dataset	Fit to observation
Spatial distribution	Poisson process with mean density from intersection and orientation distribution	Minimum information – consistency test of intersection frequency but no test of distribution or sensitivity study
Length scale	Generic Correlated to transmissivity Grown from borehole intersect	Assumed – sensitivity study from Posiva/VTT
Geometry	Assumed square or circular	Minimum information – no test or sensitivity study
Connectivity	Geometric connectivity of elements	Assumed – some sensitivity studies
Transmissivity	Integrated PFL dataset	Comparison with single-hole PFL tests could have been performed
Transport properties	Correlation with transmissivity by quadratic or cubic law	Assumed
Correlations	Length-transmissivity	Assumed. Sensitivity study from Posiva/VTT No other correlations considered

Arkitektkopia AB, Bromma, 2021

SKB is responsible for managing spent nuclear fuel and radioactive waste produced by the Swedish nuclear power plants such that man and the environment are protected in the near and distant future.

skb.se